



HAL
open science

Chemical Modification of Graphite-based Derivates and Their Uses in Elastomer Nanocomposites

Alice Pazat

► **To cite this version:**

Alice Pazat. Chemical Modification of Graphite-based Derivates and Their Uses in Elastomer Nanocomposites. Material chemistry. Université de Lyon, 2017. English. NNT : 2017LYSE1050 . tel-01537733

HAL Id: tel-01537733

<https://theses.hal.science/tel-01537733>

Submitted on 12 Jun 2017

HAL is a multi-disciplinary open access archive for the deposit and dissemination of scientific research documents, whether they are published or not. The documents may come from teaching and research institutions in France or abroad, or from public or private research centers.

L'archive ouverte pluridisciplinaire **HAL**, est destinée au dépôt et à la diffusion de documents scientifiques de niveau recherche, publiés ou non, émanant des établissements d'enseignement et de recherche français ou étrangers, des laboratoires publics ou privés.



N°d'ordre NNT :

2016LYSE1050

THESE de DOCTORAT DE L'UNIVERSITE DE LYON

opérée au sein de
l'Université Claude Bernard Lyon 1

Ecole Doctorale n°34
Matériaux

Spécialité de doctorat :
Discipline : Chimie des Matériaux

Soutenue publiquement le 24/03/2017, par :

Alice PAZAT

Chemical Modification of Graphite-based Derivates and Their Uses in Elastomer Nanocomposites

Devant le jury composé de :

ESPUCHE Éliane	Professeur	Université Lyon 1	Examinatrice
GIESE Ulrich	Professeur	DIK, Hanovre	Rapporteur
PÉNICAUD Alain	Directeur de Recherche	CNRS Bordeaux	Rapporteur
BRUNO Florence	Ingénieur	LRCCP	Examinatrice
JANIN Claude	Docteur	LRCCP	Examineur
BEYOU Emmanuel	Professeur	Université Lyon 1	Directeur de thèse
BARRÈS Claire	Maître de Conférences HDR	INSA de Lyon	Co-directrice de thèse

UNIVERSITE CLAUDE BERNARD - LYON 1

Président de l'Université

Président du Conseil Académique

Vice-président du Conseil d'Administration

Vice-président du Conseil Formation et Vie Universitaire

Vice-président de la Commission Recherche

Directeur Général des Services

M. le Professeur Frédéric FLEURY

M. le Professeur Hamda BEN HADID

M. le Professeur Didier REVEL

M. le Professeur Philippe CHEVALIER

M. Fabrice VALLÉE

M. Alain HELLEU

COMPOSANTES SANTE

Faculté de Médecine Lyon Est – Claude Bernard

Directeur : M. le Professeur J. ETIENNE

Faculté de Médecine et de Maïeutique Lyon Sud – Charles Mérieux

Directeur : Mme la Professeure C. BURILLON

Faculté d'Odontologie

Directeur : M. le Professeur D. BOURGEOIS

Institut des Sciences Pharmaceutiques et Biologiques

Directeur : Mme la Professeure C. VINCIGUERRA

Institut des Sciences et Techniques de la Réadaptation

Directeur : M. le Professeur Y. MATILLON

Département de formation et Centre de Recherche en Biologie Humaine

Directeur : Mme la Professeure A-M. SCHOTT

COMPOSANTES ET DEPARTEMENTS DE SCIENCES ET TECHNOLOGIE

Faculté des Sciences et Technologies

Directeur : M. F. DE MARCHI

Département Biologie

Directeur : M. le Professeur F. THEVENARD

Département Chimie Biochimie

Directeur : Mme C. FELIX

Département GEP

Directeur : M. Hassan HAMMOURI

Département Informatique

Directeur : M. le Professeur S. AKKOUCHE

Département Mathématiques

Directeur : M. le Professeur G. TOMANOV

Département Mécanique

Directeur : M. le Professeur H. BEN HADID

Département Physique

Directeur : M. le Professeur J-C PLENET

UFR Sciences et Techniques des Activités Physiques et Sportives

Directeur : M. Y. VANPOULLE

Observatoire des Sciences de l'Univers de Lyon

Directeur : M. B. GUIDERDONI

Polytech Lyon

Directeur : M. le Professeur E. PERRIN

Ecole Supérieure de Chimie Physique Electronique

Directeur : M. G. PIGNAULT

Institut Universitaire de Technologie de Lyon 1

Directeur : M. le Professeur C. VITON

Ecole Supérieure du Professorat et de l'Education

Directeur : M. le Professeur A. MOUGNIOTTE

Institut de Science Financière et d'Assurances

Directeur : M. N. LEBOISNE

Title and key-words

Title

Chemical Modification of Graphite-based Derivates and Their Uses in Elastomer Nanocomposites

Key-words

Graphite oxide, polyisoprene, functionalization, ionic liquids, thermal expansion, in situ polymerization, permeability, tensile properties

Titre

Modification chimique du graphite et de ses dérivés et leur utilisation dans des nanocomposites à matrice élastomère

Mots-clés

Graphite oxydé, polyisoprène, fonctionnalisation, liquides ioniques, expansion thermique, polymérisation in situ, perméabilité, propriétés mécaniques

Intitulé et adresse du laboratoire

Laboratoire Ingénierie des Matériaux Polymères (IMP@Lyon1), UMR CNRS 5223

Bâtiment Polytech'Lyon

15 boulevard Latarjet

69622 VILLEURBANNE

Discipline

Chimie des Matériaux

Abstract

The aim of this study was the investigation of various dispersion methods for graphite-based fillers in elastomers such as polyisoprene, to enhance mechanical and barrier properties. To increase graphite-rubber interactions and so decrease filler-filler aggregation, graphite-based fillers have been chemically modified. Graphite was previously oxidized into graphite oxide (GO), bearing epoxide, hydroxyl and carboxylic acid groups, which could further act as anchor sites for molecules and polymer chains. To increase the compatibility between GO and the polymeric matrix, amines and alkoxysilanes, as well as polymer chains, were grafted on GO. Grafting contents between 4-50 wt% were obtained, depending on the functionalization technique which was used. A thermal modification path of GO was also investigated and led to the formation of porous graphite structure. Polyisoprene composites containing 15 phr of these graphite-based fillers were prepared and showed decreased air permeability (-70 % for composites containing thermally-treated graphite filler, as compared to those containing carbon black only) as well as enhanced tensile properties. Finally, the use of ionic liquids as dispersing agents was investigated. Natural rubber – graphite composites with 1 wt% of ionic liquid displayed enhanced reinforcement (+ 25 % for the stress at 300 % strain) while maintaining similar strain at break to composites containing carbon black only.

Résumé

L'objectif de la thèse a été d'explorer différentes voies de dispersion de charges graphitiques dans des élastomères de type polyisoprène dans le but d'améliorer les propriétés mécaniques et barrière. Pour augmenter les interactions entre le graphite et l'élastomère et donc diminuer les interactions entre charges, les charges graphitiques ont été modifiées chimiquement. Le graphite a été préalablement oxydé pour obtenir du graphite oxydé (GO) contenant des groupements époxyde, hydroxyle et acide carboxylique, susceptibles de servir comme sites d'ancrage de molécules et de chaînes polymères. Afin d'améliorer la compatibilité du GO avec la matrice polyisoprène, des amines et des alkoxysilanes ainsi que des chaînes polyisoprène ont été greffées sur le GO. Des taux de greffage variant de 4 à 50 % en poids ont été obtenus selon la technique de fonctionnalisation utilisée. Une expansion thermique du GO a aussi été étudiée et a conduit à la formation d'une structure graphitique poreuse. Des composites polyisoprène contenant 15 pce de ces charges graphitiques modifiées ont ensuite été préparés et ont montré une diminution de la perméabilité à l'air (-70 % pour les composites graphite traité thermiquement, par rapport à ceux chargés uniquement en noir de carbone) ainsi qu'une amélioration des propriétés mécaniques. Enfin, l'utilisation de liquides ioniques comme agents dispersants a été étudiée. Des composites caoutchouc-graphite avec 1 % en poids de liquides ioniques ont montré un renforcement plus élevé (+ 25 % pour la contrainte à 300 % d'élongation) tout en conservant un allongement à la rupture similaire par rapport à des composites contenant uniquement du noir de carbone.

Acknowledgements

First, I would like to thank all the members of the jury for accepting to study my work. I would especially like to acknowledge Ulrich Giese and Alain Pénicaud who kindly accepted to review this manuscript, and Eliane Espuche who accepted to be part of this jury.

I also want to thank Philippe Cassagnau for the opportunity he gave me to perform my PhD at IMP laboratory. I also want to acknowledge my two supervisors: Emmanuel Beyou and Claire Barrès for their supervising.

I would like to address my special thanks to Florence Bruno, Claude Janin and Benoît Omnès for their very kind support, their valuable advice and for giving me the opportunity to discover the fascinating world of rubber!

I wish as well to acknowledge all members of the LRCCP, especially Florian G. for his immense patience and his very dedicated work. I would also like to thank Martin and Florian D. who gave me valuable advice and support. I would also like to cite Morgane, Benjamin, Jérôme, Laurent, Christopher, Bernard S., Alexis, James, Gonzague, Oriane, Lamisse, Houria, Slimane, Stéphane, Anna, Anildo, Natali, Nicolas, Adrien... and all those I have forgotten! Thank you all for your warm welcome each time I came to Vitry. I would also like to thank Patrick Heuillet for his support, his smile and his wise advice about my work.

On the IMP side, my very special thanks go to Flavien for his help, his smile and his ability to solve any possible problem I could face! I would also like to thank Agnès for her help and her support, Adrien, Pierre A., Guilhem (IMP@INSA), Isabelle (IMP@INSA), Olivier, Thierry T., Florian, Sabine, Valentin, Ali...and all the people who helped me during these three years. I do not forget members of the CTμ, NMR, XRD and XPS platforms who help me with my analyses.

I would also like to acknowledge researchers from IMP at Lyon 1 and INSA, especially Fabrice, Véro, Guillaume, Anatoli and François G. (IMP@INSA) for his highly valuable help with cationic polymerization.

I am also very grateful to Amélie and Coline, two students who were part of this project, and who always showed dedication to their work. It was a pleasure for me to work with them both.

My very very special thanks will go to all PhD students, post-docs and interns for the nice time we spent together in and outside the lab. Your kindness helped overcome less joyful aspects of the PhD work. Thanks to you Gautier, my faithful co-office worker: we (almost) started and finished together this PhD! Thank you as well to Fabien, Antoine L., Cyrille, Margarita, Nico, Anaïs, Mélanie, Yann, Jiji, Jingping, Imed, Bryan, Laurent V., Hend, Christophe, Loïc, Michaël, Mathilde, Abdel, Quanyi, Anthony, Pierre P., Pierre S., Guillaume, Bastien, Marie-Camille, Marjorie, Manue, Thibaud, Edwin, Célia, Seb, Amani, Romina, Élodie, Antoine J., Dimitri, Marc, Julie C., Baptiste, Asma, Amira, Mammoudou, Dandjun, Sylvain, Kévin, KDP, Thomas, Marwa, Afef, Soline, Alice G., Sarra M., Sara B., Khaled, Mona, Jimmy, Perrine, Denis, Imane, Walid, Marina, Quillaja, Imène, Alex, Imen, Thaïs, Sylvia, Renaud, Clément, Oriane, Manon, Benjamin, Clémence,...and all those I have forgotten.

To finish I would like to thank my dearest friends, my family and Franck for their support.

Abbreviations

6PPD	N-1,3-dimethylbutyl-N'-phenyl-p-phenylenediamine
ACN	Acrylonitrile
AIBN	Azobisisobutyronitrile
AMIC	1-allyl-3-methylimidazolium chloride
APTES	Aminopropyltriethoxysilane
APTMS	3-acryloxypropyltrimethoxysilane
ARGET	Activator regenerated by electron transfer
ATRP	Atom transfer radical polymerization
BIIR	Bromobutyl rubber
BPO	Benzoyl peroxide
BR	Butyl rubber
CB	Carbon black
CBS	N-cyclohexyl-2-benzothiazol sulfonamide
CNTs	Carbon nanotubes
CR	Polychloroprene (chloroprene rubber)
CTAB	Cetyltrimethylammonium Bromide
CTP	N-(cyclohexylthio) phthalimide
CVD	Chemical vapor deposition
D	Diffusion coefficient
DBSNa	Sodium dodecyl benzene sulfonate
DCC	N-N'-dicyclohexylcarbodiimide
DCP	Dicumyl peroxide
DMAP	4-dimethylaminopyridine
DMF	Dimethylformamide
DMIB	1-dodecyl-3-methylimidazolium bromide

DMIC	1-dodecyl-3-methylimidazolium chloride
DMIT	1-dodecyl-3-methylimidazolium bis(trifluoromethyl sulfonyl)imide
DOP	Diocetyl phthalate
DOS	Diocetyl sebacate
DSC	Differential scanning calorimetry
EDAX	Energy dispersive X-ray analysis
EMIM SCN	1-ethyl-3-methylimidazolium thiocyanate
EMIM TFSI	1-ethyl-3-methylimidazolium bis (trifluoromethylsulfonyl)imide
FGS	“Functionalized graphite sheets”
FTIR	Fourier-transform infrared spectroscopy
GC-MS	Gas chromatography – mass spectrometry
GE	Commercially-available expanded graphite
GIC	Graphite intercalation compound
GNPs	Graphite nanoplatelets
GO	Graphite oxide
GOX	“Home-made” expanded graphite platelets
GPC	Gel permeation chromatography
hbDBSNa	Highly-branched sodium dodecyl benzenesulfonate
HNBR	Hydrogenated nitrile rubber
IL	Ionic liquid
IR	Polyisoprene (isoprene rubber)
KPS	Potassium peroxodisulfate
LASCs	Lewis acid surfactant combined catalysts
LCM	Latex compounding method
LCST	Lowest critical solution temperature
LSR	Liquid silicone rubber
MBT	2-mercaptobenzothiazole

MBTS	Dibenzothiazyl disulfide
M_c	Molecular weight between crosslinks
MDR	Moving die rheometer
M_{HR}	Maximum torque
M_L	Minimum torque
MLG	Multilayer graphene
MMT	Montmorillonite
M_n	Molar mass
NBR	Acrylonitrile-butadiene copolymers (nitrile rubber)
NMP	N-methylpyrrolidone
NMR	Nuclear magnetic resonance
NMRP	Nitroxide mediated radical polymerization
NR	Natural rubber
NS	Nucleophilic substitutions
OBr	N-(2-aminoethyl)-2-bromo-2-methylpropanamide
OD	Oxidative debris
ODA	Octadecylamine
P	Permeability coefficient
PDI	Polydispersity index
PDMS	Polydimethylsiloxane
PEDOT	Poly (3,4-ethyldioxythiophene)
PGO	Pristine graphite oxide
phr	Part per hundred rubber
PILs	Poly ionic liquids
PMMA	Poly(methyl methacrylate)
PNIPAM	Poly(N-isopropylacrylamide)
PS	Polystyrene

PT-g-PMMA	Polythiophene-graft-poly(methyl methacrylate)
PVA	Poly(vinyl) alcohol
PVDF	Polyvinylidene fluoride
RAFT	Reversible addition fragmentation chain transfer
rGO	Reduced graphite oxide
S	Solubility coefficient
SBR	Styrene-butadiene rubber
SDS	Sodium dodecyl sulfate
SEM	Scanning electron microscopy
SrGO	Sulfonated-reduced graphite oxide
STM	Scanning tunneling microscopy
STP	Standard temperature and pressure
t_{90}	90 % of t_{max}
TBzTD	Tetrabenzylthiuram disulfide
TEM	Transmission electron microscopy
TEMPO	2,2,6,6-tetramethyl-piperidine 1-oxyl
TESPT	bis[3-(triethoxysilyl)propyl]tetrasulfide
TETD	tetraethylthiuram disulfide
TEVS	Triethoxyvinylsilane
TFSI	Bis(trifluoromethylsulfonyl)imide
T_g	Glass transition temperature
TGA	Thermogravimetric analysis
THF	Tetrahydrofuran
t_{max}	Time at which the maximum torque is reached
TMOS	Trimethoxy(7-octen-1-yl)silane
TMQ	2,2,4-trimethyl-1,2-dihydroquinoline
TPP	Tetraphenylporphyrin

TPU	Thermoplastic polyurethane
TRG	Thermally reduced graphite oxide
ts ₂	Scorch time
TTPB	Trihexyl(tetradecyl) phosphonium bromide
TTPC	Trihexyl(tetradecyl) phosphonium chloride
TTPT	Trihexyl(tetradecyl) phosphonium bis(trifluoromethyl sulfonyl)imide
UV	Ultraviolet
XNBR	Carboxylated NBR
XPS	X-ray photoelectron spectroscopy
XRD	X-ray diffraction
ZnO	Zinc oxide

Table of contents

Résumé substantiel de la thèse	19
Main introduction	23
Chapter 1: Literature study	25
Introduction.....	29
1. Graphene-based materials.....	30
2. Elastomeric materials: composition and processing principles	61
3. Properties of elastomer composites containing graphite / graphene	79
Conclusion of the literature study.....	104
Chapter 2: Functionalization of graphite oxide by using a “grafting onto” approach	106
Introduction.....	110
1. Functionalization strategies	110
2. Preparation of GO	112
3. Grafting of octadecylamine onto GO	118
4. Grafting of TESPT onto GO	122
5. Grafting of polyisoprene chains onto GO through nitrene chemistry	126
Conclusion	136
Chapter 3: In situ polymerization of isoprene onto graphite oxide	138
Introduction.....	142
1. Functionalization strategies	142
2. Grafting of acryloxy and allyl groups onto GO through a hydrolysis-condensation reaction	144
3. In situ polymerization of isoprene onto modified GO.....	148
Conclusion	164
Chapter 4: Properties of polyisoprene composites containing modified-graphite oxide	166
Introduction.....	170
1. Polyisoprene composites containing thermally-expanded graphite	170
2. Properties of composites containing graphite-based fillers	173
Conclusion	188
Chapter 5: Use of ionic liquids as dispersing agents in NR and NBR – graphite composites	190
Introduction.....	194
1. Ionic liquids as dispersing agents	194
2. NR composites.....	197
3. NBR composites.....	212

4. Brief comparison of the changes in tensile properties of NR of NBR induced by the addition of graphite and ionic liquids	216
Conclusion	216
Main conclusion	220
References.....	224
Appendices	246
1. Characterization methods	252
2. Appendix to Chapter 1.....	256
3. Appendix to Chapter 2.....	265
4. Appendix to Chapter 3.....	267
5. Appendix to Chapter 4.....	273
6. Appendix to Chapter 5.....	275

Résumé substantiel de la thèse

Dans cette étude, des composites élastomères contenant des charges graphitiques modifiées ont été préparés et caractérisés. L'influence de la modification de surface du graphite sur les propriétés des composites élastomères a été étudiée.

L'étude bibliographique s'est concentrée sur le graphène et ses dérivés ainsi que sur les stratégies pour disperser efficacement cette charge dans une matrice élastomère.

Le graphène est un monofeuillet d'atomes de carbone sp^2 dont l'empilement constitue le graphite. Il possède un module d'Young de 1 TPa et une surface spécifique de 2630 m^2/g . De nombreuses méthodes de production existent mais la plupart d'entre elles sont coûteuses et difficiles à mettre en œuvre à l'échelle industrielle. Pourtant, une méthode basée sur l'oxydation, l'exfoliation puis la réduction du graphite semble prometteuse. Un matériau proche du graphène peut ainsi être obtenu, avec des propriétés intéressantes malgré la présence de nombreux défauts structuraux par rapport au graphite. La dispersion de cette charge dans une matrice élastomère peut améliorer les propriétés mécaniques et les propriétés barrière ainsi que les conductivités thermiques et électriques. Elle est cependant délicate à réaliser, à cause de fortes interactions π - π entre les feuillets du graphite, qui limitent l'exfoliation, et conduisent à la présence d'agrégats dans la matrice.

Une méthode pour diminuer ces interactions interfeuillets est de fonctionnaliser les dérivés du graphène par l'utilisation d'interactions physiques ou chimiques. De nombreuses stratégies ont été décrites dans la littérature, incluant par exemple l'utilisation d'agents dispersants, pour limiter l'agrégation des feuillets. De plus, le graphène oxydé peut être préparé par un procédé d'oxydation, pour former des groupes hydroxyle, acide carboxylique et époxyde sur sa surface et sur les bords des feuillets. Ce matériau peut ensuite être fonctionnalisé en utilisant une large gamme de réactions de chimie organique telles que des réactions d'estérification, des additions nucléophiles, des substitutions nucléophiles, etc. Il a été rapporté que la modification chimique du graphite oxydé (GO) pouvait efficacement modifier sa dispersabilité, en réduisant par exemple son hydrophilie et en augmentant son affinité pour les solvants organiques. Ceci est intéressant pour la dispersion de cette charge dans des matrices apolaires telles que le polyisoprène, afin d'augmenter les interactions charge-matrice, et ainsi apporter un meilleur renforcement. Cependant, le GO est un isolant électrique à cause de la perturbation du réseau aromatique conjugué, aussi une restauration partielle de la conductivité électrique peut être nécessaire par un procédé chimique, thermique ou solvothermique.

Dans la deuxième partie de l'étude bibliographique, l'influence de l'addition de charges graphitiques sur les propriétés d'une matrice élastomère a été étudiée. Les élastomères sont des matériaux souples qui peuvent supporter de forts allongements mais qui présentent une rigidité limitée et une perméabilité élevée. L'ajout de charges dans des matrices élastomères a donc pour objectif de les renforcer et les principaux mécanismes de dispersion du noir de carbone et de la silice sont bien connus. Cependant, pour les charges lamellaires, les mécanismes de dispersion et d'exfoliation sont moins bien maîtrisés. De plus, la petite dimension des charges graphitiques induit de fortes interactions entre les feuillets qui entraînent des phénomènes d'agrégation. Comme discuté précédemment, la modification chimique peut être un moyen de surmonter cette difficulté. De plus, l'utilisation d'un procédé approprié peut également influencer la dispersion de la charge. Ainsi, la

dispersion en milieu solvant, a souvent montré qu'elle pouvait conduire à une dispersion efficace de la charge graphitique avec, cependant, une transposition industrielle limitée. À l'inverse, la voie du mélange direct a souvent conduit à une amélioration des propriétés des composites moins importante.

Par ailleurs, les améliorations les plus notables des propriétés mécaniques et des propriétés barrière ont été observées pour des charges avec une surface spécifique élevée et leur modification de surface a montré dans certains cas, des améliorations de la dispersion et de la qualité de l'interface. Cependant, la plupart des charges graphitiques, même non modifiées, conduisent tout de même à une amélioration significative des propriétés mécaniques et barrière ainsi que des conductivités thermiques et électriques des élastomères, même à un faible taux (quelques % en masse).

L'étude expérimentale s'est ensuite concentrée sur la modification chimique du graphite pour améliorer à la fois sa dispersion dans une matrice élastomère contenant aussi du noir de carbone et les propriétés mécaniques et barrière des composites correspondants. Différentes stratégies ont été étudiées : (i) le greffage de molécules sur le graphite oxydé, (ii) le greffage d'agents de couplage entre le graphite oxydé et l'élastomère, (iii) la polymérisation in situ d'un monomère sur le graphite oxydé, (iv) le traitement thermique du graphite oxydé et (v) l'utilisation de liquides ioniques comme agents dispersants.

Dans le premier cas, le greffage covalent d'octadécylamine (ODA) sur le GO par une réaction de substitution nucléophile a été effectué à température ambiante et a conduit à un taux de greffage de 10 % massique. Des suspensions de GO-ODA stables dans du toluène (contrairement à des suspensions de GO non modifié), à une concentration de 1 mg/mL, ont été obtenues, ce qui atteste de la diminution du caractère hydrophile apporté par le greffage de l'ODA. Une autre approche consiste à utiliser un agent de couplage de type silane, le bis [3-(triéthoxysilyl)propyl] tétrasulfide (TESPT), qui a été greffé sur le GO par une réaction d'hydrolyse-condensation. Un taux de greffage de 6 % massique a été évalué par analyse thermogravimétrique. L'intérêt majeur du GO-TESPT est de posséder des liaisons soufre-soufre, capables de se rompre sous l'effet de la chaleur, et d'agir en tant qu'agent de réticulation. Cette réaction n'a néanmoins pas été étudiée ici.

Dans la deuxième stratégie, le greffage du polyisoprène sur le GO a été effectué en deux étapes. Dans une première étape, le GO a été fonctionnalisé par le 1-azido-undecanol, par une réaction d'estérification faisant intervenir les groupements acide carboxylique du GO. Un taux de greffage d'azide de 9 % massique a été obtenu et des suspensions des charges modifiées ont montré une augmentation de leur stabilité dans du toluène, en comparaison avec des suspensions de GO. Dans une deuxième étape, le GO-azide a réagi avec le polyisoprène (IR) par une réaction de cycloaddition. Un faible taux de greffage de polyisoprène (2.5 % massique) a été déterminé par ATG. De plus, une réduction simultanée du GO-azide-IR a été observée (procédé solvothermique). Des suspensions de GO-azide-IR ont montré une amélioration de la stabilité dans du toluène à une concentration de 1 mg/mL, grâce à la fonctionnalisation (par rapport à des suspensions de GO).

Dans la troisième stratégie, la polymérisation in situ de l'isoprène sur le GO a été réalisée, en deux étapes, pour améliorer sa dispersion dans une matrice polyisoprène. Dans un premier temps, un alkoxy silane a été greffé à la surface du GO par une réaction d'hydrolyse-condensation. Puis, l'isoprène a été polymérisé in situ sur le GO-alkoxy silane, par polymérisation radicalaire en émulsion. Cependant, la réaction de polymérisation n'a pas pu se dérouler en présence de 10 % massique de GO-alkoxy silane (radicaux piégés par le GO). Dans un deuxième temps, la polymérisation cationique en émulsion de

l'isoprène a été réalisée, en utilisant des catalyseurs combinés avec des acides de Lewis et une charge GO-alkoxysilane contenant 50 % massique de polyisoprène a été obtenue.

La quatrième stratégie a consisté en la modification du graphite par un procédé thermique. Le graphite a d'abord été oxydé en utilisant la méthode de Hummers, et dans un deuxième temps, le GO a été soumis à des températures élevées (700 °C environ) avec une rampe de température très rapide, pendant 30 s. Dans ces conditions, les groupements fonctionnels sur le GO se dégradent et produisent un dégagement gazeux qui repousse les feuillets et crée une structure expansée, poreuse et froissée.

Des composites à matrice polyisoprène ont été élaborés à l'aide des différentes formes de graphite modifié obtenues. L'originalité de cette étude est d'avoir ciblé des composites à vocation industrielle. Leur composition inclut donc un taux de charge élevé (50 parts pour cent d'élastomère ou pce) comprenant du noir de carbone majoritairement. Les charges modifiées ont été incorporées en substitution d'une partie du noir de carbone, conduisant à un taux de (50-x) pce de noir de carbone et x pce de charges graphitiques.

Les propriétés de ces composites ont ensuite été étudiées. Lorsque 2 pce de noir de carbone ont été remplacés par 2 pce de graphite modifié, les propriétés mécaniques ont été peu impactées. Cependant, quand 15 pce de graphite modifié ont été ajoutés (en substitution à 15 pce de noir de carbone), des effets notables ont été observés. Alors que le GO a principalement un impact négatif sur les propriétés mécaniques, le GO fonctionnalisé a montré une amélioration des propriétés des composites polyisoprène. Ainsi, le GO-ODA a présenté un renforcement (augmentation des contraintes aux faibles allongements) avec cependant une conservation des propriétés à rupture. Des mesures de perméabilité à l'air ont été effectuées sur les composites : le GO-ODA et le graphite expansé thermiquement, ajoutés en remplacement de 15 pce de noir de carbone, ont induit les plus fortes diminutions, atteignant des diminutions 62 % et 70 %, respectivement, en comparaison avec la perméabilité du composite à matrice polyisoprène contenant uniquement du noir de carbone.

Par ailleurs la modification du graphite a conduit à des conductivités thermiques des composites du même ordre de grandeur que ceux chargés uniquement en noir de carbone, et plus faible que celle des échantillons contenant du graphite commercial.

La cinquième stratégie étudiée a consisté en l'ajout de liquides ioniques en tant qu'agents dispersants, pour améliorer la dispersion de graphite commercial dans des matrices de caoutchouc naturel (NR) et de copolymère acrylonitrile-butadiène (NBR). Une amélioration des propriétés mécaniques a été observée pour le NR : des contraintes élevées aux faibles allongements, induites par la présence de graphite, ont été obtenues en même temps que les propriétés à rupture étaient préservées grâce à la présence du liquide ionique. L'ajout de liquide ionique dans des composites NR – graphite a donc bien présenté un effet dispersant sur le graphite et le noir de carbone.

Dans le cas de l'utilisation d'une matrice NBR, une diminution des contraintes a principalement été observée, suggérant une diminution de la densité de réticulation. De plus, il a été montré que le taux de liquides ioniques dans le composite n'avait pas d'effet significatif sur les propriétés en traction du NR et du NBR. Les liquides ioniques ont montré des interactions avec le système de vulcanisation quelle que soit la matrice élastomère utilisée. Ainsi, ces élastomères présentent une réticulation plus rapide en présence de 1 % massique de liquide ionique. De plus, certains liquides ioniques tels que le chlorure de 1-allyl-3-méthylimidazolium (AMIC) peuvent inhiber la réaction de réticulation lorsqu'ils sont

incorporés à un taux de 10 % massique. Il pourrait donc être intéressant d'étudier la réaction de liquides ioniques avec le système de vulcanisation du NR et du NBR.

Dans cette étude, il a donc été montré que la modification chimique du graphite pouvait conduire à l'élaboration de composites présentant des propriétés mécaniques améliorées ainsi que des propriétés barrière à l'air intéressantes. Ainsi le GO-ODA et le GOX semblent être les deux charges préparées dans cette étude ayant le plus de potentiel pour une transposition industrielle. Cependant, l'utilisation de liquides ioniques comme agents dispersants n'a pas apporté les résultats escomptés sur les propriétés de composites à matrice caoutchouc NR et NBR.

En perspective, l'influence du procédé d'élaboration des matériaux sur les propriétés des composites pourrait être étudiée. Compte-tenu des difficultés bien connues de la dispersion de nanocharges dans les matrices polymères, il est intéressant de rechercher des alternatives. L'une d'entre elles, viable sur le plan de la transposition industrielle, est l'élaboration du mélange en milieu latex. Les élastomères utilisés dans cette étude (IR, NR et NBR), existent en phase latex et il pourrait être intéressant de regarder l'effet de l'ajout de charges graphitiques, en suspension aqueuse, directement dans le latex. La formation de morphologies complexes pourrait entraîner entre autres une forte augmentation des propriétés barrière des composites.

Main introduction

Elastomers are common materials which have a wide range of applications, including everyday life products, such as shoe soles and tires, and industrial products, such as rubber seals and gaskets in automotive industry for instance. These materials have been known for a long time. Hence, natural rubber (NR) has been known in South America for centuries but it is only in the 18th century that the French explorer Charles de la Condamine brought samples back to France. A century later, Thomas Hancock invented a “masticator”, a mixing machine able to heat and press rubber in order to shape it. However, rubber goods had a very low weather resistance, became brittle in the cold and sticky if exposed to the sun. Eventually, in 1842, Charles Goodyear discovered the vulcanization process and rubber industry really began to expand. In the end of the XIXth century, Henry Wickham sent hevea seeds to Ceylan and Singapore that are at the origin of today’s South East Asia huge rubber plantations. With this larger supply available, rubber industry continued to develop fast. With over 12 million tons produced in 2015, natural rubber is the elastomer most used worldwide.

Besides, during World War I and World War II, synthetic rubbers were developed to overcome the natural rubber latex shortage. Nowadays, a very wide variety of synthetic elastomers are produced and their structure and properties are carefully controlled. In 2015, around 17 million tons of rubber were synthesized, which accounts for around 58 % of the total rubber production. Despite a very wide use due to their exceptional elasticity, these materials display low stiffness and are permeable to most gases, which may limit their potential applications. To overcome these difficulties, various fillers are commonly added in elastomeric matrices. Among these fillers, carbon black is the most commonly used to enhance mechanical properties of elastomers. It has been used for centuries as a pigment for paper, but it is only in the first half of the XXth century that it was discovered to reinforce rubber. Nowadays, over 12 million tons of carbon black are produced worldwide, with more than 80 % of this production being used in rubber goods, mainly in tires.

Recently, a new class of fillers, nanofillers, has been described to enhance several properties of elastomer composites, at a lower loading than carbon black. Among these nanofillers, graphene, a 2D material consisting in a single atomic layer of carbon atoms, and mostly found in its stacked form (graphite), has triggered a lot of research work in recent years. Pristine graphene displays outstanding electrical, thermal, mechanical and barrier properties. Hence, it is reported to have an electronic mobility of 200,000 cm²/(V.s), which is around 45,000 times higher than copper. Such properties suggest that graphene could be of great interest as a filler in polymer materials. The preparation of pristine graphene is anyhow costly and difficult to scale-up, and graphene derivatives have often been prepared instead. They include oxidized forms of graphene (graphene oxide), small stacks of graphene layers (graphite nanoplatelets) and other graphene-based structures. Due to the presence of several defects in these graphene-based materials, their properties do not reach those of pristine graphene. However, these materials can be prepared in larger quantities than pristine graphene and may thus be added as fillers in polymer materials.

Several studies on the effect of graphite-derivatives on the properties of thermoplastics have been performed and they reported significant improvements of the corresponding composites in terms of mechanical properties, barrier properties as well as electrical and thermal conductivities. However, little work was carried out on elastomeric materials, due to a more difficult dispersion of the filler in

the elastomer. Graphite nanoplatelets are very inert chemically and thus low interactions with rubber matrices are often reported. Besides, due to their small lateral dimension, these nanoplatelets tend to agglomerate to a large extent, thus creating large-size agglomerates and thus impairing the properties of the corresponding material.

One of the solutions, already studied with thermoplastic matrices, is to modify the surface of graphene-based fillers, through covalent grafting of polymer chains for example. This enhances filler-matrix interactions, and decreases filler-filler interactions. Due to its very stable conjugated aromatic structure and the lack of functional groups, the surface modification of graphene derivatives is very challenging, especially to improve its compatibility with elastomers such as polyisoprene. In this work, several modification paths have been attempted, involving chemical covalent grafting strategies, use of dispersing agents as well as thermal treatment. The influence of these treatments on the mechanical and barrier properties of the corresponding elastomer-based composites, has been investigated.

This report is divided into a literature review and four experimental chapters. The literature review focuses on graphene derivatives and their functionalization, elastomer materials and then the properties of elastomer composites based on graphene and graphene-derived fillers. The second chapter deals with the preparation of graphite oxide (GO) and the covalent grafting of several compatibilizing agents onto the surface of GO. The third chapter describes the in situ polymerization of isoprene in presence of GO derivatives as a means to enhance GO – polyisoprene compatibility. Then, the fourth chapter discusses the properties of polyisoprene-based composites containing the modified graphite-derivates. Finally, the fifth chapter focuses on the use of a non-covalent modification strategy, using ionic liquids, to compatibilize graphite and common elastomers (natural rubber and acrylonitrile butadiene copolymer).

Chapter 1: Literature study

Table of contents of Chapter 1

Introduction.....	29
1. Graphene-based materials.....	30
1.1. Production of single graphene sheets.....	30
1.1.1. Bottom-up preparation methods.....	31
1.1.2. Top-down preparation methods.....	31
1.2. Production of graphene-based materials from graphite derivatives.....	32
1.2.1. Natural and synthetic graphite.....	32
1.2.2. Expanded graphite.....	32
1.2.3. Graphite nanoplatelets.....	33
1.2.4. Functionalization of graphite derivatives.....	34
1.3. Production of graphene-based materials from graphite oxide.....	43
1.3.1. Graphite/graphene oxide preparation.....	43
1.3.2. Graphene oxide structure.....	44
1.3.3. Graphite oxide properties.....	45
1.3.4. Functionalization of graphite oxide.....	46
1.3.5. Reduction of graphite oxide derivatives.....	55
1.4. Conclusion.....	59
2. Elastomeric materials: composition and processing principles.....	61
2.1. Polyisoprene.....	61
2.1.1. Natural polyisoprene.....	61
2.1.2. Synthetic polyisoprene.....	62
2.2. Acrylonitrile-butadiene copolymers.....	64
2.3. Elaboration of an elastomeric material.....	64
2.3.1. Crosslinking.....	64
2.3.2. Fillers.....	71
2.3.3. Rubber mixing techniques.....	76
2.4. Conclusion.....	78
3. Properties of elastomer composites containing graphite / graphene.....	79

3.1.	Barrier properties	79
3.1.1.	Permeability	79
3.1.2.	Permeability mechanisms and models in nanocomposites	80
3.1.3.	Influence of filler size, shape and aspect ratio	82
3.1.4.	Influence of filler orientation	84
3.1.5.	Influence of processing and functionalization	84
3.2.	Mechanical properties.....	88
3.2.1.	Tensile properties.....	88
3.2.2.	Viscoelastic properties	93
3.3.	Thermal properties.....	96
3.3.1.	Thermal stability.....	96
3.3.2.	Thermal conductivity.....	97
3.4.	Electrical properties	99
3.4.1.	Percolation	100
3.4.2.	Influence of processing.....	100
3.4.3.	Dielectric properties	103
3.5.	Conclusion	103
	Conclusion of the literature study.....	104

Introduction

Much research interest has been focused on graphene since the attribution of a Nobel Prize in Physics to Andre Geim and Konstantin Novoselov from Manchester University (UK) in 2010. The expectations about the exceptional theoretical properties of this material have led many researchers to work upon isolation of single graphene sheet. Nowadays industrial production of graphene is developing with many start-up companies appearing on the market. Yet, many efforts are still to be made for large quantities of defect-free graphene sheets to be produced at reasonable costs. Applications of this material are wide and include electronics, photovoltaics and energy storage as well as high-performance composites. For the latter, polymers have shown to be of great interest to produce easily processable materials with enhanced thermal or mechanical properties for instance. Graphene could be used as an additional filler or as a replacement of traditional reinforcing fillers such as carbon black. Besides, graphene can potentially enhance properties such as thermal and electrical conductivities even at a very low loading (< 1 wt%). Regardless of the application it is necessary to ensure appropriate dispersion of the graphitic filler in a polymer matrix.

Great potential in the use of graphene as a filler comes from its “nano” size. Its small dimension is of great interest since large surface areas are available to interact with the matrix. However, due to strong interactions between the graphene nanosheets, they tend to aggregate. To avoid such phenomenon, several strategies such as the use of a surfactant to decrease surface energy or the grafting of several molecules on its surface is often necessary. Many functionalization strategies have been developed over the past years. They include non-covalent and covalent attachment. To perform such modifications, the use of an oxidized form of graphene is often required. Hence, graphene oxide, a graphene layer bearing oxygen functional groups on its surface, is widely used as a starting material for chemical functionalization. In addition, through several reduction treatments, graphene oxide can be converted back to a “graphene-like material”.

This oxidation/reduction method is of considerable interest for the industry as it might open the way for large production of “graphene-like materials” at low costs. Hence, while defect-free graphene layers can be prepared through expensive CVD process, oxidation/reduction method is mostly a chemical process using low-cost graphite as a starting material. However, these fillers, often called “graphite nanoplatelets”, show inferior properties in terms of several properties such as electrical conductivity.

These nanoplatelets anyhow enable the development of polymer nanocomposites. Even if they show lower properties than defect-free graphene, they however retain the ability to enhance mechanical properties, electrical and thermal conductivities as well as barrier properties of polymer composites. Among common polymers, elastomers are widely-used materials that exhibit exceptional elasticity and damping properties. They are often reinforced with low cost carbon black to enhance mechanical properties such as tensile strength. However, it is usually necessary to use high loadings (> 25 wt%) leading thus to important reduction in strain at break. The use of graphene nanofillers could enable an increase in tensile strength while preserving strain at break of the elastomers. Besides, electrical and thermal conductivities could be induced, still a low loading. Eventually, due to its platelet shape, graphene has a great potential in increasing barrier properties of elastomers.

This section is a literature review dealing with graphene-elastomer composites. It highlights key parameters to tune rubber properties through the incorporation of graphene or its derivatives.

1. Graphene-based materials

Graphite is a well-known material present in everyday life and it displays several interesting properties such as electrical conductivity. Recently, a lot of research has been done on separating graphite layers to obtain isolated graphene sheets. This nanomaterial has theoretical outstanding properties such as exceptionally high Young's modulus, electrical and thermal conductivities. However, it is still hard to obtain defect-free single layer graphene at a competitive price for industrial use. Thereby, a number of intermediate structures such as graphite nanoplatelets have been synthesized. This section details common graphite-related materials found in the literature.

1.1. Production of single graphene sheets

Graphene is defined as a monolayer of sp^2 carbon atoms assembled in a honeycomb structure. A monolayer is made of carbon atoms with 0.142 nm interatomic distance and organized in a bidimensional crystal (Figure 1).

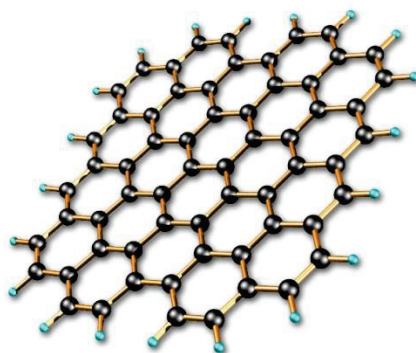
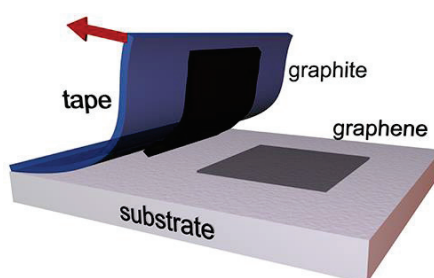


Figure 1: Single graphene sheet.

Graphene first appearance in literature can be traced back to 1970 but its isolation as a single sheet was not possible until 2004 when Andre Geim's team from Manchester University (UK) developed a micromechanical exfoliation method based on the use of scotch tape (Scheme 1) [1].



Scheme 1: Representation of micromechanical exfoliation of graphite.

Andre Geim and Konstantin Novoselov received the Nobel Prize in Physics in 2010 for their work on graphene. Graphene is of great scientific interest due to its outstanding properties. Indeed, a monolayer has a Young's modulus of 1 TPa and a yield strength of 130 GPa which makes it the toughest material ever measured [2]. Besides, graphene has a thermal conductivity of 5000 W/m.K, about twelve times higher than copper. Graphene electrical conductivity properties are also outstanding with 128 S/m² and charge mobility around 200 S.m²/C, hence 45000 times higher than copper.

In addition, due to its 2D dimension, graphene has a very high theoretical specific surface area (2630 m²/g) as well as a very low permeability to most gases including helium. Thus, even if helium has a small kinetic diameter of 2.6 Å, graphene has an even lower pore diameter as well as a high penetration energy barrier of 18.8 eV (compared to 18.6 eV kinetic energy for a helium atom) [3]. In addition, graphene is a flexible, tough material exhibiting good optical transparency properties [4].

Two main procedures are available to obtain a single graphene sheet: “bottom-up” ways in which graphene is grown from carbon atoms and “top-down” routes where graphene is obtained through graphite exfoliation.

1.1.1. Bottom-up preparation methods

1.1.1.1. Epitaxial growth

Silicon carbide is heated under vacuum at 1300 °C so that silicon atoms from outer layers evaporate. After a predetermined time, carbon atoms rearrange themselves into thin graphene layers. However, this method is very costly and enables the production of small quantities of high-quality graphene.

1.1.1.2. Chemical Vapor Deposition (CVD)

The first CVD experiment was performed by Hagstrom in 1965 [5]. In this method, graphene is produced by catalytic decomposition of a carbonaceous precursor (methane is often used but any other carbon source can work) at high temperature onto a metallic substrate that acts as a catalyst. Copper and nickel are common metal substrates. For the former, carbon atoms from the decomposition of carbonaceous gases deposit onto its surface to produce a graphene layer. For the latter, carbon atoms penetrate into the substrate and, when temperature goes down, their solubility decreases and carbon atoms move back to the surface. This technique permits to produce high-quality graphene polycrystal at a small scale.

1.1.2. Top-down preparation methods

1.1.2.1. Micromechanical exfoliation

In 2004, researchers from Manchester University (UK) developed an exfoliation method of graphite based on adhesive tape [1], as discussed previously (Scheme 1).

Layers are separated by dichotomy until small stacks or even single layers are isolated. The obtained nanosheets are then transferred onto a silicon wafer. However, similarly to the CVD method, this technique cannot be used for large-scale production of graphene.

1.1.2.2. Liquid-phase exfoliation

Graphite exfoliation can also be performed by ultrasonication in organic solvents such as N-methylpyrrolidone, dimethylformamide or water (often in presence of a surfactant) [6–11]. This method enables production of small graphite flakes but seldom leads to the obtention of single layers. However, this way is suitable for large-scale production of graphite nanoplatelets. A similar method has been developed by Coleman et al [12] by shearing in a blender to exfoliate graphite.

Other methods such as the opening of carbon nanotubes and electric-arc discharge with a graphite electrode can also lead to a graphene-like material [2, 13, 14].

1.2. Production of graphene-based materials from graphite derivatives

1.2.1. Natural and synthetic graphite

Graphite is an allotropic form of carbon. It is a non-metallic material that was named after the Greek word *graphein* (to write) by the German mineralogist AG Werner. Graphite is composed of graphene layers, stacked together by weak van der Waals forces (Figure 2).

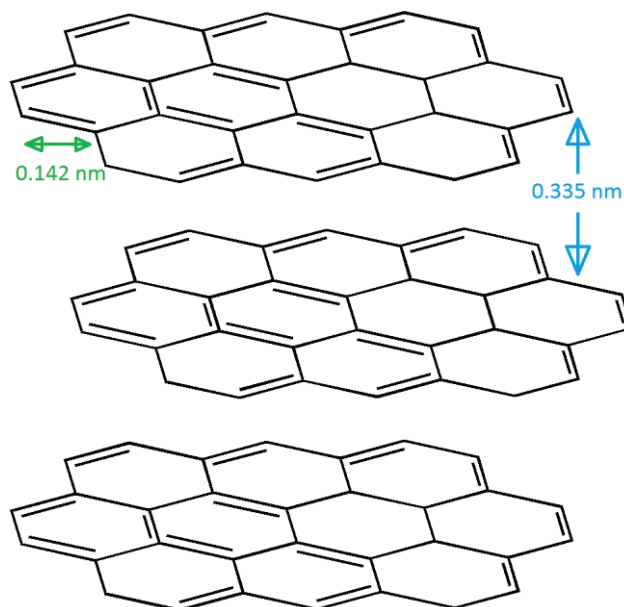


Figure 2: Graphite structure.

Graphite has a hexagonal crystalline structure with an interatomic distance of 0.142 nm in plane and an interlayer spacing of 0.335 nm. As a result, it is a highly anisotropic material and it possesses high in-plane electrical and thermal conductivities. It is also chemically inert and can thus be used for a wide range of applications: pencils, lubricants, refractory materials, batteries...

Around 80 % of worldwide natural graphite is extracted in China. Graphite-based products are classified according to their carbon content, ashes content and granulometry. Three main types of graphite are found on the market: vein graphite that is highly crystalline, graphite flakes that usually have a lateral dimension greater than 100 μm and “amorphous” graphite that is micro-crystalline and is composed of small flakes (less than 1 μm). Another class of graphite is also found on the market: synthetic graphite, which is produced by pyrolysis at 3000 $^{\circ}\text{C}$ of carbonated raw materials such as coke, oil or pitch. Synthetic graphite presents a higher porosity than natural graphite and is mostly used for Lithium-ion batteries production.

Graphite prices are strongly dependent on China’s production and exportation policy. Prices are expected to go up since there is now a need to dig quite deep to reach most graphite deposits, leading to harder extraction and so to higher costs. Besides, China’s slower economic development and greater concern about environmental regulations are expected to increase graphite prices in the upcoming years.

1.2.2. Expanded graphite

Due to weak van der Waals forces between its constitutive planes, graphite is relatively easy to intercalate.

Expanded graphite is a material produced by rapid heating of acid-intercalated graphite (also called graphite intercalation compound, GIC). These GIC are usually intercalated by sulfuric acid which infiltrates between graphitic layers and then pushes those layers apart when vaporizing under rapid heating ($> 2000\text{ }^{\circ}\text{C}/\text{min}$) at high temperature ($900\text{--}1000\text{ }^{\circ}\text{C}$) [15, 16]. The thermal process damages its structure and creates wrinkles on the sheets surface as shown in Figure 3. Therefore, the produced expanded graphite contains pores (spacing between wrinkled layers) with sizes ranging from a few nanometers to a few micrometers [17, 18].



Figure 3: SEM image of exfoliated graphite made of natural graphite by using formyl acid and microwave: Worm-like graphite under ESEM (Quanta 200F) [18].

Expanded graphite displays a worm-like morphology and is often described as a loose structure composed of collapsed and deformed parallel sheets, which results in many pores covering a wide range of sizes (Figure 3). The creation of pores leads to an increase in volume from 50 to 200 times and particle sizes ranging from 1 to $50\text{ }\mu\text{m}$, with layer thicknesses of a few hundreds nanometers [15, 16, 19–22].

1.2.3. Graphite nanoplatelets

Many industrial products are sold under the denomination “graphene nanoplatelets”. They usually refer to “stacks of a small number of graphene layers with a microscale lateral dimension”. However, this very imprecise term is not recommended by Carbon editors [23] for use in scientific community because the term “graphene” already refers to the thickness of the material and the prefix “nano” should then refer to the lateral dimension of the platelets [23]. They put forward well-defined terms such as “multilayer graphene” (a countable stack of between 2 and 10 graphene layers), “few-layer graphene” (a countable stack of 2-5 graphene layers) and “graphite nanoplates” (a stack of graphene layers with a thickness or a lateral dimension not greater than 100 nm). They also suggest the name “carbon thin films” for small stacks of discontinuous or fragmented graphene layers with a small lateral dimension.

Graphite nanoplatelets (GNPs) are a good alternative to expensive graphene sheets. They are widely available in the industry and offer the opportunity to be used as fillers in many materials. However, due to the imprecision of the term “GNPs” regarding the thickness and the lateral dimension of the product, it can be hard to compare results obtained with platelets purchased from different suppliers. Besides, the term does not refer to a special preparation method and GNPs can be obtained through an oxidation / reduction process or from acid-intercalated graphite (followed by a thermal treatment). Direct exfoliation of graphite in a solvent such as N-methylpyrrolidone (NMP), dimethylformamide (DMF) or water (with the help of a surfactant) can also lead to graphite nanoplatelets products. Ball-milling in the dry state or with the use of chemicals such as melamine is also described in the literature

as a method to produce GNPs [24]. Hence, Leon et al [24] showed the partial exfoliation of graphite into few-layer graphene using several triazine derivatives in a ball-mill with subsequent removal of the exfoliating agent after the milling process to leave a clean graphite surface [25].

Commercial so-called “graphene nanoplatelets” can then be made of stacks of layers up to 100 nm thick with a lateral dimension ranging from nano- to micrometers. The surface can be flat or wrinkled, containing or not functional groups, or with molecules covalently or non-covalently attached onto their surface and edges.

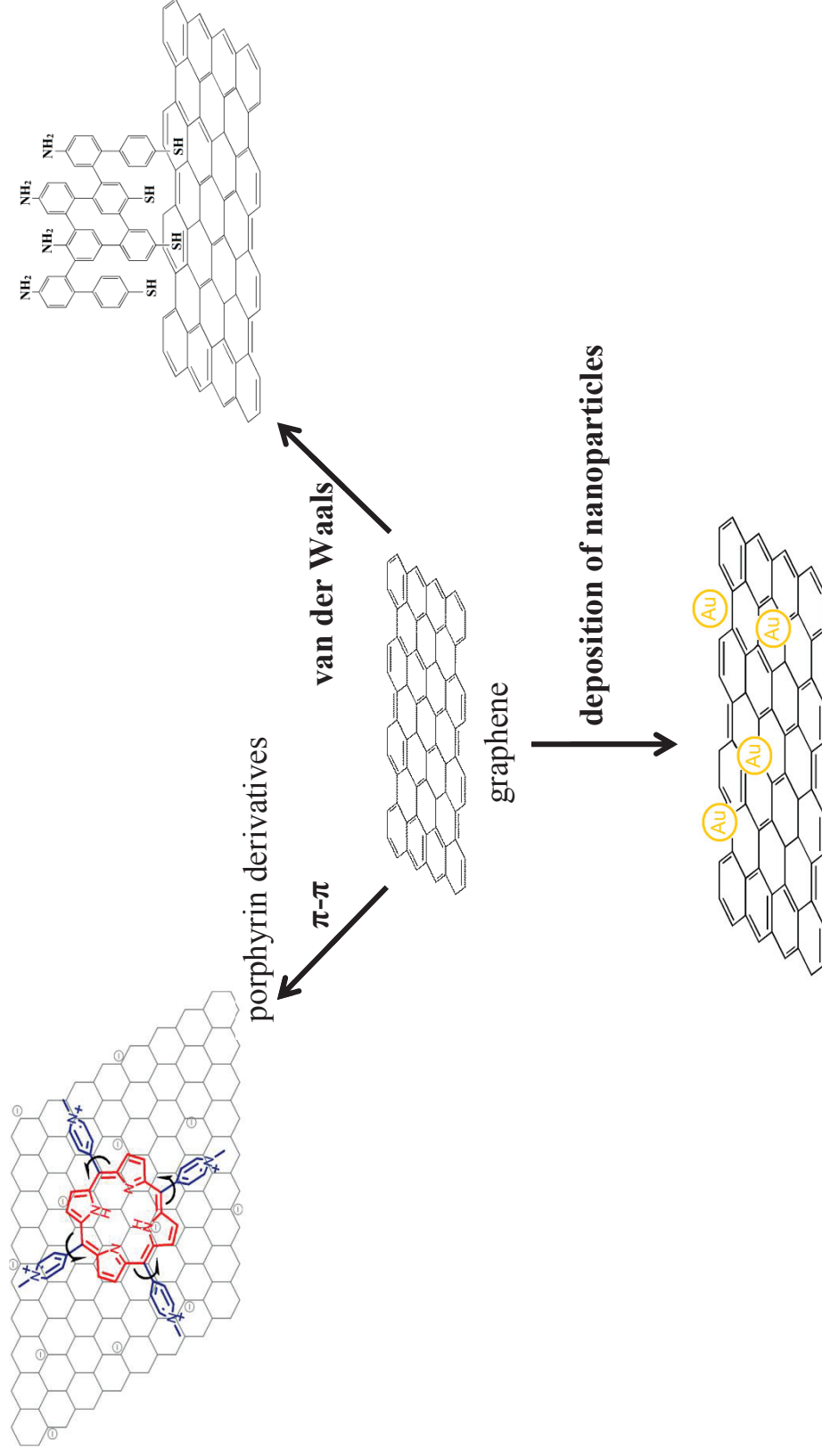
Many different graphitic structures exist and are available in the market. However, real 2D-monolayer-graphene production is still in development stage. Despite little use of graphene, graphene derivatives such as graphite nanoplatelets give rise to great expectations for use as fillers in polymer composites.

1.2.4. Functionalization of graphite derivatives

Graphene sheets undergo π - π interactions with each other, which leads to stacking of the nanosheets. To overcome the spontaneous formation of multilayer structures graphene sheets can be functionalized to reduce π - π interactions between layers. Most carbon structure modifications were initiated with CNTs and fullerenes and have been more or less successfully adapted to graphene. The main purpose is to enhance dispersibility of the nanosheets in common organic solvents, which is one of the key features for elaboration of functional nanocomposites. Several methods are available to chemically modify graphene-based sheets. They can be divided into covalent and non-covalent methods [26, 27].

1.2.4.1. Non-covalent functionalization

Non-covalent functionalization is an attractive way to modify graphene since the modifications are usually easy to perform and offer the possibility to adsorb functional molecules onto graphene surface without disturbing its conjugated structure and thus its electrical properties [28–30]. The corresponding interactions are usually weaker than covalent interactions but they can lead to the formation of rather strong bonding anyhow [31, 32]. Non-covalent attachment can happen either through van der Waals forces, deposition of nanoparticles or π - π interactions [28]. The main goal is to overcome π - π interactions between layers to prevent restacking through the adsorption of small functional molecules or polymers on graphene surface. Stable organic or aqueous suspensions can be obtained after non-covalent functionalization of graphene. Scheme 2 summarizes the main modification paths reported in the literature.



Scheme 2: Non-covalent functionalization paths for pristine graphene.

Scheme 2 shows the main paths for graphene non-covalent modification. π - π and van der Waals interactions as well as adsorption of nanoparticles are common methods to tune graphene properties without disturbing its aromatic structure. Due to the conjugated structure of graphene, π - π interactions are often reported in the literature as an efficient means to functionalize graphene.

1.2.4.1.1. π - π interactions

The main mechanism for non-covalent functionalization of graphene is π - π interactions with a molecule containing aromatic rings. Pyrene derivatives are among the most commonly used graphene modifiers (Figure 4) [28, 31, 33].

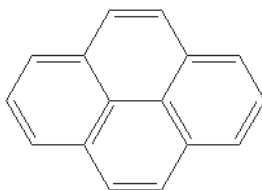


Figure 4: Pyrene structure.

π - π interactions are often reported in the literature to be an efficient means to limit graphite aggregation. Hence, Maity et al [34] used polythiophene-*graft*-poly(methyl methacrylate) (PT-g-PMMA) to non-covalently modify the graphene lattice. The modification was performed through sonication and magnetic stirring in DMF, followed by centrifugation and then washing with DMF. A graphene content of 14.2 wt% was obtained in the PT-g-PMMA-graphene composite. The interaction between PT and graphene is believed to be due to π - π interactions. The authors [34] incorporated the as-modified filler in a PVDF matrix and observed an electric percolation threshold at 0.24 vol% content of PT-g-PMMA-modified graphene as well as enhanced mechanical properties of the composites. They believe they obtained a good dispersion because the PT-g-PMMA favorably interacts with both the filler and the matrix. Polythiophene rings are adsorbed onto graphene through π - π interactions while $>C=O$ groups of PMMA undergo dipolar interactions with CF_2 groups of the PVDF matrix.

1.2.4.1.2. Van der Waals interactions

Van der Waals forces are often involved in non-covalent modification of graphene [27, 35, 36]. Hence, Woszczyna et al [35] functionalized single layer graphene through stacking into a vertical van der Waals heterostructure of a free standing amino-terminated carbon nanomembrane (cross-linked with biphenylthiols), for electrically-conductive nanodevices (Scheme 2). Upon functionalization, the graphitic structure was well preserved as evidenced by Raman analysis and the intrinsic electrical properties of this material were well retained in the modified structures.

1.2.4.1.3. Deposition of nanoparticles

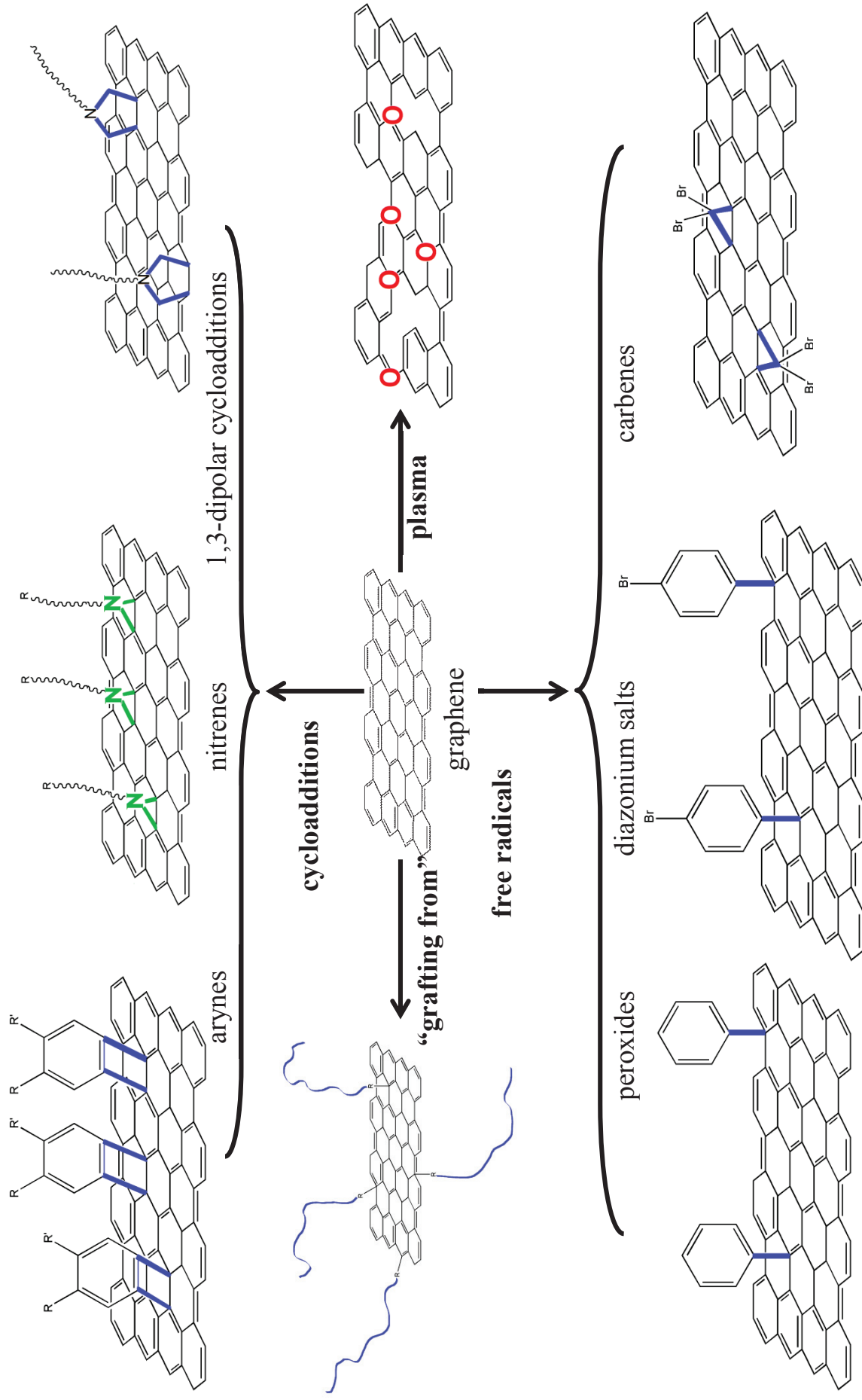
Non-covalent modification of graphene can also be performed through deposition of nanoparticles such as gold, silver or nickel. Hence, Luo et al [37] prepared graphene decorated with gold nanoparticles (Scheme 2). They deposited gold atoms onto few-layer graphene and, upon annealing, gold atoms were condensed into nanoparticles (3-30 nm in diameter).

In conclusion, non-covalent functionalization of graphene is a useful and efficient way to modify the surface while preserving the conjugated structure. Potential applications of these modified fillers are numerous, especially in the field of nanoelectronics. This method could help and disperse better the filler in a matrix with creation of a strong interface while preserving intrinsic electrical properties of graphene. However, when stronger bonds between graphene and other molecules are required,

covalent modification of the nanosheets is necessary. This modification creates strong attachment of the modifier and thus usually shows greater long-term stability than physically-sorbed species on graphene. However, contrary to the non-covalent functionalization, such modification leads to the disruption of the aromatic structure and affects electrical properties, thus requiring a final reduction step to restore the disrupted sp^2 lattice.

1.2.4.2. Covalent functionalization

Pristine graphene is very inert chemically. It does not have functional groups on its surface and its aromatic rings are very stable and thus very hard to involve in covalent linkages. However, a few chemical reactions can be used for the chemical modification of graphene sheets as shown in Scheme 3.



Scheme 3: Covalent modification paths for pristine graphene [28, 31, 38–42].

Scheme 3 presents four main functionalization paths of pristine graphene. Cycloaddition reactions are commonly reported in the literature. The use of free radicals is also a convenient way to overcome the absence of functional groups onto graphene surface. Besides, plasma modification enables selective replacement of atoms to incorporate heteroatoms onto graphene surface. Finally, polymers can be grown directly from graphene surface using the « grafting from » strategy.

1.2.4.2.1. Cycloadditions

1.2.4.2.1.1. Cycloaddition of aryne compounds

Arynes are cyclic structures derived from aromatic rings through removal of two ortho-substituents. They contain a triple bond [43] as shown in Figure 5.

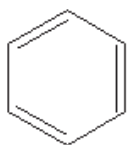


Figure 5: Benzyne structure.

These compounds can be used to covalently modify pristine graphene. Hence, graphene produced through arc-discharge was covalently modified using aryne chemistry by Zhong et al [38]. They reacted 2-(trimethylsilyl)-phenyl triate and caesium fluoride with graphene sheets in acetonitrile. The extent of functionalization was measured to be of one aryne compound per 17 carbon atoms from TGA and 1 per 16 by XPS. They obtained stable suspensions in DMF at concentrations up to 0.40 mg/mL [38].

1.2.4.2.1.2. Nitrenes

Azides are nitrogen-containing compounds that can decompose upon light or heat to form highly reactive nitrene species [43]. Azide chemistry has been widely studied to functionalize fullerenes and carbon nanotubes and has then been adapted to graphene nanosheets [29, 42, 44–50]. These compounds can be used to covalently bond to graphene since they can react through cycloaddition reactions onto carbon-carbon double bonds of graphene. Hence, Vadukumpully et al [42] functionalized graphene with various alkylazides. First cetyltrimethylammonium bromide (CTAB) was wrapped around graphene to enhance exfoliation through sonication, then hexylazide, dodecylazide, 11-azidoundecanol and 11-azidoundecanoic acid were reacted in a 1:10 ratio (graphene to modifier). The latter proved to be the best at enhancing graphene stability in common solvents such as toluene and acetone at up to 0.1 mg/mL.

In another study, Strom et al [50] functionalized micrographite sheets through nitrene cycloaddition of azido-phenylalanine in *o*-dichlorobenzene. The resulting product was shown by XPS to bear one phenylalanine molecule per 13 graphene carbon atoms [50]. Hence, azide chemistry is a useful tool to incorporate organic species onto pristine graphene without the need for functional groups on its surface.

1.2.4.2.1.3. 1,3-dipolar cycloadditions

Another direct functionalization route is the 1,3-dipolar cycloaddition reaction of azomethine ylides [51]. Hence, Quintana et al [52] modified graphene through in situ generated azomethine ylides produced from condensation of paraformaldehyde with a modified α - amino acid. They determined a grafting efficiency of 15 wt% by TGA corresponding to one functional group per 128 carbon atoms.

Similarly, Zhang et al [53] prepared porphyrin-grafted graphene through reacting modified tetraphenylporphyrin (TPP) and sarcosine with graphene. They reported that the obtained grafting was covalent and calculated a 18 % mass loss in TGA corresponding to one TPP group per 235 carbon atoms.

1.2.4.2.2. Free radicals

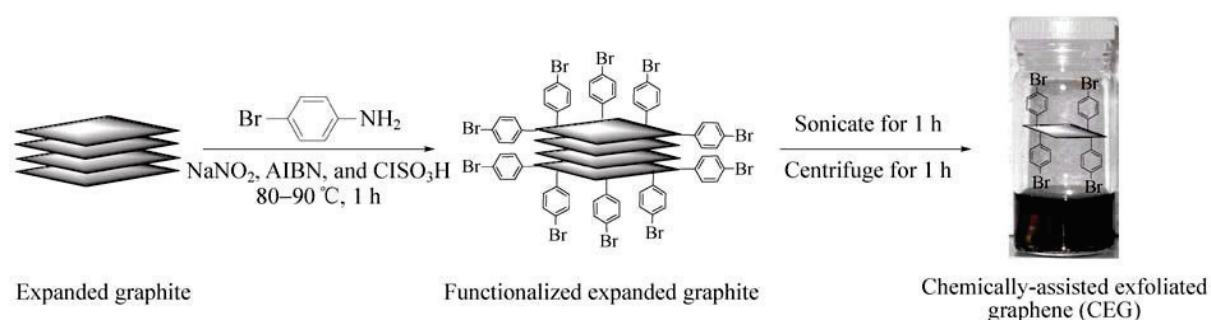
Free radicals are an efficient way to overcome the absence of functional groups onto graphene.

1.2.4.2.2.1. Peroxides

Benzoyl peroxide (BPO) can be used to covalently functionalize graphene. Hence, Liu et al [54] used a toluene/BPO solution and initiated the reaction photochemically. Raman spectroscopy indicated the attachment of phenyl groups through the appearance of a D band due to the creation of sp^3 carbons. They also observed a decrease in electrical conductivity due to the disruption of the aromatic structure as well as an increase in the level of hole doping [54].

1.2.4.2.2.2. Diazonium salts

Reaction of diazonium salts onto graphite nanosheets is often described in the literature [55, 56]. Sun et al [39] prepared soluble expanded graphite nanosheets through reacting bromoaniline onto the graphitic substrate. Hence, 4-bromoaniline in the presence of sodium nitrite and a catalytic amount of azobisisobutyronitrile (AIBN) was covalently linked to expanded graphite. Scheme 4 shows the functionalization procedure.



Scheme 4: Reaction path to attach a diazonium salt onto expanded graphite [39].

A Br concentration of about 0.6 % (XPS) was reported [39]. They also showed that the bulky diazonium groups were mainly located at the edges of the nanosheets.

Kongsfelt et al [57] also investigated properties of diazonium-modified graphene. They used epitaxial graphene to anchor nitrophenyl diazonium groups on its surface. They evidenced the grafting through XPS and scanning tunneling microscopy (STM) from which they observed irregular surface coverage.

1.2.4.2.2.3. Carbenes

Carbene chemistry is another useful tool to functionalize graphene without prior treatment. Sainsbury et al [40] prepared functionalized graphene through carbene attachment. Bromoform and a phase-transfer catalyst, trihexylamine, were added in an organic suspension of exfoliated graphene in benzene. Covalent grafting was evidenced through FTIR and XPS analysis. Besides, TGA allowed them to calculate that one carbene substituent per 37 carbon atoms (1 per nm^2) was grafted.

1.2.4.2.3. Plasma

Among other available methods, plasma modification can be done on graphene [58]. Hence, Sicinski et al [41] used graphite nanoplatelets treated with oxygen plasma for a time varying from 16 to 64 min.

They incorporated oxygen groups on graphene sheets surface and observed an increase in surface free energy from 23 to 30 mJ/m² [41].

1.2.4.2.4. Functionalization with polymers

Functionalization of graphene oxide can also be carried out with polymers. Several mechanisms can be used. Grafting of polymers onto graphene can be divided into two groups: “grafting to” and “grafting-from” techniques.

1.2.4.2.4.1. “Grafting to”

Using this procedure, grafting can be carried out in one or two steps. First the polymer can be functionalized to incorporate reactive functional groups on its backbone or on its chain-ends, if not already present. Then, addition onto graphene is performed through one of the previously presented mechanisms such as nitrene addition [33, 59–66].

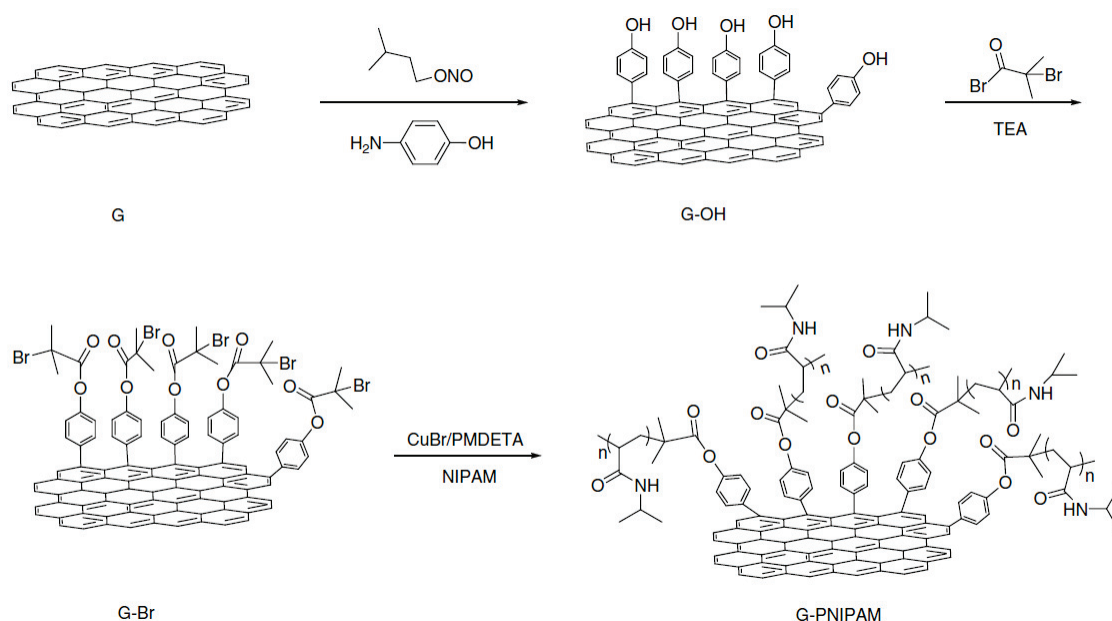
1.2.4.2.4.2. “Grafting from”

To covalently attach polymers onto graphene or graphene oxide surface another strategy is also available. In “grafting from” approach, initiators or monomers are grafted onto the graphitic substrate and then polymerization occurs in situ directly onto graphene sheets [33]. Two common mechanisms to polymerize monomers from graphene surface are atom transfer radical polymerization (ATRP) and reversible addition fragmentation chain transfer (RAFT).

1.2.4.2.4.2.1. Atom transfer radical polymerization (ATRP)

ATRP is a radical polymerization technique that permit to obtain. The obtained polymers usually have high molar masses and low polydispersity. The reaction is performed through a radical mechanism but controlled by a catalyst that keeps the number of radicals in the medium low and so limits side-reaction. The catalyst, a transition metal, and an initiator (alkyle halide) are necessary to carry out the polymerization [67–69].

This technique has been quite widely reported for polymer grafting onto graphene sheets. Hence, Ren et al [70] used ATRP mechanism to attach poly(N-isopropylacrylamide) (PNIPAM) onto graphene. The reaction path is presented in Scheme 5.



Scheme 5: NIPAM polymerization onto graphene [70].

The substrate was first functionalized with a diazonium salt followed by the attachment of bromoisobutyrate groups. Finally, NIPAM was in situ polymerized onto modified graphene. A grafted amount of up to 37.5 wt% was determined by TGA. The resulting product showed temperature-responsive solubility. Hence, while at a temperature lower than the lowest critical solution temperature (LCST) suspensions in water were stable, they quickly aggregated when the temperature was raised. This phenomenon was explained to be due to the formation of entropically favored intramolecular H-bonds at high temperature and enthalpically favored intermolecular H-bonds at low temperatures leading to aggregation – disaggregation of the PNIPAM-graphene in water. Other groups also reported interesting results in ATRP functionalization of graphene [71–75].

1.2.4.2.4.2.2. Reversible addition fragmentation chain transfer (RAFT)

Another common controlled polymerization technique is RAFT polymerization. In this process, a thiocarbonylthio compound chain transfer agent enables to reach a controlled molecular weight with a low polydispersity. Complex polymer structures such as comb-like and star polymers can be afforded [76].

To change graphene solubility in various solvents, Ye et al [77] functionalized graphene nanosheets with several polymers using RAFT process. They grafted a chain transfer agent onto graphene by reacting alkyne groups onto graphene before performing RAFT polymerization of either styrene, methylmethacrylate, 4-vinylpyridine and (dimethylamino)ethyl methacrylate [77]. The resulting polymers presented various solubilities in water, oil, acidic, alkaline solutions, polar and apolar solvents. They achieved a grafting efficiency of 2 PMMA chains per 10000 carbon atoms and they were able to disperse the modified platelets at up to 0.965 mg/mL in chloroform.

In situ polymerization is of great interest for polymer attachment onto graphene and is probably one of the most challenging modification paths. Many studies have focused on thermoplastic polymers, with polystyrene and poly(methylmethacrylate) being quite widely reported in the literature [78–85].

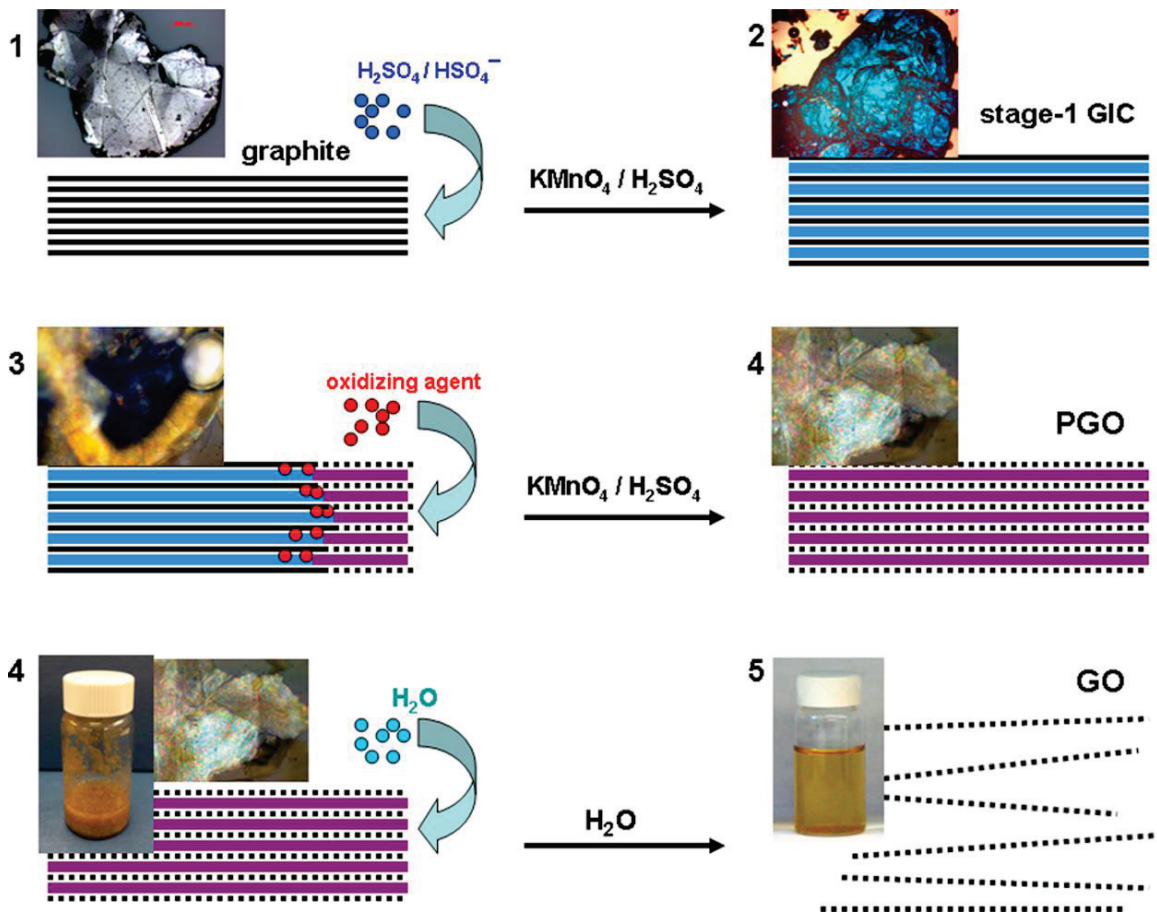
Graphene can thus be modified through a great number of methods. Non-covalent grafting usually provides a simple reaction path with no disruption of the aromatic structure while covalent modifications enable greater effects on graphene properties such as strong changes in its solubility. However, the absence of functional groups onto graphene surface limits available reaction paths that can be performed. In the next section, a method to incorporate oxygen functional groups onto graphene surface is reported.

1.3. Production of graphene-based materials from graphite oxide

Graphite oxide is a 3D material derived from graphite that contains covalent carbon-oxygen bonds. It is regarded as an intermediate material towards the production of graphene. In 1958, Hummers [86] reported a method, commonly used nowadays, to prepare graphite oxide using potassium permanganate as the oxidizing agent in a mixture of sulfuric acid and sodium nitrate.

1.3.1. Graphite/graphene oxide preparation

Moreover, Dimiev et al [87] studied the mechanism of graphene oxide formation from graphite, shown in Scheme 6.



Scheme 6: Formation of graphene oxide from bulk graphite. GIC = graphite intercalated compound, PGO = pristine graphite oxide [87].

They describe that, in a first step, a mixture of sulfuric acid and HSO_4^- ion intercalates in between graphitic layers. Then, potassium permanganate diffuses through the interlayer spacing and replaces the intercalant. Carbon atoms on the graphene layers are then attacked by the oxidant to create covalent carbon – oxygen bonds and the reduced form of potassium permanganate remains in between layers. Finally, upon addition of water, the intercalants are removed and oxidized graphene layers are exfoliated into individual graphene oxide sheets [87, 88].

1.3.2. Graphene oxide structure

Graphene oxide structure has been much investigated and several models have been proposed but the commonly accepted one comes from Lerf, Klinowski et al [89, 90]. Their model is represented in Figure 6.

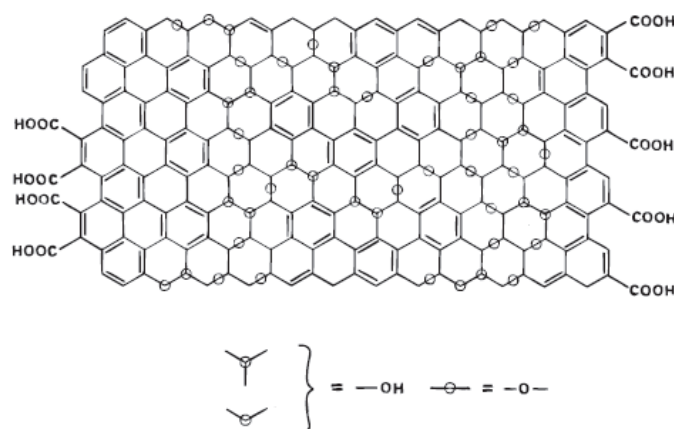


Figure 6: Graphite oxide structure according to the Lerf-Klinowski model [89].

They suggested that graphene oxide layers are composed of a lattice of sp^2 and sp^3 carbon atoms bearing hydroxyl and epoxide groups on its surface as well as carboxylic acid groups on its edges with a C:O ratio of around 2:1.

Some other models suggest the presence of other oxygen functional groups such as ketones on graphene oxide surface as discussed by Szabo et al [91]. Figure 7 shows several representations of these models.

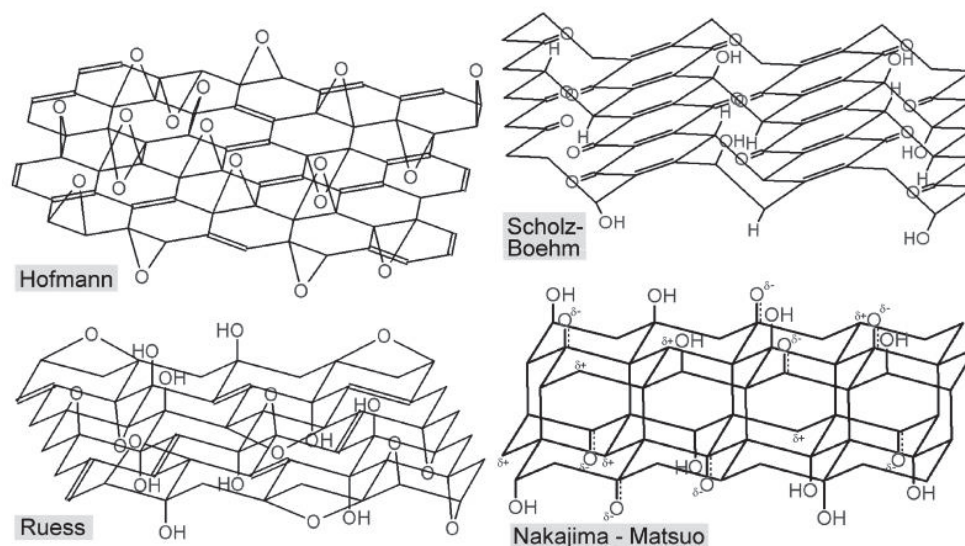


Figure 7: Some other models of graphite oxide structure [91].

Most of the models presented in Figure 7 do not acknowledge the presence of carboxylic acid groups on GO edges. However, they all attest of the presence of hydroxyl and/or epoxy groups on GO surface explaining its highly hydrophilic character [28, 92].

1.3.3. Graphite oxide properties

While graphite is usually exfoliated in hazardous organic solvents such as N-methylpyrrolidone (NMP), many research groups [93–104] have shown that graphite oxide can be exfoliated in water to single graphene oxide sheets and can be reduced back to a graphene-like compound. Besides, functional groups on its surface and edges enable covalent and non-covalent interactions with several chemical reactants [27, 28, 33]. However, the disruption of the graphene lattice impacts graphite oxide electrical conductivity. Hence, graphite oxide is a close-to-insulating material with a differential conductivity ranging from 1 to $5 \cdot 10^{-3}$ S/cm and a bias voltage of 10 V as reported by Gomez-Navarro et al [105]. Moreover, graphite oxide shows lower mechanical properties than graphene. GO paper is reported to have an elastic modulus of 32 GPa and a fracture strength of 120 MPa [106, 107].

In addition, graphite oxide has been proven not only to contain oxygen functional groups grafted on its surface but also to bear oxidative debris (OD) on its surface [108]. They are composed of small patches of strongly oxidized graphite that are deposited onto GO surface as represented in Figure 8.

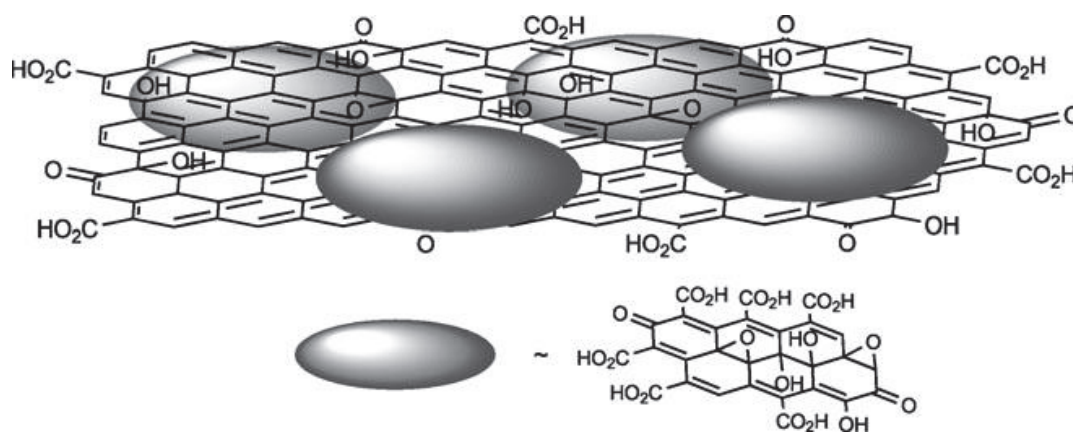


Figure 8: Oxidative debris located onto GO surface [108].

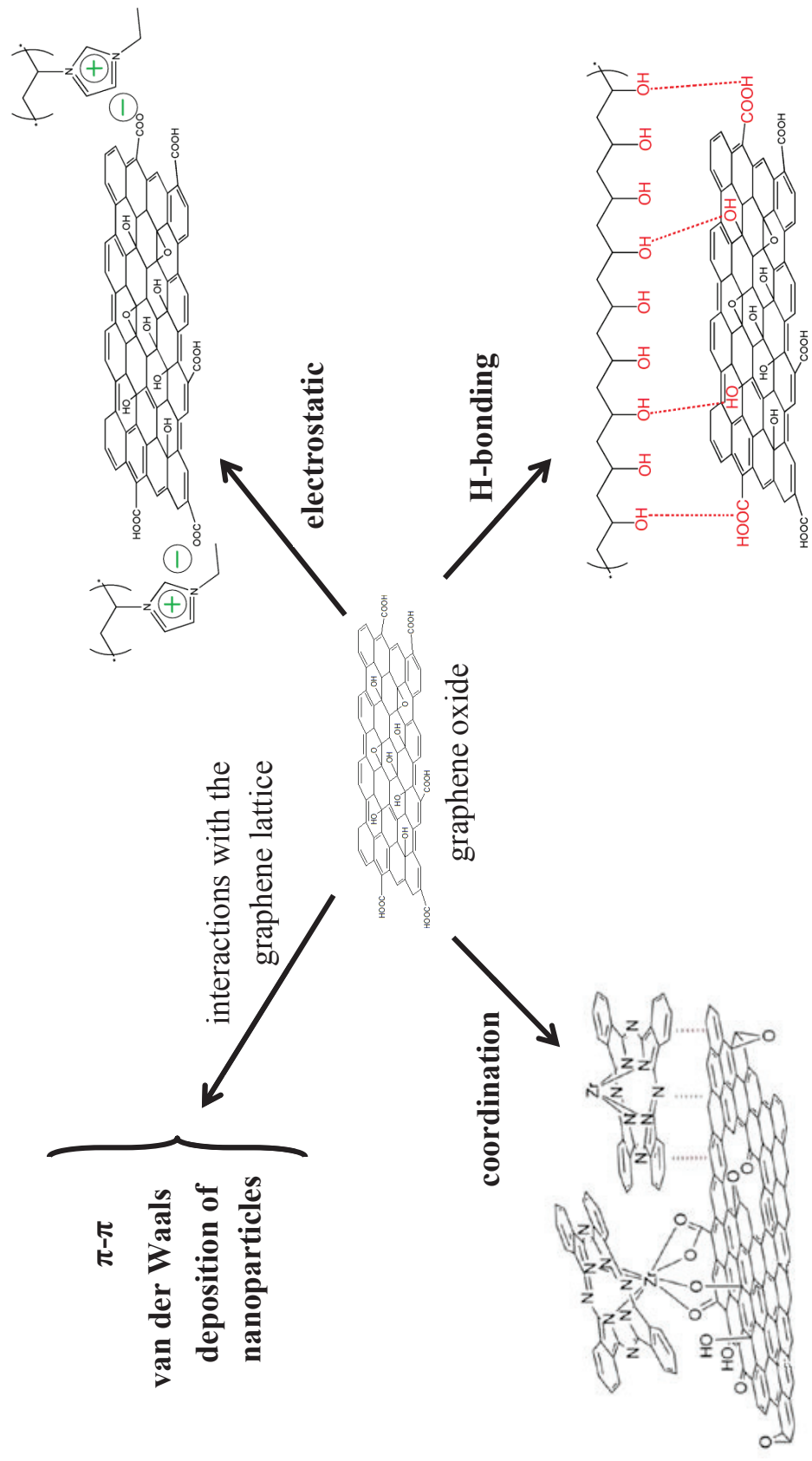
These debris adhere to GO through strong π - π interactions as well as H-bonds between anchored oxygen functional groups on GO surface and the ones located on OD. According to Rourke et al studies [108, 109], these oxidized parts account for one third of the mass of GO and can be selectively removed. A base wash process with NaOH can separate OD from GO [108]. Basic conditions create a repulsion between the negatively charged debris and GO and lead to the removal of OD. Base-washed GO possesses a carbon to oxygen ratio of 4:1 (as compared to 2:1 for GO) and shows an increase in electrical conductivity by 5 orders of magnitude. Besides, unlike GO, it does not form stable suspensions in water suggesting that OD are effective surfactants to stabilize aqueous GO suspensions. However, the base cleaning of graphite oxide does not affect grafted oxygen groups on GO surface and therefore it does not act as a reduction agent. In addition, when treated with hydrazine hydrate for example, both oxidative debris and most anchored oxygen functional groups are removed and the corresponding electrical conductivity is partially recovered [110].

1.3.4. Functionalization of graphite oxide

Similarly to pristine graphene, GO can be functionalized according to several modification. Modifications can lead to enhanced dispersibility of the nanosheets in common solvents.

1.3.4.1. Non-covalent functionalization

Non-covalent functionalization of GO has been reported in the literature [28]. All modifications previously detailed for pristine graphene can also be performed on GO. In addition, the presence of functional groups on GO surface opens the way for other methods involving the use of ionic, coordination and hydrogen bonding as shown in Scheme 7 [27, 28].



Scheme 7: Non-covalent modification paths for GO [111–113].

Scheme 7 shows the main non-covalent functionalization paths for GO. Modification through π - π and van der Waals interactions, as well as deposition of nanoparticles on GO surface, have already been presented in section 1.2.4.1. The presence of oxygen functional groups on GO enables other interactions to take place, such as ionic, H-bonding and coordination and are detailed in the following section.

1.3.4.1.1. Electrostatic interactions

GO functional groups can bear charges that may interact with other charged molecules through electrostatic interactions.

Figure 9 shows a schematic representation of electrostatic interactions between positively-charged poly (3,4-ethyldioxythiophene) (PEDOT) with negatively-charged sulfonated-reduced graphene oxide (SrGO) prepared by Xu et al [114].

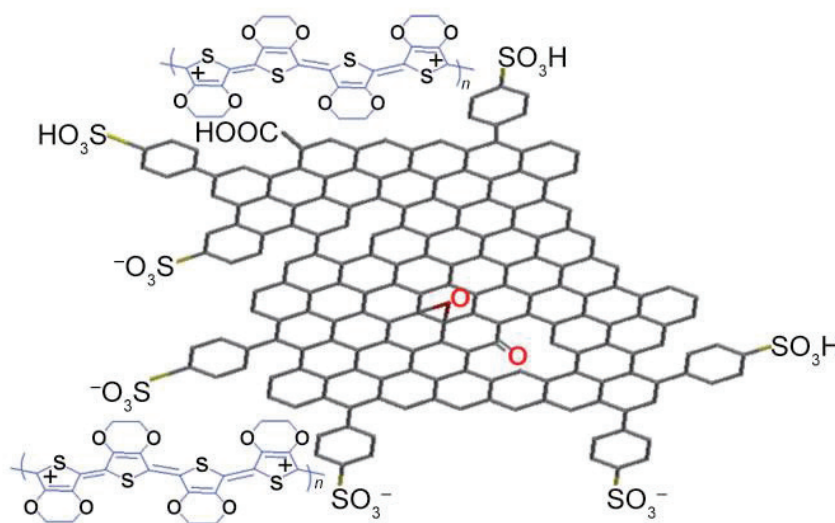


Figure 9: Schematic representation of sulfonated-rGO-PEDOT structure.

Upon incorporation of these fillers in a PEDOT matrix, the composites exhibited good electrical conductivity (up to 0.2 S/cm) as well as high transparency.

Poly ionic liquids (PILs) can also be used to modify GO surface (see Scheme 7, top right) [111]. For example, poly(1-vinyl-3-ethylimidazolium) was reported to non-covalently interact with graphene oxide leading to stable GO suspensions in both water and organic solvents through the anion exchange of the PIL in the medium. This stabilization is believed to be due to electrostatic interactions between carboxylic acid groups at the edges of GO sheets and imidazolium cations. Another possible stabilization mechanism comes from the aromatic rings of imidazolium cations that can interact through cation- π and π - π interactions with GO. In situ reduced modified-GO was reported to form stable suspensions in both water and propylene carbonate [111].

1.3.4.1.2. Hydrogen-bonding

Graphene oxide bears many oxygen functional groups that can be easily involved in H-bonding with an appropriate modifier. For example, poly(vinyl) alcohol (PVA) is a water-soluble polymer containing many hydroxyl groups. Liang et al [113] dispersed graphene oxide sheets in PVA through simple solution mixing in water. At 0.7 wt% GO, they obtained 76 % and 62 % increase in tensile strength and Young's modulus, respectively. They explained these enhanced properties by a strong polymer-filler

interface due to H-bonding between PVA and oxygen groups located on the GO surface (Scheme 7). They also observed a slight increase in the glass transition temperature (+ 3 °C) through DSC measurements, which they attributed to constrained PVA chains because of H-bonding interactions with GO (Figure 10).

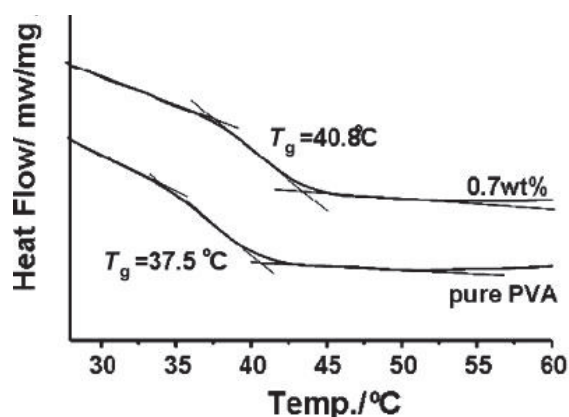


Figure 10: Differential scanning calorimetry of pure PVA and 0.7 wt% GO - PVA composites.

H-bonding thus appears as a powerful means to effectively modify GO, creating strong non-covalent bonds between GO and a modifier. These interactions are stronger when numerous.

1.3.4.1.3. Coordination bonds

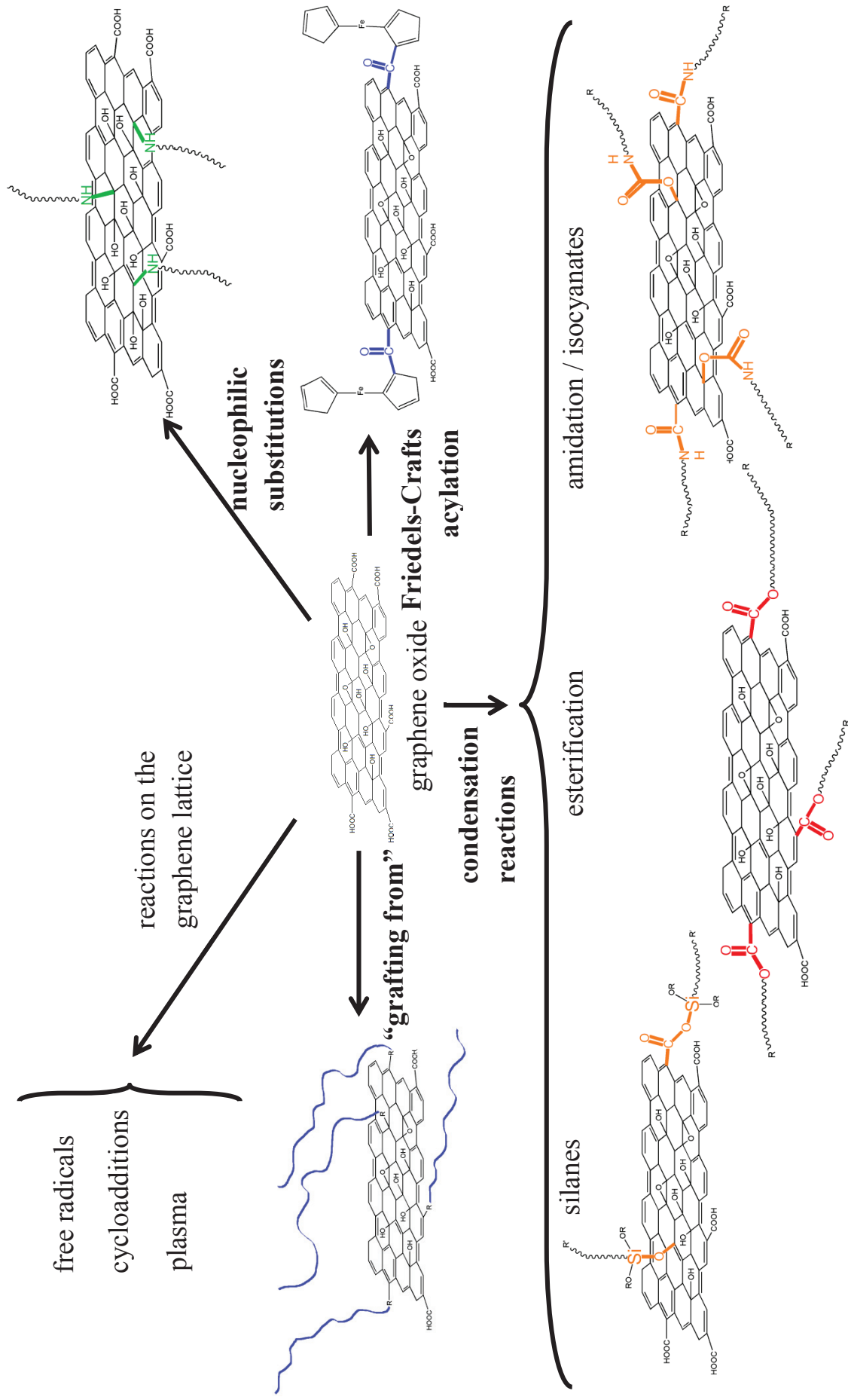
Functionalization through coordination bonds between GO and transition metal species can be performed. Hence, dyes were attached by Jurow et al [112] onto GO surface using coordination bonding. Zr(IV) porphyrinoid species were attached on GO through axial coordination between oxophilic Zr(IV) and oxygen functional groups of graphene oxide (Scheme 7). The modification was carried out at room temperature with simple sonication in THF. This supramolecular approach led to high dye loading of up to 1 chromophore per 20-50 nm², while preserving the electronic properties of both the substrate and the attached molecules. Similarly, Yamada et al [115] also prepared functionalized GO through coordination bonding. They investigated the coordination force of several metal cations with ammonia-treated graphene oxide. All metal cations were dissolved in 2-propanol and coordinated to ammonia-GO upon heating. It was found that cobalt, nickel and copper-based divalent catalyst performed best, leading to stable bonding which enables to limit aggregation of the treated GO.

Non-covalent modification of GO is an efficient way to tune its properties while preserving its conjugated structure. However, covalent functionalization of GO is most widely reported since the presence of oxygen functional groups on its surface and edges allows for very diverse chemical reactions to take place and then opens a wide range of available routes for functionalization.

1.3.4.2. Covalent functionalization of GO

Covalent functionalization of GO is widely reported in the literature [28, 33, 43, 55, 116–118]. Most covalent modifications are performed on the oxidized form of graphene since it possesses reactive functional groups on its edges and basal plane. Epoxy, hydroxyl and carboxylic acid groups are available for several molecules to react with. In addition, reduced graphene oxide often contains residual oxygen-based groups that can also be used as anchor sites for graphite modification.

Scheme 8 gathers common covalent modification paths for GO.



Scheme 8: Covalent modification paths for GO [26, 28, 33, 55].

From Scheme 8, it can be observed that several paths are available for GO covalent modification. The first class of reactions do not require functional groups and directly involve the graphene lattice. Such modifications include free radical reactions, cycloadditions and plasma modification. They will not be extensively presented here as they have already been detailed in section 1.2.4.2. Three other modifications paths do require oxygen functional groups on GO surface to be performed. Among these, nucleophilic substitutions, condensation reactions as well as Friedel-Crafts acylation have been used. They are presented in the following section.

1.3.4.2.1. Nucleophilic substitutions

Nucleophilic substitution (NS) often occurs very easily and is therefore promising for large-scale production of functionalized graphene. It can be performed through reacting an amine group with epoxy rings of graphene oxide. Many molecules are eligible for NS with GO such as aliphatic and aromatic amines, amino acids and amino-terminated polymers [28, 33, 116, 119].

For instance, Bourlinos et al [120] reacted several amines and amino acids with GO. They reported an increase in the interlayer distance of modified GO (as evidenced by XRD) dependent on the amine chain length. They also noted that GO layers inherit the physicochemical properties of the modifier. Octadecylamine-modified GO for instance led to stable suspensions in organic solvents. Liu et al [121] also prepared modified GO platelets with long-chain amines. They reported a very high grafting efficiency of 22 wt% and 25 wt% (from TGA measurements) respectively for oleyamine and octadecylamine. They also performed XPS to assess the covalent nature of the grafting. Besides, they report ionic-bonding of the amines onto GO. Similarly, Li et al [122] grafted octadecylamine (ODA) onto GO and observed very distinct dispersibility for GO and ODA-grafted-GO, as shown in Figure 11.

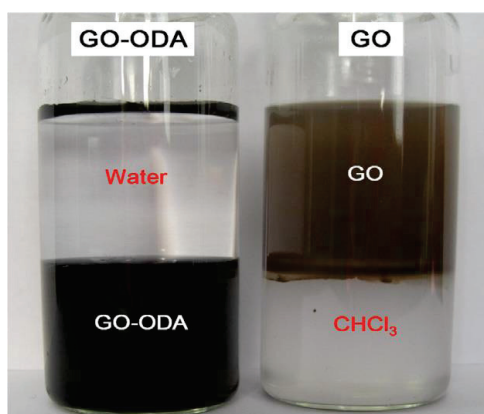


Figure 11: Stability of GO and ODA-modified-GO suspensions in a water/chloroform mixture at 0.5 mg/mL [122].

Indeed, while GO forms stable suspensions in water and does not disperse well in organic solvents, its modified counter-part shows stronger affinity for organic solvents than for water. Through elemental analysis, the authors calculated a grafting content of 32 wt%.

Nucleophilic substitutions involving amine species are thus widely reported as efficient modifications for GO [28, 33].

1.3.4.2.2. Condensation reactions

Condensation reactions can also occur on GO carboxylic acid and hydroxyl groups through several mechanisms such as sol-gel process, esterification and amidation reactions as well as reactions with isocyanates (Scheme 8). Some of these reactions are detailed below.

1.3.4.2.2.1. Reaction with silanes

Matsuo et al [123–125] were among the pioneers in reacting GO with silane compounds. Indeed, they reported GO modification with several chlorosilanes such as octadecyltrichlorosilane that can form Si-O bonds with hydroxyl groups on GO surface. They obtained a silicon content up to 1.7 mol/g of graphite oxide [125].

Many research groups also performed reactions of different alkoxysilane compounds with GO. For example, Zhang et al [126] grafted 3-aminopropyltriethoxysilane with a grafting efficiency of 16 wt%, determined by TGA. Similarly Wu et al [127] grafted bis(triethoxysilylpropyl)tetrasulfide onto GO and observed a strong decrease in hydrophilicity of the modified graphene oxide. Moreover, Beyou et al [128] studied the hydrolysis-condensation of trimethoxy(7-octen-1-yl)silane with graphene oxide and reached a grafting efficiency of 5.3 wt% (0.2 mmol/g), determined by TGA. The modified GO sheets showed enhanced dispersibility in PDMS oil at 0.1 mg/mL.

1.3.4.2.2.2. Esterification

Graphene oxide can be functionalized through a simple esterification reaction. Salavagione et al [66] covalently attached poly(vinyl alcohol) through esterification on GO. Hydroxyl groups of PVA reacted with carboxylic acid groups of GO to form ester bonds. At 10 wt% loading, an increase of 35 °C in the glass transition temperature was observed. It was attributed to the restriction of the segmental motion of PVA chains by rigid graphite flakes.

Besides, Jia et al [129] used esterification reactions to crosslink graphene oxide sheets using diols or polyols such as 1,2-ethanediol, 1,3-butanediol, 2-methyl-2,4-pentanediol, 2,2-dimethyl-1,3-propanediol, 1,2,3-propanetriol and 2,2-bis(hydroxymethyl)-1,3-propanediol. Ester bridges were created through reaction of carboxylic acid groups of GO and hydroxyl groups of diols and polyols. In a reverse manner, the authors also reacted oxalic acid, propandioic acid, succinic acid, hexanedioic acid and octanedioic acid with GO. In the latter case, carboxylic groups were provided by the modifier while GO reacted via its hydroxyl groups to form ester bridges. An increase in the interlayer spacing was observed from 6.89 Å with pristine GO to 7.65 Å and 2,2-dimethyl-1,3-propanediol-crosslinked GO.

1.3.4.2.2.3. Amidation

When put in presence of amine groups, GO often preferentially reacts by nucleophilic substitution. Amino groups react rather easily with epoxide groups at low temperature. However, when the necessary conditions are gathered, amino groups can also react with carboxylic acid groups to form amide bonds. A preliminary step is often to prepare an acyl halide from the carboxylic groups to increase their reactivity towards NH₂ groups. Thus, Niyogi et al [130] reacted thionyl chloride onto graphene oxide sheets in DMF before adding octadecylamine to create covalent amide bonds. The final compound was studied through FTIR to assess the structure, and TGA analysis showed a 7 wt% loss attributed to the ODA which had been grafted on GO.

1.3.4.2.2.4. *Reactions with isocyanates*

Modification of GO with isocyanates is also possible. Stankovich et al [131] treated graphene oxide with several isocyanates such as toluene isocyanate at room temperature. They observed reduced hydrophilicity of the treated platelets as well as an increased stability of suspensions in polar aprotic organic solvents. Several groups [70, 132–134] reported similar results such as Kim et al [135] who modified graphene oxide with phenyl diisocyanate and acetyl phenyl diisocyanate. The modified fillers were further incorporated into a thermoplastic polyurethane matrix. At 3 wt% loading, a 90 % decrease in oxygen permeation was observed.

Condensation reactions thus appear as an easy and versatile way to covalently modify GO. A wide variety of modifiers can be used, and the properties of the modified GO can be tuned to enhance its dispersability in organic solvents for example.

1.3.4.2.3. *Friedel-Crafts acylation*

Another functionalization of GO can be realized through Friedel-Crafts acylation. Monoacylation of GO using ferrocene was reported by Avinash et al [136]. They performed covalent grafting following a simple green chemistry procedure using trifluoroacetic anhydride on alumina at room temperature. Covalent grafting was evidenced from FTIR analysis. An increase in GO interlayer spacing from 0.5 nm to 2.4 nm was observed through energy dispersive X-ray analysis (EDAX). The samples showed magnetic properties.

1.3.4.2.4. Covalent grafting of polymers on GO

Functionalization of graphene oxide can also be carried out with polymers. Several mechanisms can be used. Methods of covalent grafting of polymers onto graphene or graphene oxide can be divided into two groups: “grafting to” and “grafting-from” techniques [33].

1.3.4.2.4.1. “Grafting to” approach

In these methods, grafting can be carried out in one or two steps. First, the polymer can be functionalized to incorporate reactive functional groups on its backbone or chain-ends if not already present. Then, addition onto graphite oxide is performed through one of the previously presented mechanisms such as esterification, amidation or nitrene addition for example [33].

Beyou et al [137] grafted azido-polyethylene to graphene oxide through nitrene cycloaddition. TGA measurements suggested a low grafting efficiency (1.5 wt%) leading however to a strong increase in affinity of the modified filler with heptane, as shown in Figure 12.

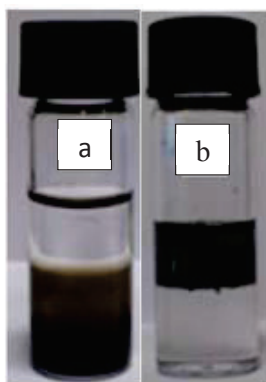


Figure 12: Suspensions of a) graphene oxide and b) azidopolyethylene-grafted graphene oxide in DMF/heptane at 0.35mg/mL. While GO suspension shows most affinity for the DMF phase (bottom), azidopolyethylene-grafted GO shows best affinity for the heptane phase (top) [137].

Many other examples of polymer grafting to GO can be found in the literature [59–66].

1.3.4.2.4.2. “Grafting from” approach

As for pristine graphene, the “grafting from” technique can also be performed with GO.

1.3.4.2.4.2.1. Atom transfer radical polymerization (ATRP)

For example, Kumar et al [79] reported the grafting of poly(methyl methacrylate) (PMMA) onto GO following an ATRP mechanism. In a first step, 2-bromoisobutyryl bromide initiator was anchored onto GO. Then MMA was in situ polymerized from functional GO. The as-synthesized products showed high grafting density (> 90 wt%) and a molar mass up to 60000 g/mol. Increased thermal stability was obtained for the grafted PMMA as compared to pure PMMA (TGA).

Other research groups also reported interesting results in ATRP functionalization of graphene [71–75].

1.3.4.2.4.2.2. Reversible addition fragmentation chain transfer (RAFT)

Beckert et al [83] developed several grafting strategies to synthesize polystyrene-grafted GO. Sulfur-based molecules were attached to GO to provide thiol, dithioester, dithiocarbonate and

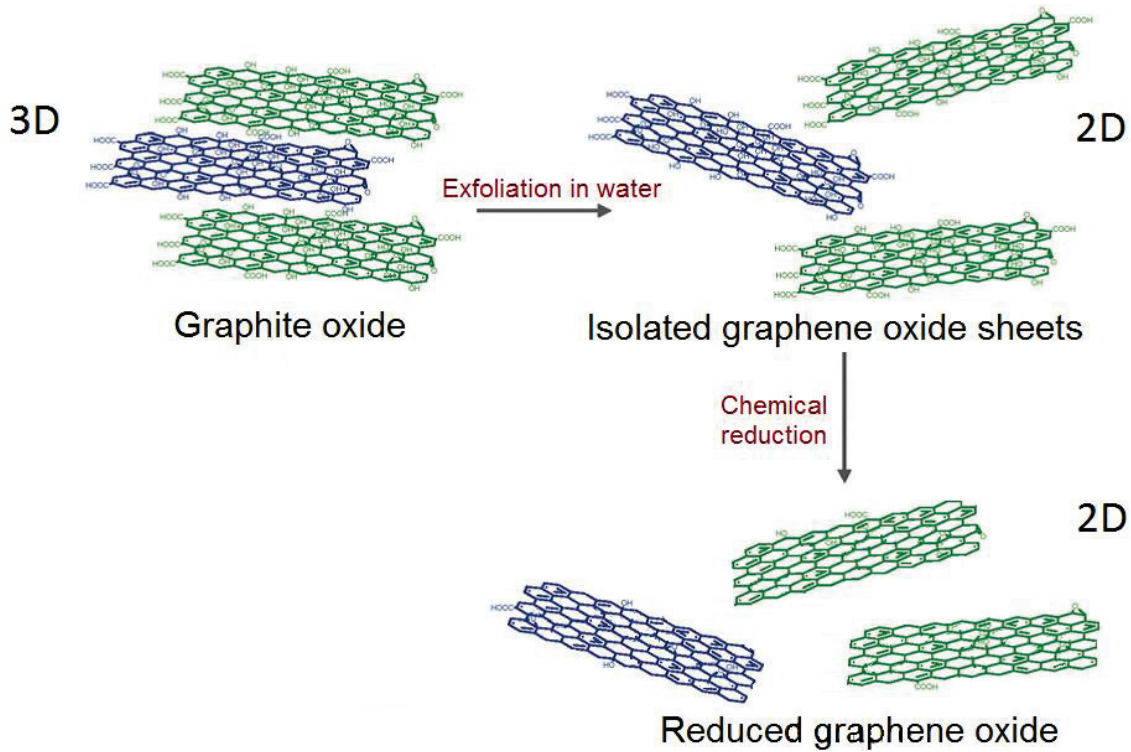
dithiourethane groups that could efficiently act as RAFT chain transfer agents for styrene polymerization. Through a rheological study the authors showed that in the case of stearyl-grafted-GO – polystyrene composites, no particle network could be obtained in the absence of covalent coupling between stearyl-grafted-GO and polystyrene [83].

Covalent bonding of polymers on GO surface is commonly reported with thermoplastic polymers such as PS and PMMA [78–85].

The presence of oxygen functional groups on GO surface allows for a wide variety of reaction paths. Functionalization can happen either through non-covalent or covalent interactions. While physical interactions lead to no disruption of the conjugated structure, covalent modification approach leads to a disruption of the aromaticity thus affecting electrical properties. Small molecules as well as polymer chains can be used to functionalize graphene sheets through different mechanisms allowing for the elaboration of high-performance composites. Apart from all the processes presented previously, multistep modifications involving various mechanisms are also often used, thus leaving many ways unexplored.

1.3.5. Reduction of graphite oxide derivatives

Graphite oxide derivatives can be finally converted into a “graphene-like” material through a reduction process. This method is interesting as it is one of the most scalable methods to produce large quantities of “graphene”. The aim is to restore the disrupted sp^2 lattice through removal of the oxygen functional groups to recover electrical conductivity. Several methods are available to prepare reduced graphene oxide from GO. However, the obtained product usually contains defects such as remaining oxygen groups, wrinkles, sp^3 carbons... and so exhibits lower properties than defect-free graphene. Scheme 9 shows the reaction steps for the preparation of “graphene” (actually, reduced graphene oxide) from graphite oxide and exfoliation into graphene oxide sheets [109].



Scheme 9: Representation of the preparation of reduced graphene oxide from graphite oxide, in aqueous phase. Adapted from [109].

Many reduction methods exist and some will be discussed in the following section. However, it is interesting to notice that the removal of oxygen groups from GO surface was not studied until Brauer [138] in 1963, about a hundred years later than the first synthesis of GO by Brodie. Figure 13 shows some of the main reduction paths to convert GO into a graphene-like material.

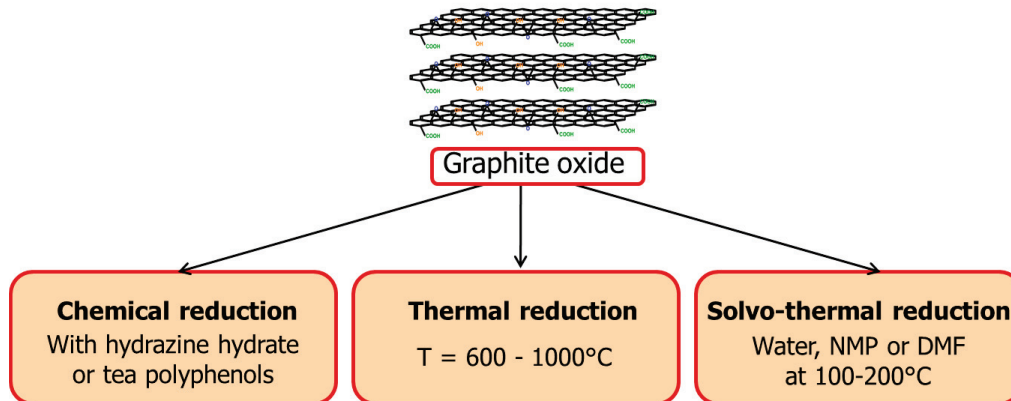
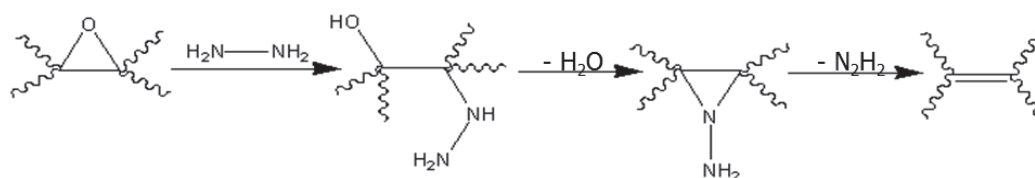


Figure 13: Main reduction paths for graphite oxide.

The most relevant parameters to compare the efficiency of the different reduction paths are both the decrease in oxygen content of the material (carbon-oxygen ratio) and the increase in electrical conductivity of the reduced material [109].

1.3.5.1. Chemical reduction of graphene oxide

Chemical reduction of graphite oxide is the most common method. Hydrazine hydrate is commonly used to restore carbon-carbon double bonds [139]. It is a highly toxic reducing agent that acts by removing oxygen functional groups from GO. Scheme 10 shows the reaction mechanism for removal of epoxide groups in presence of hydrogen.



Scheme 10: Reduction reaction of GO using hydrazine hydrate.

A carbon-oxygen ratio of 10:1 is often reported and an increase in electrical conductivity (up to 4600 S/m [140]) is also observed, but it still remains much lower than pristine graphene [141]. Other reagents such as sodium borohydride [142] or more environmentally friendly tryptophan, ascorbic acid or tea polyphenols, also proved to be efficient [143–148]. Table 1 gathers some results obtained with natural reducing agents.

Product	Carbon : oxygen ratio	Electrical conductivity
L-ascorbic acid (vitamin C)	12.5 : 1	7700 S/m
Glycine (amino-acid)	11.24 : 1	
L-aspartic acid (amino-acid)		700 S/m
Gallic acid	5.3 : 1	36 S/m
Urea		43 S/m

Table 1: Nature-based reducing agents.

Through reduction, the conjugated system is at least partially restored. This means that stronger π - π interactions may occur, leading to reagglomeration of the reduced graphene oxide sheets [149]. This restacking is undesirable since it is irreversible and reduces the specific surface area of the product and. However, a few methods are available to partly prevent the graphene from restacking. For example, the pH can be adjusted to increase zeta potential of the sheets, or a surfactant such as sodium dodecylbenzene sulfonate can be used. Else, a polymer can be adsorbed on the platelets surface to limit interlayers interactions, or the reduction process can be performed in situ in a polymer matrix [102, 141, 150, 151].

Besides, it can be observed that the corresponding reduced product is more thermally stable than GO, as shown in Figure 14 [152].

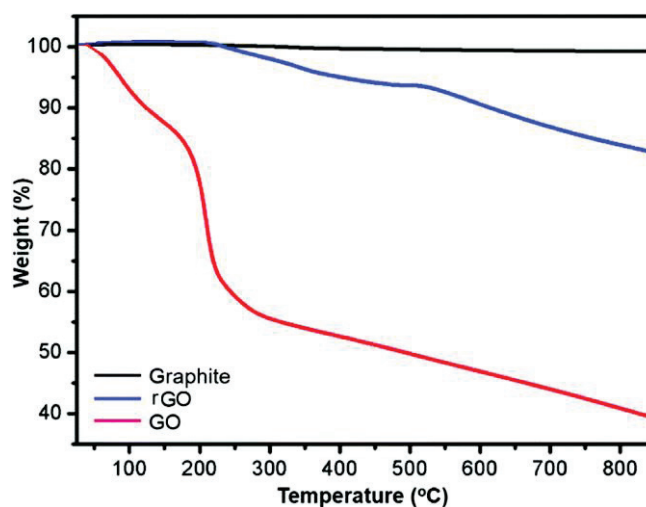


Figure 14: Thermogravimetric analysis of graphite, graphite oxide (GO) and hydrazine-reduced graphite oxide (RGO) at 10 °C/min up to 600 °C under a nitrogen flow. Adapted from [153].

Graphite does not show any degradation at 600 °C while GO shows an important mass loss (around 55 wt%). This mass loss happens in two steps: first around 100 °C where physisorbed water is released, and then the major loss occurs at 200 °C where most oxygen functional groups degrade. In contrast, reduced graphite oxide (RGO) does not exhibit more than 10 % loss at 600 °C, which proves shows greatly improved thermal stability as compared to GO. However, some degradation happens due to some remaining oxygen groups at the surface [152].

1.3.5.2. Thermal reduction of graphene oxide

Graphite oxide can also be reduced using simple heating at high temperatures. In this process GO powder is exposed to high temperatures (around 1000 °C) with a quick heating rate (> 2000 °C/min) [154]. Carbon dioxide, carbon monoxide and water vapor are generated between the layers and when this pressure overcomes van der Waals forces, it splits GO into individual sheets [154]. This method is fast and easily scalable. It is often reported to be more efficient than chemical reduction to remove oxygen functional groups but it also creates many defects in the resulting material, such as wrinkles or voids and implies an important mass loss (at least 30 %, [154]). A carbon – oxygen ratio of around 10:1 is commonly achieved [154]. It can be up to 50:1 for graphite oxide samples reduced at 1050 °C under argon atmosphere, as reported by Bai et al [155]. Thermal reduction greatly improves electrical conductivity to up to 2000 S/m [154]. A BET surface area between 700 and 1500 m²/g is also reported by Schniepp et al [154] as compared to 2600 m²/g [156] for defect-free graphene [2, 156].

However, this reduction method is incompatible with chemical functionalization of GO as any grafted species on the surface would undergo pyrolysis when exposed to high temperatures.

1.3.5.3. Solvothermal reduction of graphene oxide

Solvothermal reduction [157] is performed by heating graphene oxide in an organic solvent around its boiling point. N,N-dimethylformamide (DMF) is a suitable solvent to perform such reduction. Hence, Wang et al [158] heated graphene oxide in DMF at 180 °C (i.e. above its boiling point (153 °C)) for 12 h, and obtained a material with a C:O ratio of 14:1. Dubin et al [159] reported the use of N-methylpyrrolidone (NMP) to reduce graphene oxide. The mixture was heated at 205 °C for 24 h at

atmospheric pressure and the obtained C:O ratio was 5:1. This solvent is known to break C-O bonds from GO, hence increasing the rate of the reduction reaction.

Hydrothermal reduction of graphite oxide can also be performed. In this process, overheated supercritical water acts as a reducing agent for graphite oxide. However, this eco-friendly method requires to work at high pressure since water is heated over its boiling temperature. Hence, Zhou et al [160] autoclaved an aqueous suspension of GO at 180 °C for 6 h to obtain reduced graphene oxide. Moreover, solvothermoreduction in water is only partial. Lin et al [161] treated an aqueous suspension of GO at 100 °C for 24 h and observed that the obtained material still showed a brown reflect, typically observed for GO suspensions, with a resistivity of 6 MΩ while the same material reduced in DMF had a resistivity three orders of magnitude lower. Lin et al [161] proposed a mechanism for deoxygenation of GO in a solvent. According to their study, the release of carbon dioxide and carbon monoxide groups occurs when oxygen functional groups from GO sheets collide with one another. The polarity of the solvent promotes the diffusion of oxygen groups and therefore increases the reduction reaction rate. Lin et al [161] also showed that DMF with a dipolar moment of 3.24 D was more effective in reducing GO than ethylene glycol which possesses a lower dipolar moment (2.31 D).

Another method based on the use of microwave radiation has also been reported for the reduction of GO and compounds with a carbon-oxygen ratio of 3:1 and an electric conductivity of 270 S/m have been obtained [162, 163], which remains moderate compared to other reduction routes.

Reduction methods enable to partially recover the conjugated structure of pristine graphene, leading to electrically-conductive fillers.

1.4. Conclusion

This section has highlighted the various forms of graphene-based materials available. In addition, functionalization methods to decrease interactions between graphene nanosheets and to effectively tune the dispersibility of the modified platelets in various organic solvents have been presented.

This section has presented the numerous materials that can be derived from graphene, a 2D structure of a single sheet of carbon atoms, arranged in a honeycomb structure. Pristine graphite exhibits outstanding properties such as a very high Young's modulus of 1 TPa and a complete impermeability to all gases. However, defect-free graphene is not easily prepared and most common methods such as CVD and epitaxial growth require a high amount of energy and a long time to lead to a small number of nanosheets. Fortunately, new methods have been developed to produce cheaper "graphene-like" materials at lower costs and at a larger scale. Among these methods, oxidation, exfoliation in aqueous phase, followed by reduction of the material, can lead to graphite nanoplatelets which can be of variable thickness and contain several defects such as heteroatoms, sp³ carbon atoms and wrinkled surfaces. Anyhow, these nanoplatelets may be of significant interest as fillers in polymer composites. A main challenge is to provide efficient filler-matrix interaction and overcome the strong π-stacking interactions between graphitic layers. The modification of graphite surface by non-covalent methods, may limit aggregation of the nanoplatelets and may provide enhanced interactions with the host polymer matrix. Hence, through covalent grafting of polymers onto nanoplatelets surface, its dispersibility in common organic solvents could be improved, thus suggesting improved compatibility with a polymer matrix.

Besides, an oxidized form of graphite (GO) has been described in this section. The presence of oxygen functional groups onto the surface of GO, led many authors to investigate various functionalization paths, involving epoxide, carboxylic acid and hydroxyl groups of GO. These modifications could lead to a decrease in GO hydrophilicity and an increase in its dispersibility in common organic solvents.

Such modified platelets could be incorporated into non-polar matrices, such as polyisoprene, to enhance the matrix mechanical and barrier properties. Hence, fillers are often incorporated into elastomeric matrices, to provide mechanical reinforcement for example. The following sections deals with elastomeric materials and graphene-based elastomeric composites.

2. Elastomeric materials: composition and processing principles

Elastomers are polymeric materials that exhibit rapid and large reversible strain in response to a stress [164] and so exceptional elasticity. The Mayas were among the first to take advantage of this fantastic material to create bouncing balls. Nowadays, rubber parts are found everywhere, for example in the automotive industry (tires, gaskets, seals...), in the building sector and in the medical field (disposable gloves). Such broad range of applications was made possible by the discovery of the vulcanization process (by Goodyear in 1839) and then, by the development of a variety of elastomers, by the use of fillers and additives as well as specific processing techniques. The following section deals with the structure and properties of two main types of rubber which will be addressed in this thesis: polyisoprene and acrylonitrile-butadiene copolymers (also known as “nitrile rubber”). A last part briefly introduces the reader with rubber compounding, vulcanization reaction, as well as processing methods.

2.1. Polyisoprene

Polyisoprene is the only industrial rubber which can be found in nature in addition to its synthetic counterpart. Both will be introduced hereafter.

2.1.1. Natural polyisoprene

Natural polyisoprene (known as natural rubber, NR) is a polymer containing isoprene units. It is produced naturally by enzymatic polymerization of isopentenyl pyrophosphate, leading to a polymer with a high stereoregularity and a high percentage (> 99.9 %) of 1,4-*cis* configuration as represented in Figure 15 [164].

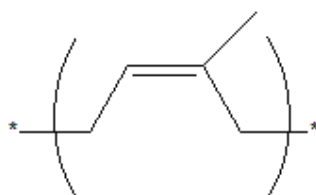


Figure 15: Chemical structure of *cis*-1,4-polyisoprene.

Molar mass distribution of natural rubber is broad with very high molar masses, ranging typically from 100,000 g/mol to 5,000,000 g/mol. Natural rubber is produced through coagulation of a latex from *hevea brasiliensis* tree and contains typically from 30 wt% to 40 wt% of polyisoprene, the rest of the product being mainly water, proteins, sugars and minerals, as shown in Table 2.

Polyisoprene	27-40 %
Water	52-70 %
Proteins	1.5-2.8 %
Acetonic extract	1.0-1.7 %
Sugars	0.5-1.5 %
Mineral materials	0.2-0.9 %

Table 2: Composition of natural rubber latex [165].

In natural rubber latex, polymer particles are dispersed in an aqueous serum, as spherically-shaped drops surrounded by proteins (responsible for “latex” allergies [166]), lipids and phospholipids that act as latex stabilizers. As a result, natural rubber does not contain only polyisoprene.

Natural rubber possesses excellent fatigue and crack propagation resistance due to its unique ability to crystallize under stress. Most common applications include tires, antivibrating systems as well as gloves and other dip-processed products prepared directly from latex. With over 12 million tons produced in 2015, NR is the elastomer most used worldwide.

2.1.2. Synthetic polyisoprene

Most attempts to synthesize a polymer that would behave like natural rubber failed. The main reasons were the lower molar masses and the lack of a controlled microstructure, especially the lack of the very high cis-1,4 structure found in natural polyisoprene. In the 1950's, with the development of Ziegler-Natta's stereospecific catalysts, a cis-1,4 content of about 90 % could be reached. A decade later, Shell Chemical Company began to sell synthetic polyisoprene (IR) synthesized in presence of an alkyl lithium catalyst. However, due to a too low cis-1,4 content (< 97 %), their polyisoprene was not able to strain-crystallize and then to reach comparable properties to those of natural rubber. A few years later, Goodyear finally commercialized a 98.5 % cis-1,4 polyisoprene product able to strain-crystallize [167, 168]. Nowadays, Goodyear, Zeon and Japan Synthetic Rubber are the main producers. However, due to the high cost of synthetic polyisoprene, natural rubber is still preferred in many applications.

Besides cis-1,4 configuration, three other polyisoprene configurations exist and are shown in Figure 16.

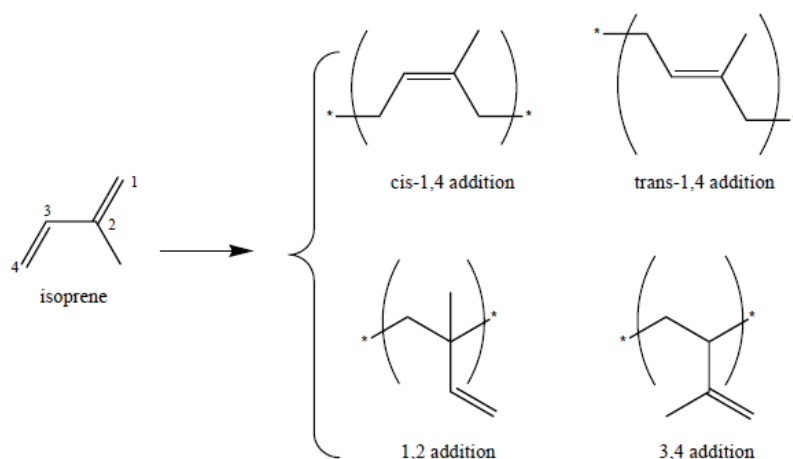


Figure 16: Isoprene and polyisoprene structures.

Cis and trans-1,4 configurations are the most common ones but most polyisoprenes include a small percentage of 1,2- and 3,4-units. As most elastomers, IR exhibits a low glass transition temperature (-73 °C for 1,4-cis configuration and -53 °C for 1,4-trans configuration) [169, 170].

Industrially, polyisoprene homopolymer and copolymers are prepared mostly through an anionic and a coordination mechanism. Table 3 gathers the main characteristics of polyisoprene products obtained through these mechanisms [169].

	Natural Rubber	Ziegler-Natta coordination IR	Anionic IR
Catalyst	/	Titanium / Aluminum catalyst	Alkyl-lithium catalyst
Branching	Yes	Yes	Linear product
Molecular weight	Up to 5 million g/mol	Up to 1 million g/mol	Up to 3 million g/mol
Molecular weight distribution	Very wide	Wide	Narrow
Cis-1,4 content	99.9 %	97 %	90 %
Gel content	> 20%	10-20 %	0 %
Impurities	Proteins and other natural products	Catalyst residuals	Traces
Reaction medium	Water (emulsion)	Organic solvent	Organic solvent

Table 3: Comparison of natural polyisoprene and the synthetic products obtained through Ziegler-Natta and anionic mechanisms [169].

The anionic polymerization process can lead to a linear polymer containing 90 % cis-1,4 product. A high molecular weight (M_w) (3,000,000 g/mol) with a narrow M_w distribution can be reached. Coordination polymerization of isoprene can lead to a higher cis-1,4 content of up to 97 % but the final product is often branched and has a lower molecular weight (1,000,000 g/mol) than the anionic-polyisoprene. The molecular weight distribution is often broad and a gel content of 10-20 % is often present. A main difference between the products obtained through these two mechanisms is their purity. Ziegler-Natta polymerization often leaves catalytic residuals, while anionic polymerization leads to a very pure product. From an environmental point of view, both systems include the use of polluting catalysts and are performed in toxic organic solvents such as cyclohexane [171, 172].

Radical polymerization of isoprene is not commonly used in the industry as it produces mainly trans-1,4 polyisoprene with a very low molecular weight. Emulsion radical polymerization, even more seldom used as it is hard to control, has a low conversion and produces a polymer with a low cis-1,4 content and high branching and gel contents. Cationic polymerization is not much used industrially either because only low molecular weight products are reached [169].

However, when no stereoselectivity or high molecular weight is desired, these polymerizations methods can be used and have been described by several authors [173–181]. Hence, Cheong et al [181] reported the use of emulsion free radical polymerization to polymerize isoprene at temperatures from 25 °C to 70 °C during 5 h to 84 h. They obtained mainly in a 1,4 trans configuration (70 %) with molar masses up to 7,600 g/mol (M_n) at a temperature of 25 °C for 9 h [181]. However, some of their polyisoprene products contained up to 91 wt% insoluble fraction (gel) (at 70 °C for 2 h) corresponding to crosslinked polymer [181]. Another simple route to polymerize isoprene has been described by Vasilenko et al [175]. Through the use of Lewis acid surfactant combined catalysts (LASCs), they reported the polymerization of isoprene through an emulsion cationic method in a one-pot reaction. When performing the reaction at 40 °C during 13 h, they obtained 1,4 trans polyisoprene (72 %) with an average molar mass of 97,000 g/mol and a polydispersity index (PDI) of 3.8. They also report that their product is fully soluble in dichloromethane, indicating that no crosslinking occurred during the polymerization reaction [175]. Such methods are not stereoselective enough to have industrial applications but they anyhow provide fast, simple and environmentally-friendly (use of water) process that can be safely handled at a laboratory scale.

2.2. Acrylonitrile-butadiene copolymers

Acrylonitrile-butadiene copolymer, also known as nitrile rubber (NBR), is a synthetic copolymer of butadiene and acrylonitrile. It was first developed as an oil-repellant rubber in the 1930's by Konrad and Tschunkur [182]. It is mostly produced through emulsion polymerization using radical initiators. The polymer can be linear or branched depending on the polymerization experimental conditions and molar masses from 3000 g/mol to 1,000,000 g/mol can be achieved. Its structure is shown in Figure 17.

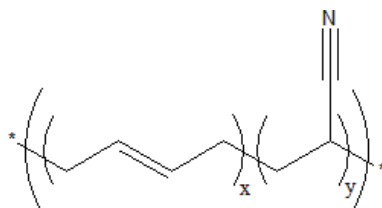


Figure 17: NBR structure with x being the number of butadiene units and y the number of acrylonitrile units.

NBR contains butadiene and acrylonitrile (ACN) units. Its properties are strongly dependent upon its ACN content (from 15 to 50 %). A high ACN content decreases its flexibility at low temperatures and thus increases its glass transition temperature (from -30 °C to 0 °C at 15 wt% and 50 wt% ACN content respectively) [183, 184]. Swelling resistance to aliphatic hydrocarbons, tensile strength and abrasion resistance are enhanced and permeability to gases is reduced in high-ACN NBRs [164, 183].

NBR displays an overall good resistance to oil, fuel, solvents and heat and a low resistance to most aromatic hydrocarbons, esters, ketones, strong oxidizing materials, acids, ozone and UV light [164].

2.3. Elaboration of an elastomeric material

Elastomeric products properties depend upon a great number of parameters including compounding and process parameters. Hence, elastomer products contain several additives to improve their properties through the use of reinforcing fillers or stabilizers (such as antioxidants) as well as additives that allow easier processing of the elastomer compound (processing oils for example). In this section, only a few aspects of elastomer processing will be described. The major role of crosslinking reactions will be described. Then, reinforcement of the elastomeric matrix through interaction with filler particles will be discussed. Finally, a short overview of conventional elastomer processing methods and parameters will be shown.

2.3.1. Crosslinking

Raw elastomers are prone to creep. They also have poor weather resistance, are sensitive to heat, cold, chemicals, UV light etc. A major breakthrough in rubber processing was the discovery of vulcanization (or curing) that is to say the creation of chemical covalent bonds between rubber chains to form a three-dimensional network. Such crosslinking is necessary to give elastomers true elastic properties with increased strength and elastic recovery as well as lower sensitivity towards temperature and solvents.

2.3.1.1. Method to crosslink elastomers

Sulfur is the oldest and most common crosslinker used in rubber industry. It is used for unsaturated elastomers such as natural rubber. Upon heating, sulfur bridges can form in between rubber chains thus creating crosslinks. Various structures are obtained during the crosslinking reaction (Figure 18).

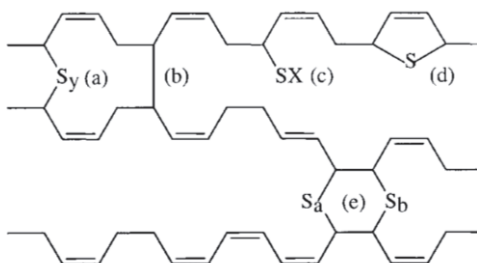


Figure 18: Schematic representation of sulfur crosslinking in a diene elastomer. Various chemical structures are obtained. (a) sulfur crosslinks ($y=1$ mono, $y=2$ di and $y > 2$ polysulfide crosslinks), (b) carbon-carbon crosslinks, (c) pendant accelerator sulfides (X stands for the accelerator), (d) cyclic sulfides and (e) vicinal crosslinks that have junction points on the same olefin chains.

Depending on the nature of the accelerator and of the accelerator to sulfur ratio, mono, bisulphidic (ratio > 1) or polysulphidic (ratio < 1) crosslinks can be produced. The mechanism will be detailed in 2.3.1.3. Short sulfide crosslinks lead to increased thermal stability whereas polysulfidic crosslinks lead to improved tensile strength of the vulcanized elastomers [164].

Peroxides such as dicumyl peroxide (DCP) can also crosslink elastomers. They enable curing of both saturated and unsaturated elastomers. They act through homolytic dissociation of peroxides to radicals and lead to the formation of carbon-carbon crosslinks. They are mostly used for saturated polymers or to co-vulcanize elastomers with thermoplastics. They usually lead to quick curing and the end-products often show good compression set and high temperature resistance. However, peroxides tend to interact with other compounds, scorch (crosslinking reaction onset) and curing times are less tunable and the end-product usually shows lower tensile and tear strength properties than with conventional sulfur curing.

Other curing agents such as phenol-formaldehyde resins (“resols”) can be used but are less common for diene polymers such as polyisoprene and acrylonitrile-butadiene copolymers. They will thus not be presented here.

2.3.1.2. Vulcanization agents and co-agents

Crosslinking reaction with sulfur is always performed in presence of many additives named “curing system”. It consists mainly in activators, accelerators, scorch retarders and the vulcanizing agent. Most common activators are zinc oxide (ZnO) and stearic acid. The former enables the formation of reactive complexes during the curing process and the latter ensures good solubility of these complexes in the rubber matrix. Accelerators mainly increase the reaction rate through addition onto sulfur and addition onto rubber chains to form crosslinking precursors. They also enable a decrease of the curing temperature. Besides, they often act as sulfur donors, reducing thus the amount of elementary sulfur to be added.

Common chemicals for this purpose are sulphenamides (such as N-cyclohexyl-2-benzothiazol sulfonamide, (CBS)), dithiocarbamates, thiuram sulfides (such as tetrabenzylthiuram disulfide (TBzTD) and tetraethylthiuram disulfide (TETD)), thiazoles (dibenzothiazyl disulfide (MBTS)) and guanidines.

Scorch retarders increase the induction period to avoid pre-curing and thus to enable a safe processing. N-(cyclohexylthio) phthalimide (CTP) is a common retarder in rubber industry. The chemical structures of these products are shown in Table 4.

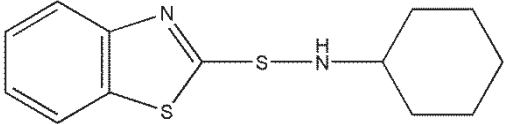
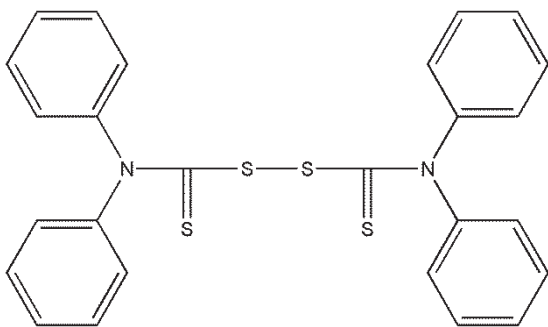
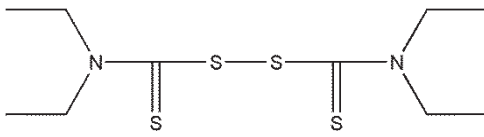
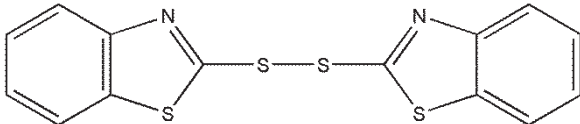
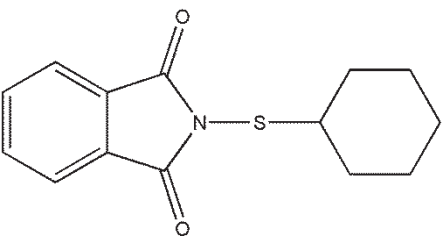
Name	Role	Structure
CBS	Accelerator	
TBzTD	Accelerator	
TETD	Accelerator	
MBTS	Accelerator	
CTP	Retarder	

Table 4: Chemical structures of common accelerators and retarders.

Sulfur crosslinker is often added as elementary sulfur, a cyclic arrangement of 8 sulfur atoms, whose S-S bond can break upon heating, with an activation energy of 252 kJ/mol [164].

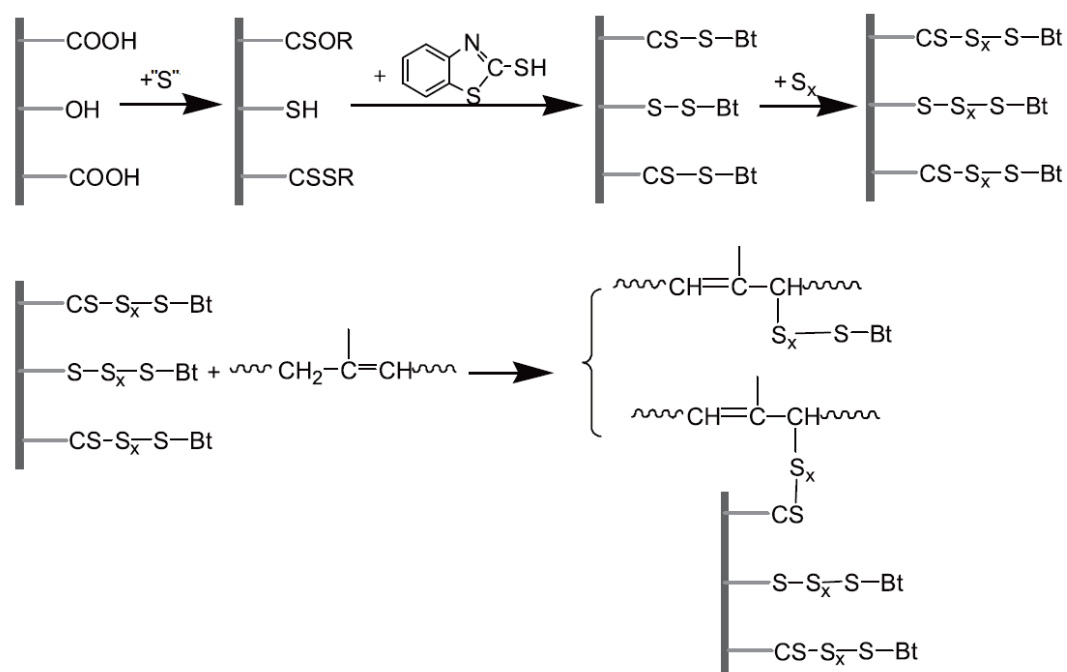
2.3.1.3. Crosslinking reaction mechanisms

Crosslinking of elastomers using sulfur-based systems is very complex. Many reactive species are involved and the reaction mechanisms are not yet fully understood. However, it is acknowledged that the following steps successively take place: accelerator dissociation and recombination, complexation with a co-agent, formation of crosslinking precursors, formation of crosslinks and post-crosslinking

reactions [185, 186]. The sulfur crosslinking of NR in presence of CBS and ZnO is detailed in Appendix 2.1.

The exact mechanism is not fully understood yet. Many side-reactions may happen and the large number of reactive species in the medium may lead to a poor control over the vulcanized elastomer properties. Besides, mixed accelerator systems are commonly used, increasing therefore the complexity of the vulcanization process. In addition, rubber formulations usually include many additives such as antioxidants, plasticizers and fillers that can interact with the curing system. Hence, Lopez-Manchado et al [187] reported acceleration of NR curing in presence of octadecylamine and even faster effect upon addition of octadecylamine-modified organoclays.

Besides, Wu et al [188] observed that reduced graphene oxide (rGO) could fasten vulcanization kinetics of NR compounds. Hence, upon addition of 5 phr of rGO, the induction time (scorch time) was decreased from 7 min to 4 min, indicating that rGO induces a faster beginning of the crosslinking reaction. Besides, the curing rate was also reported to decrease from around 13 min to 10 min (t_{90}) at 5 phr loading of rGO, showing that rGO is able to fasten the reaction. To explain these phenomena, the authors investigated the effect of rGO on the melting temperature of sulfur. Hence, it is well-known that sulfur needs to melt to be able to diffuse into the rubber and to then react with unsaturated chains to form crosslinks. Upon addition of rGO (1/2 weight of sulfur), the melting peak of sulfur was reported to decrease from 97.8 °C to 90.4 °C (DSC). This lower melting temperature of sulfur suggest that the crosslinking reaction may start earlier, thus leading to a decreased induction time. Besides, they investigated the influence of rGO on the position of the exothermal peak of the curing system and observed a decrease from 163.8 °C to 123.5 °C upon addition of rGO, thus showing that rGO accelerates the crosslinking reaction [188]. They proposed a mechanism for graphene interaction with the curing system, as displayed in Scheme 11.



Scheme 11: Vulcanization reaction of NR in presence of reduced graphene oxide [188].

Scheme 11 suggests that sulfur may react with oxygen functional groups on rGO and that further reaction with the accelerator can take place. Then, crosslinks between rGO and polyisoprene chains may be formed, following the same mechanisms as sulfur crosslinking between two polyisoprene chains. rGO may thus interact with accelerated sulfur-based curing systems [188].

Accelerators and retarders

Accelerators are mainly used to increase the curing rate. However, they tend to induce a longer “scorch time”. This delay corresponds to the period before crosslinks start to form. It is believed to be due to the thermal stability of the accelerator which is related to the time necessary to decompose C-N bonds from CBS for example [189]. Another explanation, more generally accepted, is that exchange reactions between accelerator-derived intermediates may happen, thus leading to quenching of crosslinking precursors. When most of the accelerator is consumed, crosslinking reactions may start. When the scorch delay induced by accelerators is not long enough to ensure a safe processing, other additives, known as retarders, are added. They inhibit “pre-vulcanization” but have little effect on vulcanization rate and crosslinking density [185, 190].

2.3.1.4. Practical characterization of the crosslinking kinetics

Prior to the processing of an elastomer formulation, the characteristic times of the vulcanization reactions at the processing temperatures have to be determined to guarantee that the crosslinking of the material will not occur unexpectedly. The optimum curing time is determined from rheometric measurements such as the one showed in Figure 19.

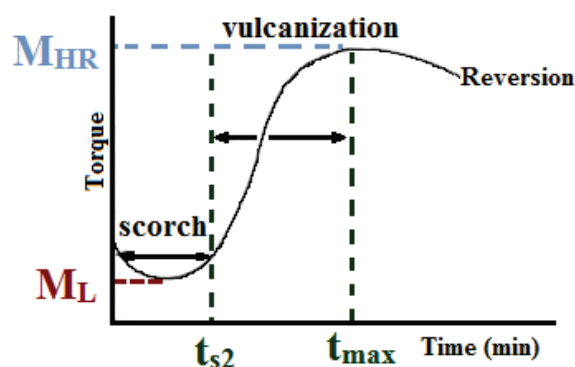


Figure 19: Rheometric curve of rubber vulcanization. M_L is the lowest torque, M_{HR} the maximum torque and t_{s2} the scorch time.

Figure 19 is a graph representing the torque, measured during an oscillatory rheological test, as a function of time. Special rotational rheometers are used, with closed cavities maintaining some pressure on the elastomer sample. The first part of the curve shows a decrease in torque due to softening of rubber with temperature. Then, the torque increases to a maximum followed by a plateau and finally decreases. The point labelled t_{s2} corresponds to the available time to process the compound before it starts curing at this temperature. Optimum vulcanization time is usually chosen as 90 to 98 % of the time necessary to reach the maximum torque (M_{HR}). After this maximum, rearrangement of polysulfide crosslinks may happen and may lead to a “reversion” which indicates a decrease in the crosslinking density (mostly for natural rubber).

2.3.1.5. Impact of crosslinking on the elastomer structure and properties

2.3.1.5.1. Crosslinking density

As for all crosslinked systems, elastomeric networks cannot be dissolved in a solvent. They can however swell and the amount of swelling can be used to determine the density of crosslinks in the network. Flory-Rehner equation (equation (1)) describes the mixing of a crosslinked polymer and a liquid.

$$-\left[\ln(1 - v_2) + v_2 + \chi_1 v_2^2\right] = V_1 n \left(v_2^{\frac{1}{3}} - \frac{v_2}{2}\right) \quad (1)$$

v_2 is the volume fraction of polymer in the swollen mass, χ_1 is the Flory-Huggins interaction parameter, V_1 is the molar volume of the solvent and n is the number of network chain segments bounded on both ends by crosslinks. It takes into consideration the heat of mixing, entropy changes due to the mixing of the polymer and the solvent and entropy changes due to the reduction of possible chain conformations because of the swelling of the polymer [191]. From this equation, it is possible to calculate the molecular weight between crosslinks (M_c) as well as the crosslinking density (v_e) of the sample (equation (2)).

$$v_e = \frac{1}{2 \times M_c} = \frac{-1}{2 \times \rho \times V_1} \times \left[\frac{\ln(1 - v_2) + v_2 + \chi_1 v_2^2}{v_2^{\frac{1}{3}} - \frac{v_2}{2}} \right] \quad (2)$$

Key parameters affecting rubber properties are the nature and density of crosslinks. Typical values for M_c in sulfur-crosslinked natural rubber are between 5 000 g/mol and 20 000 g/mol, corresponding to a crosslinking density of 1×10^{-4} mol/g and 2.5×10^{-5} mol/g, respectively (equivalent to 1.9×10^{-4} mol/cm³ and 4.8×10^{-5} mol/cm³, respectively for NR) [192–194].

The following section sums up the main properties of crosslinked polyisoprene and acrylonitrile-butadiene copolymer.

2.3.1.5.2. Properties of crosslinked IR

Crosslinked IR shows moderate tensile strength (29 MPa) and reaches high elongations at break (up to 850 %). Table 5 lists some cis-1,4-polyisoprene properties.

Property	Value
Density	920-1037 kg/m ³
Tensile strength	20-30 MPa
Elongation at break	660-1000 %
Shore A hardness	30-100
Minimum operating temperature range	-56 °C
Maximum operating temperature range	82 °C
Glass transition temperature	-73 °C
Specific heat capacity	1.830 J/(kg.K)
Thermal conductivity	0.15 W/(m.K)
Refractive index	1.52
Electrical resistivity	2.6.10 ¹⁸ Ω/cm

Table 5: Typical values of physical and mechanical properties of cis-1,4 IR [195, 196].

From Table 5, it appears that polyisoprene has limited thermal conductivity (0.15 W/m.K) and is not electrically conductive (resistivity reaches 2.6.10¹⁸ Ω/cm).

Synthetic polyisoprene shows rather similar properties to its natural counterpart. They both have good inherent tack (the ability of two uncured materials to resist separation after bringing their surfaces into contact for a short time under a light pressure) [197–199]. On the other hand they have poor oil, sunlight and ozone resistance as well as limited heat resistance [200]. Contrary to its natural counterpart, isoprene rubber enables better control of both the process and the properties of the final product since the high purity of IR (no proteins or mineral products) ensures uniform (however slower) vulcanization of the product as well as little variation between batches. Besides, synthetic polyisoprene and natural rubber are compatible and can thus be blended.

Polyisoprene main applications include tires, automotive parts, shock absorbers, gaskets, sporting equipment, adhesives, coatings as well as health care items such as gloves where the presence of allergens such as proteins can be undesirable.

2.3.1.5.3. Properties of crosslinked NBR

Crosslinked NBR is a common material in automotive industry due to good oil resistance.

Table 6 lists some of NBR properties.

Property	Value
Density	1000 kg/m ³
Tensile strength	20 MPa
Elongation at break	500 %
Shore A hardness	30-90
Minimum operating temperature range	-40 °C
Maximum operating temperature range	121 °C
Refractive index	1.52
Relative electric permittivity at 1MHz	2.5
Electrical resistivity	1.10 ¹⁵ Ω/cm

Table 6: Typical values of physical and mechanical properties of NBR [195, 196].

NBR can operate at rather more elevated temperatures than IR (121 °C and 82 °C, respectively) which is of significant interest for industrial applications.

NBR is widely used in automotive industry as gaskets, O-rings and housing in contact with oils. It is also a major health care rubber with a wide use for disposable gloves production.

2.3.2. Fillers

Most elastomers are reinforced by fillers to improve their performances such as their mechanical properties. Among these fillers, carbon black and silica are essential.

2.3.2.1. Carbon black

Carbon black is the main filler used in rubber industry. It is a form of amorphous carbon found in soots and largely produced by petrochemical industry.

Main industrial processes include thermal decomposition of natural gas (thermal black), or acetylene (acetylene black) and incomplete combustion of natural gas (tunnel black and furnace black) or coal tars (lamp black). Carbon blacks are mainly made of carbon with traces of oxygen, hydrogen, sulfur and mineral materials. Their structure is represented in Figure 20.

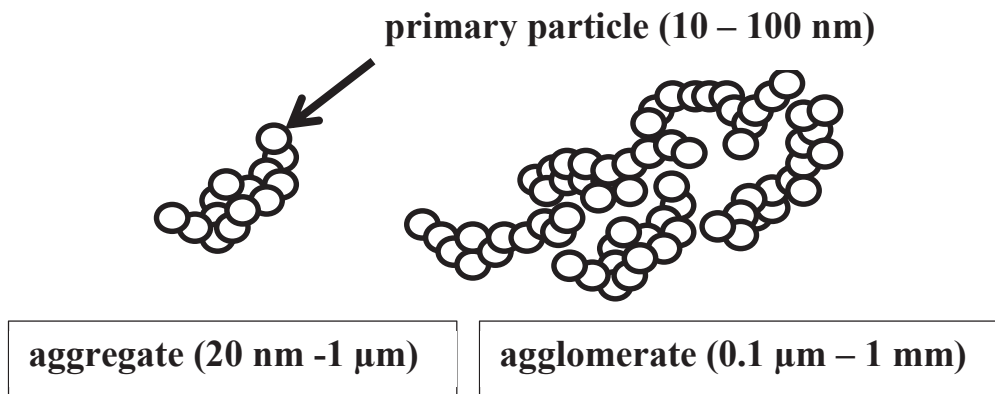


Figure 20: Carbon black structure.

Carbon black structure consists in elementary or primary particles (10 - 100 nm) stacked in unbreakable aggregates (20 nm - 1 μm) that are organized in agglomerates (0.1 - 1000 μm) and which can be further compacted into pellets (1 mm) [165]. The concept of “structure” refers to the extent to which aggregates form complex 3D arrangements [201–203]. Low structure carbon blacks usually contain around 30 primary particles per aggregate while high-structure carbon blacks aggregates can be constituted of up to 200 particles [204, 205].

Blacks are classified according to their preparation process, particle size and surface area as shown in Table 7.

Grade	ASTM number	Particle size range (nm)	Nitrogen specific area (m ² / g)	Iodine absorption number (g/kg)
Super abrasion furnace	N110	11-19	127	145
Intermediate SAF	N220	20-25	119	121
High abrasion furnace	N330	26-30	78	82
Fine furnace	400 series	31-39	-	-
Fast extruding furnace	N550	40-49	40	43
High modulus furnace	N660	49-60	35	36
Semi reinforcing furnace	N772	60-100	32	30
Fine thermal	800 series	100-200	-	-
Medium thermal	N990	200-500	8	-

Table 7: ASTM carbon blacks classification according to their specific surface areas and particle size [206].

Carbon blacks classification is based on their structure as well as their manufacturing process. ASTM standards provide a classification of carbon blacks through a letter and a number (ASTM D1765). The first digit is linked to the particle size and the second refers to the structure of the carbon black (the higher the number, the more structured the carbon black is) [164]. Carbon blacks of “100” series possess small primary particle sizes and a high specific surface area while carbon blacks from “900” series possess the largest particle sizes and the smallest specific surface area. Another feature is the shape of the aggregates that can be spheroidal, linear, ellipsoidal or branched. The reinforcing ability of carbon blacks is strongly linked to these structural aspects.

After mixing with carbon black (without crosslinking), the elastomeric matrix cannot be fully dissolved in a good solvent, leaving a highly swollen rubber-filler gel. This solid fraction is referred to as “bound rubber” and it evidences the presence of strong carbon black-elastomer interactions [204, 207]. It depends on filler loading, its structure and specific surface area, physico-chemical surface activity as well as processing parameters [208]. A pictorial description of bound rubber in carbon black-filled rubber compounds has been drawn by Leblanc [204] (Figure 21).

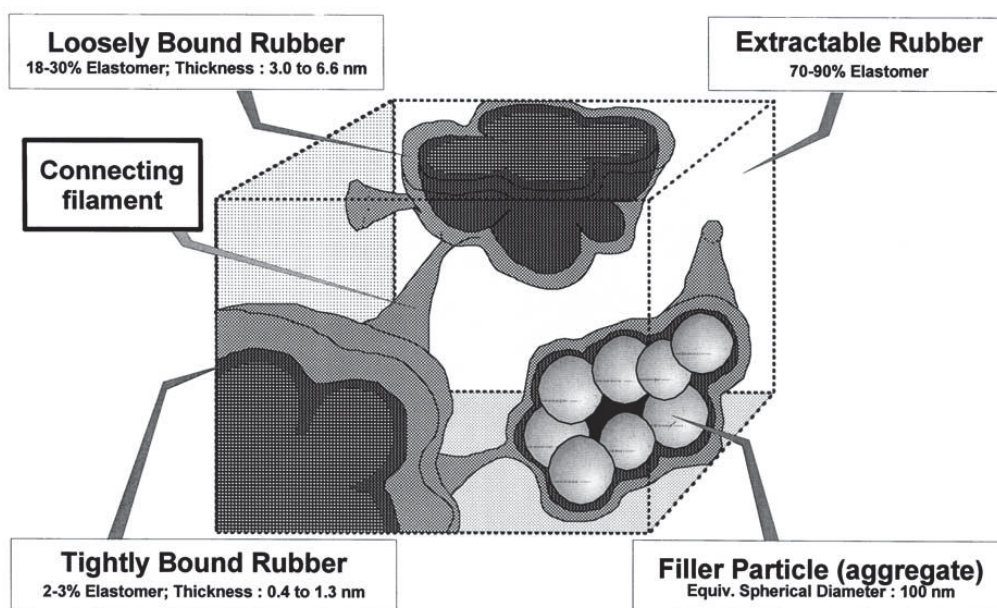


Figure 21: Representation of bound rubber in carbon black-elastomer compounds [204].

In this representation, carbon black aggregates are covered by tightly bound rubber (2-3 %), loosely bound rubber that interconnects filler aggregates (18-30 %) and free elastomer (70-90 %) that can be extracted with a good solvent, even in the uncured state. Carbon black-elastomer compounds thus consist in complex filler-elastomer networks in which interparticle interactions occur in different manners, including bridging by the polymer. This prevents good dispersion of agglomerates and thus causes poorly dispersed blends [204].

It is generally admitted that spontaneous bonds between carbon black and the elastomer consist in covalent as well as non-covalent interactions [204, 209]. Carbon black is reported to contain a variety of functional groups on its surface such as esters, hydroxyls, quinones, ketones, phenols, etc [210]. These groups are believed to be responsible for carbon black-elastomer bonding. Two hypotheses explain spontaneous generation of these bonds. First, during mixing, free radicals are formed and may react with carbon black surface to lead to the formation of bound rubber. Then, during heating (for crosslinking) polysulfide bonds may form between carbon black and the elastomer chains. In addition, van der Waals bonds are reported to occur. Filler-matrix interactions enable reinforcement of the matrix while filler-filler interactions lead to the formation of a strong carbon black network [211, 212]. When heated above 3000 °C, graphitization of carbon black occurs and functional groups are removed. The filler loses its reinforcing ability thus showing the role of strong carbon-black-elastomer interactions through functional groups on carbon black surface.

2.3.2.2. Silica

Silica (fumed or precipitated) is also a common filler in rubbers. It is used mainly for tire applications. Silica is made of spherical particles from 5 to 100 nm which arrange themselves into aggregates from 100 to 500 nm, due to physico-chemical interactions. These aggregates spontaneously form agglomerates from 1 to 40 μm because of van der Waals forces and hydrogen bonding. Silica possesses silanol functional groups on its surface which make it hydrophilic thus leading to poor spontaneous interaction with the rubber matrix and thus bad dispersion. To overcome this problem, a coupling agent is often used to favor elastomer-silica interfacial bonding. Bifunctional organosilanes containing a trialkoxysilane group allow covalent linkages with silica through hydrolysis-condensation reactions

[213]. Figure 22 shows the chemical structure of a common silane coupling agent used in rubber industry.

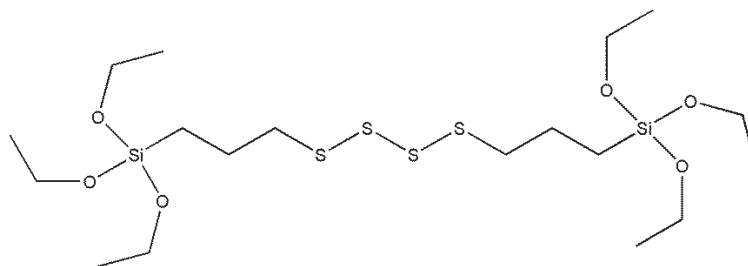


Figure 22: Chemical structure of 3-mercaptopropyltriethoxysilane (also known as TEPST, bisTESPT or Si69).

Such molecules enable a decrease of silica surface energy and thus lower filler-filler interactions to favor filler-matrix interactions.

2.3.2.3. Other fillers

Other fillers such as kaolin, sodium carbonates or inert charges such as talc are often added in rubber mixes. Their effect on the elastomer depends upon their aspect ratio, surface activity and morphology. Nanoclays such as montmorillonite also bring interesting properties mainly in terms of permeability reduction. More recently, carbonaceous nanocharges such as carbon nanotubes (CNTs) have appeared in rubber mixes to produce high-performance, thermally and electrically conductive elastomers [214]. Nanosized fillers offer the opportunity to have strong impact on the properties of the composites even at very low loading, which leads to light-weight composites, relatively low costs and easy processing. They also have a high specific surface area thus creating a large filler-matrix interfacial area which should promote efficient load transfer from the matrix to the filler [215]. These nanocharges however tend to aggregate and thus experimental results often do not reach expectations. This new category of fillers opens the way for new research areas.

2.3.2.4. Filler dispersion: mechanisms and difficulties

To be efficient, fillers need to be well dispersed in the elastomer and so they require good filler matrix compatibility. They need to interact with the rubber matrix through physical and or chemical linkages. Those interactions depend upon various parameters such as filler morphology, size and surface activity. To be well reinforcing, they need to be of small size to form a colloidal suspension within the matrix [216]. It is known that large particles ($> 5 \mu\text{m}$) tend to degrade elastomer properties, creating local heterogeneities that are often the starting points for cracks. Smaller particles (between 1 and 5 μm) are reported to be compatible with elastomers without being able to strongly reinforce the material. Thus, particle sizes smaller than 1 μm are often looked for [209]. A well-dispersed nanosized filler would be of great interest since it would provide a large interfacial area and would lower the average distance between particles in a composite. These properties allow for a lower loading and so enable to reduce weight and keep high elasticity [217].

Elastomers are highly viscous materials that need to be well mixed to be able to obtain an adequate dispersion of the filler in the matrix, in order to reach the desired properties for the final compound.

This means that through the mixing process large agglomerates (up to 1 mm for carbon black) need to be broken [209]. Rubber mixing is often reported to occur in three main stages: incorporation of the

additives, a dispersive mixing step and a distributive mixing step [218, 219]. Figure 23 schematically shows the difference between a dispersive and a distributive mixing for carbon black filler.

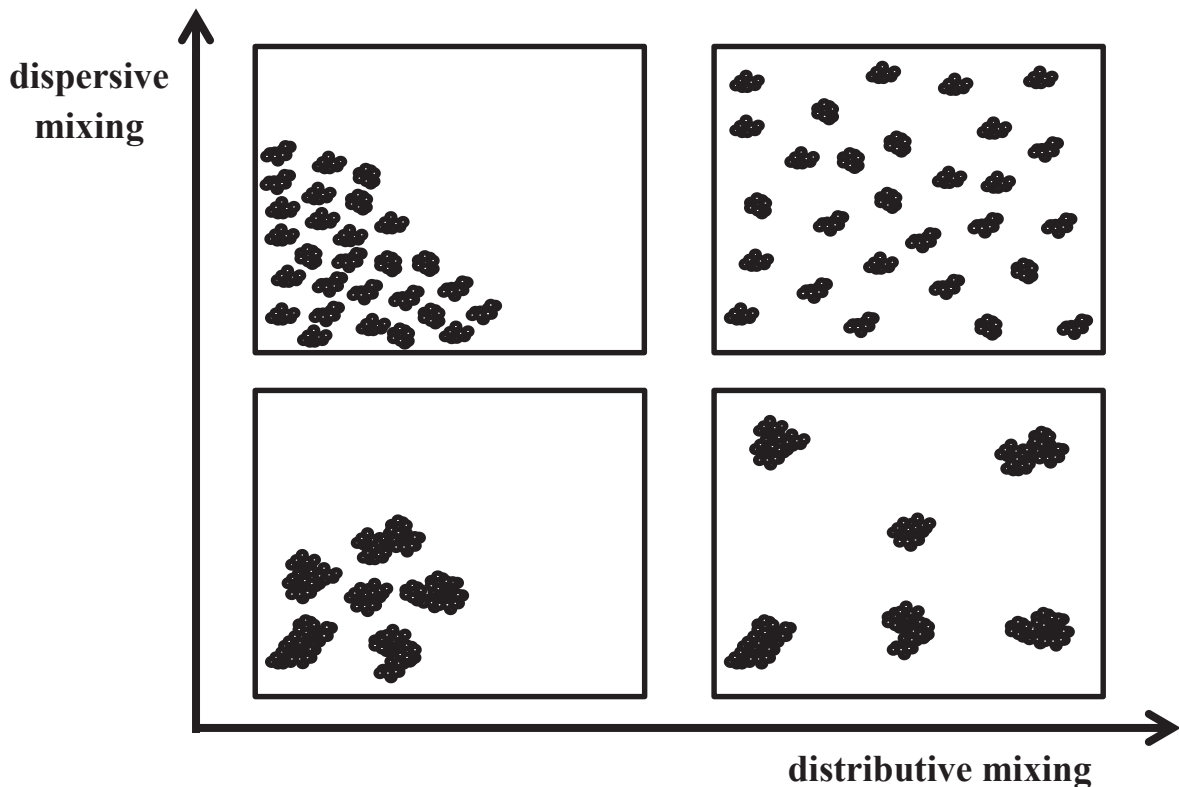


Figure 23: Dispersive and distributive mixing processes.

During the dispersive step, large components undergo size reduction by separation through erosion and rupture of the agglomerates in smaller fragments that are then separated in the matrix [220, 221]. The last step distributes the small fragments in the matrix without affecting their physical form [222]. These two last phases however do not necessarily happen one after another but most likely happen rather simultaneously.

Dispersion mechanisms of carbon black agglomerates are reported to occur through (i) rupture, a sudden fracture of the pellets into a few fragments and (ii) erosion, a progressive mechanism where small fragments are continuously detached from the periphery of the agglomerate [220, 221, 223]. Rupture occurs above a critical shear stress where hydrodynamic forces exceed cohesive forces, which depend on the carbon black pellet size. Erosion, on the contrary, proceeds through the detachment of a fixed eroded volume per strain unit and is driven by the applied shear stress and strain. It is a local mechanism which rate depends on the carbon black properties. Hence, faster erosion has been reported for carbon blacks with high structures [220].

Lamellar nanofillers dispersion occurs through different mechanisms. Ideal dispersion of platelets-like fillers requires complete exfoliation, which means that all layers should be apart from each other. The main problem to achieve such dispersion, is the strong interlayer interactions that need to be overcome in order to separate the layers. Little work on graphite dispersion mechanisms has been performed, most studies focusing on nanocomposite properties. However, clays such as Montmorillonite (MMT) have attracted much research attention over the past few years and the

exfoliation mechanisms of these materials have been studied. A major breakthrough in MMT dispersion was the development of intercalation techniques to enable a reduction in the interlayer interactions and thus to facilitate exfoliation. Another main development in MMT exfoliation in a polymer matrix was the work on MMT surface modification to lower surface energy and to enhance filler-matrix interactions [224].

Less work has been reported on graphite nanoplatelets dispersion. However, the similarities in morphology with MMT led many groups to apply similar procedures. The use of intercalated and expanded compounds has thus been reported. Besides, chemical modification of the surface has been widely performed and described in the literature to decrease the strong π - π interactions between layers [225].

Figure 24 shows a schematic representation of stacked, expanded and exfoliated graphite platelets in an elastomeric matrix.

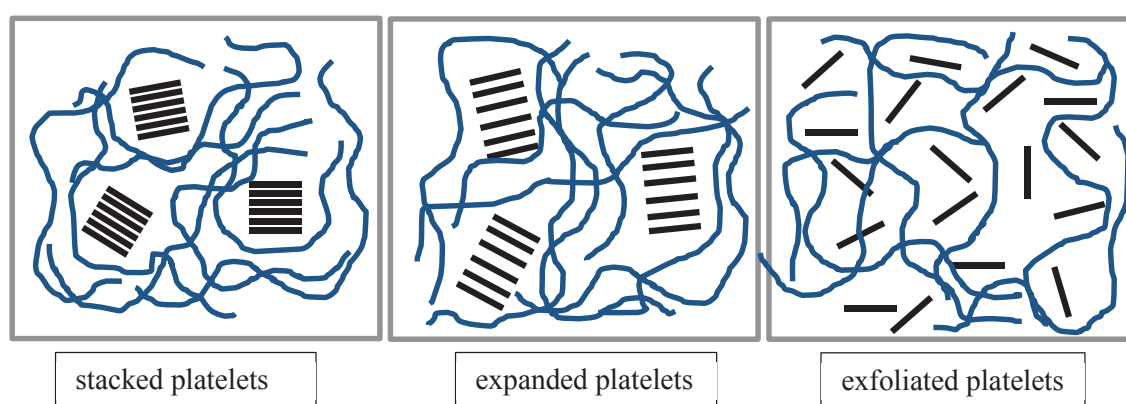


Figure 24: Representation of the dispersion of several graphite structures in an elastomer matrix.

Exfoliation of graphite nanoplatelets into an elastomer is desired to enhance the properties of the final material. Most exfoliation processes are performed in suspension rather than during bulk processing, during which, high shear is reported to break the platelets rather than exfoliate them [225].

2.3.3. Rubber mixing techniques

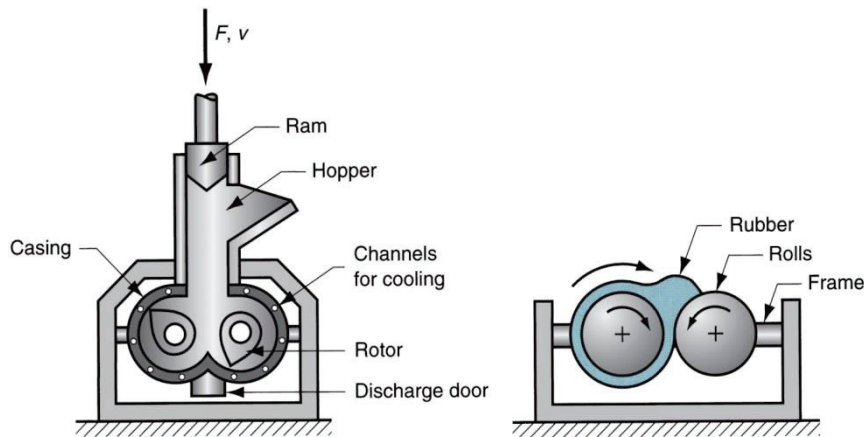
2.3.3.1. Solution blending

Solution blending, which consists in dissolving the elastomer in an appropriate solvent and adding all fillers and additives in the mixture, is very common for research purposes [135, 226–228]. It is often observed to lead to homogeneous dispersion of the fillers, added in suspension in a solvent in the dissolved rubber. However it requires long time (several hours) to dissolve the rubber and the use of large quantities of toxic organic solvents such as toluene which have to be fully evaporated to recover the solid compound. This is not desirable in industry. Besides, a less described process is the synthesis of the elastomer in presence of the fillers [135]. This is however mainly applicable for research studies. Other techniques such as in situ polymerization have also been reported and will not be detailed here.

2.3.3.2. Bulk mixing

Industrially, rubber is mostly processed through so-called “direct blending”. Compounding is carried out in an internal mixer consisting in a bi-cylindrical chamber closed by a ram and containing tangential or interpenetrating rotors. In a second step, the mix is discharged on a two-roll mill for further

homogenization and cooling. Schematic drawings of the processing equipment are shown in Scheme 12.



Scheme 12: Representation of an internal mixer and a two-roll mill.

In an internal mixer, gum and additives are fed from the hopper and the ram comes down to close the chamber containing the rotors [229]. The mix is then discharged at the bottom of the equipment. In a two-roll mill, rubber sticks to one roll and forms a bead between the two counter-rotative rolls. A sheet can be formed, which will then be transformed in bands or preforms to feed the process which will give its final shape to the product, prior to crosslinking. However, this process is often reported to lead to less homogeneous dispersion and distribution of graphite nanofillers inside an elastomeric matrix than solution-blending technique. However, high shear forces usually applied to overcome the high viscosity of the elastomeric matrix can lead to the breakage of the graphene platelets [225].

2.3.3.3. Latex compounding

Rubber mixing in latex phase is also commonly used in the industry. Natural rubber exists naturally in latex form (30-40 wt% solid content) and NBR can be synthesized in latex form. Through the use of appropriate equipment such as a high-shear mixer, it is possible to disperse fillers and other additives in an elastomeric matrix in the aqueous phase. At a laboratory scale it is often done by adding an aqueous suspension of the filler in a latex under mechanical stirring, sonication or the use of a high-shear mixer. At an industrial scale, high speed units are used and do not always require mechanical stirring of the latex with the filler, as shown in Figure 25 [230].

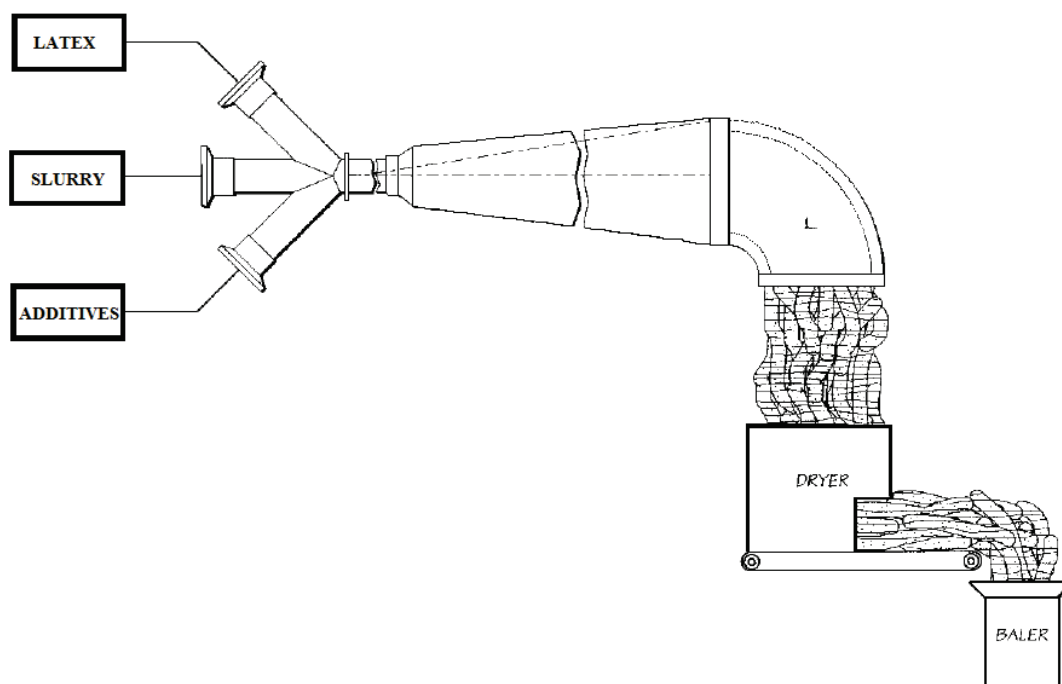


Figure 25: Representation of latex processing.

A Cabot Corporation patent describes a process to mix an elastomer latex with carbon black and additives [230]. First, an aqueous suspension of carbon black (“slurry”) is prepared and homogenized in several mixing units. A latex is slowly fed ($1.5 \text{ m}\cdot\text{s}^{-1}$) in the coagulum reactor at about atmospheric pressure. Additives are discharged in the latex, then the carbon black slurry is pushed into this medium at high speed ($150 \text{ m}\cdot\text{s}^{-1}$) and under high pressure (70 bars). Spontaneous coagulation of the latex occurs. In many processes, addition of an aqueous acid or solution salts is often reported to be necessary to coagulate the latex mix. In a last step, the coagulum is dried in an extruder to remove water and it is finally compacted into bales.

Other processes involving coagulation of the latex after shaping the product (“dipping process” for example) are also common in the industry, for gloves manufacturing for example.

2.4. Conclusion

In this section, common rubber processing techniques as well as dispersion challenges of fillers have been reported. The wide industrial use of carbon black has triggered a lot of research on dispersion mechanisms and optimization of dispersing equipment. However, with the increasing presence of nanofillers on the market, new challenges have emerged. Hence, platelet-like materials such as graphite nanoplatelets offer the opportunity to strongly enhance properties of elastomeric matrices. However, π -stacking leads to strong interactions and aggregation between fillers, so new means to reduce these interactions, such as chemical functionalization have to be developed.

3. Properties of elastomer composites containing graphite / graphene

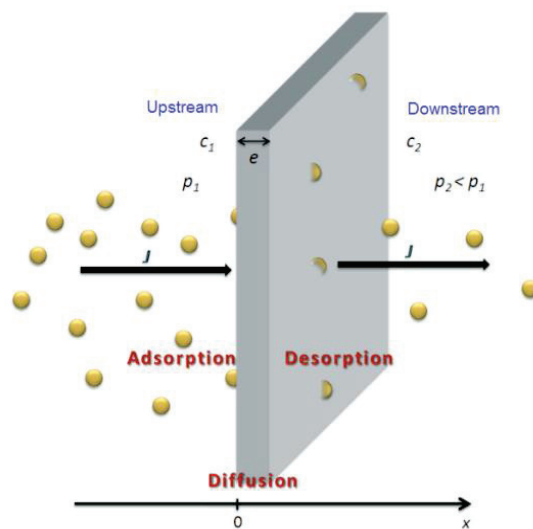
Elastomers are materials showing exceptional elasticity and are used for numerous applications. However, their low tensile strength as well as their insulating behavior can be limiting. The incorporation of graphitic nanofillers can help and improve drastically several properties. With its high Young's modulus, high electrical and thermal conductivities, graphene seems an ideal filler to effectively tune elastomers properties. With low graphene loadings, most elasticity properties of rubbers could be preserved while increasing or adding new properties to the composites to enable new applications. The following section will present some of the effects of graphene incorporation into elastomers and will highlight the key parameters to effectively monitor the changes.

3.1. Barrier properties

3.1.1. Permeability

Rubber nanocomposites can be of great interest for sealing and tightness applications for example in tires, buildings and hydraulic systems. Elastomers contain a large free volume and so are highly permeable to most gases.

Transport properties of small molecules such as gases through elastomers usually occur in three main steps: (i) adsorption of molecules onto the upstream side of the polymer membrane, (ii) dissolution and diffusion of the permeant inside the matrix and (iii) desorption of gas molecules from the downstream side of the membrane (Scheme 13) [231, 232].



Scheme 13: Steps in molecular transport through a membrane [233].

Transport properties thus depend on the affinity of the diffusion molecule for the elastomer membrane as well as the mobility of the permeant inside the matrix. Adsorption and desorption of the gas molecules onto and from the surface are considered very fast and the rate-limiting step in transport of gas molecules through a matrix is the dissolution-diffusion step [234].

The driving force for the diffusion of gas molecules into an elastomer is the presence of a concentration gradient in gas molecules between the two surfaces of an elastomer membrane. Gas molecules diffuse from areas of high concentrations to areas of low concentration until equilibrium is reached. The

diffusion phenomenon is often described by Fick's law (3), describing the linear diffusion of a molecule through a membrane [231, 235].

$$J = -D \frac{\partial c}{\partial x} \quad (3)$$

where J is the flow in diffusing molecules by unit of time and area ($\text{cm}^3_{\text{STP}} \cdot \text{cm}^{-2} \cdot \text{s}^{-1}$), c is the local volume concentration in diffusing molecules (cm^3_{STP}) and D is the diffusion coefficient ($\text{cm}^2 \cdot \text{s}^{-1}$) with STP standing for standard temperature and pressure.

In a Fickian diffusion process, the main parameters affecting transport properties of small molecules through a membrane are related according to equation (4).

$$P = D \times S \quad (4)$$

where P is the permeability coefficient ($\text{cm}^3_{\text{STP}} \cdot \text{cm} \cdot \text{cm}^2 \cdot \text{s} \cdot \text{cm}_{\text{Hg}}$ or also expressed in $\text{mol} \cdot \text{m} \cdot \text{m}^2 \cdot \text{s}^{-1} \cdot \text{Pa}^{-1}$), D , the diffusion coefficient ($\text{cm}^2 \cdot \text{s}^{-1}$) and S , the solubility coefficient ($\text{cm}^3_{\text{STP}} \cdot \text{cm}^{-3} \cdot \text{cm}_{\text{Hg}}$).

The permeability coefficient P characterizes the ability of the gas molecules to go through an elastomeric membrane when a pressure gradient is applied (5).

$$P = \frac{e \times J}{(p_1 - p_2)} \quad (5)$$

where e is the thickness (cm, considered constant), p_1 is the upstream partial pressure (cm_{Hg}) and p_2 is the downstream partial pressure (cm_{Hg}).

The diffusion coefficient characterizes the ability of the permeant to go through the matrix and the solubility coefficient is related to the affinity of the permeant for the matrix.

Several factors influence transport of gas molecules through an elastomeric membrane such as (i) environmental factors such as temperature, pressure, concentration, (ii) intrinsic properties of the elastomer such as free volume and glass transition temperature (related to the chain mobility), (iii) the presence of plasticizers and (iv) the affinity of gas molecules for the elastomer [232–234].

3.1.2. Permeability mechanisms and models in nanocomposites

The addition of impermeable fillers can enhance the barrier properties of the rubber matrix. Defect-free graphene is impermeable to all gases including helium and it is thus an ideal candidate to effectively reduce permeability of rubber composites [135, 225, 227, 236–241]. While graphene derivatives are not fully impermeable to gases, they however retain elevated barrier properties to most gases. For example, GO-PDMS barrier properties towards nitrogen, oxygen, hydrogen, methane and carbon dioxide gases were investigated by Ha et al [242] who reported a 35 % decrease in permeability of the composites towards these gases at 1 wt% GO content in a PDMS matrix.

Many parameters such as filler shape, size, orientation and dispersion in the host matrix play a significant role in barrier properties of the composites. Platelet-like nanofillers are the most promising since they are able to form a tortuous path to effectively slow down the diffusion of gas molecules inside the material, as illustrated in Figure 26.

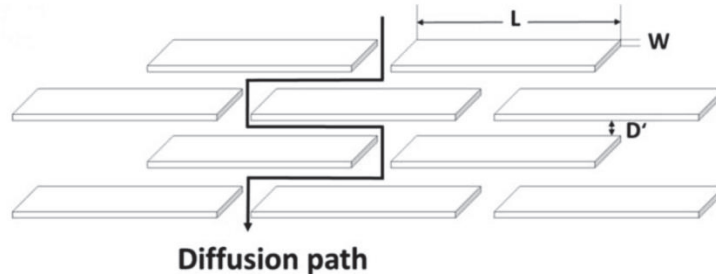


Figure 26: Gas diffusion path inside the material [3].

Hence, at 5 phr loading in styrene-butadiene rubber (SBR), Song et al [236] reported a 35 % decrease in permeability of composites containing low defect graphene (exhibiting a platelet morphology) as compared to composites with carbon black, whose aspect ratio is much lower [236].

Several models can be used to describe permeability as a function of the filler content [3, 228, 243–248]. Nielsen’s model [244] is the most common one and it is also referred to as “classic tortuosity model”. It assumes that impermeable flakes with a certain aspect ratio associated to their cross-section are uniformly dispersed in a permeable matrix [3]. Nielsen’s equation can be written as follows:

$$\frac{P}{P_0} = \frac{1 - \Phi}{1 + \tau} \quad (6)$$

where P is the gas permeability of the composite, P_0 the gas permeability of the pure polymer matrix, Φ the volume fraction of the filler and τ the tortuosity factor. P/P_0 is called the relative permeability. This model assumes random orientation of the fillers in the matrix, ignoring the significantly different behavior of aligned platelets.

According to the model used, the tortuosity factor will have a different expression. In Nielsen’s classical model, it is expressed as follows:

$$\tau = \frac{\alpha}{2} \Phi \quad (7)$$

with α the aspect ratio of the filler [249]. Cussler [248] proposed a model similar to Nielsen’s in which two different tortuosity factors were added: one for random alignment of the fillers and another one for perfectly aligned fillers [228, 248]. Another attempt to include filler orientation in the composite has been done by Bharadwaj [245] who included S' , an orientation parameter equal to a value of -0.5 for parallel orientation (no tortuosity), 0 for random orientation and 1 for perpendicular alignment of the platelets in the material, as shown in Figure 27.

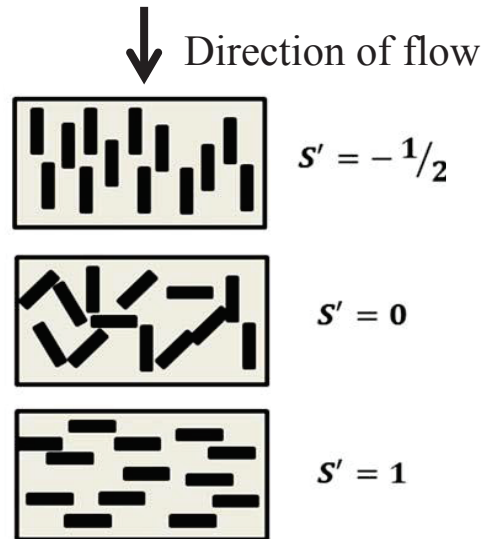


Figure 27: Schematic representation of the orientation parameter.

Bharadwaj's equation with tortuosity factor can then be expressed as follows:

$$\frac{P}{P_0} = \frac{1 - \phi}{1 + \frac{\alpha}{2} \phi \frac{2}{3} (S' + \frac{1}{2}) \phi} \quad (8)$$

It is very similar to Nielsen's model but is more versatile as it takes into account more parameters to fit the system. From Figure 27, it is suggested that alignment of the platelets perpendicular to the flow will create greater tortuosity and thus will increase the diffusion length of the permeant in the composite.

Other models such as Gusev-Lusti [246], Fredrickson and Bicerano [247] also exist but they will not be extensively presented here. It was shown by Dunkerley et al [249] that most models provide similar results at low filler content (< 10 vol%). With most studies on graphitic fillers being performed at low loadings (under 10 vol%), any of these models can be used.

3.1.3. Influence of filler size, shape and aspect ratio.

A high aspect ratio of the filler is of significant importance since large fillers will divert more the diffusion path and so will increase the total path length, as shown in Figure 26. This leads to reduced permeability of the material. It was shown by Ozbas et al [227] that increased surface area of thermally-reduced graphene oxide flakes (referred to as "functionalized graphene sheets", FGS) led to more efficient barrier properties of PDMS composites as displayed in Figure 28.

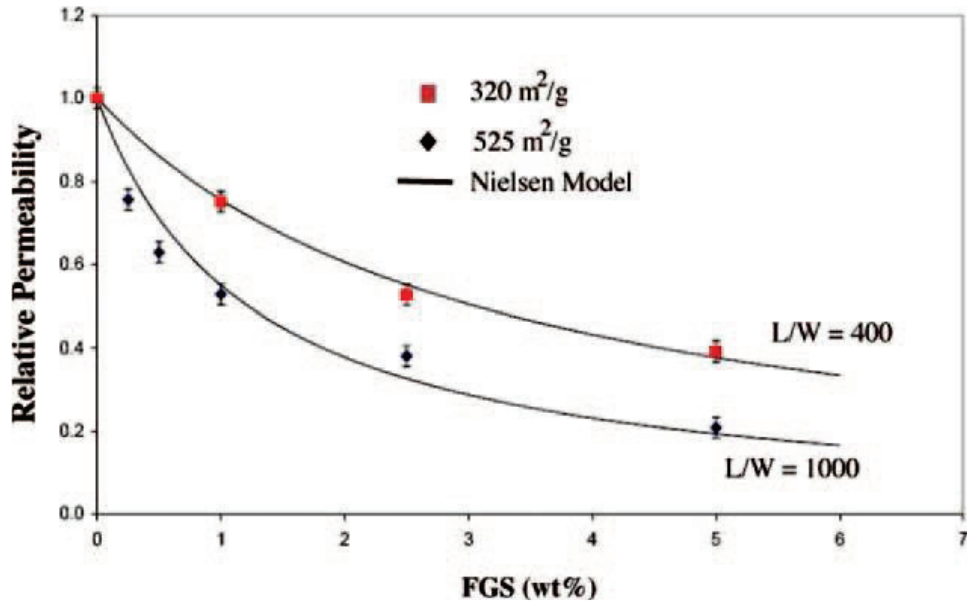


Figure 28: Reduction in air permeability as a function of functionalized graphite flakes (FGS) loading in PDMS (as compared to neat PDMS). Solid lines represent Nielsen's model predictions [227]. L/W is the aspect ratio (length/width) of the filler particles in the sample.

The FGS sample with the highest aspect ratio provides the lowest permeability. These plots show the decrease in air permeability of PDMS-FGS composites with increasing filler loading, with FGS fillers exhibiting different specific surface area, associated with different aspect ratios of the particles (L/W) [227]. 60 % and 80 % decrease in air permeability were reached for FGS exhibiting a specific surface area of 320 m²/g and 525 m²/g, respectively, at 5 wt% loading in PDMS. This emphasizes the significant effect of filler aspect ratio on the barrier properties of the corresponding composites. Besides, Ozbas et al [227] observed a fine fit of Nielsen's curve with their experimental values.

Moreover, Yoo et al [3] investigated the effect of aspect ratio, orientation and aggregation of graphene or graphene oxide sheets over the oxygen permeability. The calculations confirmed that a high aspect ratio is preferred to decrease permeability of the composites, as shown in Figure 29 a. At 1 vol% of graphene-based filler, by increasing the aspect ratio of the platelets (α) from 30 to 3000, the relative permeability of the composites with respect to the neat matrix decreased by 10 % and 90 %, respectively, which shows the major effect of filler aspect ratio over permeation properties.

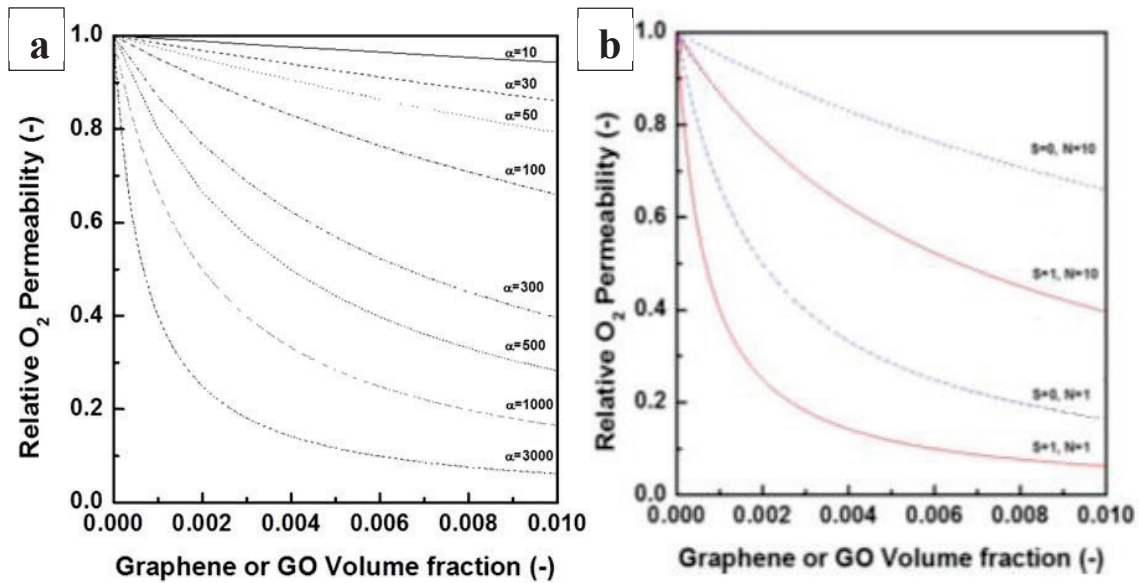


Figure 29: a) Effect of graphene nanosheets aspect ratio on the O₂ permeability of a polymer matrix and b) influence of the graphene nanosheets orientation and stacking on O₂ permeability. Adapted from [3].

Figure 29 b shows the decrease in permeability of the composites as a function of graphene loading for various numbers of layers. For perpendicular orientation ($S'=1$), a single layer of graphene will provide a decrease in permeability greater than 90 % while for a stack of 10 layers (lower aspect ratio), a value of only 60 % can be reached. While well exfoliated platelets create a very tortuous path, stacks of nanosheets will significantly reduce the diffusion path. At the same volume fraction, the probability for a gas molecule to meet a graphene nanosheet will be lowered if the stacking parameter (N , number of layers) is high [3].

3.1.4. Influence of filler orientation

The influence of filler orientation on the permeability of the composites was also computed by Yoo et al [3]. Perpendicular orientation of the platelets ($S'=1$) showed superior permeability reduction than the randomly-oriented ones, as displayed in Figure 29 b. The former configuration led to 60 % decrease in oxygen permeability whereas the latter only reached 35 % reduction for 10 layer-nanosheets at 1 vol% loading, as compared to the pure polymer. The main factor in improving barrier properties is then tortuosity. For perpendicular orientation ($S'=1$), tortuosity is maximized and, therefore, this configuration is the most effective one in increasing the diffusion path of gas molecules inside the composite.

These studies have shown the effect of filler shape, size and aspect ratio, on permeability. Besides, filler orientation has proven to be of significant influence on permeability of the composites. This feature is much related to processing. Several research groups thus investigated the influence of processing conditions, and composites morphologies, on barrier properties of elastomer composites.

3.1.5. Influence of processing and functionalization

Kim et al [135] showed that the same thermally reduced graphene oxide (TRG) filler, dispersed according to three different routes, resulted in three distinct behaviors in permeation. The main permeation results of their study are shown in Figure 30.

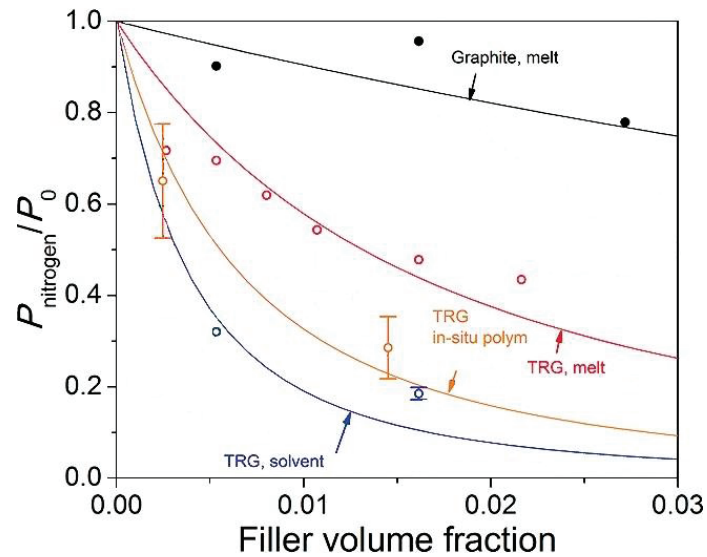


Figure 30: N_2 permeability of TPU composites. Solid lines are predictions according to the model of Lape et al [228]. Adapted from [135].

Figure 30 shows a decrease in relative permeability to nitrogen gas as a function of the volume fraction of several graphitic fillers in TPU composites. The influence of processing can be seen. Hence, composites with 1.6 vol% of TRG prepared through direct melt mixing led to a 50 % decrease in nitrogen gas permeability while in situ polymerized composites induced a 70 % decrease. Solution-blended samples at the same loading were even more efficient (up to 80 % permeability reduction) [135].

In addition, the effects of surface functionalization and processing route obviously result in variations of the state of dispersion of the filler, which is a key factor regarding the composite properties. Thus, morphologies of the composites provide some understanding of the permeability results. Figure 31 shows TEM images of TPU composites containing graphitic fillers.

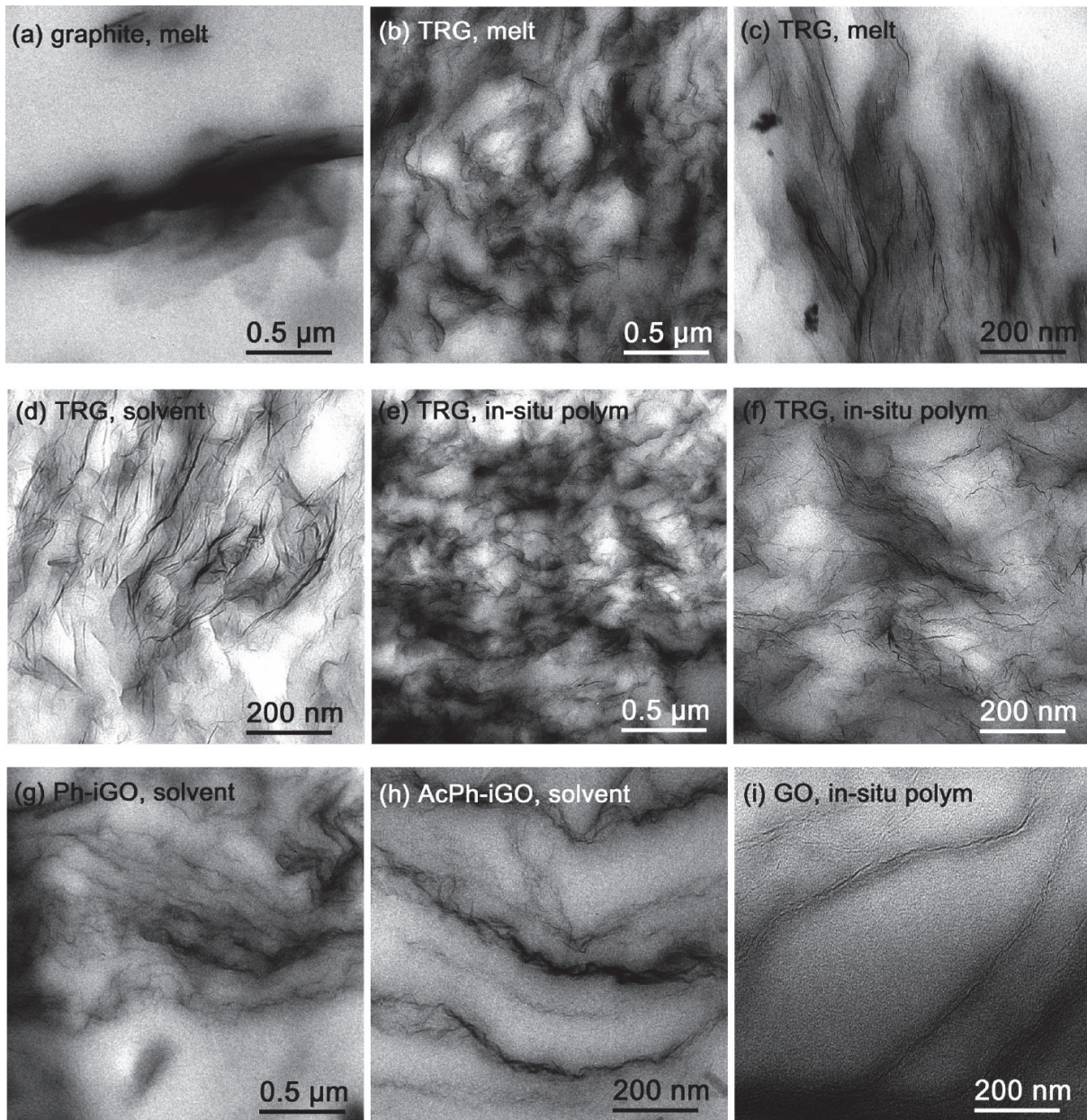


Figure 31: TEM micrographs of TPU composites filled with (a) 5 wt% (2.7 vol%) graphite, (b,c) 3 wt% (1.6 vol%) melt-processed TRG, (d) 3 wt% (1.6 vol%) solution blended TRG (e,f) 3 wt% (1.6 vol%) in situ polymerized TRG, (g) 3 wt% (1.6 vol%) phenyl isocyanate-modified GO, (h) 3 wt% (1.6 vol%) acetyl phenyl isocyanate-modified GO and (i) 2.8 wt% (1.5 vol%) in situ polymerized GO.

Figure 31 a shows the morphology of melt-compounded composites containing graphite aggregates of at least 1.5 μm in length while the materials containing TRG (Figure 31 b and c) display a rather homogeneous distribution. TRG particles incorporated through solution blending (Figure 31 d) or in situ polymerization (Figure 31 e and f) look slightly more homogeneously distributed in the matrix. The performance of the composite in permeation seems to be directly related to the state of dispersion. Indeed, solution-blended TRG (Figure 31 d) are more homogeneously dispersed in the TPU matrix and lead to better barrier properties of the composites.

In addition, the effect of surface functionalization was investigated by comparing morphologies of composites containing pristine or modified GO. Images of GO (Figure 31 i) and modified GO composites (Figure 31 g and h) reveal thinner aggregates than TRG and suggest interconnection between fillers

[135]. Phenylisocyanate and acetylphenyl isocyanate-functionalized GO appear to be rather homogeneously dispersed in the matrix. They also display the largest decrease of permeability (-98 % and -94 %, respectively). Thanks to its effect on dispersion, functionalization can thus be an efficient way to enhance barrier properties of the composites. Such large decreases in permeability are not widely reported in the literature for elastomer-based composites but it illustrates anyhow a tendency.

However, surprisingly, homogeneous dispersion of the filler in the matrix does not always lead to the best performance in permeation. Indeed, Yan et al [237] have reported that a specifically segregated morphology obtained by the latex compounding method (LCM) could lead to improved barrier efficiency as compared to homogeneously dispersed and aligned platelets. Thus, Yan et al [237] prepared natural rubber composites containing 4 phr of reduced graphene oxide through a latex co-coagulation method. Some samples were obtained directly from compression molding the coagulated material while others were homogenized on a two-roll mill prior to compression molding. Figure 32 shows the morphologies obtained with the two compounding methods.

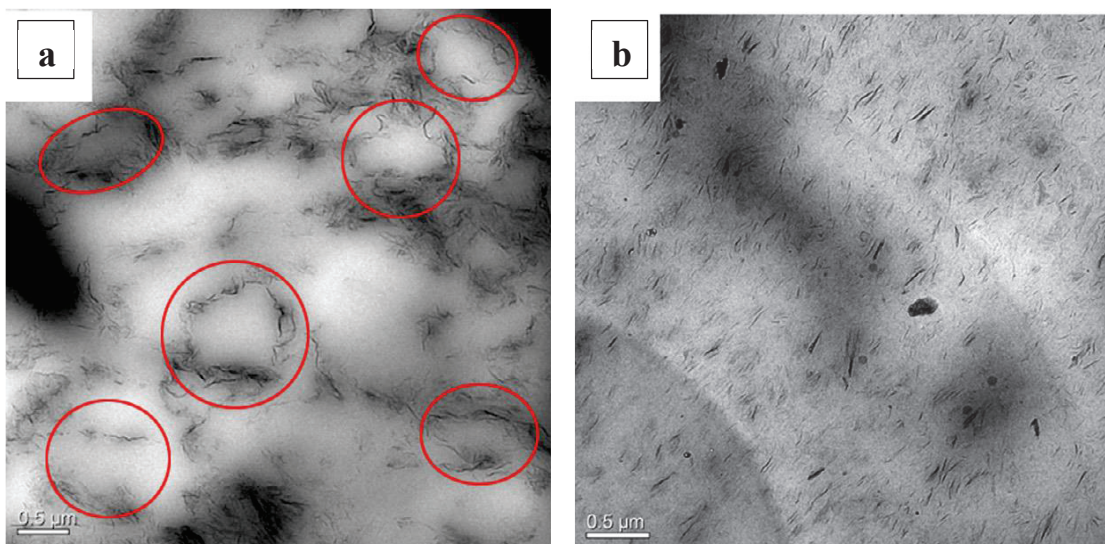


Figure 32: Composites containing 4 phr of reduced graphene oxide in natural rubber (NR) matrix prepared through two methods: a) latex compounding, and b) homogenization in a two-roll mill [237].

While Figure 32 a shows a segregated morphology, with the nanosheets being localized at the interface, between latex particles, Figure 32 b displays a more homogeneous dispersion in the rubber matrix. Oxygen permeability of the composites was also investigated (Figure 33).

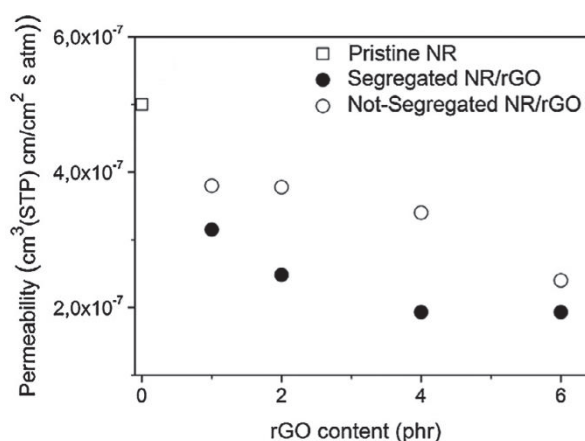


Figure 33: Oxygen permeability of NR-rGO composites as a function of rGO loading for the two types of morphologies.

Both morphologies exhibited increased barrier properties of the composites in comparison with pristine natural rubber but samples with a segregated structure showed greater permeability reduction as compared to homogenized samples (70 % towards 30 % at 4 phr loading). These results indicate that the connected network formed by rGO platelets is more efficient in diverting the permeant path than homogeneously dispersed platelets. The segregated morphology ensures a smaller inter-particle distance than homogeneous distribution, thus creating barrier zones able to divert and slow down the permeant diffusion to a greater extent. Optimum dispersion for improvement of barrier properties is thus very dependent on processing conditions.

Other impermeable fillers with appropriate platelet morphology such as clays have also been used to increase barrier properties of polymers. However, graphene and its derivatives have a significant advantage over clays as they usually perform better in permeability reduction while preserving good mechanical properties of the composites and increased thermal and electrical conductivity [3, 243, 250, 251].

A short literature review regarding permeation properties of graphitic fillers-based elastomer composites is available in Appendix 2.2.

3.2. Mechanical properties

Single-layer graphene has outstanding mechanical properties. It is stiff, flexible, has a Young's modulus of 1 TPa and an ultimate strength of 130 GPa. On the contrary, rubber materials have low stiffness and break at relatively small stresses around 20 MPa. Due to this important contrast, many attempts have been made to reinforce rubbers through incorporation of graphene or graphitic fillers in an elastomeric matrix [17, 225, 252–254].

3.2.1. Tensile properties

Many reports have shown improvement of mechanical properties due to graphitic filler incorporation. Most studies deal with the incorporation of small content of graphite nanoplatelets into a polymeric matrix through direct or solution mixing. They mainly report an increase in Young's modulus, and in tensile strength and a decrease in elongation at break. However, these results appear to strongly depend upon the type of filler (lateral size, thickness, surface chemistry) and the mixing procedure.

3.2.1.1. Influence of filler size, shape and aspect ratio

Different carbon fillers have been investigated by Schopp et al [255]. They prepared SBR composites containing 25 phr loading of respectively carbon black (CB), expanded graphite (EG), multilayer graphene (MLG, < 10 layers), chemically reduced graphene oxide (CRGO) and thermally reduced graphene oxide (TRGO). They used latex mixing followed by internal mixer and two-roll mill mixing. Stress-strain plots in Figure 34 clearly indicate that TRGO and MLG lead to the most pronounced stiffening of the material with stress at 50 % strain up to 14 times higher than pure SBR matrix [255].

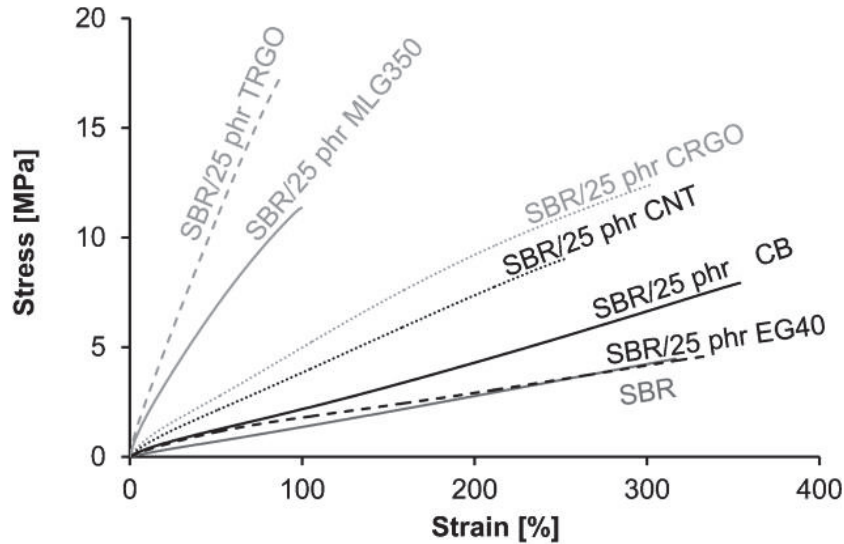


Figure 34: Stress-strain curves of SBR-carbon fillers composites at 25 phr [255].

Tensile strength is also greatly increased (more than 3 times higher than neat SBR) but elongation at break is strongly impacted and is decreased by a factor 3. CRG and CNT lead to moderate increases in tensile strength ($\times 2$) and stiffness ($\times 3$) with a less pronounced loss in strain at break. CB and EG did not bring much changes compared to neat matrix properties, leading to a slight increase in stiffness and in tensile strength with no impact on elongation at break. The stiffening effect of these carbon fillers could be ranked the following way: TRGO>MLG>CRGO>CNT>CB>EG. Hence, platelet-like carbon fillers with small thickness exhibited the highest reinforcing effect on the matrix. However, a strong reduction in strain at break is usually not desirable and CRGO filler might be more satisfactory for most common rubber applications where ability to withstand large deformations is required. Another feature, not investigated in this study, is the influence of the filler over the crosslinking density of the elastomer. Hence, the filler may interact with the curing system and lead to differences in crosslinking densities of the final composites, thus affecting their mechanical properties [188].

Similarly, Mao et al [256] compared the efficiency of carbon black as compared to graphite oxide and observed that around 13 vol% (~ 32 phr) of carbon black (N330) were necessary to reach the same tensile strength as SBR composites containing only 2 vol% of GO [256]. Similar results were reported by Ozbas et al [227] who showed that 1 wt% of thermally reduced graphene oxide in NR lead to similar moduli values as composites containing as much as 16 wt% of carbon black. Thus, graphitic fillers show promising results for reinforcement of elastomers at low loading.

3.2.1.2. Influence of processing

Mechanical properties of elastomer composites are very dependent upon many parameters linked to the process. As a matter of fact, filler dispersion is strongly impacted by the processing technique and

is of significant influence over the behavior of the composite. Besides, the elastomeric matrix may undergo degradation such as molar mass reduction during mixing. Another key feature is the nature and the amount of crosslinks formed during the vulcanization process. However, the features of the vulcanized network in the composites (crosslinking density and nature of crosslinks) compared to the pristine matrix is seldom studied in the literature. The following section will thus focus on process parameters affecting filler dispersion without taking into account any modification of the crosslinked network in the presence of the filler.

Potts et al [257] investigated the preparation of thermally reduced graphene oxide – natural rubber composites prepared either in bulk by two-roll mill mixing or from latex via a latex mixing phase preceding twin-roll mill mixing. They observed a slight decrease in modulus at 100 % and 300 % strain for bulk-compounded composites at 2 phr loading of TRGO as compared to neat NR. On the contrary, latex-compounded composites with 2 phr showed over 40 % improvement in 100 % modulus, as compared to the matrix [257]. Moreover, it was observed by transmission electronic microscopy that the latex pre-mixing step improved the dispersion of reduced graphene oxide in NR, which improves the moduli of the composites.

Similarly, Yang et al [239] observed better dispersion for expanded graphite – NBR composites prepared through latex compounding followed by internal mixing than for composites that underwent no latex precompounding phase. Figure 35 shows SEM pictures of composites with 5 phr loading of expanded graphite prepared either through direct bulk mixing and including a predispersion in latex phase [239].

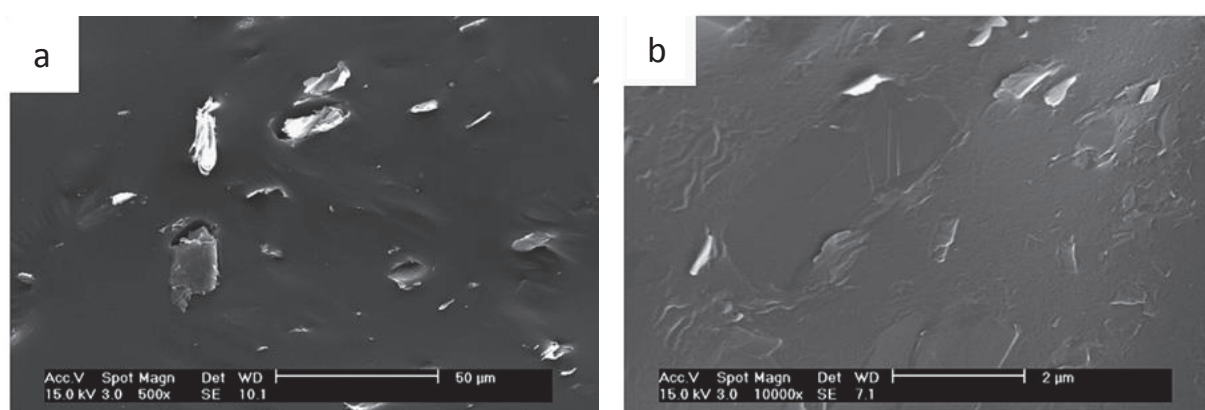


Figure 35: SEM images of NBR-based composites with 5 phr expanded graphite prepared with (a) direct blending and (b) latex compounding method [239].

It can be seen clearly that aggregates are much smaller (from 25 μm to less than 1 μm) in the composite prepared through a latex premixing method.

Moreover, tensile properties of composites prepared through latex mixing showed a significant increase of stresses even at 3 phr loading. The authors achieved 3 times higher tensile strength at 10 phr loading than with unfilled NBR and a strongly reduced elongation at break (110 % vs 410 % for pure NBR) [239].

The effect of latex compounding was further investigated by Yan et al [237]. They dispersed reduced graphene oxide (rGO) in natural rubber latex using a latex co-coagulation method with or without

further homogenization on a twin-roll mill. Morphologies of the composites are shown in Figure 32. They showed that samples prepared through a one-step latex mixing exhibited a segregated morphology and performed better in permeability measurements. Figure 36 shows stress-strain curves of pure NR and composites with 2 phr loading of rGO with a segregated (not homogenized) or homogeneous dispersion.

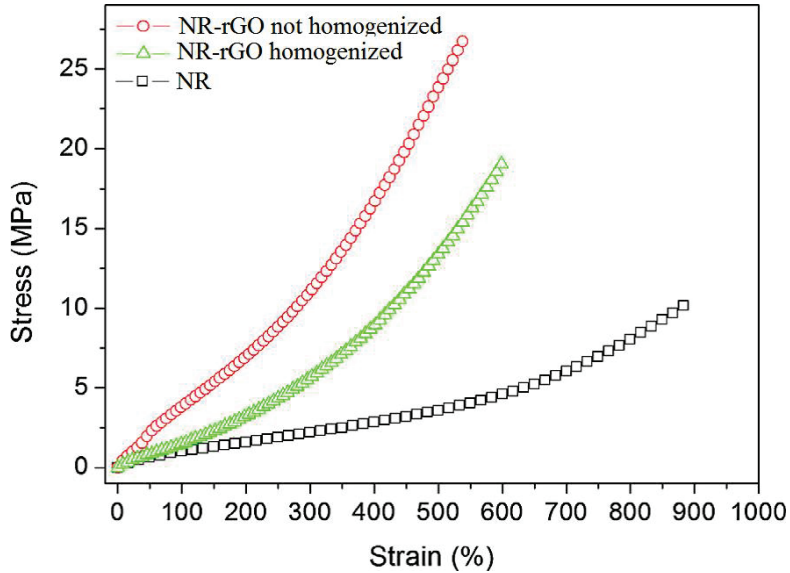


Figure 36: Stress-strain curves of pure NR and of NR composite with 2 phr loading of reduced graphite oxide (rGO), homogenized or not. Adapted from [237].

In Figure 36, it can be observed that samples prepared through a one-step latex mixing exhibit higher modulus at 100 % and 300 % elongation, higher tensile strength (27 MPa vs 19 MPa for homogenized samples) with only a small decrease in elongation at break. These enhanced values for segregated composites may be related to the formation of a stronger rGO network [237].

3.2.1.3. Influence of functionalization

Influence of graphite functionalization over mechanical properties was investigated by Zhao et al [258]. First, they functionalized GO using triethoxyvinylsilane (TEVS) and in situ polymerized liquid silicone rubber (LSR), performed in presence of TEVS-grafted GO. They prepared un-functionalized composites with the same method and investigated mechanical properties of the composites at different filler content. Figure 37 shows the tensile properties of the corresponding LSR composites.

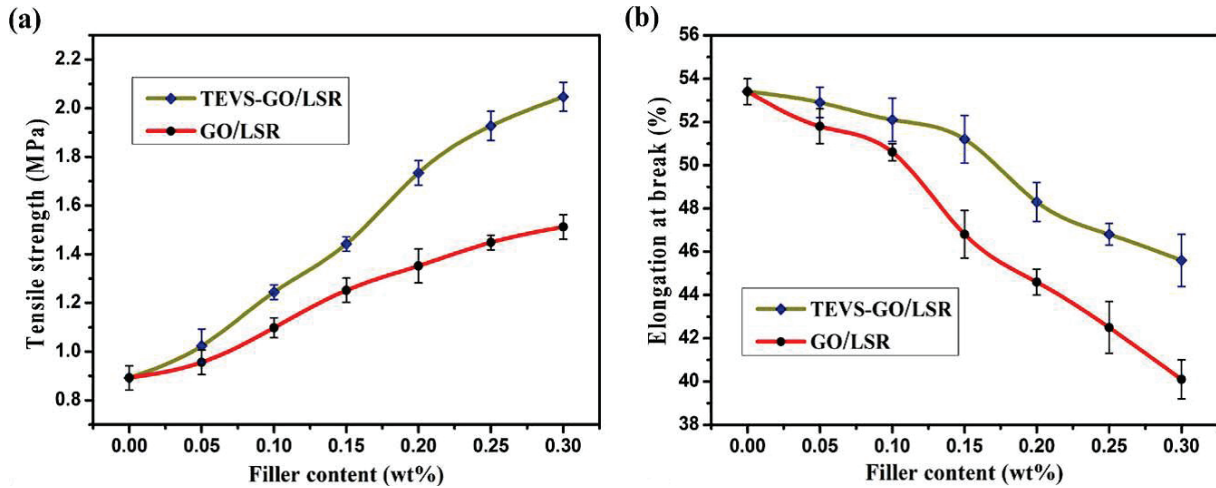


Figure 37: Mechanical properties of LSR composites (a) tensile strength and (b) elongation at break [258].

Composites containing 0.3 wt% of functionalized GO showed slightly greater tensile strength (2 MPa vs 1.5 MPa) as well as comparable strain at break (46 % vs 40 %). These changes are anyhow very small and the functionalization did not bring significant enhancement in tensile properties of LSR composites.

Wang et al [259] also investigated the effect of GO functionalization on tensile properties. They grafted octadecylamine onto GO and prepared SBR composites through melt compounding, with the filler being incorporated as a “paste” with ethanol, and by ensuring subsequent evaporation of the solvent during mixing on a twin-roll mill. Figure 38 shows stress-strain curves of SBR composites containing 3 wt% of modified and neat GO.

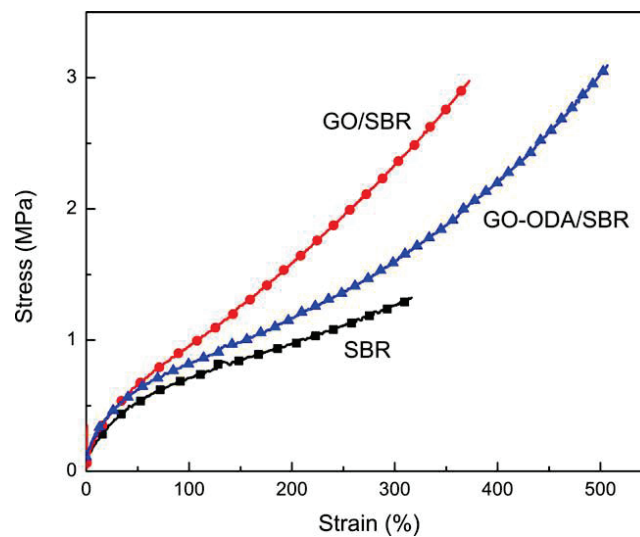


Figure 38: Stress-strain curves of pure SBR, GO-SBR and GO-ODA composites at 3 phr [259].

The composite containing the modified filler exhibited higher tensile strength but lower stiffness than pristine GO. Both fillers led to increases in tensile strength, stresses at 100 % and 300 % elongation as well as strain at break compared to the pure SBR matrix. In this study, functionalization did not bring much improvement in tensile properties of the composites at low loading (3 phr). Thus, functionalization can be a means to improve filler dispersion but does not always lead to improved

mechanical properties. Intrinsic filler parameters such as size, shape and aspect ratio have shown to be of greater influence over properties of the composites.

A literature review regarding tensile properties of graphite fillers-elastomer composites is available in Appendix 2.3.

3.2.2. Viscoelastic properties

Studying viscoelastic properties of the composites by dynamic mechanical analysis (DMA) provides information regarding molecular mobility of the polymer chains and about the composite structure. The α relaxation temperature, $T_{\alpha 1}$ associated with the glass transition temperature is obtained from $\tan\delta$ maximum in a temperature sweep. It is related to molecular mobility which may be affected by strong interactions between rubber chains and fillers. Reinforcement of the matrix due to filler incorporation can be observed through an increase in the storage modulus.

Figure 39 shows a typical example of the evolutions of the storage modulus and $\tan\delta$ with temperature for graphite-based NBR composites [260]. The samples referred to as “micro-composites” are prepared through simple twin-roll mill mixing while “nanocomposites” are prepared with previous latex mixing dispersion stage.

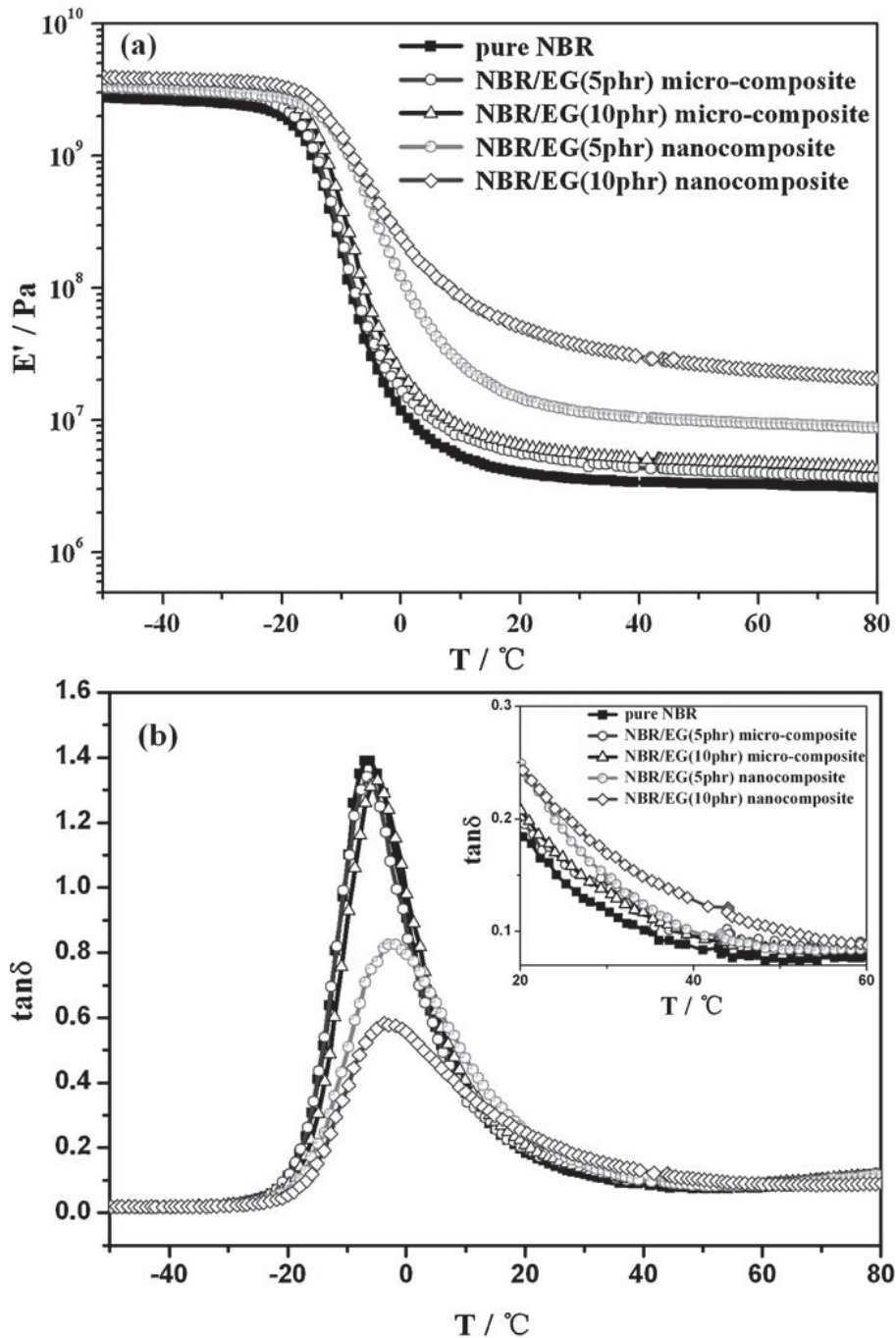


Figure 39: (a) Storage modulus of NBR composites containing 5 phr and 10 phr of expanded graphite (EG) and (b) $\tan\delta$ values [260]. The measurements were recorded under a tension mode at a frequency of 1 Hz with a strain amplitude of 0.1 % in the temperature range from -50 °C to - 80 °C. The heating rate was 3 °C/min.

From Figure 39 a, an increase in the storage modulus (E') in the rubbery state (above T_{α}) can be observed for all composites due to some reinforcing effect which is more pronounced for “nanocomposites” that underwent a latex pre-dispersion step, than for “micro-composites” that were prepared through direct twin-roll mill mixing. Due to poor dispersion and distribution, “micro-composites” exhibit a very weak reinforcement, whereas the increase of E' for “nanocomposites” can be attributed to a better dispersion state [261, 262]. Rubber-filler and filler-filler interactions (“filler networks”) lead to a significant increase in E' . Besides, the increase in filler loading from 5 phr to 10 phr leads to a small increase of the storage modulus, from 1×10^7 Pa to 2×10^7 Pa at 60 °C.

On Figure 39 b, the loss factor ($\tan\delta$) is represented as a function of temperature. Upon incorporation of expanded graphite filler, no effect is observed for “micro-composites” as compared to neat NBR, while a broadening and a decrease in $\tan\delta$ peaks after T_{α} is observed for “nanocomposites”. According to the authors, the decreased volume fraction of elastomer in these “nanocomposites” associated with rubber-filler interactions are responsible for more heterogeneous behavior of NBR molecules (broadening) and a decrease of intramolecular hysteresis in the T_{α} region. The authors point out a slight increase of $\tan\delta$ beyond T_{α} , which they attribute to enhanced hysteretic mechanisms (friction between rubber molecules, rubber-filler and filler-filler interactions) when the filler volume fraction increases. However, it can be noted that this effect is very small (Figure 39 b).

Payne effect

The viscoelastic behavior of filled elastomers typically exhibit enhanced non-linearity, known as the Payne effect. It is characterized by a drop of the storage modulus and the occurrence of a maximum of the loss modulus when strain is increased. It occurs at low strain, whereas unfilled elastomers present non linearity at larger strains without peak on the loss modulus plot. Hence, unfilled rubbers show a linear behavior up to quite large strains while the elastic modulus of a filled rubber decreases with strain. It can be explained by adsorption and desorption of polymer chains on the filler surface under mechanical sollicitation, leading to network collapse [263, 264].

Wang et al [259] studied the behavior of SBR composites containing octadecylamine-modified GO. Figure 40 shows plots of the storage modulus as a function of strain amplitude for various GO-ODA contents.

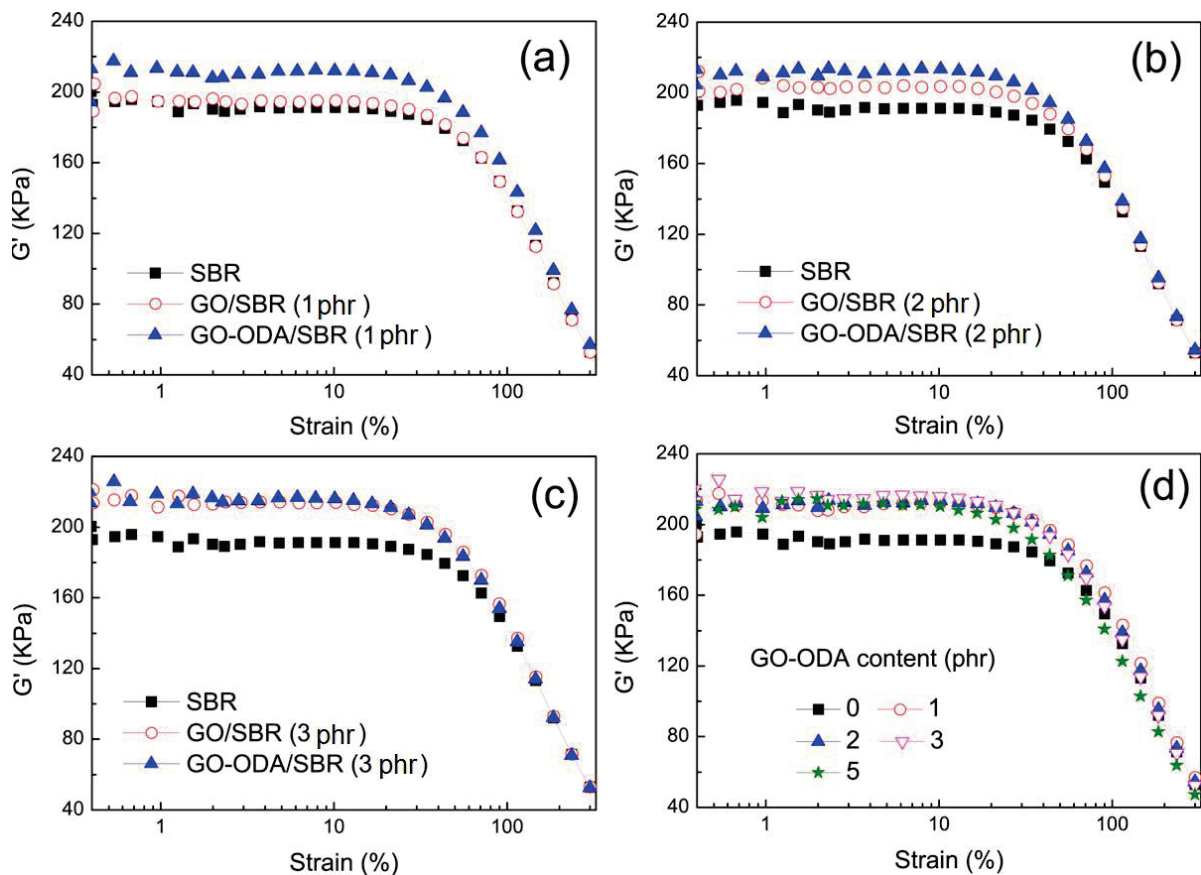


Figure 40: Storage modulus as a function of strain amplitude for crosslinked SBR composites with a filler content of (a) 1 phr, (b) 2 phr, (c) 3 phr, and (d) various GO-ODA content [259] recorded at 1 Hz at 60 °C.

In Figure 40, it can be observed that all compounds exhibit linear viscoelastic behavior at low strain amplitude and non-linear viscoelastic behavior at high strain rates. At 1 phr and 2 phr loading, composites containing GO-ODA filler show slightly greater storage modulus than GO-filled samples, which according to the authors, indicates a small reinforcement effect which may be attributed to a stronger interface due to ODA grafting onto GO [259]. Figure 40 d shows that increased GO-ODA loading (5 phr) led to a smaller linear zone which can be attributed to the formation of a weak filler network which is more strain-sensitive. It can be pointed out though, that the influence of functionalization on viscoelastic properties of GO/SBR composites is very limited in this study.

The numerous studies on graphene incorporation into elastomers to enhance mechanical properties reveal the strong potential of this nanofiller that might be used as a partial replacement of the very common carbon black filler in the future.

3.3. Thermal properties

3.3.1. Thermal stability

Graphene is thermally stable up to more than 1000 °C and can thus increase thermal stability of a polymer composite. Nevertheless, most studies deal with the introduction of reduced graphene oxide, graphite nanoplatelets or expanded graphite in elastomers, rather than graphene itself. Kim et al [265] thus reported increased thermal stability of SBR/multilayer graphene composites at 1 wt% loading. In addition, some groups also observed an enhanced thermal stability for composites containing GO which however is itself quite unstable. Hence, Gan et al [238] reported an increase of 44 °C in the onset degradation temperature of liquid silicone rubber composites filled with 1 wt% loading of graphite oxide, as shown in Figure 41.

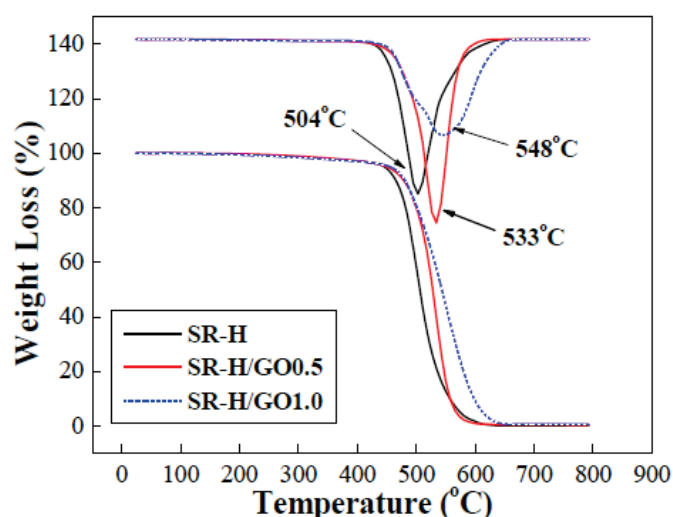


Figure 41: TGA data of silicone rubber (SR-H) composites filled with GO at 0.5 and 1 wt% [238].

Therefore, incorporation of graphic fillers can be a good means to enhance thermal stability of elastomer composites.

3.3.2. Thermal conductivity

Graphene and its derivatives are very often reported to be efficient in increasing thermal conductivity of elastomers. Graphene displays a very high thermal conductivity and, if well dispersed in a matrix, it can lead to strong enhancements in thermal conductivities of rubbers. Its sheet morphology is moreover well adapted for thermal conduction, providing low interfacial resistance. Typical increase in thermal conductivity upon addition of graphite nanoplatelets is represented in Figure 42.

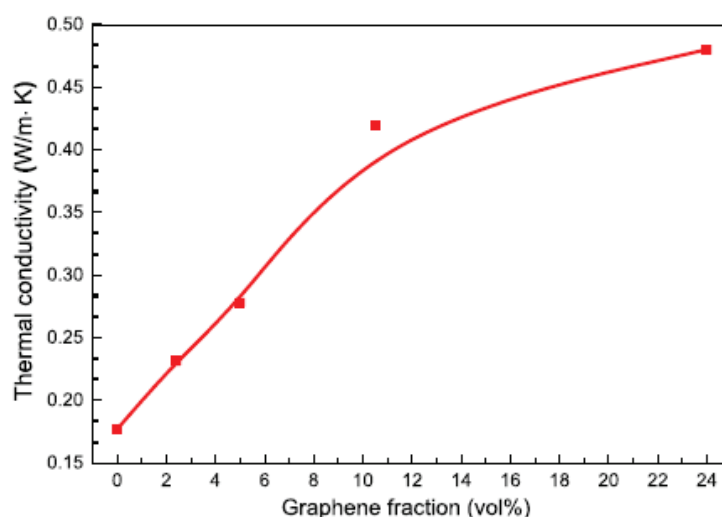


Figure 42: Thermal conductivity of SBR compounds as a function of GNPs loading (using a thermal conductivity tester HC-110 according to ASTM C 518. The temperatures at the top and bottom molds were set at 50 °C and 30 °C with a sample size ϕ 51 mm * 6 mm) [266].

As shown in Figure 42, an enhancement in thermal conductivity from 0.17 W/m.K for pristine SBR to 0.27 W/m.K upon addition of 5 vol% of graphite nanoplatelets was achieved by Araby et al [266]. They used a solution-blending technique followed by two-roll-mill mixing for the preparation of the composites and a thermal conductivity as high as 0.48 W/m.K was reached at 24 vol% of graphite nanoplatelets content [266]. However, such a high loading of graphite nanoplatelets may strongly impact strain at break of the composites and will lead to high costs.

3.3.2.1. Influence of processing

Good contact between fillers is necessary for thermal conductivity enhancement. The final conductivity will thus depend on the dispersion quality, which results from filler geometry as well as the mixing process. To investigate the latter, Mu et al [267] dispersed expanded graphite in silicon rubber at various loadings according to two methods: solution blending and direct melt mixing. Figure 43 shows the increase in thermal conductivity of these silicon composites as a function of the filler content.

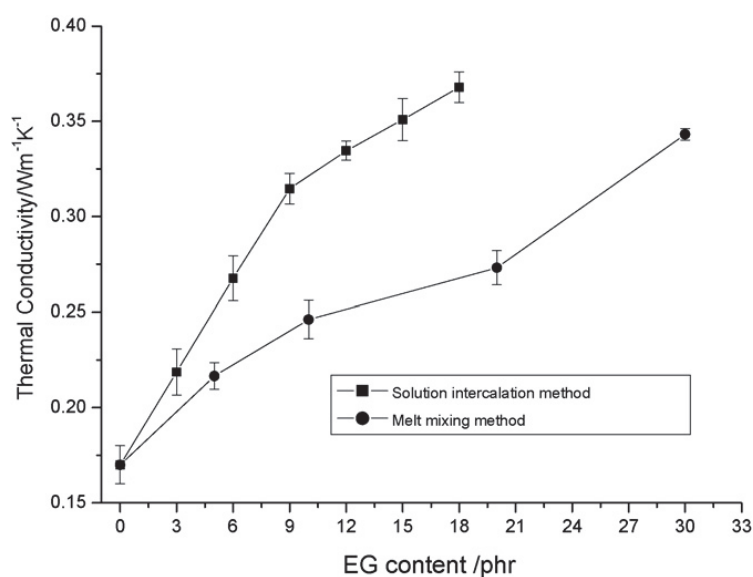


Figure 43: Thermal conductivity of expanded graphite-PDMS composites at various expanded graphite loadings [267].

Pure silicon matrix exhibited a 0.17 W/m.K thermal conductivity that was increased to 0.24 W/m.K and 0.32 W/m.K for melt-processed and solution-processed samples, respectively, at 9 phr loading. The authors observed enhanced thermal conductivities for both composites with a greater effect for solution-blended samples, which exhibited better dispersion. They reported that the expanded graphite network was disrupted in the melt-blended composites while the solution process preserved the graphite network structure. By this method, more exfoliation and intercalation of rubber chains between graphite layers can be achieved [267]. The authors suggested a structural interpretation for the origin of the higher thermal conductivity of solution-processed samples, as shown in Figure 44.

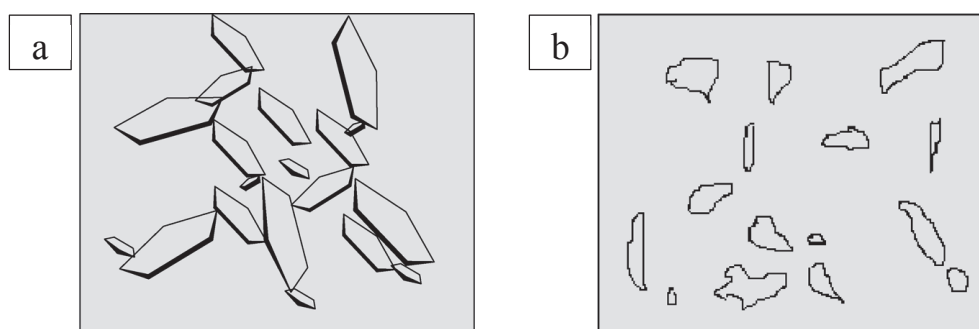


Figure 44: Schematic morphologies of silicon - expanded graphite composites prepared by (a) solution-processing and (b) melt-processing [267].

Figure 44 a represents large EG particles whose shapes and dimensions were not affected by the solution mixing. However, Figure 44 b shows particles that are much smaller and whose shape changed drastically under shear during melt mixing. The surface-to-volume ratio is then largely reduced and so higher loadings are necessary to achieve elevated thermal conductivity compared to solution-processed samples containing large EG particles [267].

3.3.2.2. Functionalization

Phonons are known to be responsible for the heat conduction in materials. To maximize their action, scattering should be minimized. One method is to modify the graphene filler by covalent coupling to

the matrix to enhance filler-matrix interactions. Zhao et al [258] introduced pristine and modified GO in liquid silicon rubber and observed that thermal conductivity was enhanced upon addition of fillers from 0.19 (pristine elastomer) to up to 0.38 W/m.K for composites containing 0.3 wt% of the modified filler. Figure 45 shows the increase in thermal conductivity as a function of the filler content.

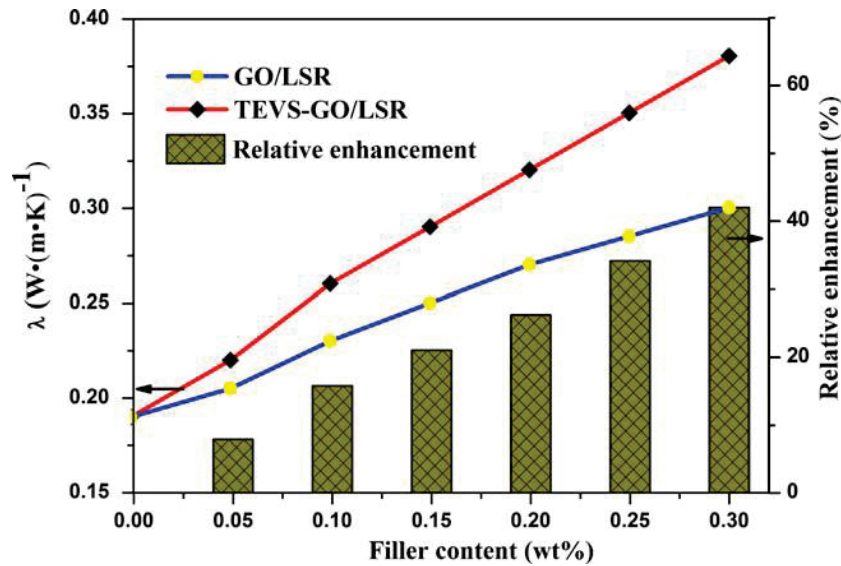


Figure 45: Thermal conductivity of silicon rubber (LSR) composites containing GO and TEVS-GO [258].

Both fillers increase thermal conductivity but the effect is more pronounced for triethoxyvinyl silane (TEVS)-modified GO. A relative enhancement of up to 42 % for TEVS-GO as compared to pristine GO / LSR composites was calculated at around 30 wt% loading.

Graphene derivatives have thus proven to be effective in enhancing thermal stability and conductivity of elastomeric matrices. However, the increase in thermal conductivity is often limited by high interfacial thermal resistance between nanosheets and rubber. This phenomenon is known as Kapitza resistance [268, 269] and is due to poor thermal coupling between graphite nanoplatelets and the elastomeric matrix [266]. Functionalization can thus be a means to improve this coupling by favouring the interfacial interaction between the graphitic filler and the elastomeric matrix.

3.4. Electrical properties

Elastomers are insulating materials. However, upon the addition of a conductive filler (carbon black, carbon fiber, CNT, graphene...) they can become electrically conductive. This electrical conductivity is dependent on the filler electrical properties, its loading, size and dispersion state in the host matrix. Carbon black is commonly used to achieve electrical conductivity in elastomers. However, high loadings are usually necessary, impacting failure properties of the material. Carbon nanofillers are promising alternatives to carbon blacks in this application since their intrinsic electrical properties are some orders of magnitude higher, which offers the possibility to produce conductive elastomers at much lower filler loading [270]. Carbon nanotubes have been reported to be very efficient in increasing electrical conductivity of polymers at a very low content (less than 1 vol%). Graphene also appears to be very promising for this application.

3.4.1. Percolation

A major challenge when dealing with electrical conductivity is to ensure the creation of a conducting path inside the material. When filler loading is substantially low, the average distance between filler particles is greater than their size range and the fillers form individual particles rather than a conducting network. When a critical loading is reached, conduction can take place by a tunneling effect through the polymer layers surrounding the filler and electrical conductivity increases quickly. This critical concentration is called “percolation threshold” [271]. It depends upon the filler content, size, morphology and the state of dispersion and distribution in the material.

The “ideal” dispersion of the filler in the matrix to increase electrical conductivity might not be the homogeneous dispersion needed for good mechanical properties, but rather a partial segregation that would create conductive paths. Close wrapping of the matrix on fillers would act negatively on electrical conductivity [225]. Araby et al [266] investigated electrical properties of SBR filled with graphite nanoplatelets. They measured the electrical volume resistivity of the materials and observed a slight decrease below 5 vol% and a pronounced drop from 5 to 7 vol%, as shown on Figure 46.

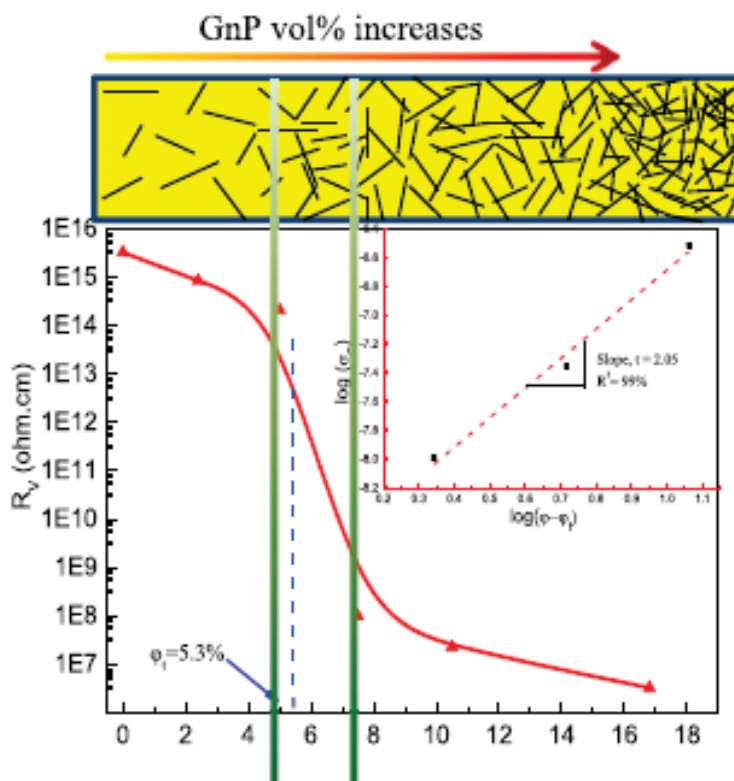


Figure 46: Electrical volume resistivity of SBR composites as a function of graphite nanoplatelets volume fraction [266].

They interpreted these results using percolation theory. At low volume fraction, fillers cannot connect with each other. At a certain concentration (about 5 vol% in this study), the filler volume fraction is high enough to enable formation of conductive paths and so, to rapidly decrease electrical volume resistivity.

3.4.2. Influence of processing

The effect of processing on electrical surface resistance of composites filled with thermally reduced graphene flakes has been studied [135]. Their results are reported in Figure 47.

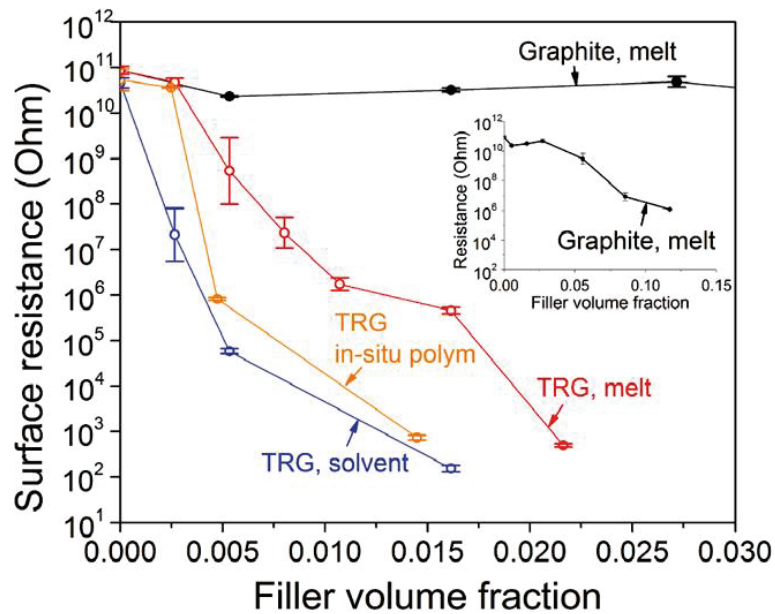


Figure 47: Surface resistance of graphite-TPU composites prepared through different methods [135].

It appears that solution-blending is the most effective process in reaching low percolation threshold, with a value smaller than 0.1 vol%. In situ polymerized and melt-compounded samples show a similar percolation threshold of 0.25 vol% but the former show a faster decrease in electrical surface resistance at higher loadings. The lowest resistance value (of around $10^2 \Omega$) was reached for TRG – TPU samples prepared from solution blending at around 1.7 vol%. Another interesting feature in this work is the influence of filler size and specific surface area on the electrical properties. Graphite used in this study has a specific surface area of $29 \text{ m}^2/\text{g}$ while TRG has a much higher specific surface area of $800 \text{ m}^2/\text{g}$. Graphite – TPU composites prepared through melt mixing showed a decrease in electrical surface resistance of about 5 orders of magnitude at more than 10 vol% while TRG - TPU composites achieved values 8 orders of magnitude lower than the neat matrix at only 2.2 vol%.

Despite these spectacular results, it can be mentioned that surface resistance measurements are very sensitive to surface defects of the samples, which can be caused by processing. Moreover, the surface of a sample may not be much representative of the bulk (except for thin films). Therefore, volume resistivity measurements would have been preferable to draw suitable conclusions on the influence of processing.

Influence of processing conditions upon the electrical conductivity of reduced graphene oxide – natural rubber latex composites has also been investigated by Zhan et al [272]. They prepared composites using several mixing procedures. Some samples were prepared through direct latex coagulation, others were further homogenized on a twin-roll mill and others were obtained through direct blending. The results from the electrical conductivity measurements are shown in Figure 48.

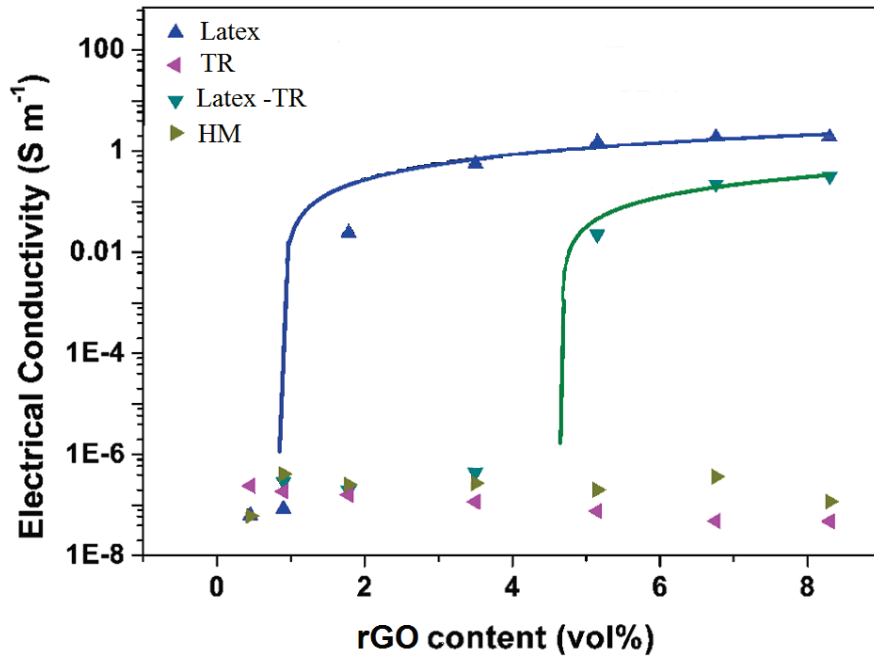


Figure 48: Electrical conductivity of natural rubber - reduced graphene oxide composites prepared according to different methods. Latex: direct latex blending, TR: twin-roll mill mixing, Latex-TR: latex blending followed by twin-roll mill homogenization and HM: HAAKE mixing.

From these experiments, it appears clearly that samples prepared by direct melt mixing (HM and TR) did not again significantly increase electrical conductivity even at 8 vol% content. However, samples combining a latex mixing step with a twin-roll mill homogenization showed an increase in electrical conductivity of about 6 orders of magnitude with a percolation threshold lower than 5 vol%. Besides, samples prepared by latex mixing only performed best with an increase of about 7 orders of magnitude as compared to direct blended composites. They also showed a very low percolation threshold of less than 1 vol%. TEM pictures presented in Figure 49 help to understand this phenomenon.

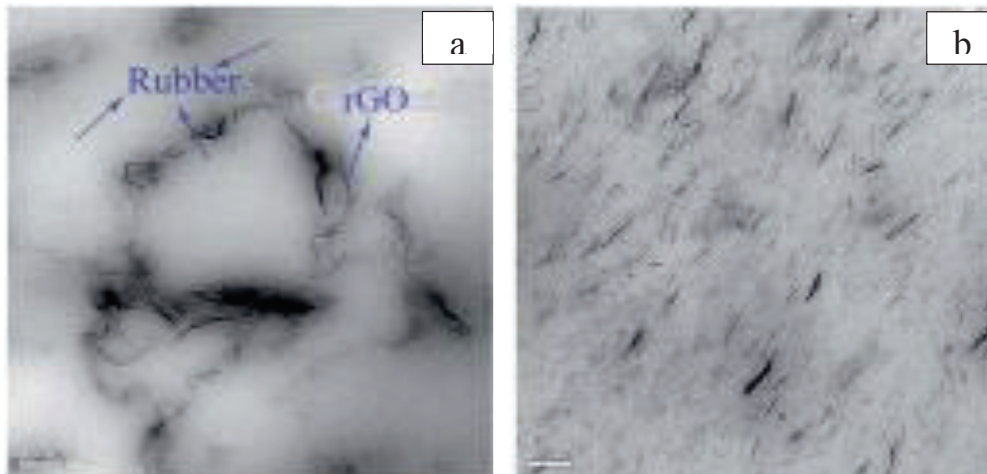


Figure 49: TEM images of NR-rGO composites prepared through (a) latex mixing and (b) latex assembly followed by twin-roll mixing.

Figure 49 a shows samples prepared through latex assembly. Segregated morphology can be observed with rGO platelets being arranged in circular shapes at the periphery of rubber latex particles, forming a network. On the contrary, samples that have been homogenized in a twin-roll mill show rather

homogeneous dispersion with orientation of the fillers along the milling direction. The formation of a conductive path in the segregated morphology is responsible for the higher electrical conductivity of the corresponding composites.

Filler orientation also plays a significant role in reducing the percolation threshold and increasing electrical conductivity of the resulting material [273–276]. Higher electrical conductivities are achieved when fillers are interconnected. Random dispersion is thus often preferred to aligned platelets since there is a greater probability of platelets coming in contact with one another. Functionalization of the filler may also be a means to increase electrical conductivity through improving dispersion and creating a stronger filler-matrix interface [277]. Combining different conductive fillers is also sometimes reported in the literature [278].

Outstanding electrical properties of graphene are thus of great interest in creating electrically-conductive elastomer composites. Applications are numerous. Coleman et al [279] for example, reported the use of graphene-rubber composites as strain sensors to monitor body motion.

A short literature review on the electrical properties of graphene-rubber composites is available in Appendix 2.4.

3.4.3. Dielectric properties

Macromolecular dynamics can be studied through dielectric measurements. Hence, information on intermolecular motion as well as dipolar rotations can be evidenced from the dielectric relaxation spectrum.

Most studies report an increase in dielectric permittivity of the composite upon addition of conductive fillers. Romasanta et al [280] compared CNT and reduced graphene oxide sheets in a PDMS matrix and observed a 6-fold and 10-fold increase in the dielectric constant for reduced GO sheets and carbon nanotubes composites respectively. This difference may be due to the presence of some functional groups on rGO surface that reduce polarization process and thus improve the polymer-matrix interface. Several other groups performed dielectric studies on graphene based-rubber composites. Parameters affecting dielectric properties were found to be the loading, morphology, size and dispersion state of the fillers, as for most of the properties of such composites [127, 281–286].

3.5. Conclusion

This section has given an insight of the effect of graphene-based fillers in elastomers. Decreased permeability, increased stiffness with or without an impact on elongation at break, increased thermal conductivity as well as increased electrical conductivity of the composites are often reported. A key parameter in enhancing the matrix properties is the appropriate dispersion of the filler in the matrix as well as strong matrix-filler interactions. A way to tune these interactions is to functionalize graphitic fillers to incorporate new functionalities on their surface. Moreover, enhanced compatibility with the polymer matrix has a significant impact on the distribution of the filler.

Conclusion of the literature study

Graphene is a promising nanomaterial that shows outstanding mechanical, thermal, electrical and barrier properties. It is however hard to obtain perfect, defect-free graphene. Methods such as chemical vapor deposition have proven to be efficient in growing graphene single layers of high-quality graphene on very small surfaces limiting thus its applications to nanoelectronics and research. Other techniques such as oxidation/reduction processes enable the production of much larger quantities at lower costs. Yet, materials prepared through this way usually present many defects like disruption of the conjugated π system, leading to inferior electrical properties. Such graphene-like material anyhow retains some interesting features of graphene such as relatively high mechanical and barrier properties and can thus be of great interest for use as fillers in polymers. Due to differences of several orders of magnitude in terms of mechanical, thermal and electrical properties, significant effect of these nanofillers upon incorporation in polymeric materials such as elastomers can be expected.

Several studies have shown the great potential of this filler in several elastomers on mechanical, thermal, electrical and barrier properties of the composites. Several parameters affecting these enhancements were highlighted. Intrinsic characteristics of filler as size, shape and aspect ratio were proven to be of significant impact as well as processing conditions. Morphologies of the composites were observed to be affected by the process. Filler orientation was shown to be a key issue in permeability enhancement while the formation of a filler network inside the matrix was evidenced to be of major importance for electrical conductivity issues. Functionalization of the filler was also proven to be of significant interest to improve the filler dispersion and exfoliation in the matrix and thus its mechanical, thermal, electrical and barrier properties. Two main methods were highlighted: weak non-covalent attachment of modifiers onto graphene or GO without disruption of its conjugated structure, and strong covalent attachment of a molecule onto the graphitic surface. For the latter, prior oxidation to provide functional groups is often required. The last section evidenced the possibility to graft polymers onto graphene or GO through many different mechanisms including in situ polymerization of the monomer onto the substrate.

The forthcoming chapters will deal mostly with functionalization strategies to enhance dispersion of graphite into polyisoprene rubber to improve mechanical and barrier properties.

Chapter 2: Functionalization of graphite oxide by using a “grafting onto” approach

Table of contents of Chapter 2

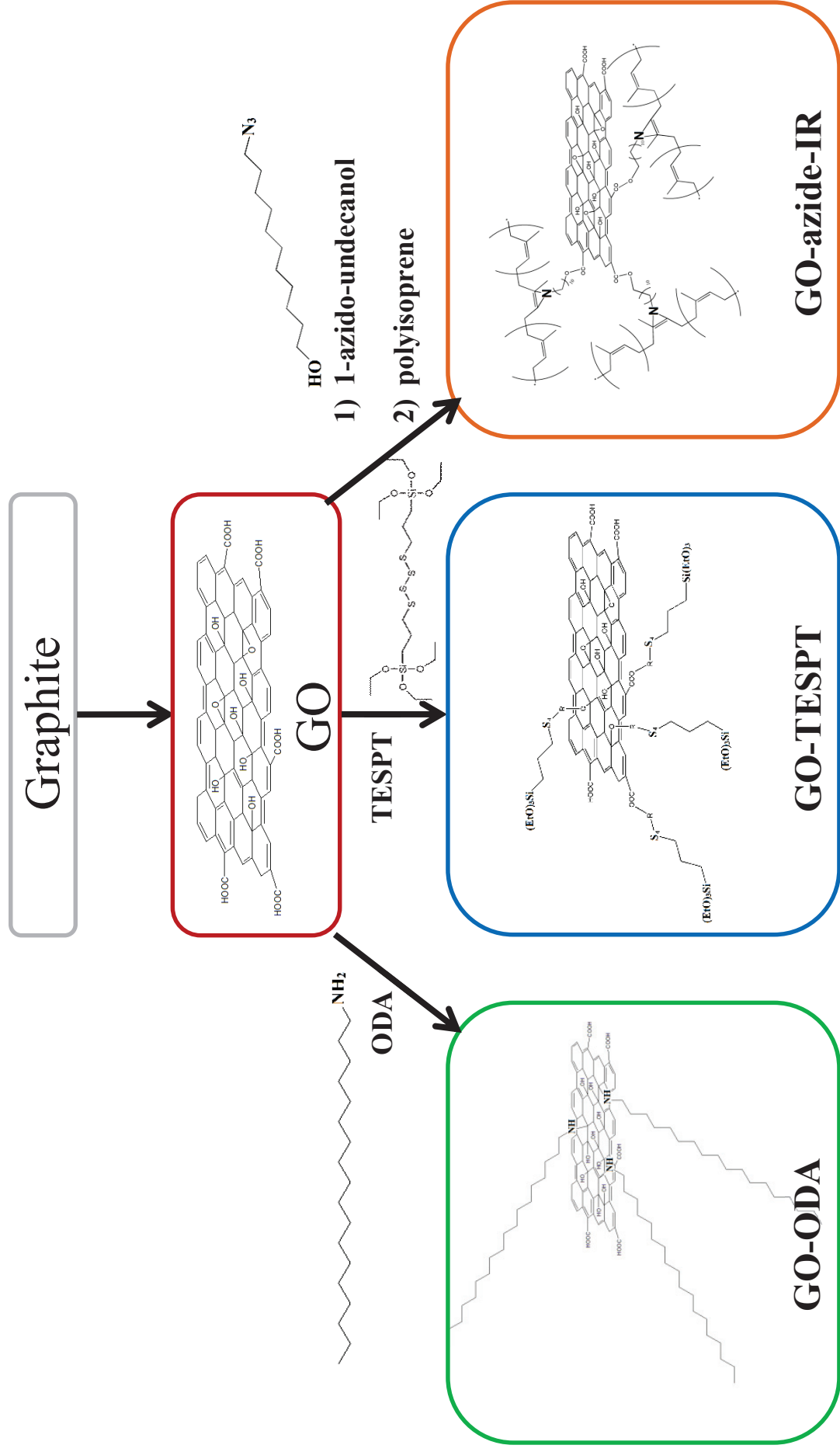
Introduction.....	110
1. Functionalization strategies	110
2. Preparation of GO	112
3. Grafting of octadecylamine onto GO	118
4. Grafting of TESPT onto GO	122
5. Grafting of polyisoprene chains onto GO through nitrene chemistry	126
5.1. Esterification of 1-azido-undecanol onto GO	127
5.2. Cycloaddition of GO-azide onto polyisoprene	133
Conclusion	136

Introduction

Covalent modification of GO is often reported in the literature to limit aggregation of the nanoplatelets and to enhance their dispersion in a matrix. Many studies have been performed with thermoplastic matrices [85, 122, 277, 287, 288], while fewer papers have been published on elastomer composites containing functionalized GO. In this section, three strategies are reported. First, the use of a hydrophobic alkyl amine is discussed to decrease GO hydrophilicity and, therefore, to enhance its dispersion in polyisoprene. Then, a second strategy is based on the use of a common silane coupling agent, TESPT, to effectively modify GO. Finally, an attempt to anchor polyisoprene chains onto GO through the use of a bifunctional molecule is reported.

1. Functionalization strategies

Several chemical covalent functionalization reactions can be performed directly on graphite. However, graphite oxide, a material prepared by oxidation of graphite, that contains oxygen functional groups on its surface and edges, may be functionalized using a wider range of chemical reactions, as described in Chapter 1. In the present study, three main functionalization paths are reported and are summarized in Scheme 14.



Scheme 14: Functionalization strategies for the grafting of ODA, TESPT and IR onto GO.

First graphite was oxidized into GO to provide oxygen functional groups which can be used for further modification steps. One strategy is based on the grafting of ODA, an amine bearing a long, non-polar alkyl chain onto GO. The reaction was performed by a nucleophilic substitution path, as described by Liu et al [289]. A second functionalization path was carried out by using TESPT, a common silane coupling agent used for further vulcanization, and able to react with GO through a hydrolysis-condensation reaction [127]. Finally, a third reaction path attempted in this study is the covalent attachment of polyisoprene chains on the surface of GO sheets. From the grafting of 1-azido-undecanol, a bifunctional modifier, onto GO. The reaction was performed in two steps: (i) esterification of hydroxyl groups of 1-azido-undecanol with carboxylic acid groups of GO and (ii) cycloaddition of azide-modified GO on polyisoprene (through the formation of nitrenes). All these chemical modifications were characterized using common analytical techniques such as FTIR and TGA. The grafting content and the influence of the grafted molecules over the affinity of the modified platelets for non-polar solvents were evaluated.

This chapter first details the synthesis and characterization of GO, which is the starting material for most chemical modifications performed in this study.

2. Preparation of GO

Graphite can be oxidized according to several well-known methods to incorporate oxygen-based functional groups on its surface and then provide reactive anchor sites for further modification. Brodie [290] was the first to synthesize GO using a mixture of potassium chlorate and fuming nitric acid. However, the process was long (over a week) and hazardous due to the formation of explosive chlorine dioxide gas. In 1958, Hummers [86] introduced an improved process to oxidize graphite using strong acids and potassium permanganate as the oxidant, as described in Chapter 1. The latter method has been used in this study (see Appendix 3.1. for the experimental procedure).

Graphite oxide was characterized by FTIR, Raman, XRD, XPS, TGA measurements as well as TEM and SEM.

First, FTIR analysis evidenced the presence of oxygen functional groups on its surface (Figure 50).

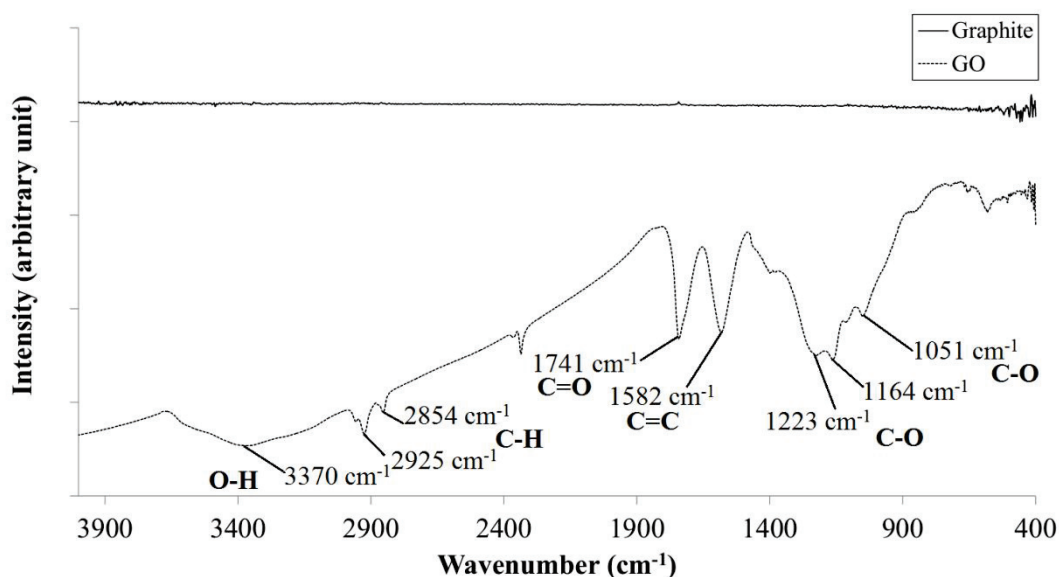


Figure 50: FTIR spectrum of graphite oxide.

No functional groups could be evidenced on the surface of graphite, its FTIR spectrum being a flat signal. On the contrary, several functional groups could be evidenced onto the surface of GO. A wide peak at around 3370 cm^{-1} is attributed to O-H stretching vibration band while C=O elongation band of carboxylic acids appears on the spectrum at 1741 cm^{-1} . C-O absorption bands are visible at 1223 cm^{-1} , 1164 cm^{-1} and 1051 cm^{-1} and are related to carboxylic acid, epoxide and hydroxyl groups, respectively. Carbon-hydrogen elongation bands are observed at 2925 cm^{-1} and 2854 cm^{-1} (for asymmetrical and symmetrical elongations respectively) and C=C elongation band is visible at 1582 cm^{-1} . This analysis is thus consistent with the presence of hydroxyl, carboxylic acids as well as epoxide groups on the surface of GO [100].

Moreover, Raman spectroscopy is a useful tool to study graphitic structures so both graphite and GO spectra are displayed in Figure 51.

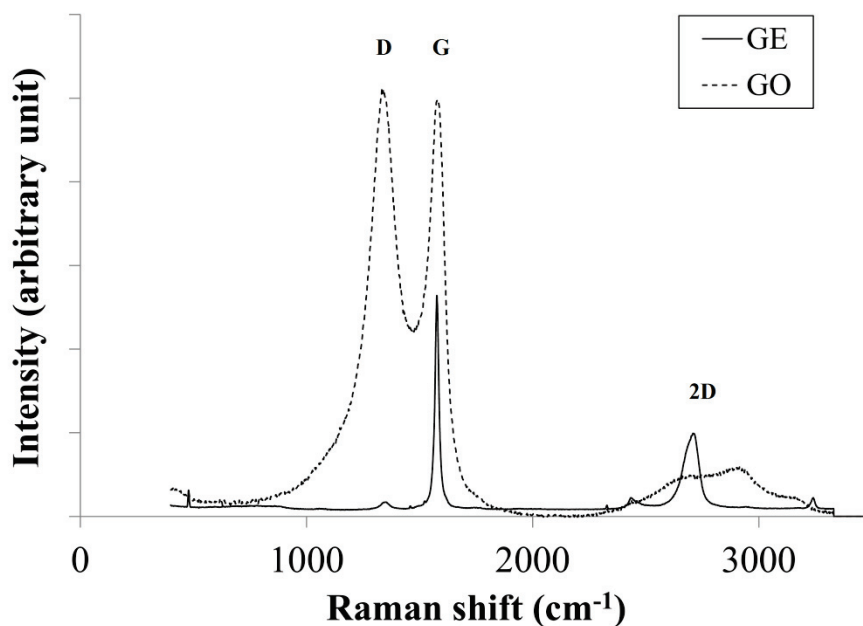


Figure 51: Raman spectra of graphite (GE) and GO.

Graphite exhibits a strong G band at 1576 cm^{-1} , characteristic of ordered sp^2 aromatic carbons, a weak D band at 1345 cm^{-1} related to structure defects such as sp^3 carbons and a neat 2D band at 2711 cm^{-1} . GO shows a greatly increased D band due to the formation of many sp^3 carbons and a broad 2D band as compared to pristine graphite. The intensity ratio of D and G bands (I_D/I_G) is found to increase from 0.20 for graphite to 1.02 for GO, which is known to be related to the incorporation of oxygen functional groups onto GO surface. The widening of the 2D peak can be attributed to the irregular shape (wrinkles) of GO. Moreover, graphitic structure is preserved as evidenced by the presence of a strong G band. A more detailed study of GO Raman spectrum has been reported by Kudin et al [291].

XRD measurements were also performed and revealed an increased interlayer spacing in GO compared to pristine graphite (Figure 52).

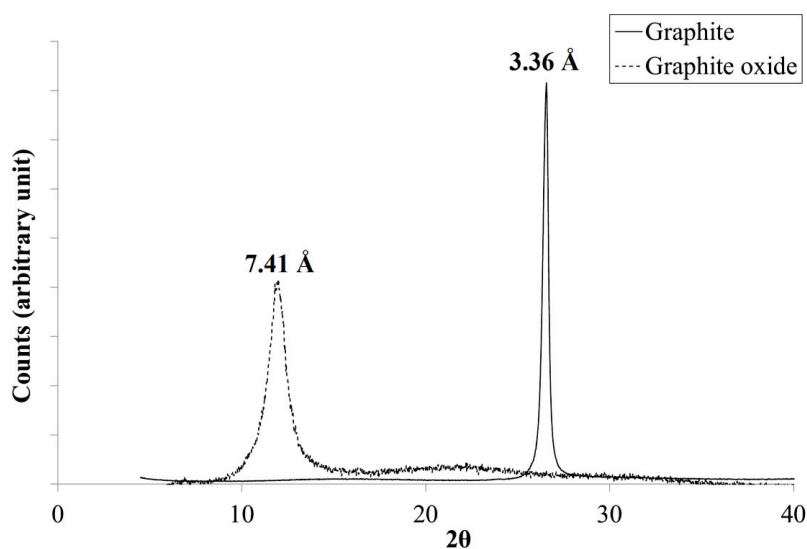


Figure 52: XRD analysis of graphite and graphite oxide.

Indeed, while pristine graphite shows an interlayer spacing of around 3.36 Å, GO displays an increased interlayer distance of 7.41 Å due to the anchoring of oxygen functional groups on the nanosheets surface [2, 73, 292].

Moreover, X-ray photoelectron spectroscopy was performed on GO to provide additional proof of the presence of different oxygen-based groups (Figure 53).

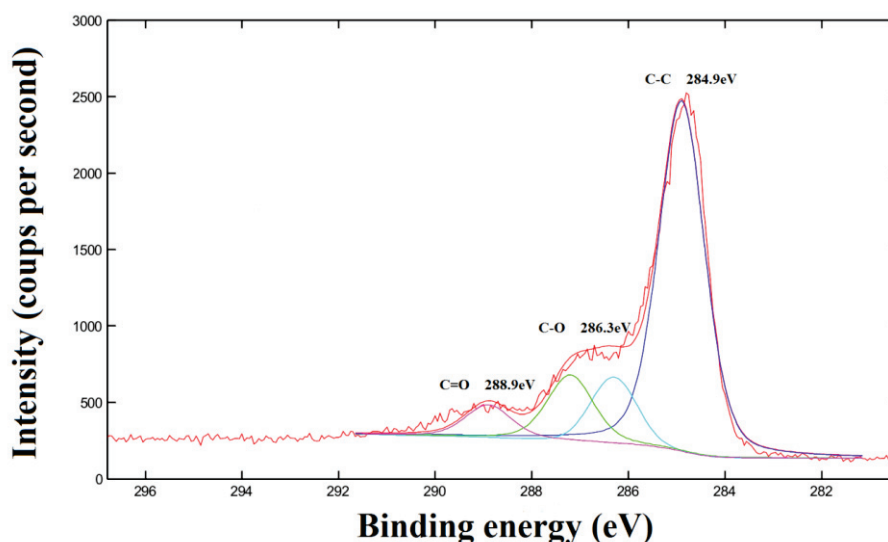


Figure 53: XPS C 1s spectrum of GO.

Three main types of carbon binding can be evidenced. A first major peak at 284.9 eV is related to carbon-carbon bonds, a second peak at 286.3 eV is attributed to single carbon-oxygen bonds and a third peak at 288.9 eV is linked to carbon-oxygen double bonds. This analysis is thus consistent with the presence of carboxylic acid, epoxide and hydroxyl groups onto GO surface and corroborates the analysis [100].

In order to get a more quantitative picture of oxygen-based groups in GO, TGA was performed (Figure 54).

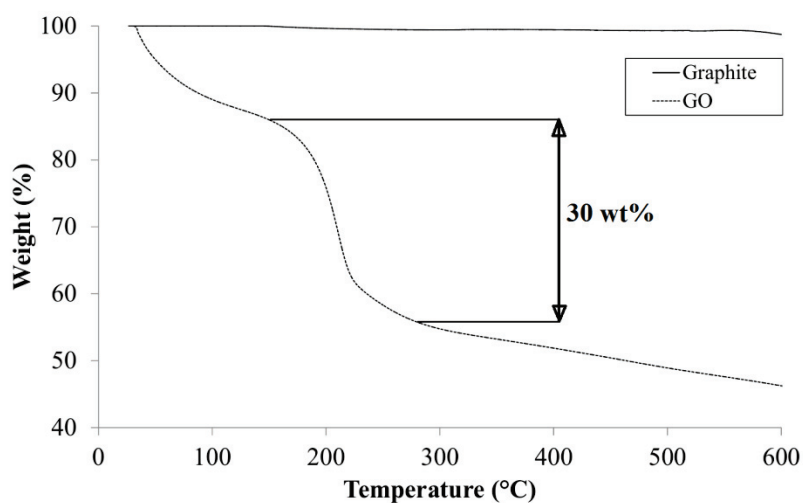


Figure 54: TGA analysis of graphite oxide under helium with a heating rate of 5 °C/min.

TGA data shows no significant weight loss for graphite up to 600 °C while GO undergoes around 50 % weight loss before the temperature reaches 600 °C. GO thermogram can be divided into several domains: at temperatures below 150 °C, the weight loss can be attributed to the release of physisorbed water while the main weight loss (of around 30 wt%) at temperatures between 150 °C and 250 °C is attributed to the pyrolysis of oxygen functional groups. At higher temperatures, more stable oxygen functional groups eventually degrade. GO is thus thermally unstable due to the presence of heat-sensitive oxygen functional groups on its surface [73, 293].

Then, morphological studies of graphite and graphite oxide have been performed using TEM and SEM (Figure 55 and Figure 56, respectively).

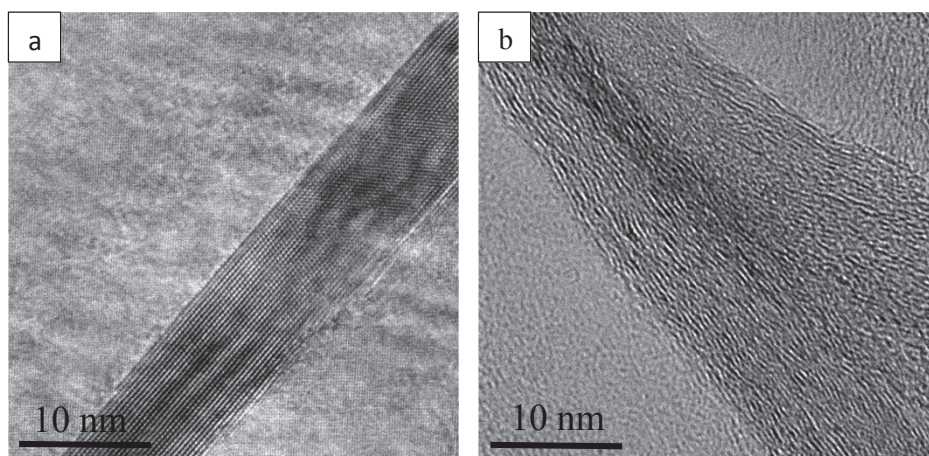


Figure 55: High-resolution TEM images of a) graphite and b) graphite oxide.

TEM image of graphite shows parallel lines corresponding to stacked graphene layers. An average interlayer spacing of around 0.34 nm and a number of layers of about 30 per stack were measured (Figure 55 a). In comparison with graphite, TEM image of GO shows a much more irregular structure with strongly wrinkled sheets and an irregular interlayer spacing that could be averaged to 0.41 nm. This is consistent with the incorporation of functional groups onto graphene layers (Figure 55 b). However, this measure lacks of precision as it is highly sensitive to the orientation of the sample towards the beam. Hence, the interlayer spacing of 0.74 nm measured by XRD may be more accurate.

At a wider scale, SEM also provides interesting information on GO morphology, as shown in Figure 56.

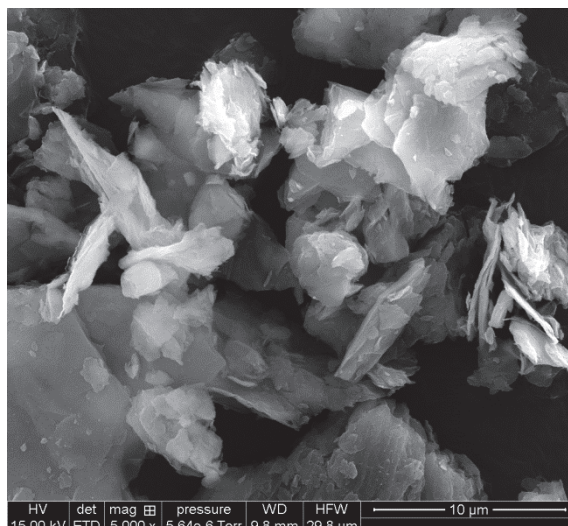


Figure 56: SEM image of GO.

Irregularly-shaped stacks of nanosheets can be seen on the SEM picture of GO. A wide size distribution is observed as well as the presence of small « patches » on the surface of GO nanosheets. These small graphitic units can be interpreted as strongly-oxidized graphite small flakes that are adsorbed on GO surface and that may be removed with an appropriate base wash, as described by Rourke et al [108, 110].

Due to the presence of oxygen-based moieties on GO, the hydrophilicity of graphite and GO is expected to be very different, which can be confirmed by studying the stability of their suspensions in water (Figure 57).

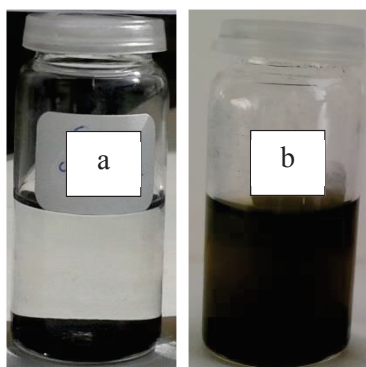


Figure 57: Suspensions of a) graphite and b) GO in water at 1 mg/mL.

Indeed, when dispersed in water at a concentration of 1 mg/mL, graphite sediments immediately (Figure 57 a) while GO sheets disperse well and yield a brown suspension which remains stable after 24 h (Figure 57 b).

All these characterizations have allowed to determine the nature of the chemical moieties present on GO surface and, to a lesser extent, to give an estimate of their weight fraction (from TGA) in the

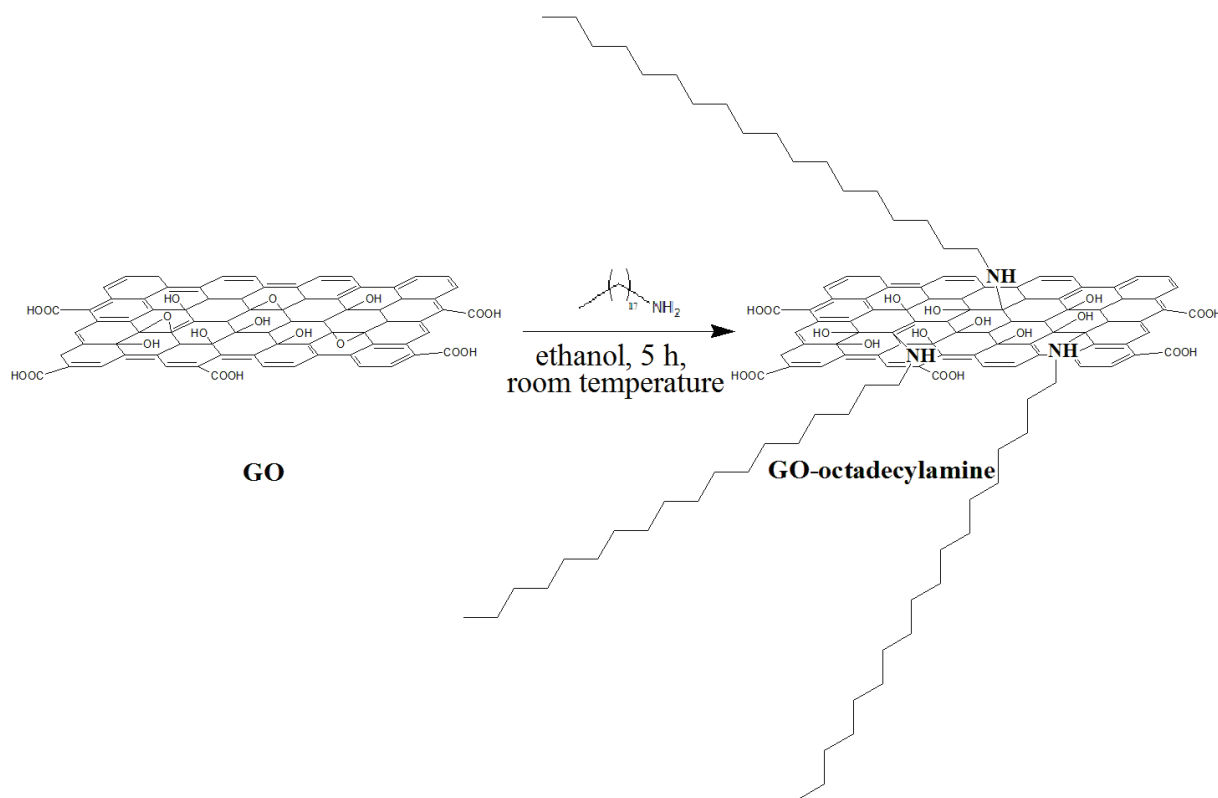
modified filler. Then, chemical modification of GO can be performed using these oxygen—based functions.

3. Grafting of octadecylamine onto GO

To improve dispersion of polar graphite oxide sheets in a non-polar elastomeric matrix, grafting of alkyl chains onto its surface can be performed. Octadecylamine (ODA) is a primary amine with a 18-carbon alkyl chain that has been very widely used for clay modification [187, 294–300] and it has been successfully adapted for GO functionalization [120–122, 130, 226, 259, 301–303]. Amine end-groups on ODA are able to react with GO epoxy groups through a nucleophilic substitution (NS) reaction and through an amidation with carboxylic acid groups on GO edges. However, in presence of amino groups, GO often reacts mainly by nucleophilic substitution. Indeed, amino groups are reported to react preferentially with epoxide groups of GO rather than with carboxylic acid groups, which often require the preparation of an acyl halide functionalized GO to enhance reactivity through an amidation reaction path [120, 130, 304].

For example, Bourlinos et al [120] reacted ODA onto GO and reported an increase in the interlayer spacing of the modified GO from 6.78 Å to 14.8 Å by XRD measurements. Using amines with various alkyl chain lengths, they showed that the interlayer spacing was increasing with increasing alkyl chain length. Besides, a neat change in solubility of GO upon functionalization with ODA was reported by Li et al [122]. They prepared immiscible chloroform / water mixtures and they observed that pristine GO was entirely localized in the water phase while GO-ODA was well dispersed in the organic phase. Upon a thermal treatment of the modified GO, they reported an increase in electrical conductivities of polystyrene films by 3 orders of magnitude due to ODA grafting onto GO [122].

In the present study, ODA reacted with GO through a nucleophilic substitution path. It was performed according to Scheme 15.



Scheme 15: ODA grafting onto GO through a nucleophilic substitution reaction.

GO was grafted with ODA in a one-step reaction involving the nucleophilic substitution of ODA onto GO at room temperature in ethanol (see Appendix 3.2. for the experimental procedure).

ODA grafting onto GO is reported to be performed either at room temperature or under reflux for 5 h to 24 h [121, 122, 259]. Li et al [122], performing NS of ODA under reflux in ethanol, reported simultaneous partial reduction of GO upon a solvothermal process. Hence, after refluxing ODA with GO for 20 h in ethanol, they observed a darker color of the suspension from brown to black and evidenced increased thermal stability of GO-ODA as compared to pristine GO, that they attributed to reduction of the functionalized GO.

In the present study, octadecylamine was grafted onto GO and it is expected that the compatibility with non-polar polyisoprene will be improved by the presence of long non-polar alkyl chains.

First, the grafting of octadecylamine onto GO was evidenced through FTIR characterization (Figure 58).

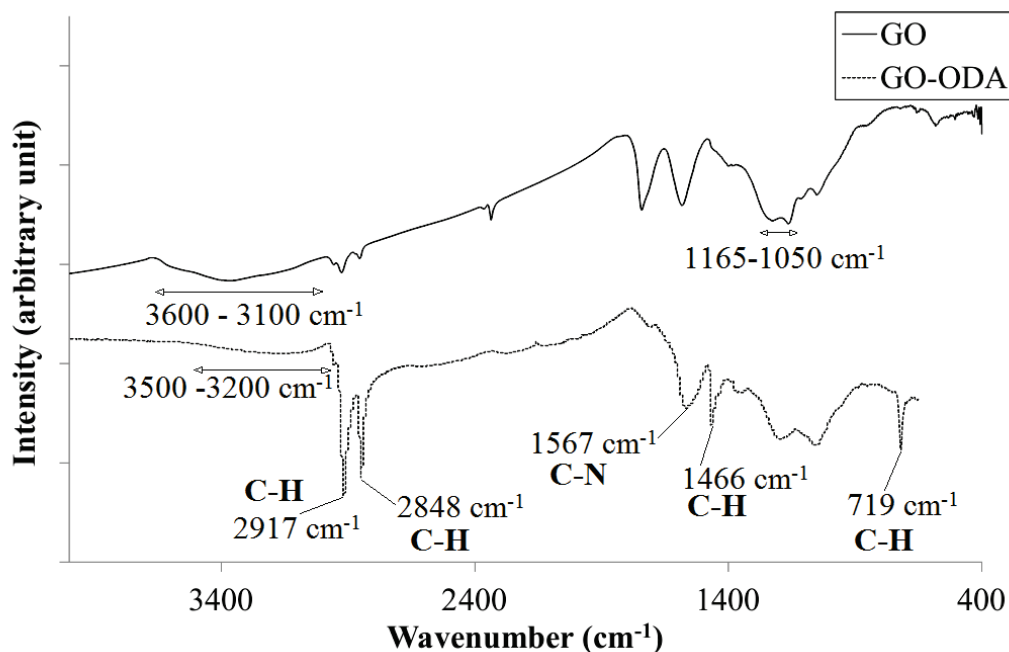


Figure 58: FTIR spectra of GO and GO-ODA.

From Figure 58, it can be seen that GO-ODA shows a reduced O-H absorption band in the 3500-3100 cm^{-1} range. Additional bands at 2917 cm^{-1} , 2848 cm^{-1} , 1466 cm^{-1} and 719 cm^{-1} , attributed to the C-H bands of CH_2 groups of the octadecyl chain, are also visible. They can be related to C-H asymmetric stretching, C-H symmetric stretching, C-H asymmetric bending and C-H rocking bands, respectively. Besides, a new peak at 1567 cm^{-1} attests for the presence of C-N bonds of ODA. Moreover, it is suggested that no free ODA remains in the sample, as the characteristic band of primary amines in the 3300-3200 cm^{-1} region is not visible. Finally, FTIR analyses suggest that ODA reacted mostly through a nucleophilic substitution on epoxide groups of GO as the intensities of C-O-C peaks in the 1165-1050 cm^{-1} region are reduced as compared to pristine GO, as discussed by Li et al [122].

A quantitative analysis of the product was also performed through TGA (Figure 59).

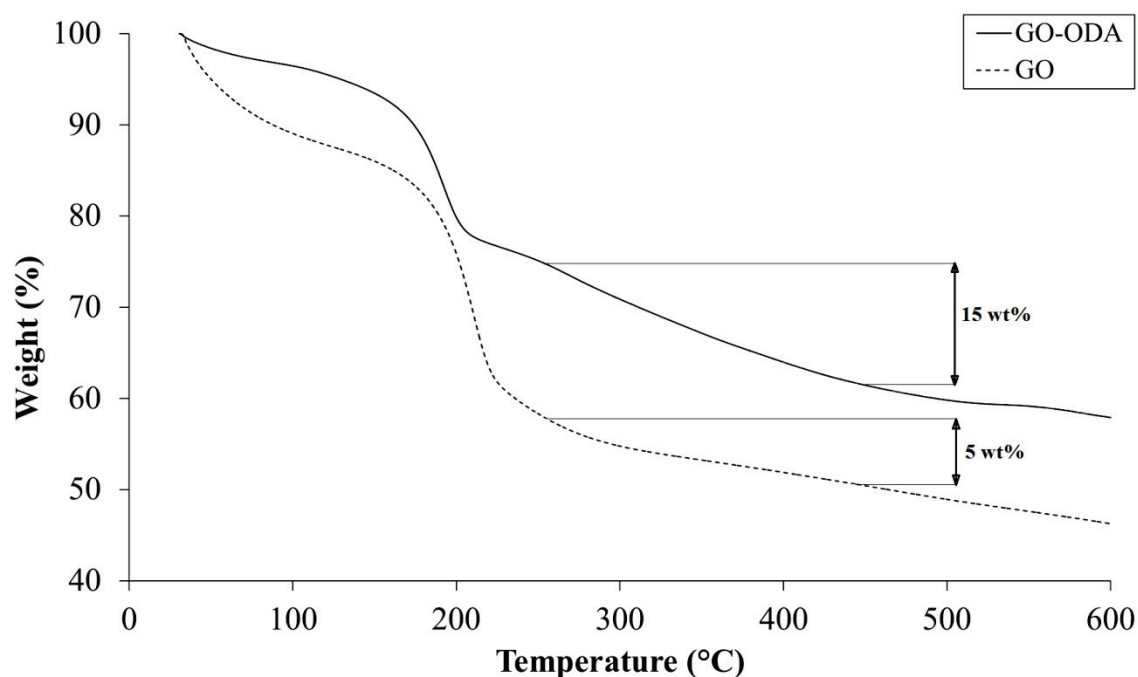


Figure 59: TGA thermogram of GO and GO-ODA under helium at 5 °C/ min.

GO-ODA exhibits a main weight loss at around 200 °C attributed to the degradation of GO functional groups. A second weight loss between 250 °C and 450 °C can be attributed to ODA degradation. A grafting content of 10 wt% could be calculated from the thermogram (after subtracting the contribution of pristine GO). This grafting content (10 wt%) is lower than the value reported by Zhang et al [301] who obtained a grafting content of 37 wt% after one night at 75 °C. Liu et al [121] reported a value of 25 wt% after reaction for 2 h at 78 °C. Besides, contrary to several studies, no simultaneous reduction of GO platelets occurred during the NS reaction [121, 122].

Moreover, the modified platelets exhibited strongly enhanced stability in toluene at a concentration of 1 mg/mL, as compared to pristine GO (Figure 60).

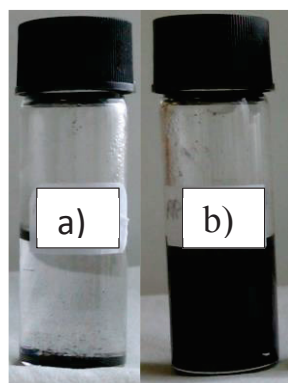


Figure 60: Suspensions of a) graphite oxide and b) graphite oxide - octadecylamine in toluene at a concentration of 1 mg/mL.

Indeed, the organic octadecyl tail of ODA enables a greatly increased compatibility of GO with non-polar organic solvents such as toluene which is a good solvent for polyisoprene (Figure 60 b). An

increased compatibility of GO with polyisoprene rubber is thus expected after functionalization with ODA.

The morphology of the platelets was observed by SEM (Figure 61).

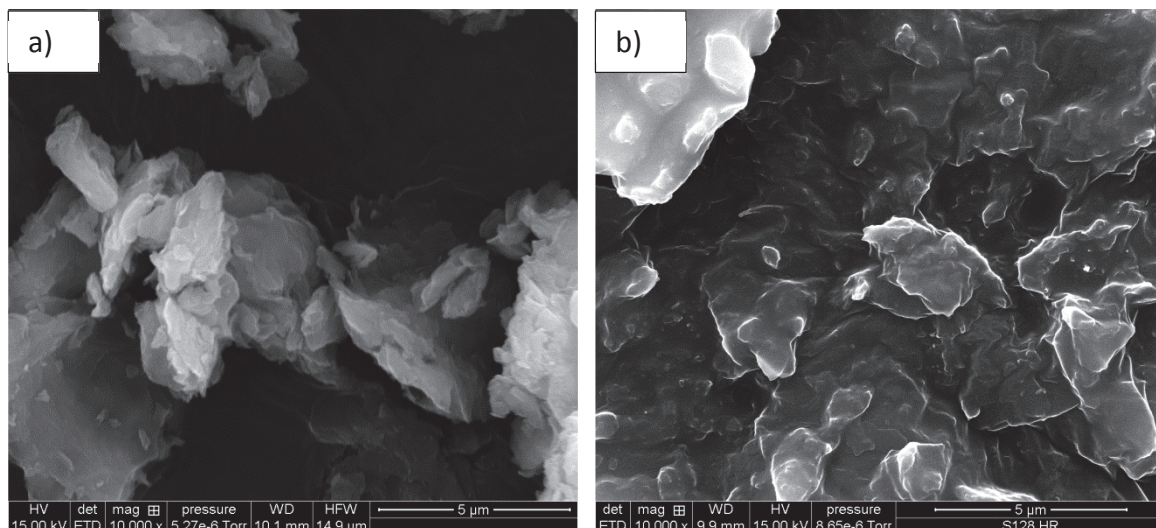


Figure 61: SEM pictures of a) GO and b) GO-ODA.

Both GO and GO-ODA platelets exhibit the same morphologies with oxidative debris visible on top of the platelets. Besides, no decrease in the platelets lateral dimensions was observed (with lateral dimensions ranging from 2 μm to 10 μm). Thus, the functionalization did not induce significant changes in the morphology of the platelets.

In conclusion, grafting of ODA onto GO through a NS has been performed and the corresponding modified platelets were characterized. The presence of long, non-polar alkyl chains was confirmed by FTIR and a grafting content of 10 wt% was calculated from TGA measurements. Suspensions of the grafted GO platelets exhibited enhanced stability in toluene at concentrations up to 1 mg/mL, thus suggesting increased compatibility with non-polar polyisoprene matrix. In the next section, a second functionalization path is reported, involving TESPT, a common silane coupling agent.

4. Grafting of TESPT onto GO

Silane coupling agents are very commonly used in elastomer compounds for silica compatibilization [305–308]. They react with silica through hydrolysis-condensation of the trimethoxysilane groups onto the silanol groups of silica to create Si-O-Si covalent bonds. These coupling agents enable a lowering of silica surface energy and decreased hydrophilicity of the silica particles, thus increasing their compatibility with elastomers. The use of silane coupling agents leads to better dispersion of silica particles in the rubber matrix that otherwise tend to aggregate due to strong particle-particle interactions.

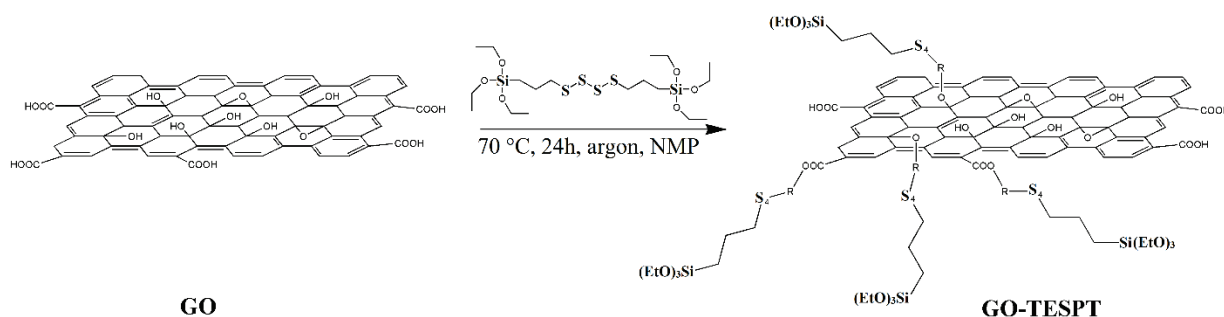
Similar studies were performed with other fillers such as CNTs [309–312]. Hence, Nakaramontri et al [309, 310] investigated the effect of two common silica coupling agents: aminopropyltriethoxysilane (APTES) and bis[3-(triethoxysilyl)propyl]tetrasulfide (TESPT) on the properties of epoxidized natural rubber (ENR) – CNTs composites. They observed enhanced dispersions of the nanotubes treated with

APTES or TESPT and increases in electrical conductivity and tensile properties. The stress at 100 % strain was found to increase from 2.2 MPa to 4.7 MPa upon addition of TESPT at a concentration of 0.06 mL/(g of CNTs) in ENR composites containing 5 phr of CNTs. Using Flory-Rehner equation, they also observed a small increase in crosslinking density from 251 mol/m³ to 264 mol/m³ upon addition of TEPST in ENR – CNTs composites at 5 phr. They reported chemical bonding of the silica coupling agent with CNTs and ENR [310].

Similarly to silica, graphite oxide is a hydrophilic material that tends to aggregate when incorporated into elastomeric matrices. This similarity led some authors to apply traditional silica modifications techniques to GO [127, 313].

Bis[3-(triethoxysilyl)propyl]tetrasulfide (bisTESPT or TESPT or Si69) is a very common silane coupling agent used in rubber industry. It combines the ability to bind to silica through hydrolysis-condensation reactions and the ability to provide sulfur for covalent bonding with diene elastomers, such as polyisoprene, during vulcanization. Wu et al [127] reported that TESPT could also be used as a GO – elastomer coupling agent. Hence, they grafted TESPT onto GO through hydrolysis-condensation reactions and then, in situ reacted sulfur with natural rubber during vulcanization. They observed increased tensile strength of NR composites from 10 MPa for pristine GO to 15 MPa for GO-TESPT at 1 wt%. Besides, they reported a 55 % decrease in air permeability of GO-TESPT composites at 1 wt% loading, compared to the neat elastomeric matrix.

In the present study, TESPT has been grafted onto GO through a hydrolysis-condensation reaction, as shown in Scheme 16.



Scheme 16: Hydrolysis-condensation of TESPT onto GO.

TESPT is grafted onto GO through hydrolysis-condensation of trimethoxysilane groups onto both hydroxyl and carboxylic acid groups of GO (see Appendix 3.3. for the experimental procedure). The resulting modified fillers contain TESPT chains that may then split upon heating to higher temperature to create sulfur bridges with polyisoprene.

The resulting product was characterized through FTIR, TGA and SEM.

FTIR spectrum is displayed in Figure 62.

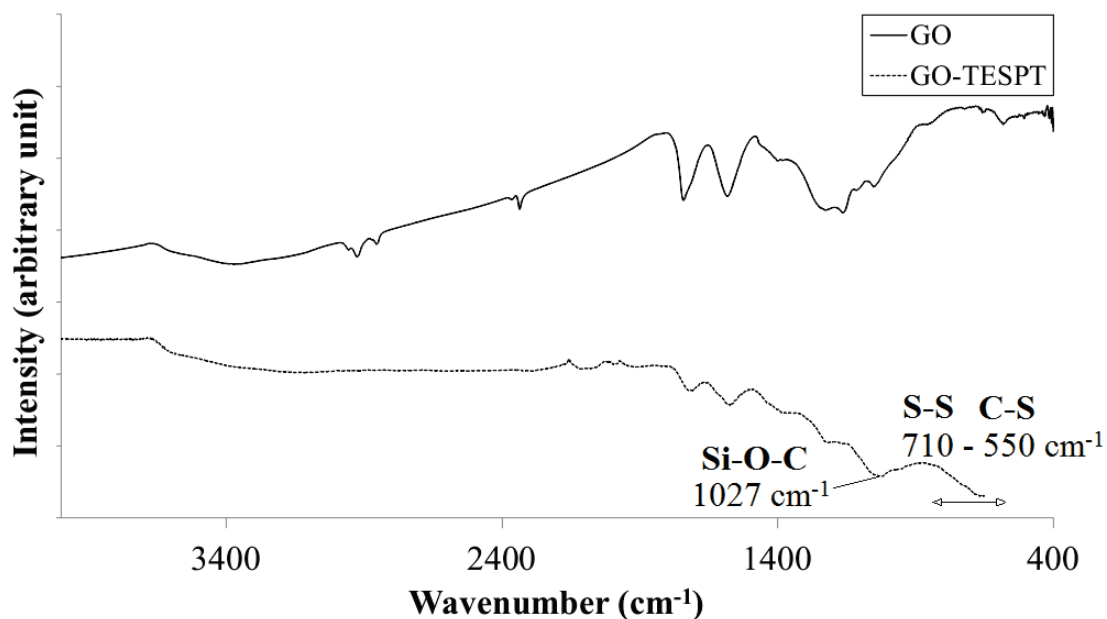


Figure 62: FTIR spectra of GO and GO-TESPT.

The FTIR spectrum of TESPT is not straightforward. Sulfur-sulfur as well as sulfur – carbon bonds usually exhibit very weak absorption bands in the $710\text{-}550 \text{ cm}^{-1}$ region. However, in the $1100\text{-}1000 \text{ cm}^{-1}$ wavenumber range, a band at 1027 cm^{-1} is observed and may be attributed to Si-O-C stretching of grafted TEPST grafted onto GO. Wu et al [127] reported similar results upon grafting TESPT onto GO. Besides, no signal in the $2900\text{-}2500 \text{ cm}^{-1}$ region is observed thus showing that no thiol (S-H bond) were formed and suggesting that polysulfide bonds in TESPT were not affected. The FTIR spectrum of GO-TESPT is thus not inconsistent with the grafting of TESPT onto GO through a hydrolysis-condensation reaction.

To investigate the amount of TESPT grafted onto GO, TGA analysis was performed (Figure 63).

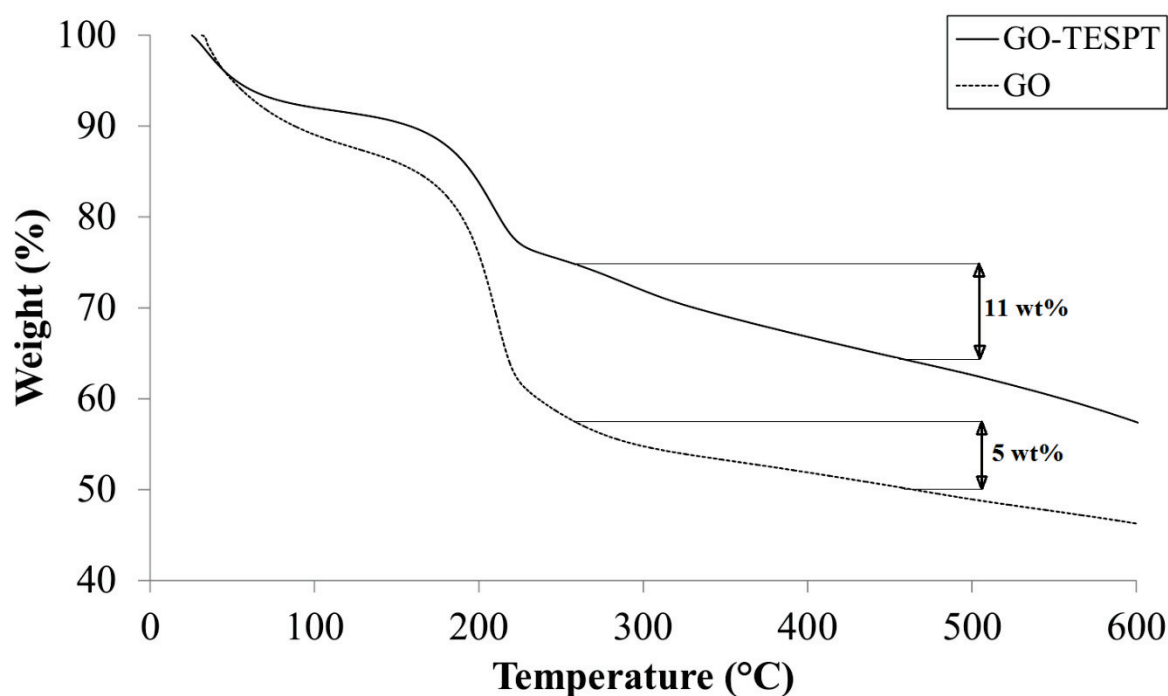


Figure 63: TGA thermogram of GO and GO-TESPT under helium at 5 °C/min.

The first weight loss below 100 °C is decreased as compared to pristine GO thus showing decreased hydrophilicity of GO-TESPT. Two main domains are then observed: one around 200 °C attributed to the degradation of GO functional groups and the other one in the temperature range 250 °C-450 °C related to TESPT degradation. The difference between GO-TESPT weight loss in that region and pristine GO weight loss gives a TESPT grafting content of 6 wt%. This grafting content is consistent with other results reported in the literature for trimethoxysilane grafting onto GO. Hence, Guimont et al [128] reported a 5.3 wt% grafting for alkoxy(7-octen-1-yl)silane onto GO using a similar procedure.

Besides, the grafting of TESPT onto GO led to an increase in the stability of its corresponding suspensions in toluene, as shown in Figure 64.

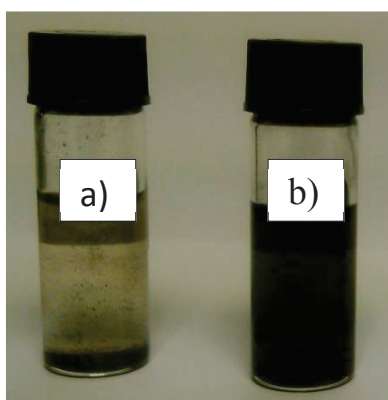


Figure 64: Digital images of suspensions of a) GO and b) GO-TESPT in toluene, at a concentration of 1 mg/mL.

GO-TESPT exhibits better dispersibility than pristine GO in toluene at a concentration of 1 mg/mL, thus indicating better compatibility with non-polar molecules than pristine GO. It can thus be expected that GO-TESPT will disperse better than GO in non-polar elastomeric matrices such as polyisoprene.

Moreover, the morphology of the modified platelets was investigated by SEM (Figure 65).

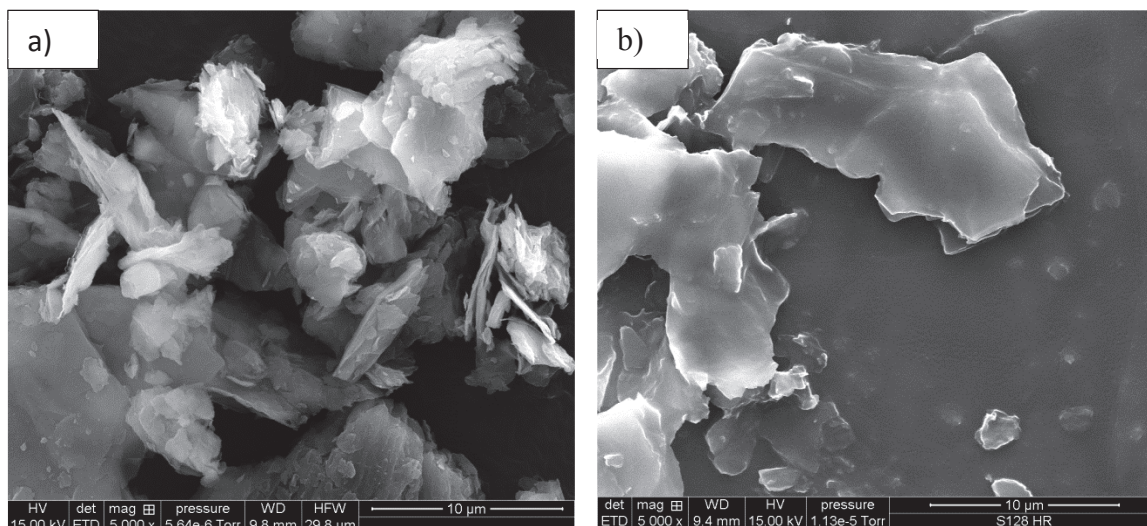


Figure 65: SEM pictures of a) pristine GO and b) GO-TESPT.

SEM pictures show no significant difference between GO and GO-TESPT. Platelets with lateral dimensions ranging from 20 µm to less than 2 µm were observed for GO-TESPT material. Oxidized debris are still observed on top of GO-TESPT platelets (Figure 65), due to the oxidation process [108, 110]. The small changes observed indicate that GO morphology was well preserved after the functionalization reaction.

TESPT could thus be grafted onto GO by a hydrolysis-condensation reaction. A grafting content of 6 wt% was evidenced by TGA, and a significant increase in stability of suspensions of modified GO in toluene could be achieved up to a concentration of 1 mg/mL. In a further study, the grafting of polyisoprene on GO-TESPT could be performed. Hence, TESPT bears sulfur atoms that may react with polyisoprene double bonds to form crosslinks between GO-TESPT and polyisoprene.

In the last section, the covalent attachment of polyisoprene chains on the surface of GO has been attempted, in two steps, using a bifunctional modifier.

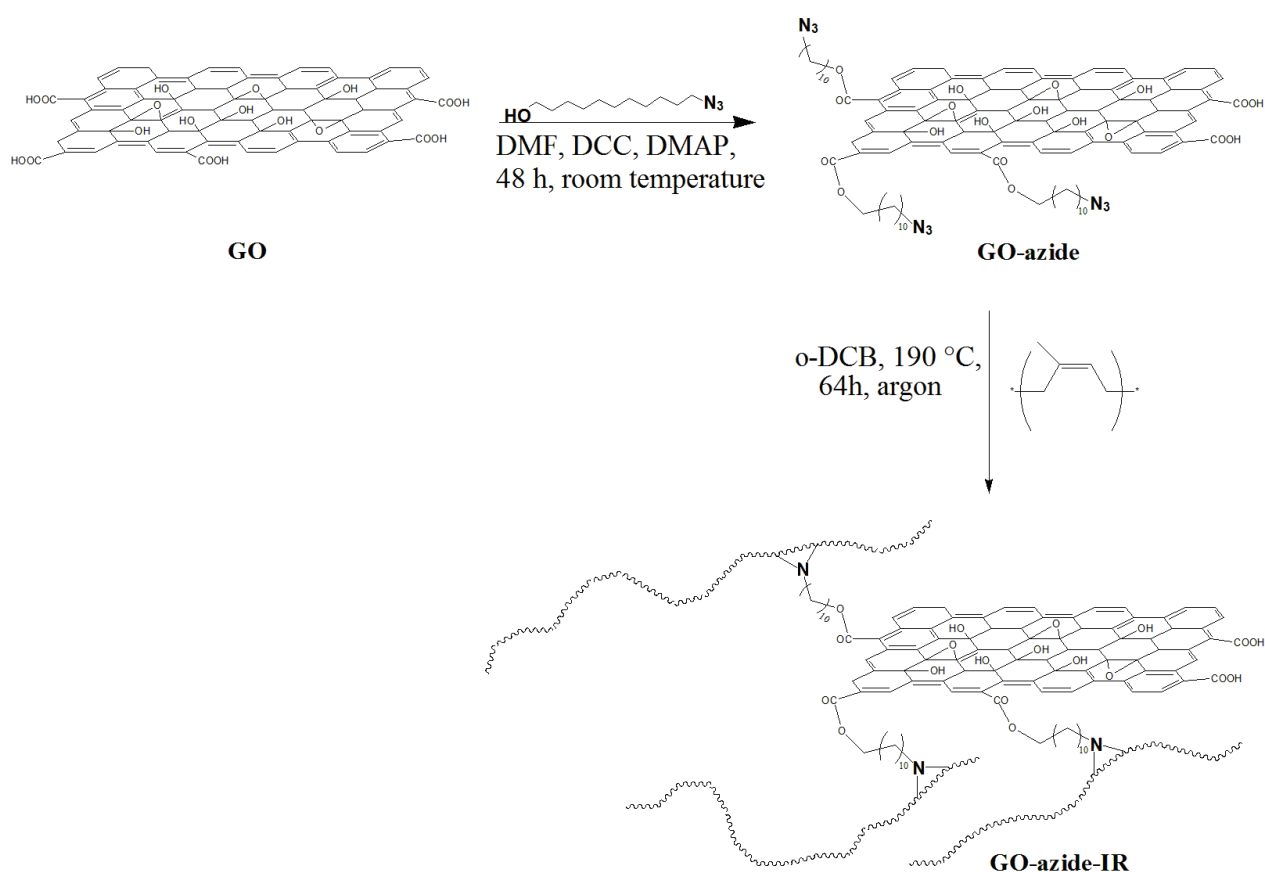
5. Grafting of polyisoprene chains onto GO through nitrene chemistry

Grafting of polymer chains onto GO has been widely reported in the literature [137, 314–318]. A wide range of chemical reactions may be used. Hence, Sun et al [318] reported the grafting of polystyrene chains onto the surface of GO using azide chemistry and they obtained a polystyrene weight content of 20 % (one chain per 1500 carbons in the graphene lattice). They also reported enhanced dispersibility of the modified platelets in organic solvents such as DMF [318]. Similarly, Guimont et al [137] reacted azido-polyethylene onto GO. They achieved a polyethylene grafting content of less than

1 wt%, but they noticed anyhow a strong increase in affinity of the platelets for heptane as compared to unfunctionalized reduced GO platelets that sediment immediately in heptane.

In this study, a “grafting to” procedure was applied to anchor polyisoprene chains onto the surface of GO. This reaction path requires adequate functional groups on GO and the polymer or the use of an appropriate modifier, able to react with both the graphitic substrate and the elastomer.

Compatibilization of GO sheets with polyisoprene was attempted through the grafting of polyisoprene chains onto the surface of GO in two steps, using a bifunctional molecule as a modifier, as shown in Scheme 17.



Scheme 17: Grafting of polyisoprene onto azide-modified GO.

The reaction involves the use of a bifunctional molecule such as 1-azido-undecanol, able to react with GO and IR. First, the hydroxyl functionality of the modifier can react with carboxylic acid groups of GO through an esterification reaction, leading to GO bearing azide functionalities, that can further react with polyisoprene double bonds through nitrene chemistry (cycloaddition reactions).

5.1. Esterification of 1-azido-undecanol onto GO

Esterification reaction onto GO has been widely described in the literature [66, 319–321]. Many authors reported the use of either carboxylic or hydroxyl groups on GO to react with a functional molecule. Hence, Jia et al [129] reacted either polyols and dicarboxylic acids onto GO to create crosslinked membranes. The membranes were reported to be ion selective and showed a 15.6 times higher elastic modulus than pristine GO [129]. Similarly, Cano et al [319] prepared modified GO

membrane through ester bonding between PVA and GO. The resulting modified membranes containing PVA with molecular weights from 50 to 150 kg/mol exhibited improved Young’s modulus by 60 % and improved tensile strength by 40 % as compared to pristine GO membranes [319].

In the present study, ester bonds between 1-azido-undecanol and GO were formed (see Appendix 3.4.1. for the experimental procedure). The resulting product was characterized by FTIR, TGA, UV-vis spectroscopy, GC-MS and XPS.

FTIR is a fast and convenient technique to investigate the structure of a material. Herein, GO-azide was characterized by FTIR, as shown in Figure 66.

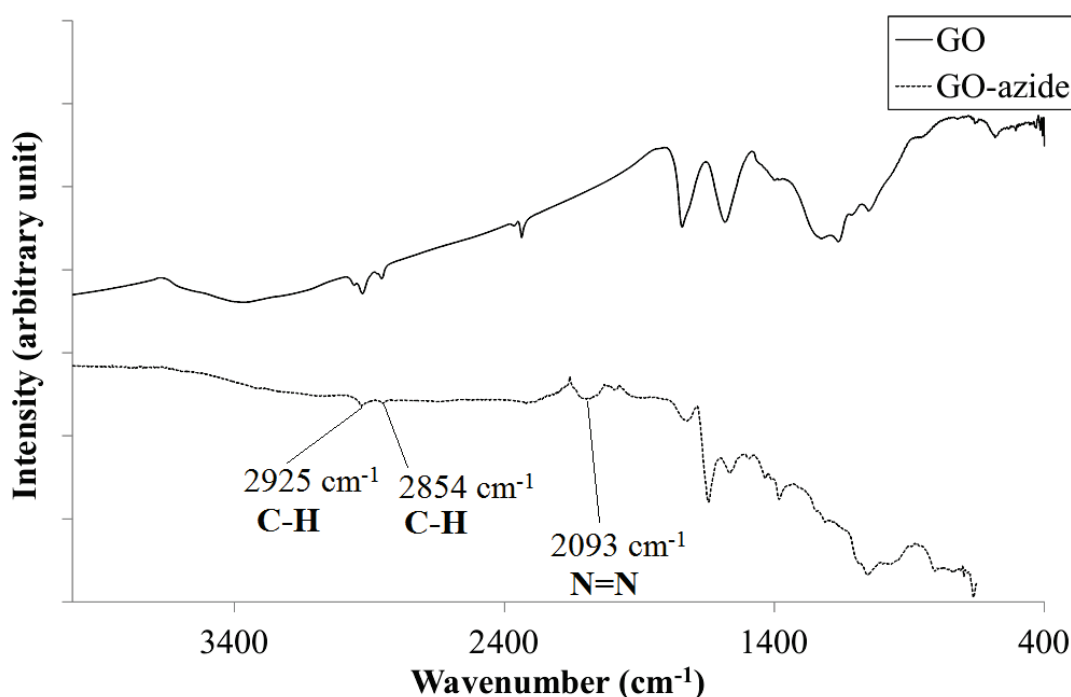


Figure 66: FTIR spectra of GO and GO-azide.

Characteristic vibration peaks of GO are visible. Besides, two new peaks at 2925 cm^{-1} and 2854 cm^{-1} may be observed and may be attributed to C-H asymmetric and symmetric stretching bands respectively of the CH_2 groups of the C_{11} alkyl chain of the grafted 1-azido-undecanol. However, these peaks are in the same region as vibration bands of aromatic carbons of GO and their attribution is not straightforward. In the $3600\text{--}3100\text{ cm}^{-1}$ region, O-H stretching vibration band is almost not observed, thus showing a strong decrease in the hydrophilicity of the material, due to the grafting of 1-azido-undecanol. Besides, a peak at 2093 cm^{-1} may be attributed to N=N vibration band of the azide groups [322]. FTIR spectrum may thus confirm the presence of 1-azido-undecanol onto GO.

To ensure that all 1-azido-undecanol is grafted onto GO, several washing steps were performed and their efficiency was followed by UV-vis spectroscopy. Figure 67 shows the UV-vis absorption spectra of the supernatants resulting from the last 4 washing steps (numbered from 8 to 12).

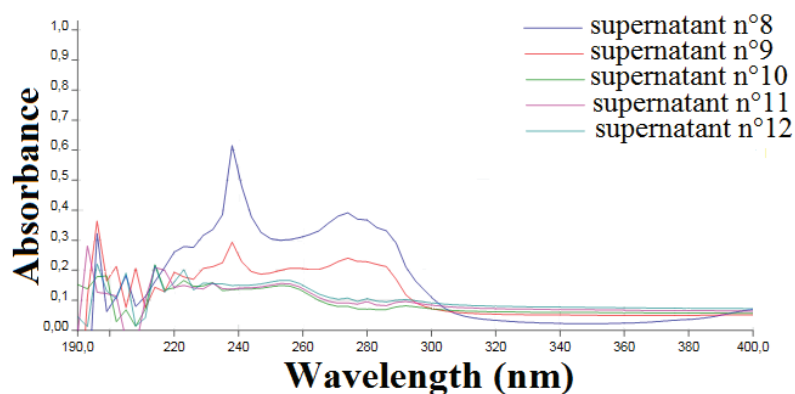


Figure 67: UV-vis absorption spectra of supernatants n°8 to 12 from GO-azide washing with THF.

In the supernatant n°8, a broad absorption band at 280 nm is observed and can be attributed to the presence of 1-azido-undecanol [323]. In the supernatant n°11, the intensity of this absorption band is largely reduced. It can be observed that no further decrease is seen in the supernatant n°12, suggesting that all extractible 1-azido-undecanol has been removed.

XPS analysis was also performed on GO-azide. The low-resolution spectrum and the high-resolution C 1s spectrum are displayed in Figure 68.

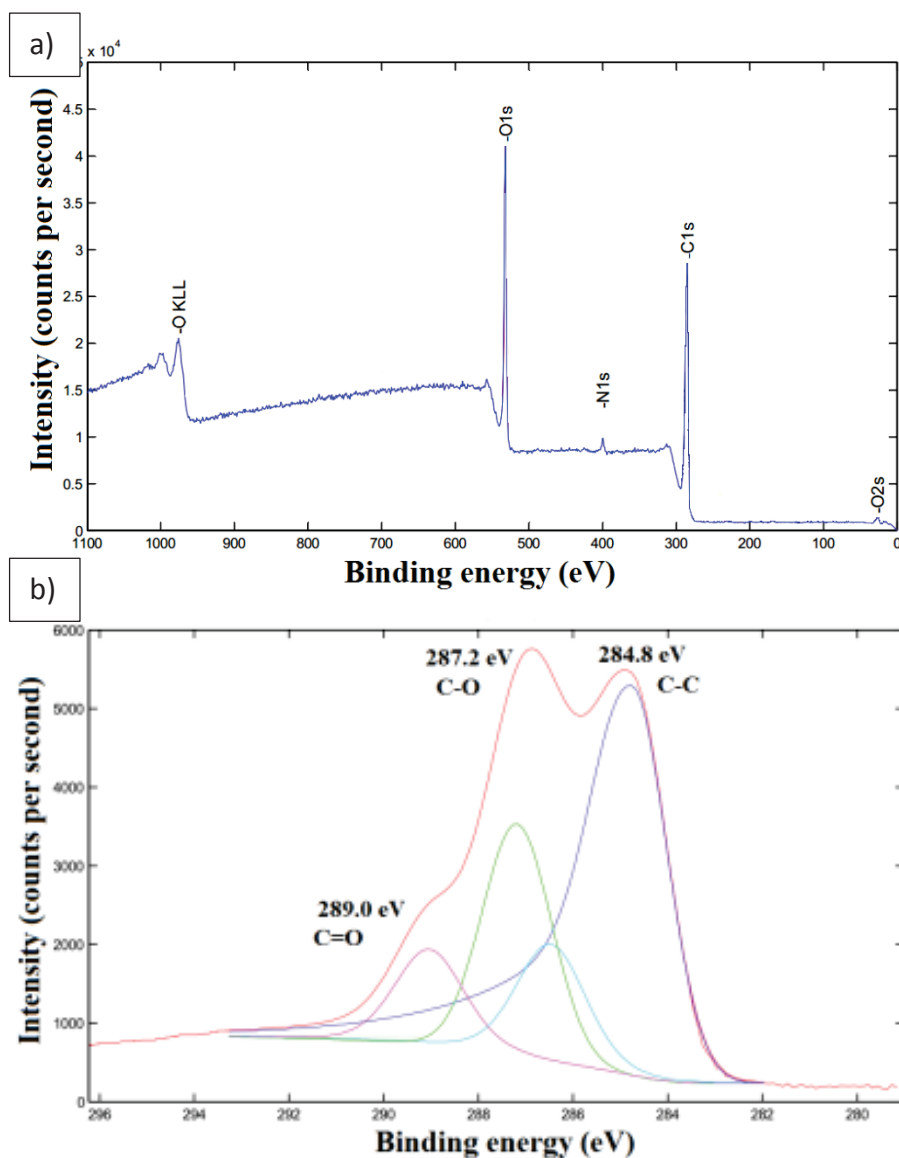


Figure 68: XPS spectra of GO-azide. a) low resolution spectrum of GO-azide and b) high resolution C 1s spectrum of GO-azide.

The appearance of a peak attributed to N 1s at 400 eV can be observed and corresponds to the presence of azide groups (Figure 68a). Moreover, the C 1s spectrum of GO-azide shows characteristic C=O, C-O and C-C peaks of GO suggesting that GO structure was well preserved.

Then, thermogravimetric analysis of azide-modified GO was performed to quantify the amount of 1-azido-undecanol grafted onto the surface (Figure 69).

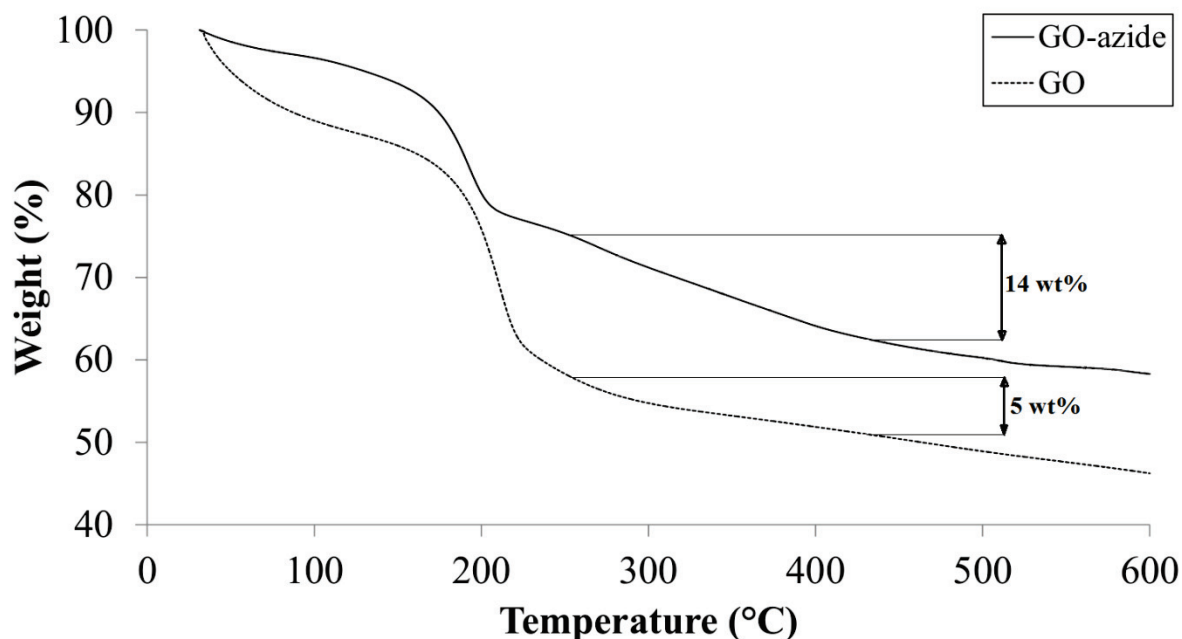


Figure 69: TGA thermogram of GO and GO-azide under helium at 5 °C/min.

As for GO, three main domains are seen. A first mass loss below 100 °C is attributed to the removal of physisorbed water from the surface. This loss is lower than for pristine GO, suggesting a more hydrophobic material. At a temperature of around 200 °C, a main mass loss due to the degradation of oxygen functional groups (pyrolysis) is visible. Finally, at higher temperatures, a greater mass loss than pristine GO is observed and is attributed to the grafted azide onto GO. The weight loss difference in the 250 °C-450 °C temperature range is of 9 wt%, corresponding to an “azide” grafting density of 0.435 mmol/g.

In addition, the stability of azide-modified GO platelets in toluene was investigated (Figure 70).

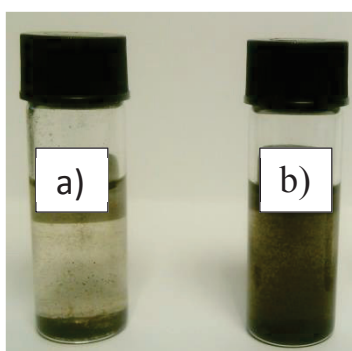


Figure 70 : Suspensions of a) GO and b) GO-azide in toluene at a concentration of 1 mg/mL.

The modified platelets showed slightly enhanced stability as compared to pristine GO dispersions in toluene at a concentration of 1 mg/mL.

Besides, gas chromatography - mass spectrometry (GC-MS) has been performed to investigate whether the azide functionality had been degraded during grafting. Even if its FTIR spectrum seems to

indicate that the N_3 group is still present, GC-MS is more accurate in determining the presence of azide functional group onto modified GO. Two different experimental conditions were used (Figure 71).

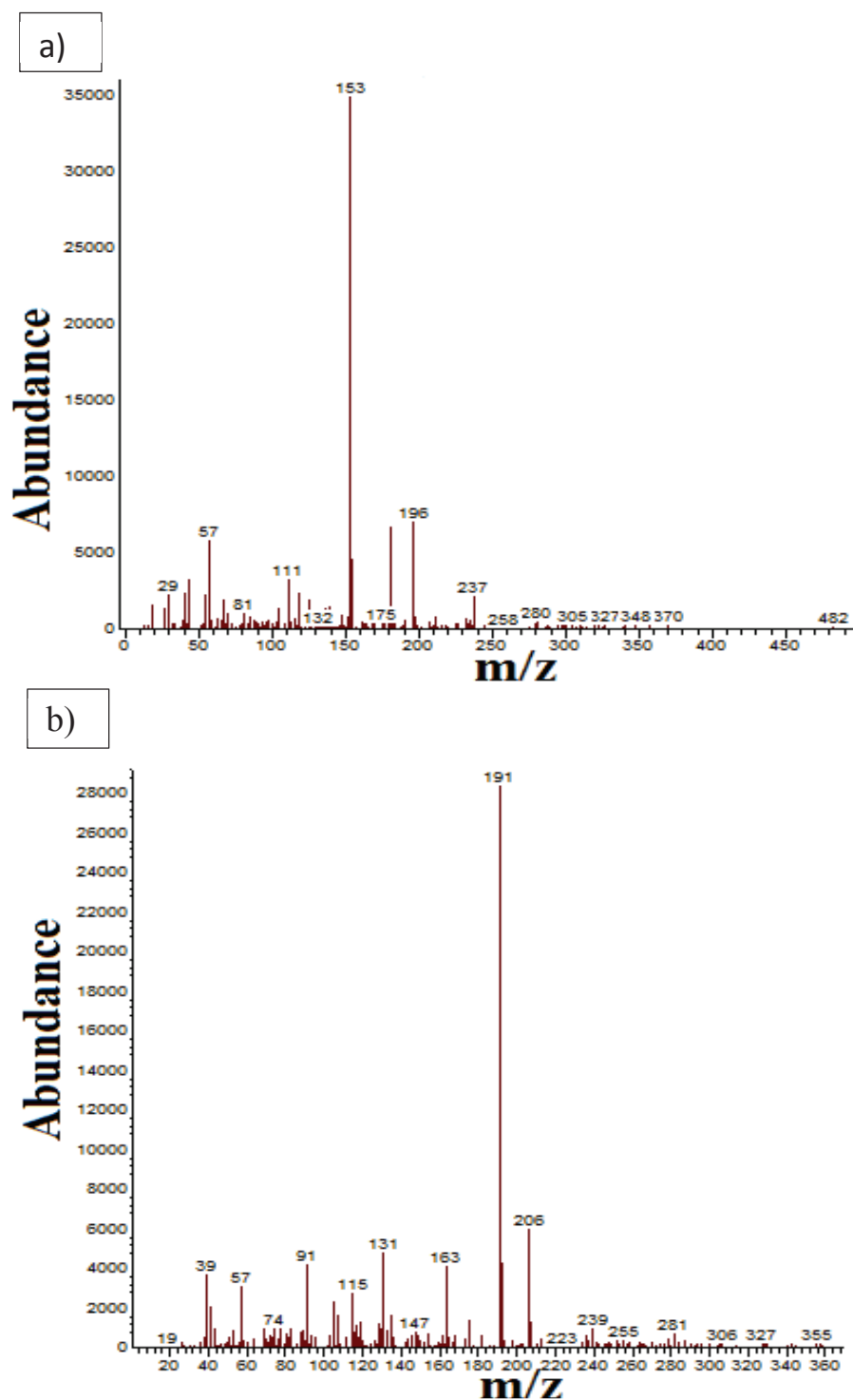


Figure 71: GC-MS spectra of GO-azide after heating at a) 180 °C and b) 275 °C.

The first sample was heated at 180 °C for 30 min under argon (no degradation of the azide group to nitrene radical expected) and the second one was heated at 275 °C for 30 min under argon prior to analysis. For the sample heated at 180 °C, fragments such as $C_{11}H_{22}N_3$ (153), $C_{11}H_{21}$ (196) and CH_3N_3 (57) were identified and are consistent with the presence of azide groups onto the surface of GO.

However, when GO-azide is heated at higher temperatures prior to GC-MS analysis, no such fragments can be identified, suggesting that the azide groups are degraded [324]. This analysis is thus consistent with the previous analyses and enables the reaction of azide groups onto modified GO to potentially react with polyisoprene in a second step, through a cycloaddition reaction. Indeed, it is expected that azide groups will lead to the formation of nitrene radicals, at temperatures higher than 180 °C, that are able to react with polyisoprene double bonds through a cycloaddition reaction.

Finally, the morphology of the platelets was investigated by SEM (Figure 72).

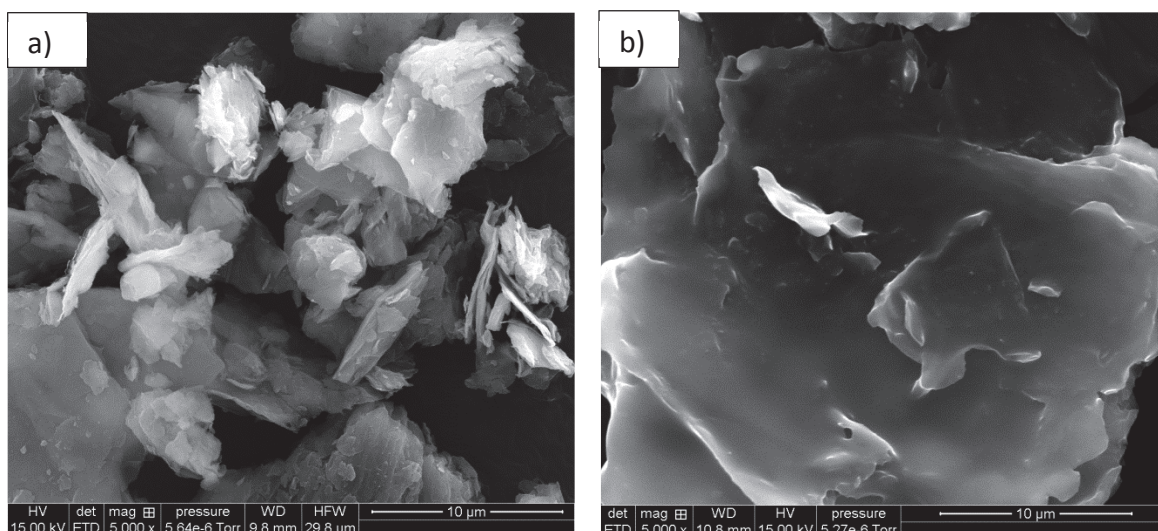


Figure 72: SEM pictures of a) GO and b) GO-azide.

Both materials exhibit similar morphology. GO-azide sample is made of wrinkled platelets of 10 µm to 20 µm, containing few oxidative debris [108, 110].

In this section, GO-azide has thus been successfully prepared with azide groups available for further modification steps.

1-azido-undecanol could thus be grafted on GO by an esterification reaction. A grafting content of 9 wt% was achieved, and a significant increase in stability of suspensions of modified GO in toluene could be achieved up to a concentration of 1 mg/mL. Besides, GC-MS analysis evidenced that azide groups were not degraded during the grafting of 1-azido-undecanol onto GO, which enables further functionalization of GO using azide groups of GO-azide.

5.2. Cycloaddition of GO-azide onto polyisoprene

As discussed before, nitrenes are reactive species that are often regarded as carbene analogues and they are formed from decomposition of azides by removal of nitrogen gas. Thus, the resulting product contains a nitrogen atom with six electrons available and is therefore an electrophilic species. These species are however too reactive to be isolated and they can react through cycloaddition reactions with unsaturated bonds to form aziridines groups [46, 325–327].

Several groups have reported the use of azide compounds to crosslink elastomers [328–331]. For example, Damiron et al [328] used 1,12-diazidododecane to crosslink poly(dimethylsiloxane-co-

methylvinylsiloxane) elastomer. They achieved a fraction of elastically active crosslinks of 160 mol/m^3 . They claimed that their system could also be adapted to a wide range of unsaturated polymers [328].

In the present study, nitrene chemistry is performed to graft polyisoprene chains onto azide-functionalized GO surface (see Appendix 3.4.2. and 3.4.3. for the experimental procedures). Upon heating at a temperature of $190 \text{ }^\circ\text{C}$, azide-grafted GO reacts onto polyisoprene through the addition of nitrene radicals located on GO with polyisoprene double bonds, as previously shown in Scheme 17. The product (GO-azide-IR) was characterized by TGA, XPS and SEM.

TGA thermograms of GO, GO-azide, GO-azide-IR and GO heated at $190 \text{ }^\circ\text{C}$ are presented in Figure 73.

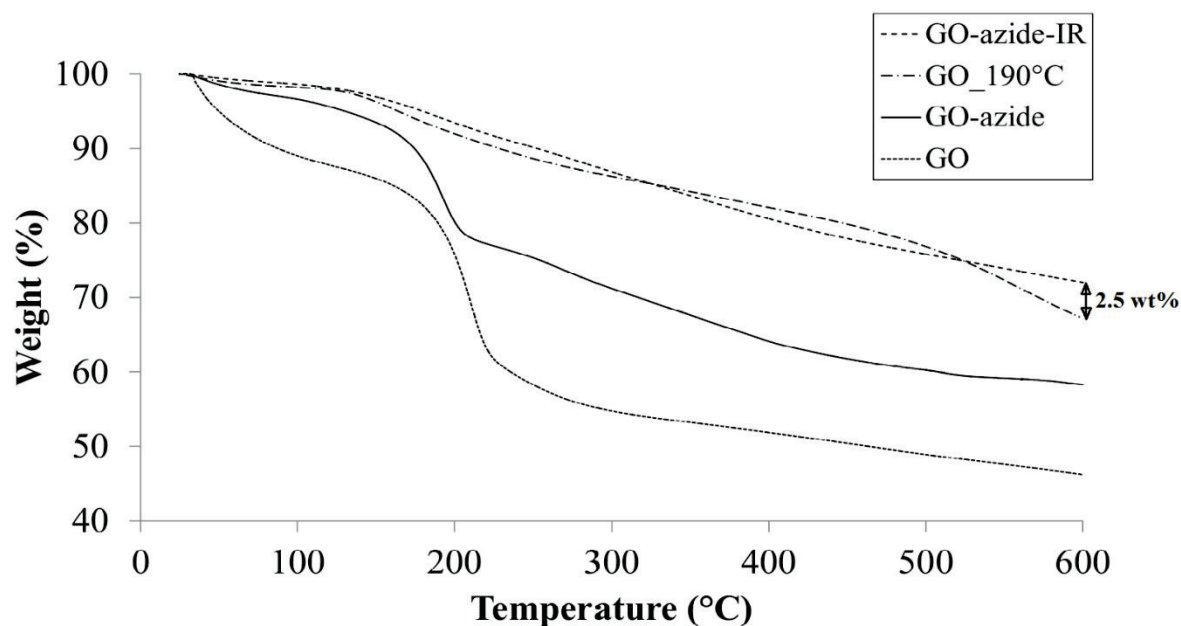


Figure 73: TGA thermograms of pristine GO, GO-azide, pristine GO heated at $190 \text{ }^\circ\text{C}$ during 64 h under argon (GO_190 °C) and GO-azide-IR.

The first observation one can make is that GO underwent reduction during the reaction. Hence, upon heating pristine GO at $190 \text{ }^\circ\text{C}$, a strong decrease in the total mass loss is seen. In the $150\text{--}250 \text{ }^\circ\text{C}$ region, 12 wt% loss is measured for pristine GO heated at $190 \text{ }^\circ\text{C}$ while pristine GO shows more than 32 wt% mass loss in the same region. The reduction of GO occurred through a solvothermal process in which thermal decomposition of oxygen functional groups occurs when heated in a solvent. Hence, Dubin et al [159] reported the solvothermal reduction of GO in NMP without the use of any reducing agent. Other groups reported similar observation for solvothermally reduced GO [128, 137, 152]. GO-azide-IR shows a very similar behavior than solvothermally reduced GO (GO_190 °C). It can thus be guessed that very low amount of polyisoprene has been grafted onto GO-azide. A difference of 2.5 wt% at $600 \text{ }^\circ\text{C}$ can be observed between the GO_190 °C sample and the GO-azide-IR one. However it is questionable whether such a small value is significant.

To further characterize the material, XPS analysis was also performed (Table 8 and Table 9). The following tables gather atomic compositions as well as the nature of the chemical bondings in pristine GO, GO-azide and GO-azide-IR samples.

	C	O	N
GO	75.1	24.0	/
GO-azide	69.6	27.8	2.5
GO-azide-IR	84.7	11.8	2.0

Table 8: Atomic compositions of pristine GO, GO-azide and GO-azide-IR samples.

	C-C / C-H	C-O / C-N	O-C-O / N-C-O	O-C=O / O-C=N / N-C=O
GO	69	11	13	6
GO-azide	56	12	22	10
GO-azide-IR	94	2	1	3

Table 9: Chemical bondings in pristine GO, GO-azide and GO-azide-IR samples.

From Table 8, it can be seen that GO contains no nitrogen while GO-azide samples contain 2.5 %. In GO-azide-IR sample, a small decrease of 0.5 % is observed. This change is however too low to be considered as significant. However, the decrease in oxygen content from 27.8 % to 11.8 % for GO-azide and GO-azide-IR respectively, is significant and can be attributed to the reduction of GO during heating at 190 °C, corresponding to the removal of most oxygen groups from GO surface. Table 9 confirms that C-C and C-H bonds content increase from 56 % to 94 % from GO-azide to GO-azide-IR, due to the solvothermal reduction occurring during the reaction. Dubin et al [159] also reported a significant increase in the intensity of the peak corresponding to C=C bond, while the oxygen content decreased markedly upon reduction of GO.

Then, the stability of suspensions of GO-azide-IR in toluene was investigated (Figure 74).

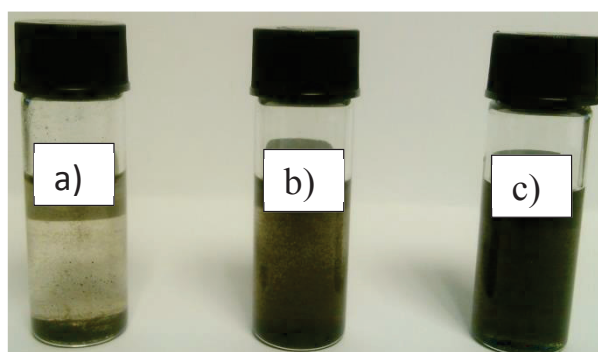


Figure 74: Digital images of suspensions of a) GO, b) GO-azide and c) GO-azide-IR in toluene at a concentration of 1 mg/mL.

Increased stability in toluene at a concentration of 1 mg/mL was observed for GO-azide-IR, as compared to pristine GO and to GO-azide. This difference is expected to be due to the reduction of the hydrophilicity of GO through removal of most oxygen groups during reduction. Several groups reported that reduced GO exhibited enhanced dispersibility in organic solvents such as DMF, NMP and DMSO but little stability in toluene was often reported due to a low polarity of this solvent [159, 332]. It is thus possible that the modified platelets in this study show a good dispersibility in toluene due to grafting of a few polyisoprene chains on the surface of GO as well as remaining alkyl chains from 1-azido-undecanol grafting.

Scanning electron microscopy was also performed on the modified platelets to study the morphology of GO-azide-IR nanosheets (Figure 75).

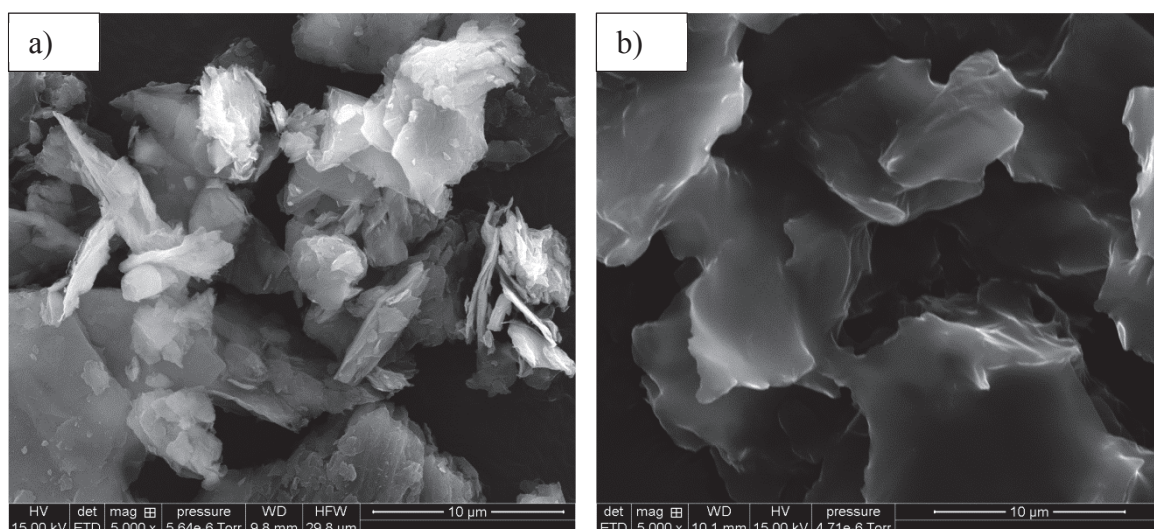


Figure 75: SEM pictures of a) pristine GO and b) GO-azide-IR.

Both materials exhibit platelet morphology with wrinkled surface. On GO-azide-IR sample no oxidative debris are observed indicating that they have been removed by the reduction process and by the washing procedure [110]. However, the very low content of polyisoprene chains on the surface of GO is not able to change its morphology.

In conclusion, GO has been modified with 1-azido-undecanol through an esterification reaction with a grafting content of 9 wt%. Through GC-MS analysis, it has been shown that azide functionalities were not degraded during the process. In a second step, GO-azide was reacted onto polyisoprene through a cycloaddition reaction. However, no significant efficiency of the reaction was observed and it was concluded that the platelets underwent mainly reduction due to a solvothermal process. Suspensions of the modified GO exhibited anyhow an increase in the stability of suspensions in toluene at up to a concentration of 1 mg/mL.

Conclusion

In this chapter, several modification pathways of GO have been investigated. First, the preparation and characterization of GO, a graphitic material containing oxygen functional groups such as epoxide, carboxylic acid groups and hydroxyl groups, has been reported. The presence of these reactive sites was evidenced through FTIR. Besides, TGA showed a degradation profile in three steps: (i) loss of physisorbed water (~ 10-15 wt%), (ii) pyrolysis of most oxygen-based functional groups (~ 30 wt%) at a temperature around 200 °C and (iii) pyrolysis of most stable oxygen groups (~ 5wt%). GO platelets were observed to lead to stable suspensions in water at concentrations of 1 mg/mL. Then, several functionalization reactions have been performed on GO platelets, involving its oxygen-based functional groups.

In a first functionalization path, octadecylamine has been grafted onto GO for compatibilization with polyisoprene. Hence, its long non-polar alkyl chains reduced GO hydrophilicity and increased its affinity for organic solvents such as toluene at 10 wt% grafting content, thus suggesting enhanced GO-ODA / polyisoprene compatibility. The reaction was performed through a NS reaction path and, in a further

study, the use of different experimental conditions could enable amidation reactions to occur and thus, could increase the ODA grafting density onto GO.

In a second section, the grafting of TESPT, a common silane coupling agent, onto GO was performed. The reaction led to a 6 wt% grafting content and increased stability of suspensions of the modified filler in toluene at a concentration of 1 mg/mL. In a further study, GO-TESPT could react with polyisoprene double bonds to form sulfur crosslinks between GO-TESPT and polyisoprene, to enhance compatibility of GO-TESPT with a polyisoprene matrix.

In a last section, a functionalization in two steps, involving the grafting of bifunctional molecule onto GO and IR chains has been performed. 1-azido-undecanol could be grafted onto GO surface through an esterification reaction at room temperature with a grafting content of 9 wt%. In a second step, the cycloaddition of GO-azide onto IR chains has been performed. The material was shown to undergo solvothermal reduction (i.e. removal of most oxygen functional groups present on the surface of GO) during the heating process. A low grafting content of 2.5 wt% was achieved and was anyhow able to significantly increase the stability of GO suspensions in toluene at a concentration of 1 mg/mL.

Grafting of short molecules onto GO has thus proven to be of significant interest in enhancing dispersibility and compatibility of GO-based fillers in a polyisoprene matrix. The covalent attachment of polyisoprene chains onto the surface of GO has been attempted but did not lead to a high grafting content. However, other methods such as in situ polymerization can be attempted in order to incorporate a greater amount of IR chains onto GO. Chapter 3 will thus deal with in situ polymerization onto GO, through several methods.

Chapter 3: In situ polymerization of isoprene onto graphite oxide

Table of contents of Chapter 3

Introduction.....	142
1. Functionalization strategies	142
2. Grafting of acryloxy and allyl groups onto GO through a hydrolysis-condensation reaction.....	144
2.1. APTMS grafting onto GO	144
2.2. Allyltrimethoxysilane grafting onto GO.....	145
3. In situ polymerization of isoprene onto modified GO.....	148
3.1. Emulsion free radical polymerization of isoprene in the presence of GO-APTMS.....	148
3.1.1. Blank experiment	149
3.1.2. Grafting of polyisoprene onto GO-APTMS	153
3.2. Emulsion cationic polymerization of isoprene in presence of GO-allyl.....	157
3.2.1. Blank experiment	158
3.2.2. Grafting of polyisoprene in presence of GO-allyl	159
Conclusion	164

Introduction

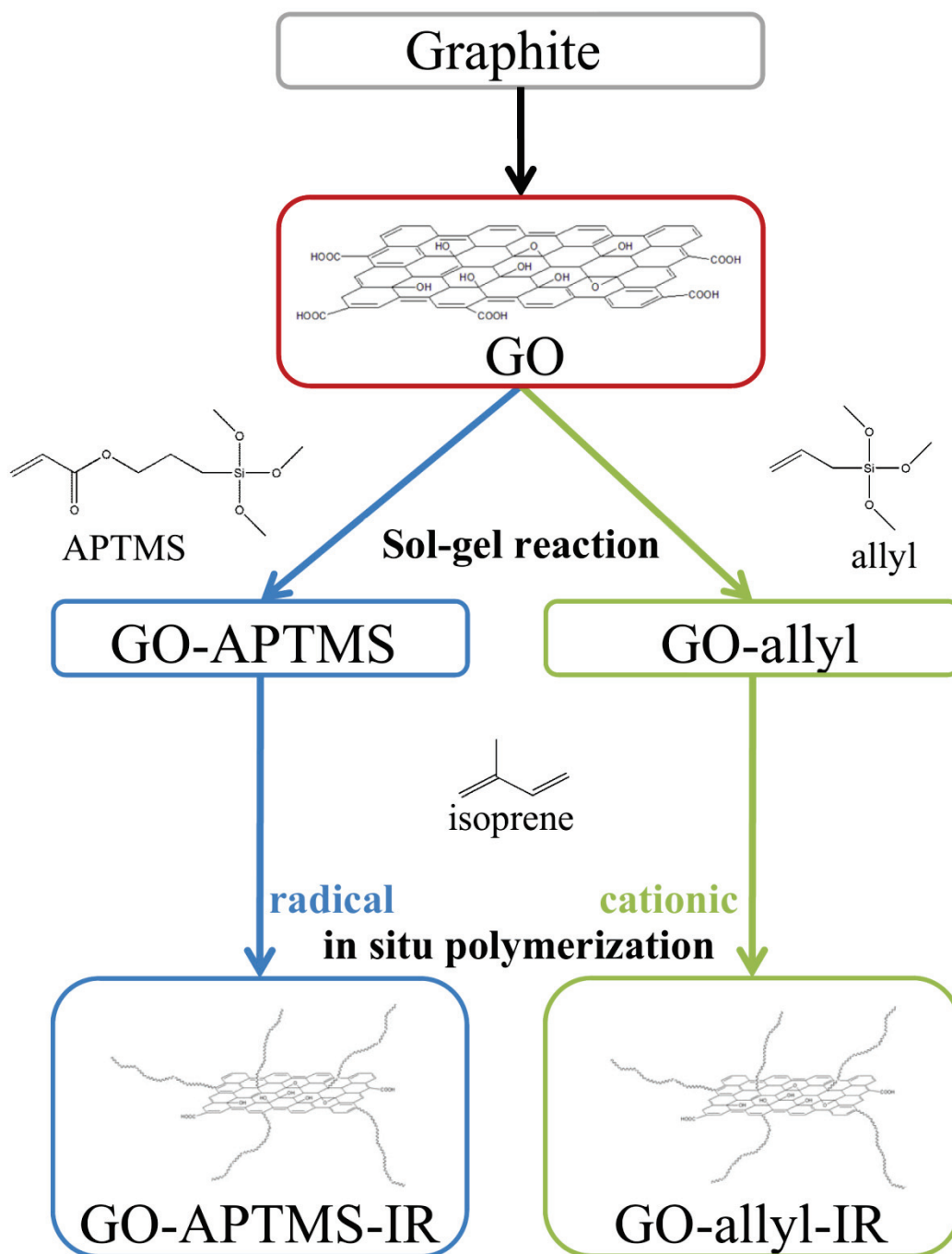
To achieve enhanced dispersion and compatibility with various matrices, grafting of polymer chains onto GO surface has been performed in chapter 2 by addition of short compatibilizing molecules or polymers. The latter yielded a low grafting content of only 2.5 wt% when prepared using cycloaddition reaction. Another method to covalently anchor polymers onto GO surface has been reported and consists in in situ polymerization of a monomer in presence of GO. In situ polymerization strategies are often complex to perform and it may be difficult to control properly the structure and molecular weight of the final polymer [314]. Besides, this method often requires modification of the graphitic substrate prior to the polymerization reaction (chemical modification with an initiator for example). For example, the grafting of N-(2-aminoethyl)-2-bromo-2-methylpropanamide (OBr) onto GO for styrene ATRP polymerization has been reported [333]. However, many research groups have achieved interesting results and a great number of studies have been published in the field of thermoplastics [73–75, 334, 335]. However, little work has been performed with elastomers. Anyhow, Garcia-Valdez et al [336] have studied the in situ polymerization of isoprene onto GO through nitroxide mediated radical polymerization. They obtained 68 wt% of polyisoprene grafted on GO surface with an average molar mass of 760 g/mol. Other groups also reported in situ polymerization of isoprene onto GO or carbon nanotubes [337, 338].

In the present study, in situ polymerization of isoprene according to two strategies has been carried out.

1. Functionalization strategies

To increase compatibility between non-polar polyisoprene (IR) and polar GO, covalent functionalization of GO has been performed through the grafting of IR chains onto the surface of GO. A “grafting through” method has been chosen, involving in situ polymerization of isoprene monomer onto functionalized GO sheets. In a first step, GO has been grafted with alkoxysilanes bearing dangling double bonds that can act as “anchor sites” for polyisoprene chains. Indeed, hydrolysis-condensation reaction of alkoxysilane reagents with the carboxylic acid and hydroxyl groups of GO is well-known and has already been widely reported in the literature [28, 123–125, 128]. In a second step, isoprene has been in situ polymerized onto previously functionalized GO through a radical or a cationic process. This reaction is challenging as it has not often been reported in the literature. Moreover, blank experiments without GO have been performed to show the ability of isoprene to polymerize through a radical and a cationic method.

Scheme 18 sums up the functionalization strategies developed in this section.



Scheme 18: Functionalization strategies for the grafting of IR onto GO.

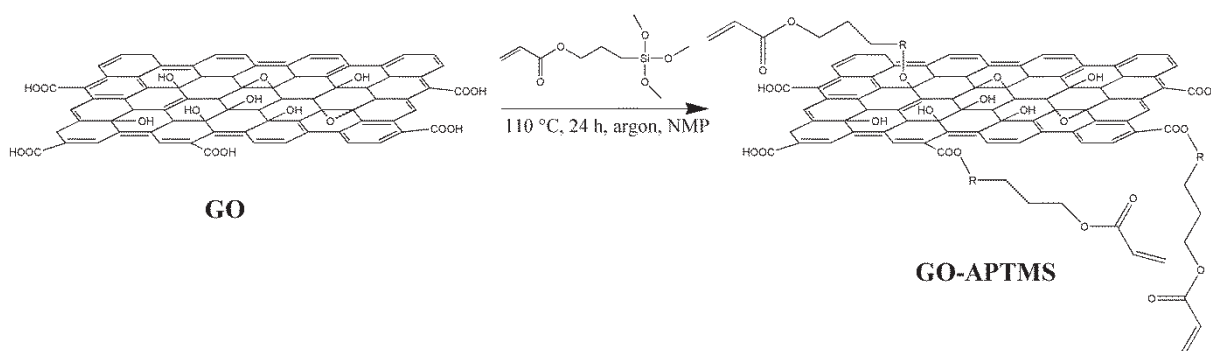
Graphite oxide was first modified by 3-acryloxypropyltrimethoxysilane (APTMS) or allyltrimethoxysilane (allyl) through a sol-gel process, followed by in situ free radical or cationic polymerization of isoprene onto the resulting modified GO. Then, polyisoprene-functionalized GO nanosheets were isolated and characterized [339].

2. Grafting of acryloxy and allyl groups onto GO through a hydrolysis-condensation reaction

2.1. APTMS grafting onto GO

To reduce GO hydrophilicity and to increase its compatibility with a polyisoprene matrix, it has been chosen in the present study to graft polyisoprene chains onto the surface of GO. A grafting through procedure, involving in situ free radical polymerization of isoprene on functionalized GO, has been performed.

To polymerize isoprene in situ on GO, anchor sites are necessary. Hence, GO needs to be modified in order to bear easily available double bonds for isoprene units attachment in presence of an initiator. In this study, GO was first modified with 3-acryloxypropyl trimethoxysilane (APTMS) to provide an acrylic double bond for isoprene polymerization. Indeed, APTMS is a reactive molecule bearing methoxysilane groups that can react with GO carboxylic acid and hydroxyl groups via a hydrolysis-condensation reaction (Scheme 19).



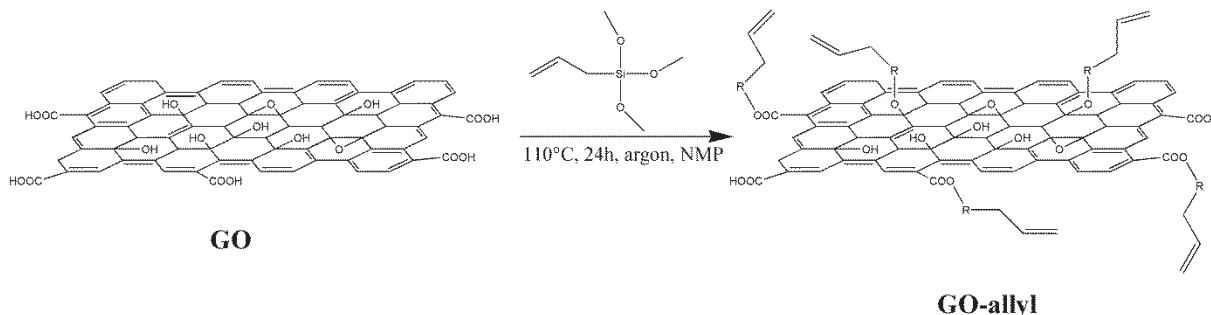
Scheme 19: APTMS grafting onto GO.

APTMS is grafted onto GO via a hydrolysis-condensation reaction involving Si-O-C linkages. Anchoring alkoxy silanes on GO surface has already been reported by several groups such as Matsuo et al [340, 341] who used various aminopropyltriethoxysilanes and reached a grafting density of around 4 mmol/g, as determined by TGA. Guimont et al [128] also grafted trimethoxy(7-octen-1-yl)silane (TMOS) through a similar procedure and obtained a grafting density of about 0.2 mmol/g. They showed that the use of increasing quantities of TMOS had no significant effect on the grafting density and they obtained stable suspensions of GO-TMOS in PDMS oil at a concentration of 0.1 mg/mL. Besides, they were able to use dangling TMOS double bonds to graft PDMS through a hydrosilylation reaction.

In the present study, APTMS-grafted GO (GO-APTMS) was synthesized according to the method of Guimont et al [342] and similar results were obtained (the experimental procedure is described in Appendix 4.1.1.). GO sheets containing 4 wt% of APTMS (0.24 mmol/g) and bearing acrylic double bonds have been prepared and the APTMS grafting did not affect the morphology of the platelets observed by SEM, nor the stacking structure, as revealed by XRD and Raman spectroscopy (see Appendix 4.3.). However, a significant reduction in hydrophilicity of the platelets has been achieved. GO-APTMS sheets showed good affinity for toluene, thus suggesting potentially good compatibility with both isoprene and polyisoprene.

2.2. Allyltrimethoxysilane grafting onto GO

Similarly to APTMS, allyltrimethoxysilane was grafted onto GO through a hydrolysis-condensation reaction. Allyl group was preferred over acrylic group because allyltrimethoxysilane is less polar than APTMS. The reaction path is shown in Scheme 20. GO-allyl stands for “allyltrimethoxysilane-grafted GO”.



Scheme 20: Grafting of allyltrimethoxysilane onto GO.

The experimental procedure is similar to APTMS grafting onto GO (see Appendix 4.1.4.).

GO-allyl was characterized qualitatively and quantitatively. FTIR analysis provided evidence of allyltrimethoxysilane presence on GO (Figure 76).

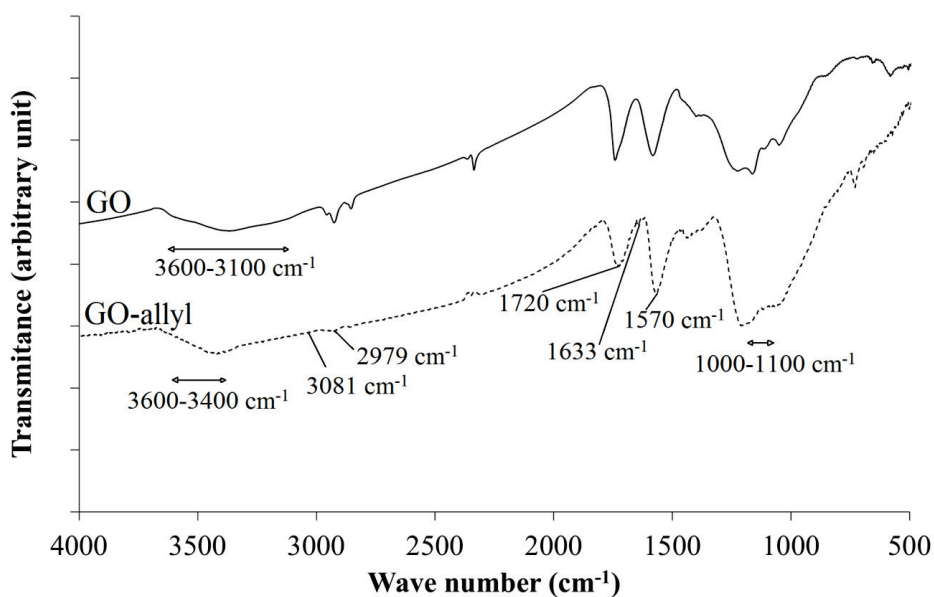


Figure 76: FTIR spectra of GO (top) and GO-allyl (bottom).

In pristine GO, the hydroxyl region exhibits a wide OH stretching vibration band in the range 3600-3100 cm^{-1} due to physisorbed water while the GO-allyl spectrum displays a reduced OH stretching vibration band due to grafting. The peak at 1720 cm^{-1} may stem from the stretching vibrations of C=O bonds. However, the FTIR analysis did not permit to clearly attest for the presence of both C=C—H asymmetric and symmetric stretching at 3081 cm^{-1} and 2979 cm^{-1} , respectively and C=C bending at 1633 cm^{-1} . Moreover, the expected Si-O bonds in the range 1000-1100 cm^{-1} are difficult to distinguish from the absorption bands of neat GO [343, 344].

In addition, XPS analysis were performed but no clear evidence of the allyltrimethoxysilane grafting onto GO could be observed (see Appendix 4.2.).

Then, XRD measurements were performed to investigate the influence of allyltrimethoxysilane grafting onto the interlayer spacing of GO (Figure 77).

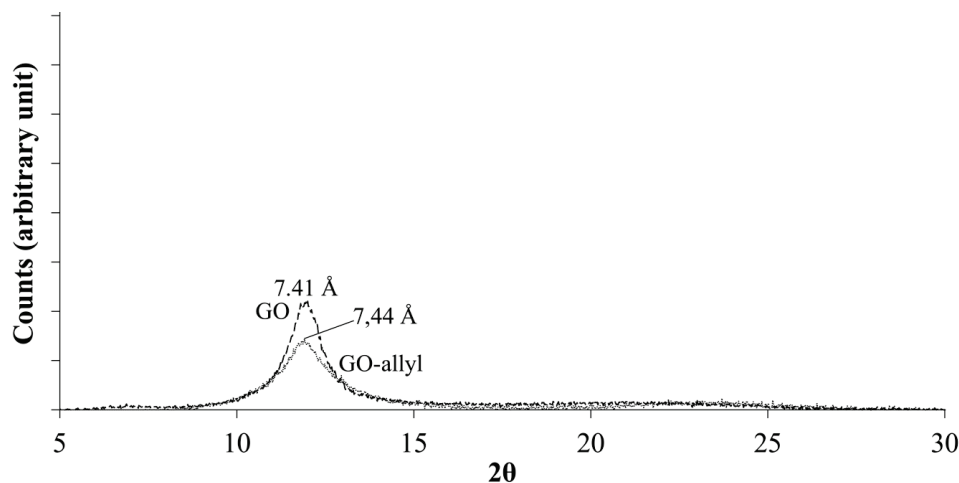


Figure 77: XRD spectra of GO and GO-allyl.

No significant increase in interlayer spacing of GO-allyl was observed in comparison with pristine GO (Figure 77). A similar interlayer distance of 7.4 Å was measured. This may indicate that allyltrimethoxysilane molecules are mainly grafted on the edges rather than between GO layers. Other studies also reported very small effect of the chemical grafting on the interlayer distance [128, 345]

A quantitative approach by thermogravimetric analysis (TGA) allowed accurate determination of the grafting density of the allyl units on the surface. TGA curves of unmodified GO and GO-allyl were recorded in helium atmosphere and are displayed in Figure 78.

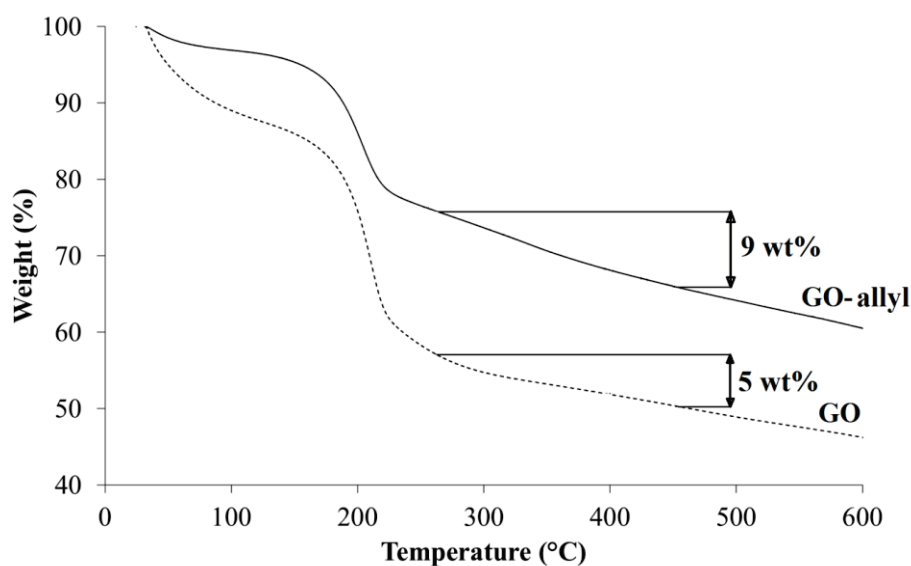


Figure 78: TGA thermogram of GO and GO-allyl.

Allyl-functionalized GO sheets show reduced weight loss below 100°C as compared to pristine GO because attachment of allyltrimethoxysilane makes the surface of GO more hydrophobic. The amount of grafted allyltrimethoxysilane on GO can be calculated from the TGA data by measuring the difference in weight loss observed in the temperature range 250-450 °C (Figure 78). Considering a weight loss of 4 % after subtracting the contribution of GO decomposition in the same temperature range, the calculation gives an allyltrimethoxysilane graft density of 0.24 mmol.g⁻¹. For comparison, Guimont et al. [128] reported a weight loss of 5.3 % (0.2 mmol.g⁻¹) for the grafting of trimethoxy(7-octen-1-yl)silane onto the GO surface. The stability of GO-based dispersions in toluene was also observed directly and the aspect of the suspensions confirms that the hydrophobicity of GO is decreased after allyltrimethoxysilane grafting (Figure 79).

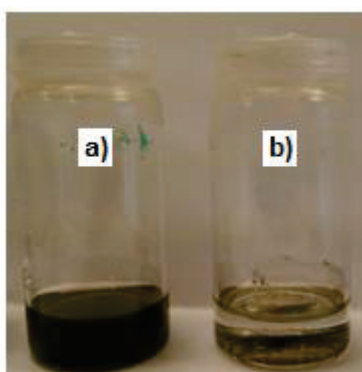


Figure 79: Suspensions of a) GO-allyl and b) GO at a concentration of 1mg/mL in toluene.

Indeed, when placed in toluene, GO sheets sediment almost immediately while GO-allyl sheets, at a concentration of 1 mg.mL⁻¹, disperse well and yield a homogeneous black suspension for at least 24 h.

Then, the morphology of allyl-modified GO was investigated by SEM.

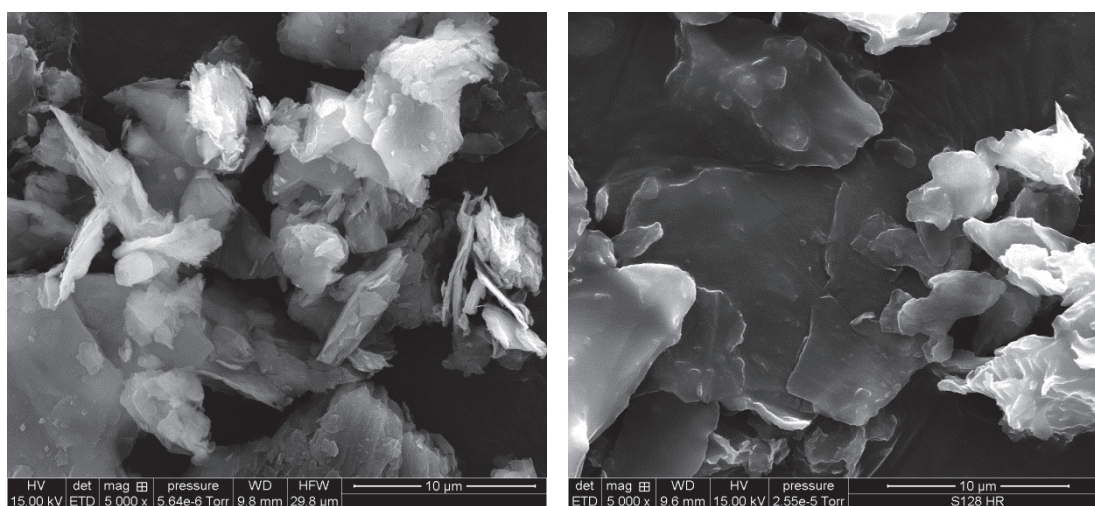


Figure 80: SEM pictures of a) GO and b) GO-allyl.

No significant changes were observed in the morphology of the GO-allyl sample, indicating that the structure of GO is preserved. Wrinkled sheets of various sizes with small “oxidized patches” on the surface of the platelets are seen [108, 110]. Sheet sizes in GO and GO-allyl are similar (< 5 μm).

Thus, through several characterization methods, it has been shown that allyltrimethoxysilane-grafted GO sheets have been successfully prepared with a grafting content of 4 wt%, as determined by TGA. The modified nanoplatelets exhibit enhanced stability in toluene, thus indicating increased compatibility with non-polar media, and then expectedly with elastomers.

The presence of dangling allyl groups on GO-allyl nanosheets was the prerequisite for polyisoprene covalent attachment through in situ polymerization.

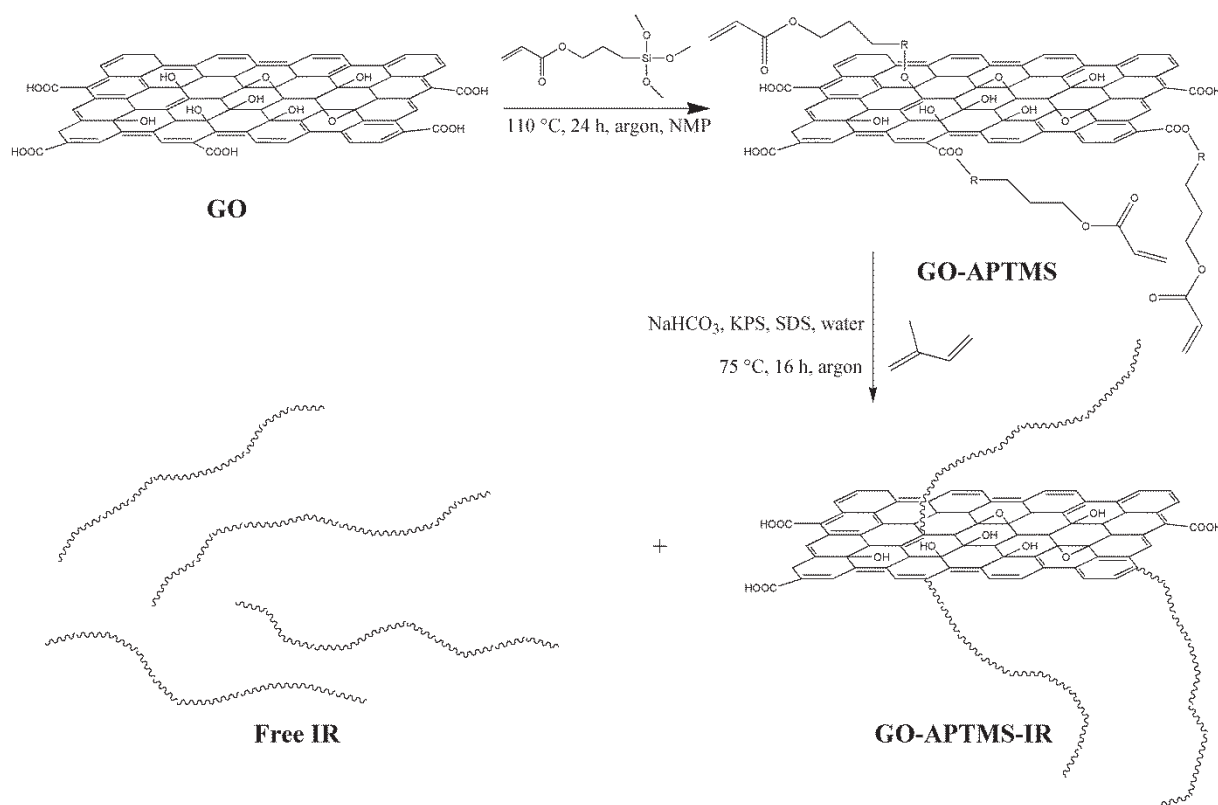
3. In situ polymerization of isoprene onto modified GO

3.1. Emulsion free radical polymerization of isoprene in the presence of GO-APTMS

In situ polymerization of isoprene on GO has been reported by Garcia-Valdez et al [336], using nitroxide mediated radical polymerization (NMRP). Surface modification and functionalization of GO was achieved by using 2,2,6,6-tetramethyl-piperidine 1-oxyl (TEMPO, T), thus allowing the “grafting from” polymerization technique. GO-T acted as a multifunctional macroalkoxyamine initiator thus controlling the polymerization of isoprene [336]. The polymerization reaction was performed at 130 °C during 144 h under 150 psi to obtain polyisoprene-GO. A grafting content of 68 wt% was determined by TGA and a IR molar mass of 760 g/mol was calculated corresponding to 11 monomer units per polyisoprene chain [336].

For comparison, radical polymerization of isoprene has also been performed on carbon nanotubes using ARGET ATRP method to in situ polymerize isoprene from 2-bromoisobutyryl bromide-GO. The authors gravimetrically calculated a CNT content decreasing from 14.7 wt% to 9.6 wt% with increasing polymerization time due to a greater polyisoprene content [337].

In this work, emulsion free radical polymerization of isoprene onto the acrylic double bond of GO-APTMS has been attempted (Scheme 21).



Scheme 21: Emulsion radical polymerization of isoprene onto GO-APTMS.

In a first step, GO was functionalized with APTMS through a sol-gel reaction, as described in section 2 (see Appendix 4.1.1.). In a second step, isoprene was in situ polymerized onto GO-APTMS according to a free radical method.

Before achieving in situ polymerization, a blank experiment was carried out to study isoprene radical polymerization.

3.1.1. Blank experiment

Isoprene polymerization has been reported in the literature. A wide range of polymerization methods have been described: anionic [346–348], cationic [173, 174, 349–352], coordinate [353–359] and radical polymerization [177–181, 360–363] methods. In this study, the use of a free radical polymerization has been chosen. Based on the study of Cheong et al [181], isoprene radical polymerization has been performed in emulsion. In their work, they investigated several redox couples to provide polymerization with a high conversion (up to 95 %) and a gel content below 10 wt%.

In emulsion free radical polymerization, radicals are formed in aqueous phase from the thermal decomposition of an initiator, they then propagate (or recombine) until oligomeric radicals with a certain critical degree of polymerization are formed so that growing chains become hydrophobic enough to enter monomer micelles and finally form latex particles [364, 365]. Using this method, there is no control over the stereochemistry of the resulting polyisoprene and a mixture of 1,2 ; 3,4 and 1,4 cis and trans species are expected. Besides, crosslinking reactions are also prone to occur, leading to insoluble fractions of the product (gel).

Free radical polymerization of isoprene was not straightforward to achieve. Difficulties due to the very low boiling point of isoprene (35 °C), the need to work under slight overpressure and the choice of an

appropriate solvent for polyisoprene coagulation after reaction thus led to adapt the experimental procedure: the work of Kongsinlark et al [366], in which isoprene was in situ polymerized through emulsion free radical polymerization was adapted to this study (see Appendix 4.1.2. for the experimental procedure).

A conversion of 80 % was determined gravimetrically and FTIR was used to investigate the structure of the resulting product (Figure 81).

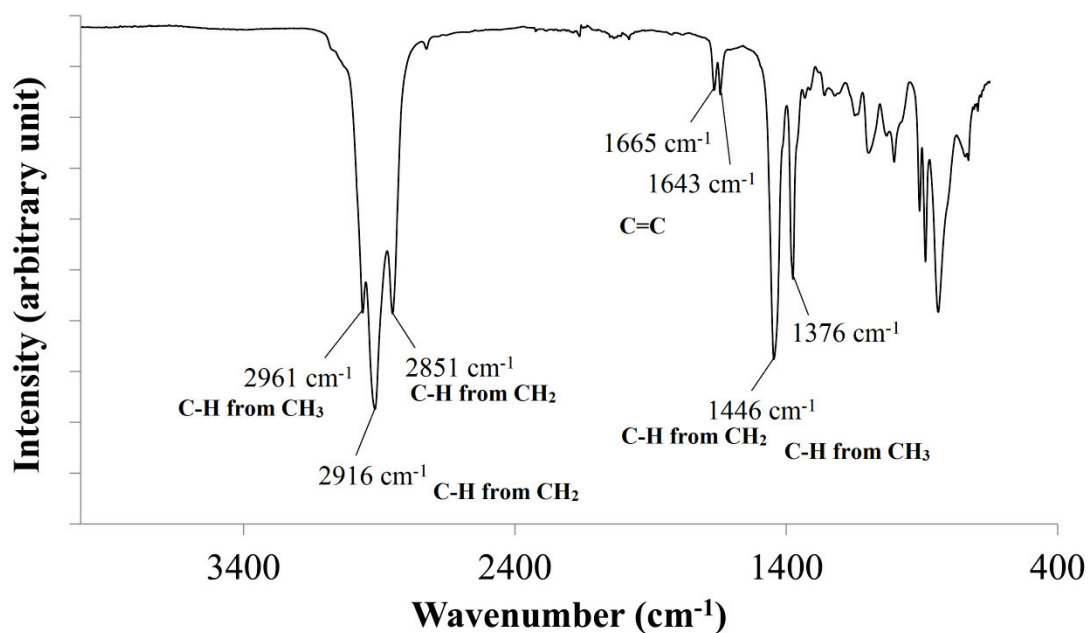


Figure 81: FTIR spectrum of the product obtained through emulsion radical polymerization of isoprene.

FTIR investigation confirmed the formation of polyisoprene. Peaks at 2961 cm⁻¹ and 1376 cm⁻¹ can be attributed to asymmetric elongation and vibration bands of C-H bond from CH₃ group. Peaks at 2916 cm⁻¹, 2851 cm⁻¹ and 1446 cm⁻¹ correspond respectively to asymmetric elongation, symmetric elongation and vibration bands of C-H bond in CH₂ groups. Peaks at 1665 cm⁻¹ and 1643 cm⁻¹ are attributed to C=C elongation bands. Hence, FTIR spectrum is consistent with the formation of polyisoprene [367–369].

¹H NMR in toluene was used to further investigate polyisoprene architecture (Figure 82).

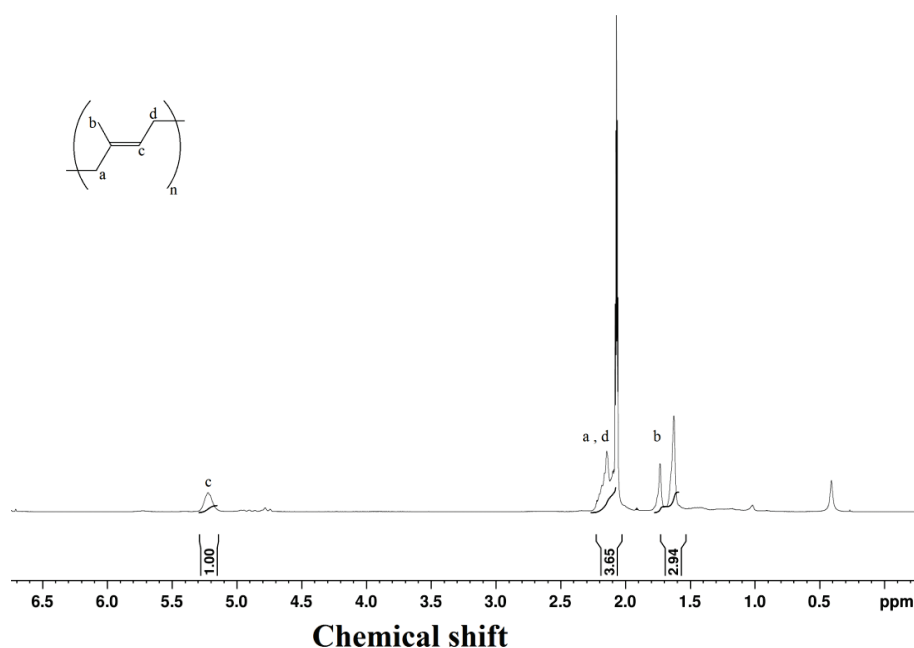


Figure 82: ^1H NMR spectrum of IR.

^1H NMR spectrum represented in Figure 82 displays a peak at 5.2 ppm corresponding to ethylenic hydrogens and peaks at 2.1 ppm and 1.7 ppm that are attributed to hydrogens coming from CH_2 and CH_3 groups, respectively. Moreover, the hydrogen molar ratio of ethylenic hydrogens and hydrogens coming from CH_2 and CH_3 groups are approximately in agreement with the architecture of the polyisoprene unit. A magnification of this spectrum in the region of ethylenic hydrogens is displayed in Figure 83.

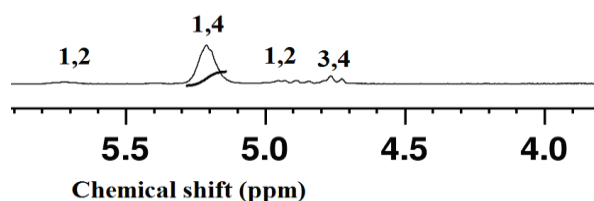


Figure 83: NMR spectrum of polyisoprene at greater magnification.

At around 5 ppm, a main peak corresponding to 1,4 species is observed. Besides, a very small shouldering at around 5.5 ppm and broad "peaks" at 4.8 ppm are related to the presence of 1,2 and 3,4 isomers, respectively [181, 351]. The product is thus mainly composed of cis and trans 1,4 units. Cheong et al [181] also reported mainly trans 1,4 configuration (70 %) for free radical polymerization of isoprene.

The molar mass of the product (M_n) was investigated by GPC in toluene. M_n values of around 7 000 g/mol were found (with a PDI of 1.28). Cheong et al [181] reported similar results (molecular

weight of 6 800 g/mol and PDI of 3.6) for polyisoprene polymerized in emulsion with a free radical method at 25 °C during 15 h.

Anyhow, the GPC results may not be representative for the whole sample, as only the soluble fraction could be analyzed. To determine the gel content in the samples, a washing procedure with hot toluene during 3 hours was performed. The samples were then centrifuged and the supernatant containing the soluble fraction was pipetted off. The pellet was dried and weighed. A high gel content of 50 wt% was obtained. The presence of such gel is due to the ability of polyisoprene chains to crosslink during radical polymerization. Values of 10-80 wt% gel content have been reported in the literature [181, 370]. As a result, polyisoprene obtained through emulsion free radical polymerization may have higher molar masses than the one given by GPC measurements as it is likely that long chains are more prone to crosslinking than short chains.

Then, thermal analyses were performed to study the behavior of polyisoprene. The DSC thermogram is shown in Figure 84.

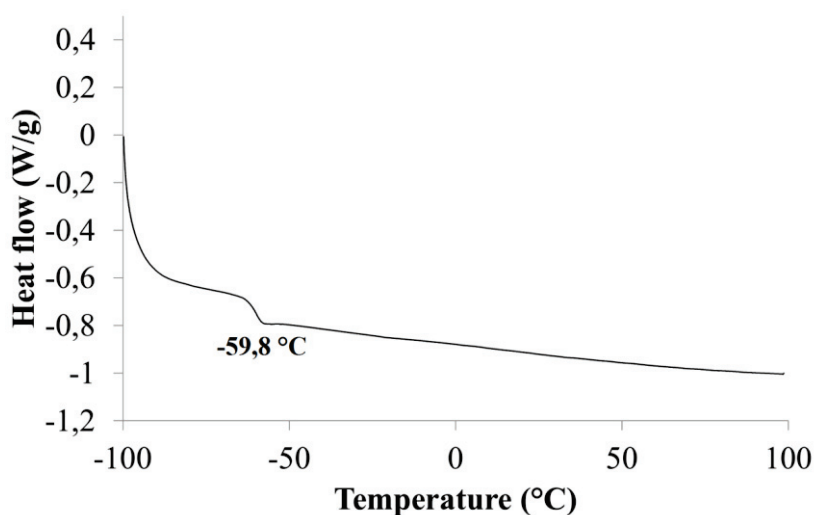


Figure 84: DSC thermogram of polyisoprene obtained through the emulsion radical polymerization of isoprene.

DSC provides interesting information about the relaxation behavior of polymers, evidencing the glass transition temperature by a neat step in the thermogram. Polyisoprene prepared through free radical polymerization showed a clear T_g of around -60 °C. This value indicates that isoprene units are mostly in trans configuration [371]. Cis 1,4 polyisoprene (such as natural rubber) usually shows lower T_g values, around -70 °C [372]. Annunziata et al [358] also obtained mainly the trans product (90 %) and measured a T_g of -57 °C.

Moreover, the thermal decomposition behavior of the polyisoprene sample was studied by using thermogravimetric analysis (TGA) (Figure 85).

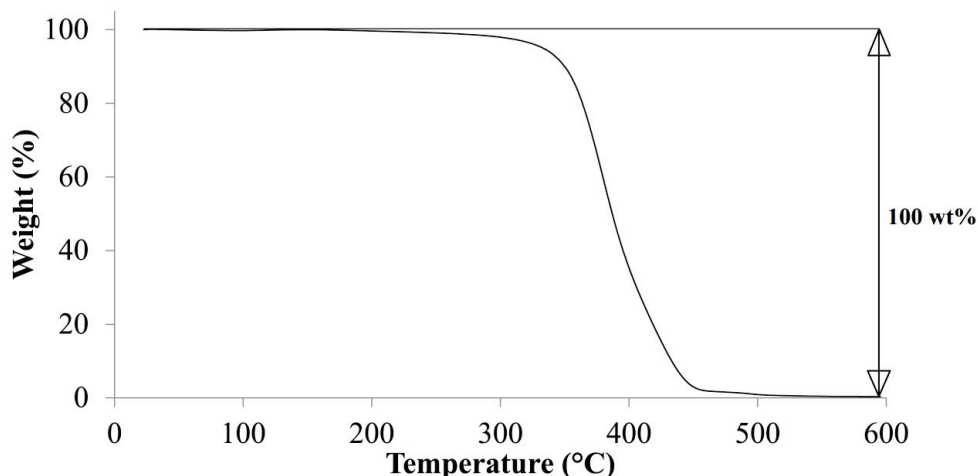


Figure 85: TGA thermogram of polyisoprene polymerized through a free radical method.

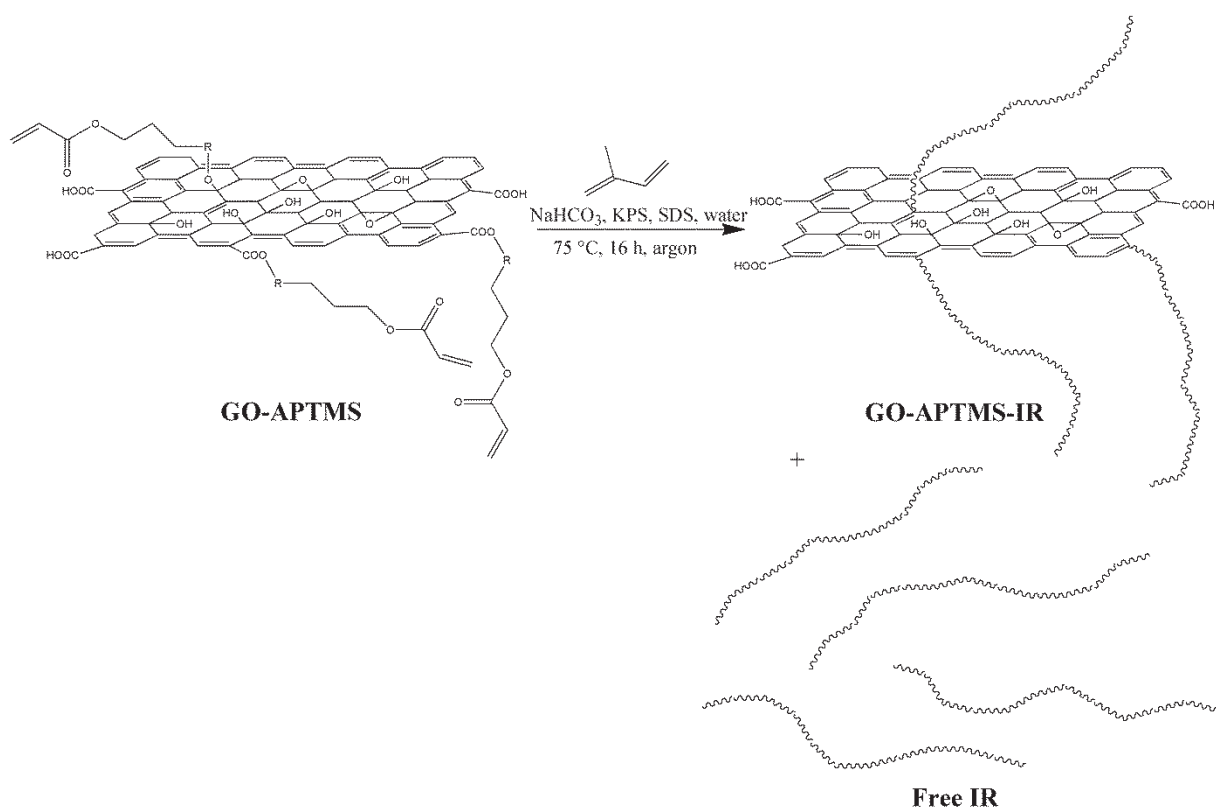
The thermogram shows full degradation of polyisoprene in one step between 300 °C and 500 °C. Other groups reported similar values [366, 373]. However, TGA does not provide information about the architecture of the polymer, which can undergo chain scission or crosslinking before 300 °C [374].

In the present study, free radical polymerization of isoprene was easy to perform and led to mostly trans 1,4 polyisoprene. This polymer fully degrades at 500 °C and has a T_g of -60 °C. A major drawback using free radical polymerization of isoprene is the lack of precise control over the reaction. As a result, many crosslinking reactions occur during the polymerization, leading to a polymer containing a high gel fraction (50 wt%).

In a second approach, emulsion radical polymerization of isoprene in presence of GO-APTMS has been attempted.

3.1.2. Grafting of polyisoprene onto GO-APTMS

The grafting of IR onto GO was performed accordingly to Scheme 22.



Scheme 22: In situ emulsion radical polymerization of isoprene in presence of GO-APTMS.

Isoprene radical polymerization was performed in presence of GO-APTMS nanosheets, so grafted and free polyisoprene chains were expected to be obtained (see Appendix 4.1.3. for the experimental procedure).

Two loadings of GO-APTMS were used: 1 wt% (GO-APTMS-p1) and 10 wt% (GO-APTMS-p10) with respect to the polymer. The two products will be described separately.

3.1.2.1. GO-APTMS-p1 (1 wt% loading)

After completion of the reaction, two phases are obtained in the reagent flask: a milky white phase and a black solid one, as shown in Figure 86.

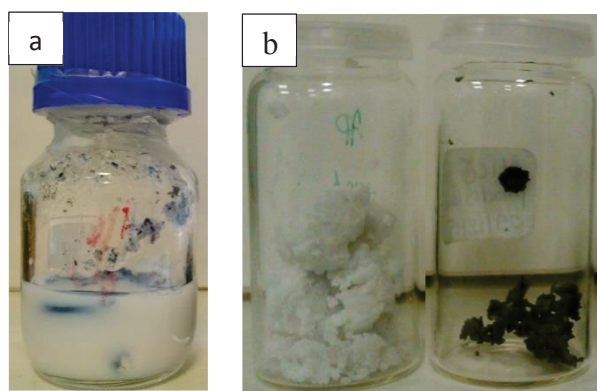


Figure 86: GO-APTMS-p1 a) before coagulation and b) after coagulation, washing and drying.

The two phases are separated by decantation and analyzed separately. The isolated white product (Figure 86 b) corresponds to 87 % of the total sample weight and it was evidenced to contain no graphite sheets. Indeed, FTIR, ^1H NMR, DSC and TGA measurements confirmed that the whole white solid product was pure polyisoprene and a T_g of $-60\text{ }^\circ\text{C}$ was determined by DSC. To remove ungrafted polyisoprene, washing of the black solid phase with hot toluene was performed and the obtained product was subsequently dried and collected. Only 40 mg (9.2 wt% relative to the black product before washing) of pure polyisoprene were extracted from the initial product. The remaining is then the APTMS-grafted GO (GO-APTMS-p1). The washed sample was then characterized using FTIR, DSC and TGA. The FTIR spectrum is displayed in Figure 87.

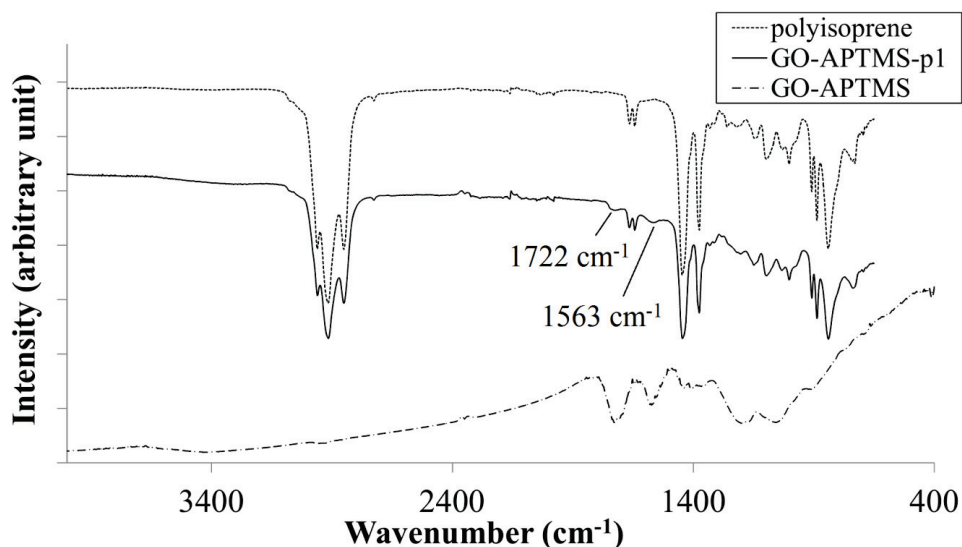


Figure 87: FTIR spectra of polyisoprene (top), GO-APTMS-p1 (middle) and GO-APTMS (bottom).

The FTIR spectrum of GO-APTMS-p1 displays the same characteristic peaks as the polyisoprene structure, with two additional peaks at 1722 cm^{-1} and 1563 cm^{-1} that may be attributed respectively to C=O and C=C vibration bands, respectively. This is an evidence of the presence of GO-APTMS in the sample. Besides, the broad O-H absorption peak in the GO-APTMS spectrum, around 3400 cm^{-1} becomes significantly weak for GO-APTMS-p1 suggesting that hydrophobic polyisoprene chains are attached onto GO-APTMS surface. Using a grafting from procedure to graft IR onto carbon nanotubes surface, Wang et al [337] also reported a strong decrease in the intensity of the O-H absorption band at 3470 cm^{-1} , which they attributed to the grafting of IR onto the CNTs.

To quantify the GO-APTMS content in the sample, TGA measurement was performed, as shown in Figure 88.

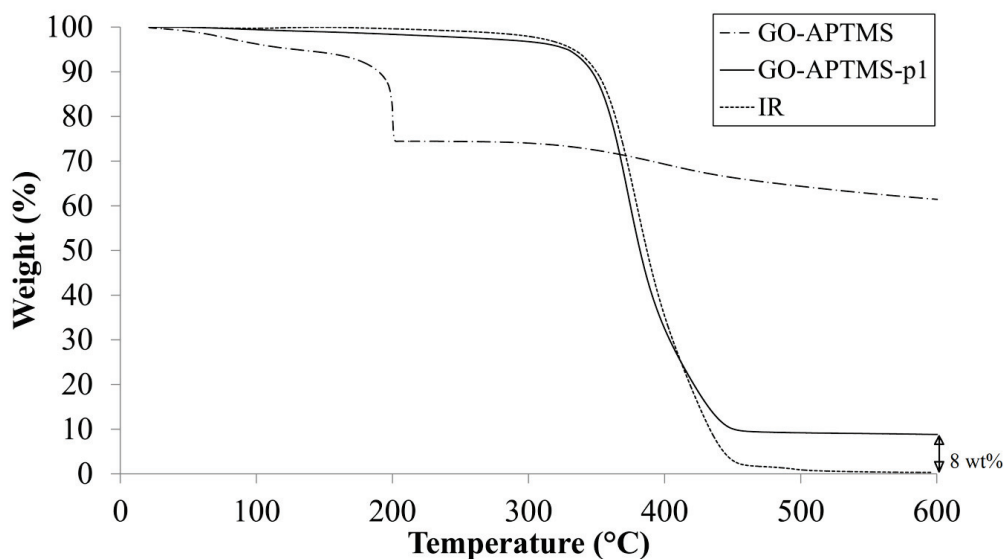


Figure 88: TGA thermogram of GO-APTMS, GO-APTMS-p1 and polyisoprene.

GO-APTMS-p1 shows a slight weight loss (2 wt%) before 300 °C followed by a major weight loss between 300 °C and 450 °C which can be attributed to polyisoprene degradation. A residue of 8 wt% was found after 450 °C due to the remaining presence of graphite-based filler. We can thus calculate a GO-APTMS content of 13 wt%. Wang et al [337] reported similar CNT content (9.6-14.7 wt%) for in situ polymerization of isoprene by using ARGET ATRP method.

Then, differential scanning calorimetry was used to study interactions between GO-APTMS and polyisoprene and the thermograms are displayed in Figure 89.

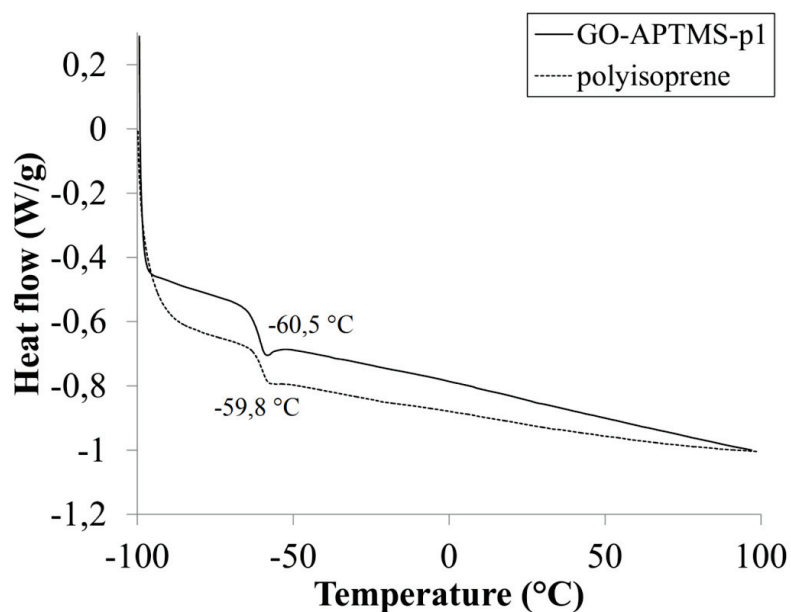


Figure 89: DSC thermogram of GO-APTMS-p1 and polyisoprene.

Studies on thermoplastics have shown that polymer chains grafted on a surface could exhibit higher glass transition temperature than free polymer chains due to restrained segmental mobility of the

grafted macromolecules [338, 375–377]. However, no shift in T_g is usually evidenced by DSC measurements of elastomer composites containing graphene-based nanofillers. Hence, GO-APTMS-p1 sample (Figure 89) showed similar T_g as pure polyisoprene ($-60\text{ }^\circ\text{C}$). Zhan et al [378] reported similar results for rGO-NR composites.

3.1.2.2. GO-APTMS-p10 (10 wt% loading)

The same experimental procedure was applied with 10 wt% GO-APTMS (relative to polyisoprene in the final composite). However, no polymer could be obtained in these experimental conditions. FTIR, DSC and TGA measurements evidenced that the product did not contain any polyisoprene chains on its surface. It suggests that GO-APTMS acts as a radical scavenger and might explain that polymerization can occur at a low loading (1 wt%) but is inhibited for higher GO-APTMS content in the reaction medium. Radical scavenging ability of graphene and GO has been reported by several groups [379–383]. This radical scavenging behavior is believed to be associated to the presence of sp^2 carbon lattice that can act through electron-transfer or adduct formation. Graphene and its derivatives could thus be used as oxidation retarders in a polymeric matrix to limit photochemical degradation for example [381].

To conclude, in situ polymerization of isoprene onto functionalized GO could thus be carried out at small GO-APTMS loading (1 wt%). However, at higher loading (10 wt%), GO free radical scavenging ability did not permit the polymerization to take place. For comparison, another strategy involving a cationic polymerization method has then been considered and is described in the next section.

3.2. Emulsion cationic polymerization of isoprene in presence of GO-allyl

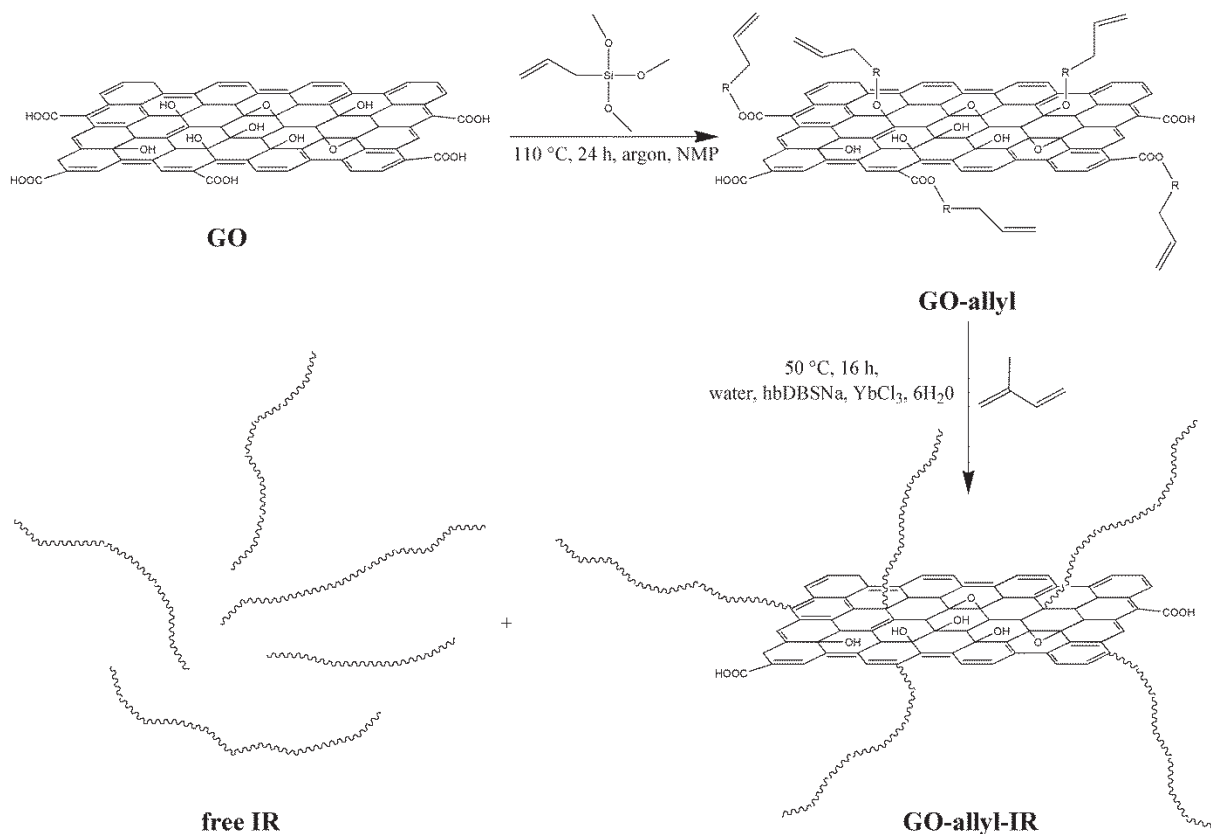
In situ emulsion radical polymerization of isoprene onto GO has shown some limitations. Other polymerization methods of isoprene have been described in the literature including cationic polymerization of isoprene. Hence, Li et al [338] reported in situ polymerization of styrene-isoprene onto GO through a cationic polymerization method using GO itself as the initiator. In this section, attachment of polyisoprene chains onto GO has been performed in two steps. Similarly to the free radical polymerization, an organic silane coupling agent has been grafted onto GO to provide anchor sites for isoprene in situ polymerization. The APTMS previously used has been replaced by the less polar allyltrimethoxysilane.

The catalytic activity of GO towards cationic polymerization of various monomers has already been reported. Indeed, GO displays acidic functionalities that may initiate cationic polymerization. Hence, Dreyer et al [269] showed the efficiency of GO as a heterogeneous catalyst in *n*-butyl vinyl ether polymerization at only 0.1-5 wt% content. After completion of the reaction, GO catalyst could be effectively recovered and was shown to retain its catalytic ability.

Moreover, Li et al [338] used GO as a cationic initiator in styrene-isoprene copolymerization. Acidic functionalities on GO surface were used to enable proton transfer to both styrene and isoprene monomers to form an ion pair thus initiating the polymerization. Styrene homopolymerization as well as styrene-isoprene copolymerization were studied. The poly (styrene-isoprene)-grafted GO sheets could be dispersed in THF at 0.2 mg/mL and displayed enhanced stability compared to pristine GO.

However, homopolymerization of isoprene could not be achieved due to difficulties in initiating the reaction.

However, in the present study the cationic polymerization of isoprene has been performed in situ onto GO-allyl using an emulsion cationic polymerization involving the use of Lewis Acid Surfactants combined Catalysts has been chosen [175] (Scheme 23).



Scheme 23: In situ emulsion cationic polymerization of isoprene onto GO-allyl.

In a first step, a blank experiment (without GO) was performed to study the emulsion cationic polymerization of isoprene.

3.2.1. Blank experiment

Cationic polymerization of isoprene has been studied by several groups [173, 174, 176, 384–386] and usually requires demanding experimental conditions in terms of inert atmosphere, monomer pressure, complex catalytic systems, use of organic solvent and low temperatures [387]. Recently, Vasilenko [175] and Kostjuk [350] demonstrated that sodium dodecyl benzene sulfonate (DBSNa) surfactants, with a polydisperse and hyperbranched structure, combined with different rare earth metal salts, generated highly water-dispersible Lewis acid surfactant combined catalysts (LASCs) which promoted fast and efficient cationic polymerization of industrially relevant monomers in direct emulsion at moderate temperature (40-60 °C) [175, 350]. Herein, the polymerization reaction was performed at 50 °C using a LASC complex which was prepared by simple mixing of ytterbium chloride hexahydrate rare earth salt and a highly branched sodium dodecylbenzene sulfonate in slight excess, in water. As discussed by Vasilenko et al [175], when the milky solution is stirred, it slowly takes a homogeneous translucent orange coloration and then the added monomer forms small droplets, stabilized by the LASCs complexes, in which polymerization occurs. A blank experiment (without the use of GO-allyl)

permitted to reach a 88 % conversion (determined gravimetrically) in 16 h. The molar mass (M_n) of the resulting polyisoprene was 23 400 g.mol⁻¹ with a polydispersity index of 1.66. It was also shown that after refluxing the obtained product in toluene, no gel was obtained, which suggests that no crosslinking reactions occurred (see Appendix 4.1.5. for the experimental procedure).

The product obtained through cationic polymerization was studied by FTIR, NMR, GPC, DSC and TGA. Cationic polyisoprene led to higher molar masses than polyisoprene polymerized through free radical polymerization, presented previously.

To conclude, isoprene cationic polymerization could thus be performed in a simple and fast one-pot reaction involving the use of LASCs. Polyisoprene product is mainly in trans 1,4 configuration with a molar mass around 20,000 g/mol and low branching degree. Indeed, a low glass transition temperature of -61 °C, typically observed for trans 1,4 polyisoprene, was measured. Besides, no gel was detected, indicating that no crosslinking occurred during the reaction.

The same protocol was then applied in presence of GO-allyl to attempt in situ emulsion cationic polymerization of isoprene onto the surface of GO-allyl.

3.2.2. Grafting of polyisoprene in presence of GO-allyl

As mentioned earlier, previous work by Li et al [338] failed in achieving homopolymerization of isoprene onto GO. In the present study, cationic polymerization of isoprene has been performed through the use of LASCs, as previously described. The reaction was proven to work on a blank experiment. Then, using the same experimental conditions, the polymerization of isoprene was studied in presence of GO-allyl. As illustrated in Scheme 23, both grafted and free polyisoprene chains were formed after the polymerization reaction in presence of GO-allyl, so the free polyisoprene chains were removed by extensive washings in hot toluene (see Appendix 4.1.6. for the experimental procedure).

Analysis of the recovered GO-containing elastomer by FTIR gave clear evidence for polyisoprene grafting (Figure 90).

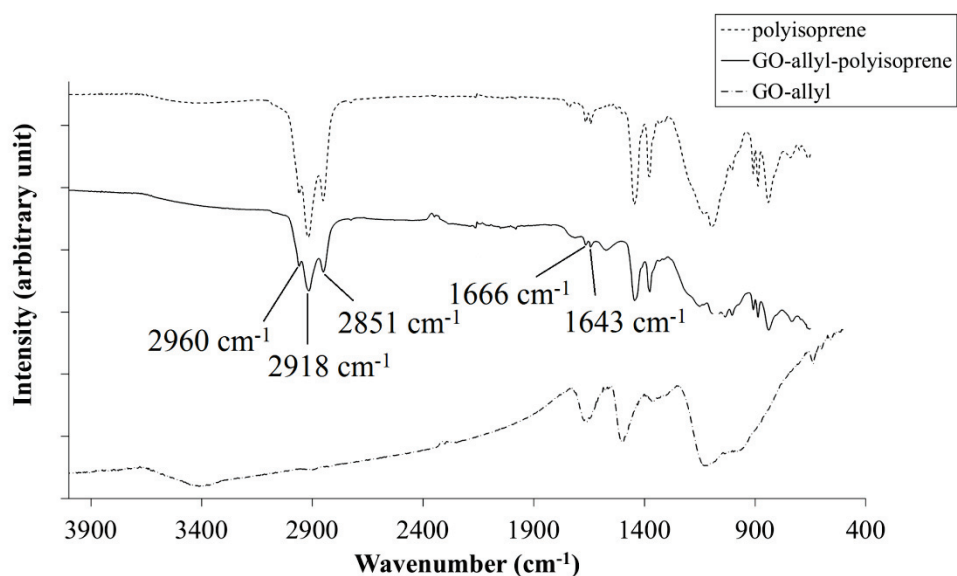


Figure 90: FTIR spectra of polyisoprene, GO-allyl-polyisoprene and GO-allyl.

Indeed, upon grafting of polyisoprene, the so-called GO-allyl-polyisoprene sample exhibits a very similar spectrum to the one of polyisoprene. Intense peaks from 2851 cm^{-1} to 2960 cm^{-1} can be seen, characteristic of the stretching vibrations of methyl C-H bonds. Additional peaks that may originate from C-C and C=C bonding modes are observed at 1666 cm^{-1} and 1643 cm^{-1} while the 1445 cm^{-1} one can be ascribed to C-H bending vibrations.

Further insight into the grafting reaction was obtained by determining the amount of polymer chains grafted on GO-allyl. XPS spectra provide additional proof for polyisoprene grafting (Figure 91).

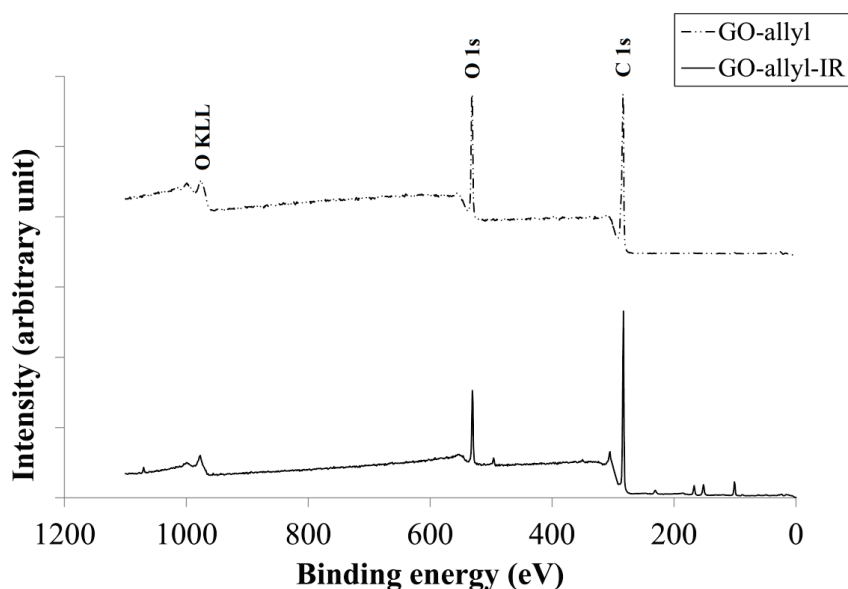


Figure 91: Low resolution XPS spectrum of GO-allyl and GO-allyl-IR.

As shown in Figure 91, the low-resolution XPS spectra of GO-allyl and GO-allyl-IR indicate an increase of the C/O ratio which is also consistent with polyisoprene grafting. Moreover, Figure 92 presents a comparison of TGA thermograms. The typical thermogram for free polyisoprene homopolymer

exhibits complete decomposition temperature before 450 °C. The major step of degradation of GO-allyl occurs at around 200 °C (decomposition of oxygen functional groups), then followed by gradual decomposition of grafted allyltrimethoxysilane. The GO-allyl-IR thermogram possesses different significant features. First, it exhibits a major degradation step at a temperature close to the one of pristine IR, thus assessing the presence of a significant amount of polymer.

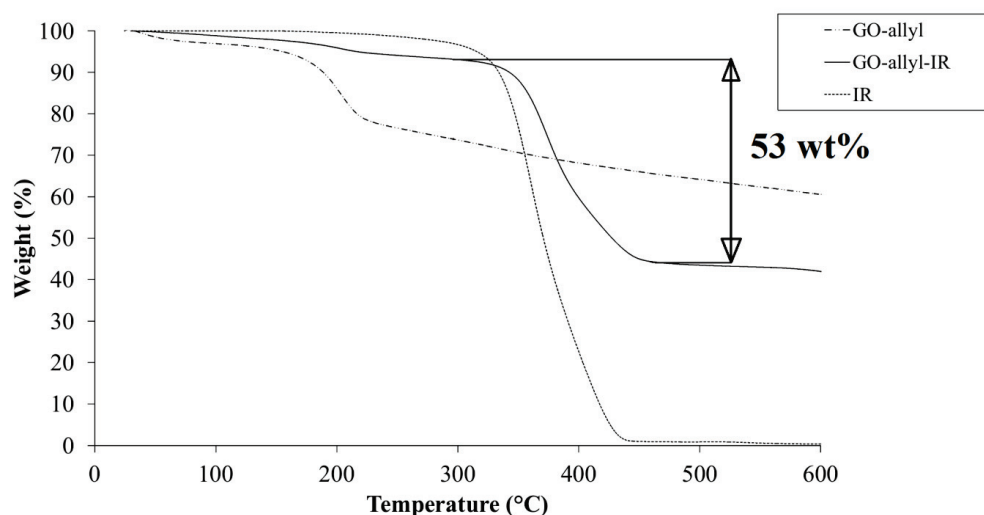


Figure 92: TGA thermogram of GO-allyl, GO-allyl-polyisoprene and polyisoprene.

Moreover, the decomposition temperature of polyisoprene increases by about 20 °C – 30 °C after grafting onto the GO-allyl sheets, as expected (Figure 92). TGA results also show that free polyisoprene chains can be completely decomposed at a temperature of 450 °C. Therefore, the amount of polyisoprene that is covalently attached to GO-allyl surface can be estimated by the weight loss of GO-allyl-IR sample between 250 °C and 450 °C (Figure 92). From Figure 92, the weight of grafted polyisoprene is around 49 % ($0.044 \text{ mmol.g}^{-1}$) in the present polymerization conditions (16 hours) and considering an allyltrimethoxysilane weight content of 4 %. For comparison, Garcia-Valdez et al [336] reported a value of 0.9 mmol.g^{-1} (TGA weight loss = 68 %) for a reaction time of 144 h at 130 °C by using the “grafting from” technique combined to nitroxide mediated polymerization. In the latter case, it should be noted that the molar mass of the grafted polyisoprene was estimated to be 760 g/mol instead of 23 400 g/mol in the present study, which explains the large difference in molecular content of grafted polyisoprene per g of solid [336]. Herein, the molar mass of the non-extractible IR is assumed to be close to the extractible IR one (i.e. 23 400 g/mol), as discussed by numerous authors. For example, Kim et al [388] have studied the in situ polymerization of isobutylene from silica particles using a living cationic surface-initiated process and it was shown that the molar masses of both grafted and non-grafted polyisobutylene chains were similar.

To obtain more understanding of the morphology developed as a result of the grafting of polyisoprene onto the surface of GO sheets, electron microscopy (SEM) was conducted (Figure 93).

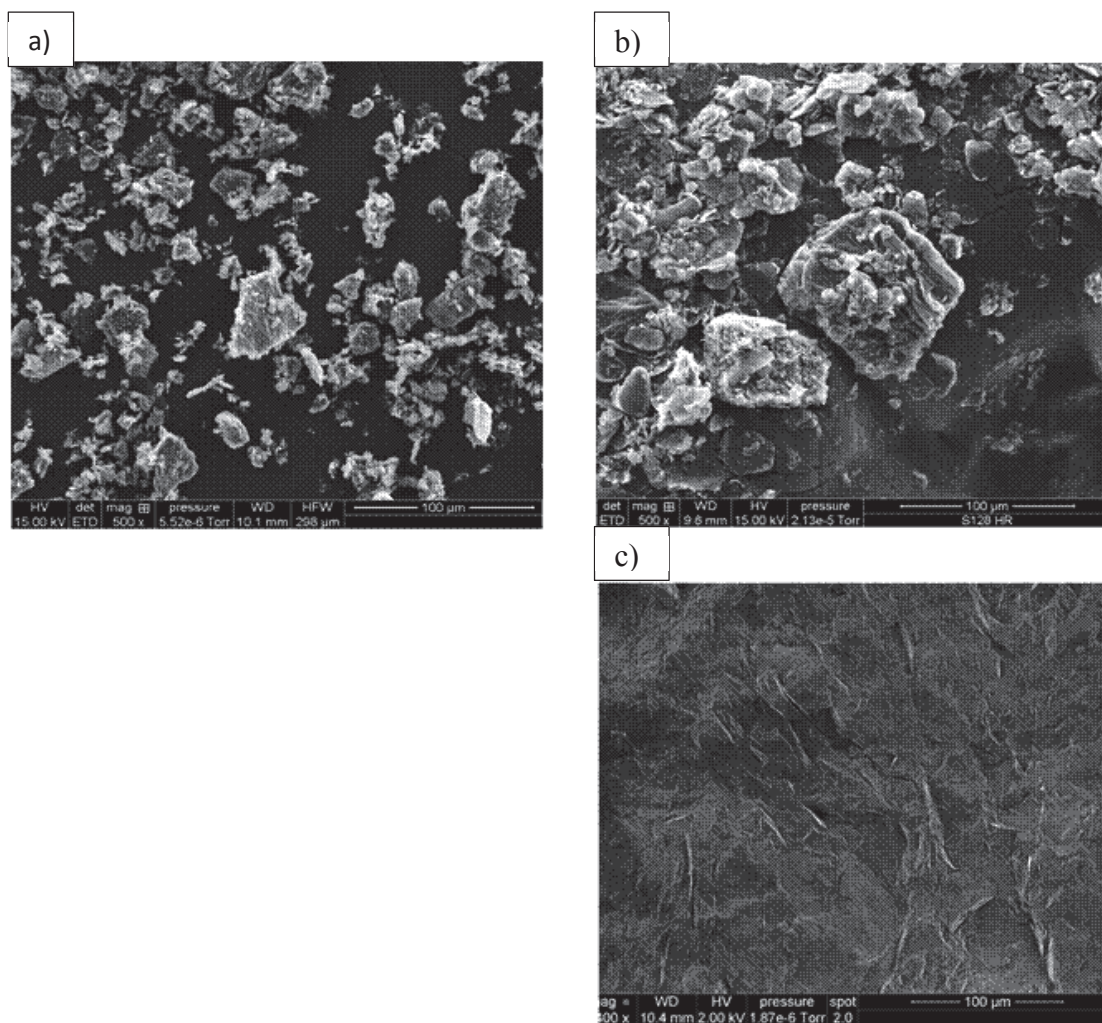


Figure 93: SEM pictures of a) GO, b) GO-allyl and c) GO-allyl-polyisoprene.

The morphology of GO is known to display a flaky texture, reflecting its layered microstructure and Figure 93 a demonstrates the structure of stacked GO layers, which results in a large particle size (up to 50 μm) while the grafting of allyltrimethoxysilane onto the surface of GO was not able to ensure a decrease of the GO particles sizes (Figure 93 b). In contrary, after polyisoprene grafting, randomly aggregated thin large flakes with wavy wrinkles surrounded by large polyisoprene domains can be observed (Figure 93 c).

Moreover, to investigate the role of the pendent allyl groups on the grafting of polyisoprene onto the surface of GO, the cationic polymerization of isoprene was also performed in presence of un-modified graphite oxide sheets. The TGA analysis of the resulting solid phase (after hot toluene washing) is illustrated in Figure 94.

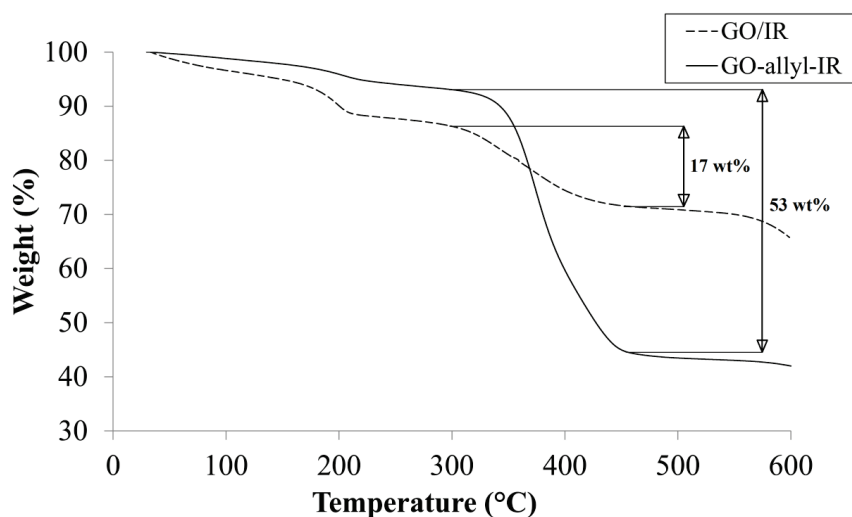


Figure 94: TGA thermogram of GO/IR (in situ polymerization of isoprene onto pristine GO) and GO-allyl-IR (in situ polymerization of isoprene onto GO-allyl).

From Figure 94, it was possible to evaluate a polyisoprene weight content of 17 % indicating a decrease by a factor 3 in comparison with the GO-allyl-IR sample.

As for GO-APTMS, DSC measurements have been done on the GO-allyl-IR sample to characterize the type of interaction between phases, such as covalent bonding, can be evaluated through the relaxation behavior of polymer chains (Figure 95).

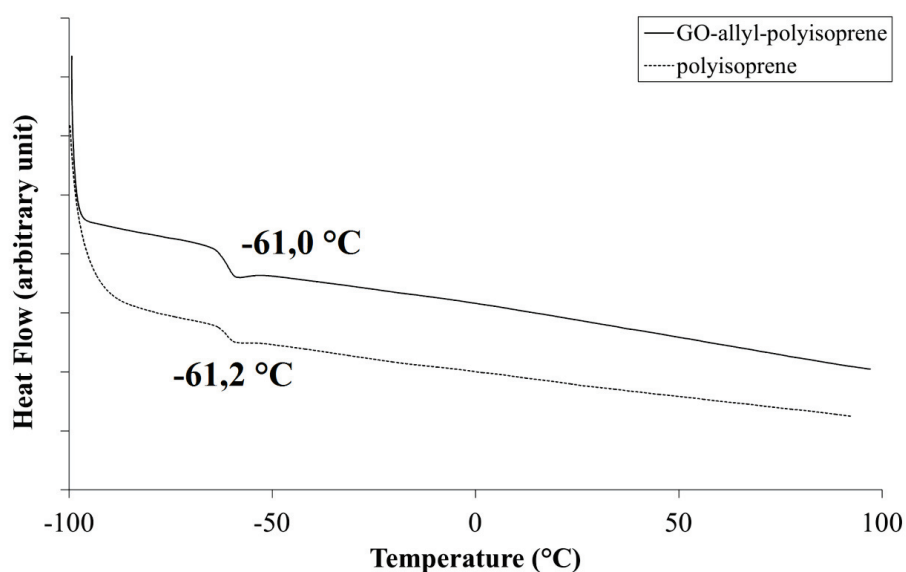


Figure 95: DSC thermogram of GO-allyl-polyisoprene and free polyisoprene.

Indeed, as discussed previously, it is expected that the glass transition temperature (T_g) of polymer chains grafted to a substrate will be higher than free or entangled chains [375, 376, 389]. For example, the T_g of polystyrene was reportedly increased by 15 °C with a GO weight content of 12 wt%, a phenomenon attributed to a strong particle-polymer interaction [338]. Herein, Figure 95 shows a glass transition temperature of -61 °C for free polyisoprene which indicates that most double bonds of the formed polyisoprene are intact, as discussed by Kostjuk et al [350]. As noticed with GO-APTMS, the

presence of GO-based sheets was not able to increase the T_g of polyisoprene which may be due to the low grafting density of polyisoprene.

This section has thus highlighted the successful grafting of polyisoprene onto GO. Cationic polymerization has proven to be easy to carry out and it was not affected by the presence of GO in the reaction medium (same conversion). A polyisoprene content of 50 wt% was determined by TGA. The composites exhibited enhanced thermal stability as compared to free polyisoprene chains. Despite little use of cationic polymerization of isoprene in the literature, this study has shown the great potential of this procedure to obtain GO-allyl-polyisoprene through an in situ process. Polyisoprene-functionalized GO has thus been prepared and could be further incorporated in a polyisoprene matrix to improve the elastomer properties.

Conclusion

In situ polymerization of isoprene onto GO has shown to be challenging, involving several crucial steps which have been addressed here with different approaches.

In this chapter, GO has been synthesized according to Hummers method and a material containing hydroxyl, carboxylic acid and epoxide functional groups with a C:O ratio of 2:1 has been obtained. Such modification led to increased hydrophilicity of the material. XRD and TEM measurements evidenced that the incorporation of functional groups induced an increase in the interlayer spacing from 3.34 Å to 7.41 Å.

Hydrolysis-condensation reactions of APTMS and allyltrimethoxysilane onto GO have been performed and showed similar results to those commonly reported in the literature with a grafting density of 0.2 mmol/g. The functionalized GO sheets have been characterized using FTIR, TGA, XDR and SEM. No change in the graphitic structure has been observed during the reaction. However, the hydrophilicity of GO has been reduced and dispersions of the functionalized platelets exhibited enhanced stability in toluene.

In a second step, isoprene has been in situ polymerized onto functionalized GO. The free radical polymerization method performed relatively well in blank experiments leading to mainly 1,4 trans polyisoprene with a molar mass of around 7,000 g/mol at 80 % conversion. However, 50 wt% of gel was produced in the reaction due to crosslinking reactions. In presence of GO-APTMS at low loading (1 wt% relative to the polymer), a similar conversion (80 %) was observed. A weight content of 13 % of GO in the composite was calculated through TGA. No shift in the glass transition of the resulting product was observed, which may be due to a low polyisoprene grafting density onto GO-APTMS. However, at higher GO-APTMS loadings (10 wt% relative to the polymer), polymerization was not able to proceed due to the radical scavenging ability of GO. This result is anyhow interesting as GO could be used as an antioxidant filler in a polymer matrix.

Thus, cationic polymerization of isoprene in emulsion was performed using a highly water-dispersible Lewis acids surfactant combined catalyst (LASC) and allowed the synthesis of polyisoprene in a simple one-pot reaction. Blank experiment led to 88 % conversion with mainly 1,4 trans configuration and a

glass transition temperature of - 61 °C. Moreover, a higher molar mass could be obtained (~20,000 g/mol) and no gel was detected.

The reaction was then able to proceed in presence of GO-allyl leading to a material containing 50 wt% of polyisoprene. The composite showed enhanced thermal stability (+ 25 °C). Besides, SEM images evidenced randomly aggregated thin large sheets surrounded by large polyisoprene domains. The role of allyltrimethoxysilane was then attested by carrying out the polymerization reaction with pristine GO instead of GO-allyl. A 3-fold lower content of polyisoprene was detected on GO showing thus the essential role of allyltrimethoxysilane on the grafting of isoprene units onto GO substrate.

In this study, the successful in situ polymerization of isoprene onto functionalized GO has thus been reported according to two methods. In a further study, other monomers could be in situ polymerized according to the same protocol.

Chapter 4: Properties of polyisoprene composites containing modified-graphite oxide

Table of contents of Chapter 4

Introduction.....	170
1. Polyisoprene composites containing thermally-expanded graphite	170
1.1. Preparation of graphite oxide	170
1.2. Thermal expansion of graphite oxide.....	171
1.2.1. Temperature dependence.....	172
1.2.2. Influence of the expansion time.....	173
Conclusion	173
2. Properties of composites containing graphite-based fillers	173
2.1. Morphologies of graphite-based polyisoprene composites	174
2.2. Thermal conductivity of graphite-based polyisoprene composites.....	176
2.3. Barrier properties of graphite-based polyisoprene composites.....	177
2.4. Tensile properties of graphite-based polyisoprene composites.....	179
2.4.1. Effect of graphite content	180
2.4.2. Effect of commercial GE (expanded graphite)	183
2.4.3. Effect of GO (graphite oxide).....	183
2.4.4. Effect of modified GO on the tensile properties of polyisoprene composites.....	184
2.4.5. Comparison of the effect of different graphite-based fillers on the tensile properties	187
Conclusion	188

Introduction

In the previous chapters, chemical covalent functionalization of GO has been performed, involving several modification paths. In the literature, other methods for the modification of GO have been reported. The use of a thermal process has been widely described in several research papers [21, 22, 134, 390, 391] and patents [392–395]. For example, Prud'Homme et al [392] reported the preparation of a graphite-like material with a porous structure and reduced oxygen content and so, lower polarity than GO, thus allowing better compatibility with non-polar polyisoprene.

Hence, in this chapter, the expansion of graphite using a thermal process, has been performed. In a second section, the properties of polyisoprene composites containing the modified graphite-based fillers described in the previous chapters, have been investigated. As shown in Chapter 1 (section 3), the addition of a graphitic filler into a polyisoprene matrix can enhance several properties of elastomer composites such as barrier or tensile properties. For example, Potts et al [396] reported a 5-fold increase in tensile strength (from 2 MPa to 10 MPa) of NR composites at 5 phr loading of chemically-reduced GO. The effect of several parameters such as filler dimensions and processing routes have been highlighted.

In this chapter, the effect of graphite modification on the dispersion of the filler in the matrix has been observed through microscopy analysis. Besides, the air permeability, mechanical properties as well as thermal conductivity of the polyisoprene composites have been investigated. The influence of the functionalization on the performance of the materials has been evaluated and the properties of modified graphite-based composites have been compared to commercial graphite-based polyisoprene composites.

1. Polyisoprene composites containing thermally-expanded graphite

Beside chemical functionalization, other graphite modification methods have been developed. Many patents [392–395, 397–400] and publications [20–22, 134, 260, 262, 390, 401–407] have reported the use of thermal processes to produce expanded graphite. This material is often prepared through intercalation of acidic species between graphite layers followed by quick heating at elevated temperatures (around 900 °C). The thermal treatment leads to pyrolysis of these acidic compounds that can induce the formation of carbon dioxide, carbon monoxide as well as water vapor which push graphite layers apart when escaping from the structure. The resulting material contains highly-wrinkled sheets and pores ranging from a few nanometers to a few micrometers. This worm-like material has been used as a filler in many polymers and has led to enhanced mechanical properties as compared to pristine graphite or graphite oxide.

1.1. Preparation of graphite oxide

The synthesis of graphite oxide from graphite using Hummers' method was fully described in Chapter 2. As a reminder, a material containing carboxylic acid, hydroxyl and epoxide groups with a C:O ratio of 2:1 was obtained. This material thermally degrades above 200 °C, at which temperature most oxygen functional groups undergo pyrolysis, resulting in a weight loss around 50 % at 600 °C.

1.2. Thermal expansion of graphite oxide

Graphite oxide can be thermally treated to prepare “expanded graphite”. When heated at elevated temperatures, oxygen functional groups can vaporize and push graphite layers away from each other, thus creating a worm-like structure, as described in Chapter 1 (section 1). In this work, the expansion was performed in a muffle furnace, under air. Figure 96 displays SEM images of pristine graphite, graphite oxide and expanded graphite morphologies.

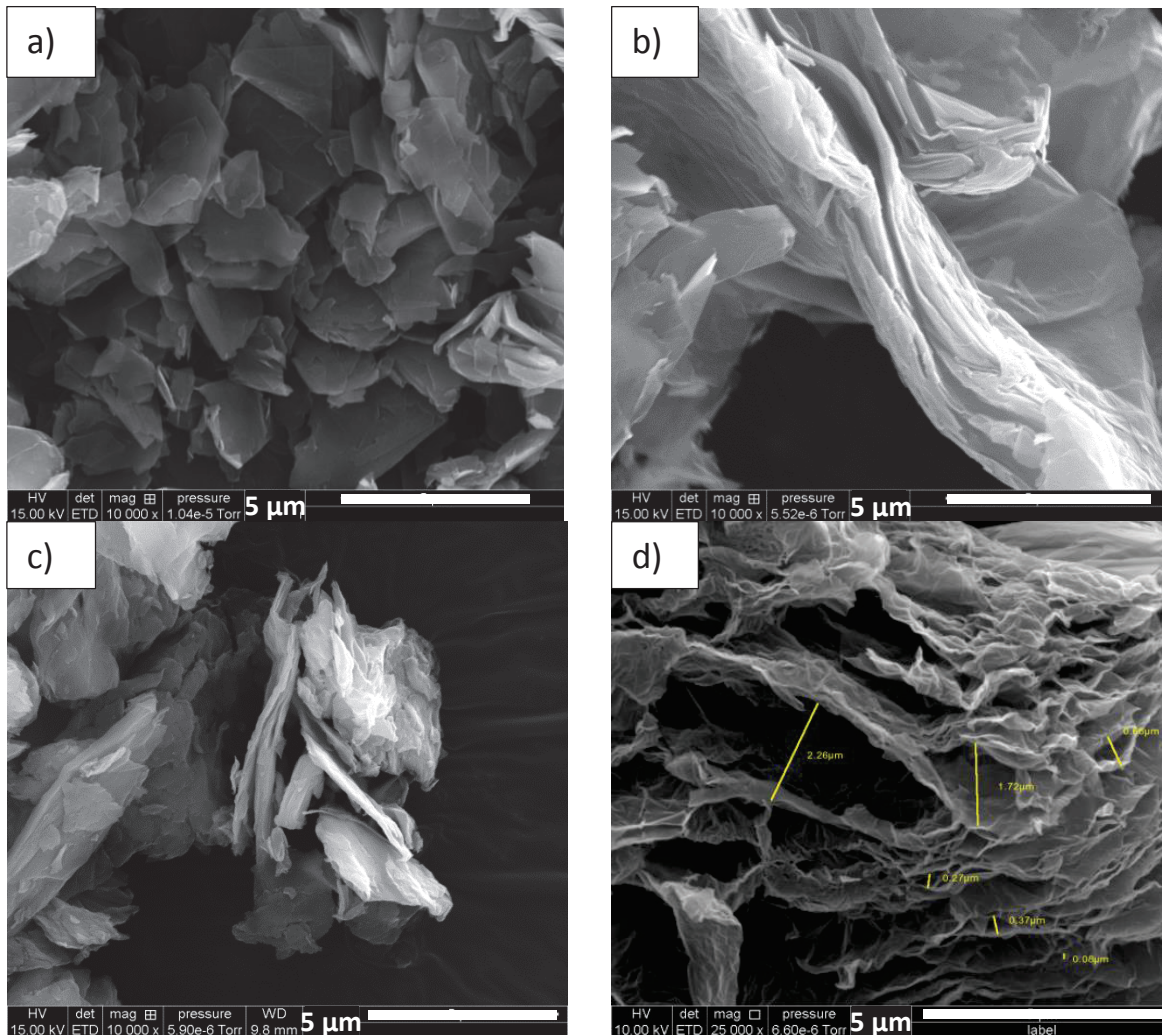


Figure 96 : SEM pictures of a) commercially-available graphite, b) commercially-available expanded graphite, c) graphite oxide prepared from commercially-available expanded graphite and d) expanded product obtained after heating graphite oxide at 700 °C during 30 s.

Commercially-available graphite (Figure 96 a) is composed of stacked platelets with an average lateral dimension around 5 μm. The platelets appear to be very plain, with a clean surface. On Figure 96 c, SEM images of graphite oxide platelets are displayed and a wrinkled structure with various lateral dimensions (from 2 μm to 7 μm) can be observed. The presence of small fragmented oxidative debris, which may be removed by an appropriate base wash, as described by Rourke et al [108, 110], is also evidenced.

From Figure 96 b, it can be observed that commercially-available expanded graphite (GE) also exhibits a wrinkled structure and spacing between stacks of layers of around 0.1 μm. Figure 96 d represents “home-made” expanded graphite platelets (GOX), which show a highly wrinkled morphology with large pores up to 2.3 μm between stacks of layers. The expanded graphite prepared from graphite oxide

displays a greater expansion than the commercial product. Several studies, such as the work of Hong et al [408] reported similar morphologies of graphite (plain, stacked layers) and expanded graphite (wrinkled sheets with pores). It can thus be of significant interest to study the thermal expansion of graphite oxide to see the effect of the expanded structure on the properties of polyisoprene composites.

1.2.1. Temperature dependence

To study the influence of the temperature on the expansion, graphite oxide samples were submitted to temperatures varying from 200 °C to 900 °C during 30 s. The morphologies of the samples were then observed by SEM (Figure 97).

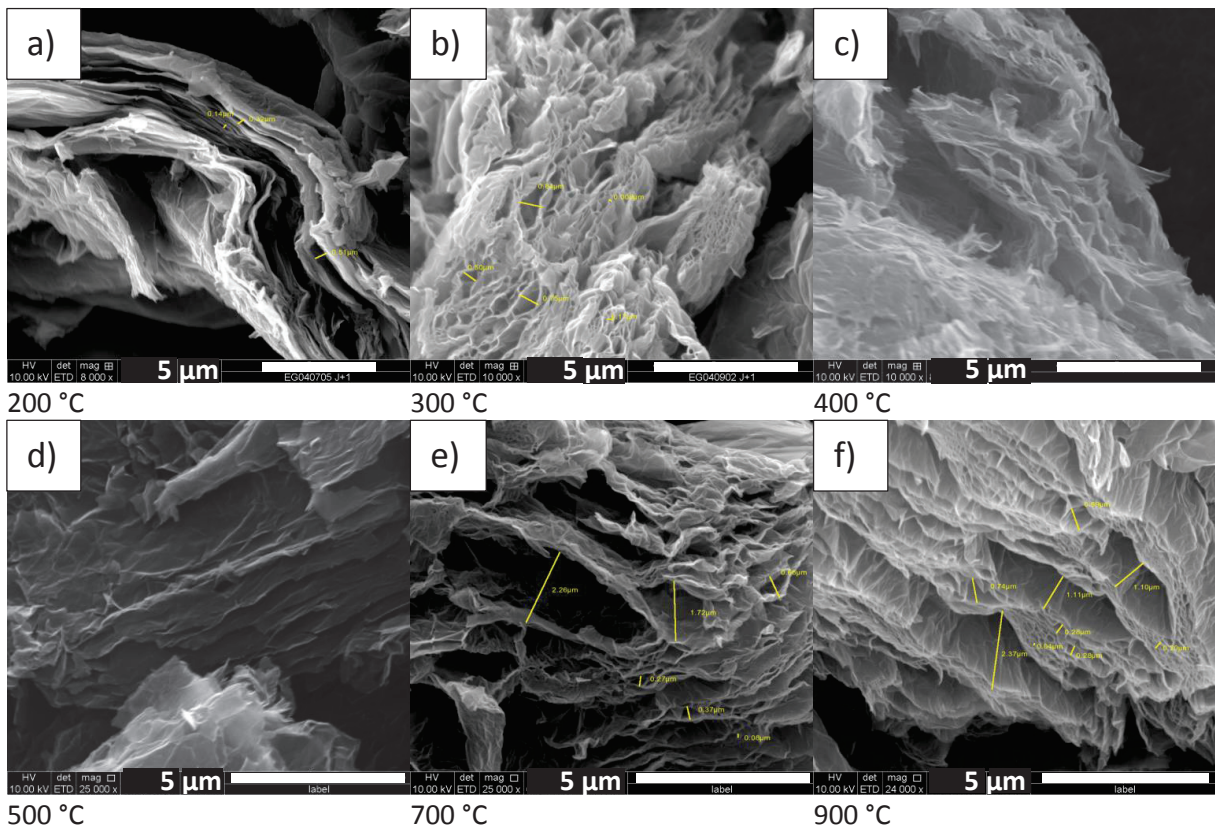


Figure 97 : SEM pictures of graphite oxide treated 30 seconds at a temperature of a) 200 °C, b) 300 °C, c) 400 °C, d) 500 °C, e) 700 °C and f) 900 °C.

From Figure 97 a, it can be observed that a similar morphology to pristine GO is retained, thus suggesting that no significant expansion occurred at 200 °C during 30 s. At higher temperatures, a worm-like structure is formed with pores of sizes ranging from 0.04 μm to 2.37 μm. From Figure 97 e and f, it appears that larger pores up to 2.37 μm (only up to 1.29 μm at 500 °C) are formed when GO is heated at temperatures higher than 700 °C. In addition, no significant difference could be observed between samples treated at 700 °C and 900 °C. It was thus chosen to prepare the expanded products at a temperature of 700 °C. Inagaki et al [402] also investigated the influence of the temperature over the morphology of expanded graphite. They reported a quick increase in the exfoliation below 650 °C, and only a small increase in pore sizes between 650 °C and 800 °C. They reported the preparation of thermally expanded graphite flakes with an exfoliation volume of 0.06 m³/kg (bulk density of 20 kg/m³) and an average pore area of 200 μm² (and up to a few mm² for the largest pores).

1.2.2. Influence of the expansion time

A similar study to investigate the effect of expansion time over the morphologies of the samples has been performed. No influence on the morphology (SEM) of the samples was observed between GO powders treated at 700 °C during 30 s, 1 min and 5 min. As a result, an expansion time of 30 s was chosen.

The experimental procedure is detailed in Appendix 5.1 and 5.2.

The use of expanded graphite in elastomer composites has been widely reported in the literature. Hence, Potts et al [257] added 5 phr of expanded graphite in NR through a twin-roll mill mixing procedure and a 3-fold increase in tensile strength was achieved. Besides, Kim et al [135] reported a 50 % decrease in N₂ permeability of TPU composites containing 1.6 vol% of thermally expanded graphite, prepared by a melt-mixing procedure.

Conclusion

In this section, the thermal expansion of home-made graphite oxide has been successfully performed. An expanded graphite powder was thus prepared, showing highly-wrinkled sheets with pores of irregular sizes up to 2.3 µm between layers which yields a much more expanded morphology compared to commercially-available expanded graphite in which pores of 0.1 µm were observed). It was shown that an increase in expansion temperature up to 700 °C led to increased pore sizes, whereas expansion time did not have a significant effect over the morphologies of the expanded products. The conditions selected for expansion are 700 °C during 30 s in a muffle furnace under air.

2. Properties of composites containing graphite-based fillers

In the previous chapters, several modifications paths of graphite have been studied. These modified fillers exhibited improved dispersion in a polyisoprene matrix. Surface modification of graphite has been reported to enable improved properties of elastomer composites [121, 127, 226, 258]. Hence, the barrier properties, the thermal conductivity as well as the mechanical properties of the modified-graphite elastomer composites have been investigated and are detailed in this section.

Most published studies deal with the addition of graphite-based fillers in a neat elastomeric matrix (which does not contain any other fillers) and compare the properties of these composites to those of the neat matrix. However, in this study, a more industrial point of view has been chosen. Hence, all materials contain carbon black, and graphite-based fillers have been used as partial substitution for carbon black. The total filler content thus remains constant. This approach enables a comparison of the effect of graphite to the one of the same amount of carbon black, in formulations which are close to industrial formulations.

Hence, polyisoprene composites with a total filler content of 50 phr have been prepared. The reference sample (named IR on the figures) contains 50 phr (20 vol%) of carbon black. Then, polyisoprene composites with graphite-based fillers have been prepared with the following loadings: 2 phr (0.6 vol%) and 15 phr (5 vol%) of modified graphite, with 48 phr and 35 phr of carbon black, respectively. The compounding and curing procedures, as well as the composites formulations are given in Appendix 5.2. These composites will be addressed throughout the present chapter for different properties. They will be named after the nature and amount of graphite-based filler partially substituted for carbon

black (for example, GO-ODA 2 phr refers to the composite with 2 phr of ODA-functionalized GO and 48 phr of carbon black).

First, the influence of graphite modification on the dispersion of graphite-based fillers in the polyisoprene composites has been investigated.

2.1. Morphologies of graphite-based polyisoprene composites

Surface functionalization has been reported to decrease filler-filler interactions (thus decreasing the size of the aggregates after dispersion in the composites), and to increase filler-matrix interactions. An overall improved dispersion can be reached, as for example with oleyamine-functionalized graphite oxide at 7 phr loading in SBR, as compared to pristine GO [121]. Aggregates with a lateral dimension of 2 μm were measured for GO while GO-oleylamine composites did not contain aggregates larger than 1 μm [121].

Herein, the morphologies of the polyisoprene composites have been investigated by SEM. The morphologies displayed in Figure 98 are those of compounds with 15 phr of modified graphite.

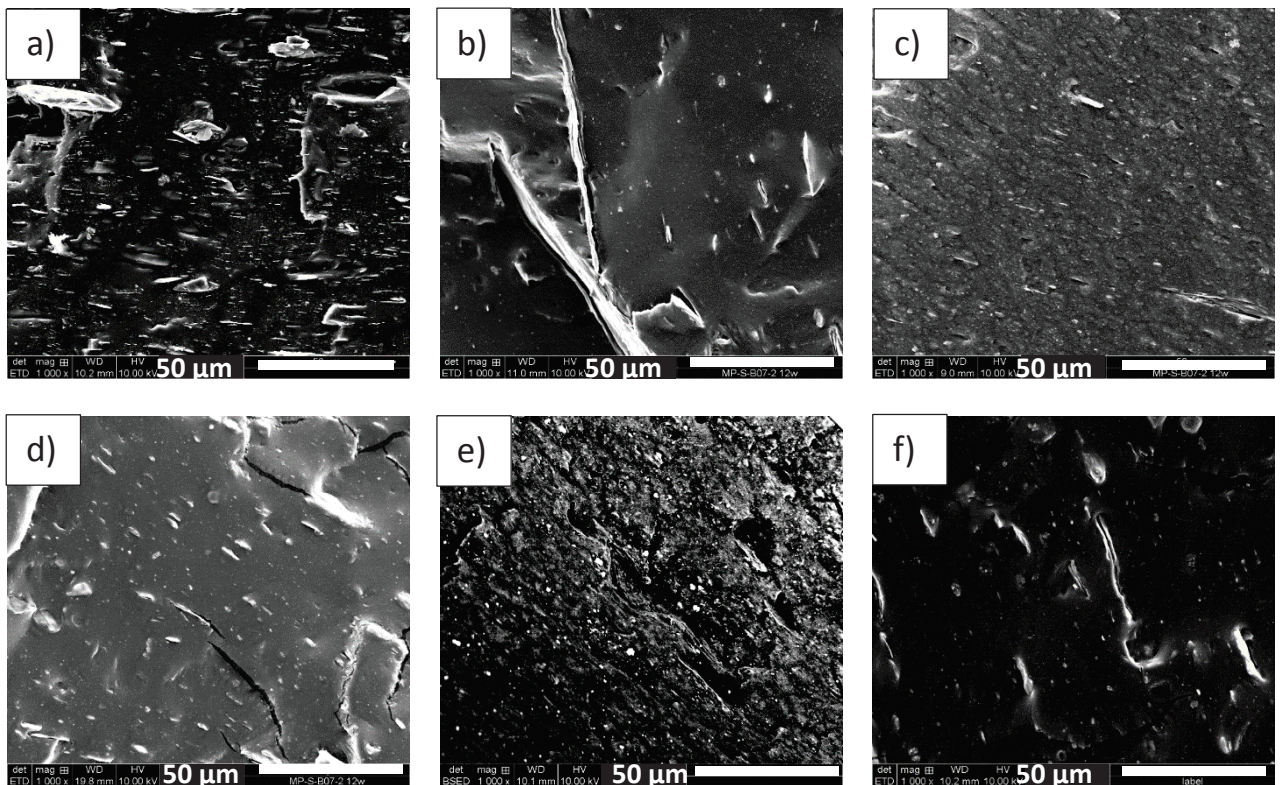


Figure 98: Morphologies of graphite-based polyisoprene composites containing 15 phr of graphite-based filler and 35 phr of carbon black, a) commercial GE, b) GO, c) GO-ODA, d) GO-TESPT, e) GOX and f) GO-allyl-IR.

From the SEM images displayed in Figure 98, aligned platelets of various sizes can be observed. Commercial graphite (GE) based composites display platelets whose lateral dimension range from a few μm to around 50 μm (Figure 98 a). GO-based composites display a rather heterogeneous dispersion with large platelets (> 100 μm) as well as platelets of a few μm (Figure 98 b). All modified-GO-based composites display enhanced dispersion and decreased thicknesses of stacks, as compared to pristine GO-based ones. Pristine GO composites contain stacks of platelets up to 10 μm thick (Figure 98 b), while the maximum thickness remains less than a few μm in all modified-GO composites. From

the four different modifications, GO-ODA polyisoprene composites seem to exhibit the smallest stacks (all lateral dimensions are below 20 μm).

In addition, in Figure 98 e, GOX platelets are hard to distinguish precisely. A few thin platelets (less than 1 μm thick), with lateral dimensions around 40 μm for the largest ones, can be observed. However, smaller platelets are not observed and may be of small lateral dimension (< 1 μm). Wang et al [260] reported similar expanded graphite platelets dimensions of a few μm in NBR composites containing 10 phr of expanded graphite. It can also be observed that most platelets are well aligned and parallel to each other due to the twin-roll mill mixing step.

Therefore, from the observation of the morphologies of GO-based composites, GO-ODA polyisoprene composites seem to display the most homogeneous dispersion with the smallest lateral dimensions. Besides, it may be pointed out that GO-allyl-IR based composites display enhanced dispersion as compared to pristine GO, which may thus reveal enhanced compatibility with the polyisoprene matrix.

Similar observations can be made for composites containing 2 phr of graphite-based fillers and their morphologies are shown in Appendix 5.3.

In addition, to investigate the role of the covalent grafting, composites containing bis[3-(triethoxysilyl)propyl]tetrasulfide (TESPT), either grafted onto GO or merely blended with GO, were prepared. Their morphologies are displayed in Figure 99.

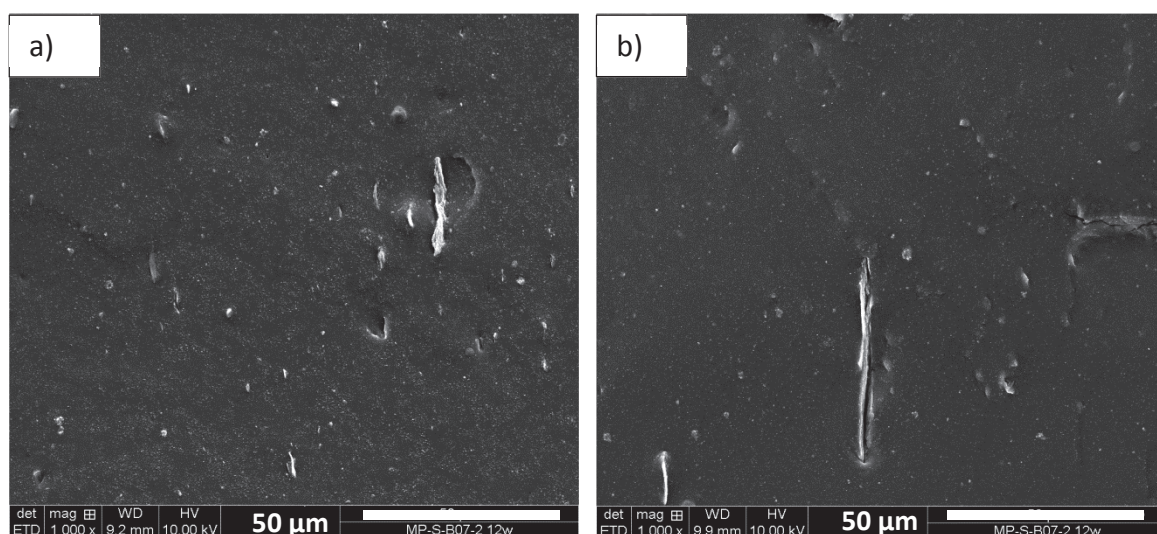


Figure 99: Polyisoprene composites containing 48 phr of carbon black and 2 phr of a) GO-TESPT (grafted) and b) GO + TESPT (just mixed, not grafted).

Composites containing TESPT-grafted-GO seem to show better dispersion and display smaller agglomerates than simply blended samples. Stacks of platelets with lateral dimension up to 50 μm are visible in Figure 99 b (mixed TESPT) whereas grafted TESPT-GO composites show smaller sizes (no more than 25 μm). The covalent grafting of TESPT on GO appears to promote better dispersion of GO-based platelets in polyisoprene.

From the morphological study, it could thus be observed that most polyisoprene composites exhibit aligned platelets along the milling direction. The most homogeneous dispersions were reached for

modified GO composites, especially for GO-ODA composites, exhibiting the smallest platelet sizes (lateral dimension of a few μm in average).

The enhanced dispersion of modified GO is generally interpreted as a consequence of improved interfacial compatibility and it is thus expected to lead to better physical properties of the corresponding polyisoprene-based composites.

2.2. Thermal conductivity of graphite-based polyisoprene composites

Graphite derivatives usually exhibit high thermal conductivity while most elastomers have a poor thermal conductivity (around $0.17 \text{ W}/(\text{m}\cdot\text{K})$). Hence, several studies have shown the ability of graphite-based fillers to increase thermal conductivity of elastomer composites [258, 266, 267].

In this study, composites were prepared as described in Appendix 5.2. All composites contain a total filler fraction of 50 phr (carbon black + graphite). It was chosen to incorporate graphite at loadings of 2 phr and 15 phr. The thermal conductivity of the samples was measured using a Hot Disk, following the method described in Appendix 1.18. In Figure 100, the variation of thermal conductivity with respect to the reference compound (ie: IR with 50 phr of carbon black, simply named IR), is reported.

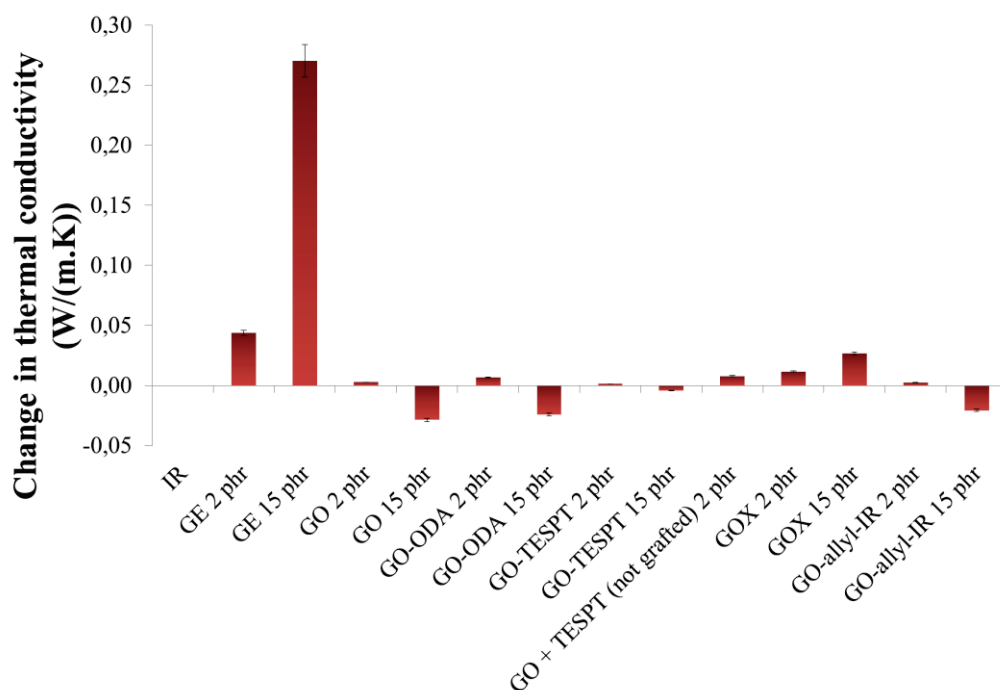


Figure 100: Relative variation of thermal conductivity of graphite-based polyisoprene composites as compared to a reference polyisoprene sample containing 50 phr of carbon black (“IR” sample with a conductivity of $0.29 \text{ W}/(\text{m}\cdot\text{K})$).

The thermal conductivity of the reference polyisoprene vulcanizate, containing 50 phr of carbon black, is $0.29 \text{ W}/(\text{m}\cdot\text{K})$. From Figure 100, it can be observed that, by replacing 15 phr of carbon black by 15 phr of commercial GE, the thermal conductivity increases by almost 100 % (up to a value of $0.56 \text{ W}/(\text{m}\cdot\text{K})$). It could also be interesting to further increase graphite loading which may lead to higher thermal conductivities. All other graphitic fillers display changes smaller than $0.05 \text{ W}/(\text{m}\cdot\text{K})$, i.e. lower than 20 %. The GOX composite loaded with 15 phr shows a moderate improvement of $0.03 \text{ W}/(\text{m}\cdot\text{K})$ (around 10 %). GO, GO-ODA, GO-TESPT and GO-allyl-IR composites containing 15 phr of the modified filler display a decrease in thermal conductivity of around $0.03 \text{ W}/(\text{m}\cdot\text{K})$. Functionalization

thus does not seem to promote efficient heat transfer between the graphitic filler and the polyisoprene matrix.

Gao et al [409] investigated the effect of grafting on the thermal conductivity of graphene platelets and graphene-polymer nanocomposites. They analyzed the effect of polyamide grafting density and grafting chain length on the thermal conductivity of graphene platelets as such or compounded with polyamide. They showed that the interfacial thermal conductivity of the platelets increased with increasing grafting density whereas the bulk thermal conductivity decreased in the same experimental conditions. These two competing phenomena led to an overall increase in thermal conductivity of the nanocomposites at low loading (< 10 vol%) and then a constant decrease at higher volume fractions [409]. Hence, in the present study, the same tendency is observed for GO-ODA composites: a very small increase (0.01 W/(m.K)) occurs at 2 phr while a stronger decrease (0.03 W/(m.K)) is observed at 15 phr.

Following a similar approach, Gulotty et al [410] studied the effect of functionalization on thermal conductivity of carbon nanotubes-epoxy composites. They reported a smaller effect of oxidized CNTs than pristine CNTs on the thermal conductivity of epoxy composites. Pristine single-wall carbon nanotubes (SWCNTs) composites displayed a thermal conductivity of 0.22 W/(m.K) at 25 °C while oxidized SWCNTs only reached a value of 0.18 W/(m.K), close to the neat epoxy matrix (0.17 W/(m.K)). The authors explained that surface functionalization could increase the interfacial interactions between CNTs and the matrix but could also lead to the formation of structural defects (such as sp^3 carbon atoms), which strongly impede the acoustic phonon transport in the CNTs, leading to a decreased thermal conductivity of the composites [410].

Functionalization of graphite fillers has thus appeared to be of little use to increase the thermal conductivity of polyisoprene composites. Materials containing modified fillers exhibit a rather similar thermal conductivity as those containing only carbon black. It is anyhow interesting to note that thermal conductivity is not much decreased either. These modified fillers could then be used to enhance other properties, such as barrier or mechanical properties, without impairing the thermal conductivity of the composites.

2.3. Barrier properties of graphite-based polyisoprene composites

Elastomers are widely used for tightness and sealing applications. As a result, it is highly desirable that they exhibit good barrier properties towards most liquids and gases. As described in Chapter 1, elastomers contain a large free volume and are intrinsically very permeable. However, upon the addition of fillers, it is possible to effectively reduce permeability of elastomeric materials. Graphite derivatives, which exhibit a platelet-like morphology, are promising for this application since they are able to create tortuosity inside the material, thus slowing down the permeant diffusion path [135, 225, 227, 236–239, 242].

Reduction of permeability of NR composites has been reported by Wu et al [127]. First they surface-functionalized GO platelets with TESPT and then they prepared composites at 1 wt% loading. They observed a decrease in permeability of 55 % as compared to neat NR. However, comparison between pristine and functionalized graphite is not often studied in elastomers. Anyhow, in their work concerning TPU composites, Kim et al [135] reported a 10 % decrease in permeability of TPU composites containing acetyl-phenyl isocyanate-modified GO as compared to pristine GO.

In the present study, the influence of graphite modification upon the barrier properties of polyisoprene composites has been investigated via air permeability measurements at room temperature (Figure 101).

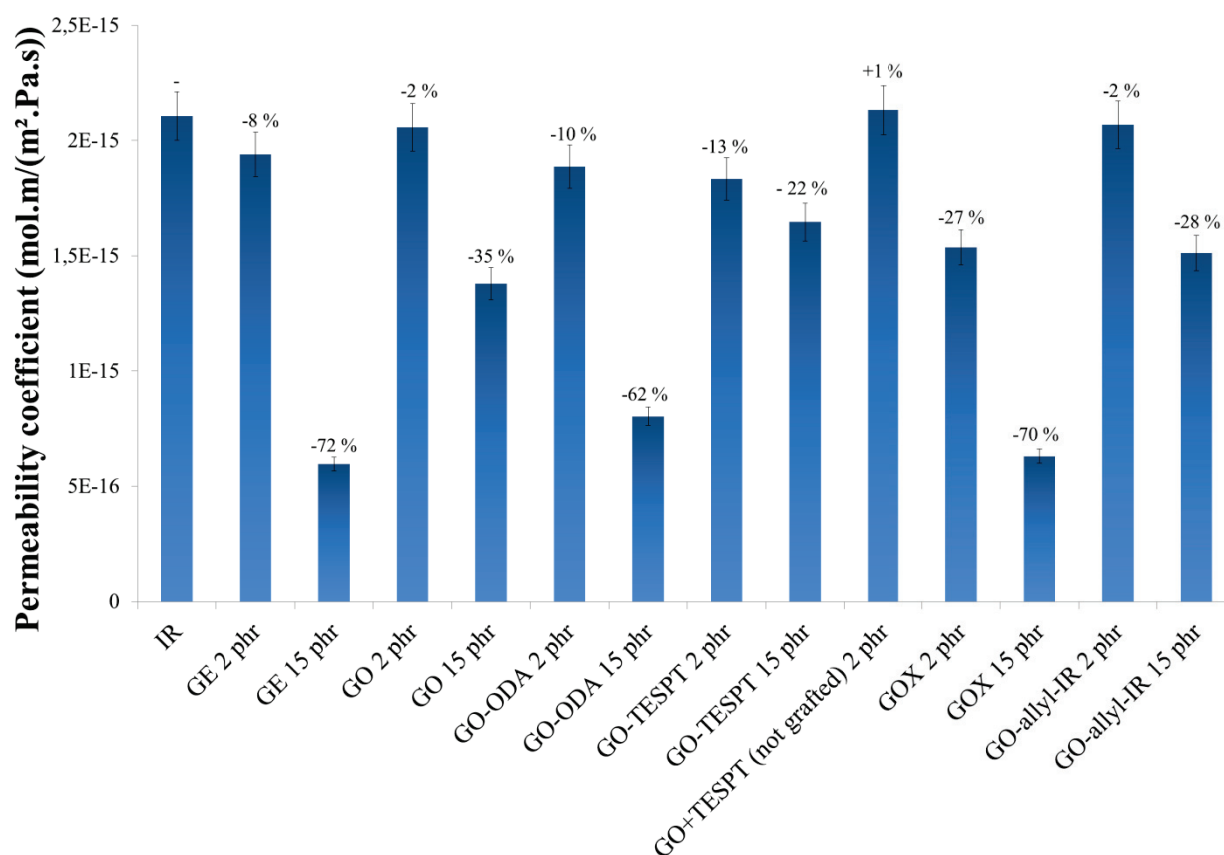


Figure 101: Air permeability coefficient of graphite-based polyisoprene composites (23 °C). The differences with respect to the “IR” reference are shown as bars.

From Figure 101, it is observed that most composites exhibit decreased air permeability as compared to polyisoprene containing 50 phr of carbon black. Although the density of filler particles (including carbon black) is high, the platelet-like morphology of graphite fillers is thus efficient in creating a tortuous path and thus decreasing permeability of the composites, as expected. However, it can be noticed that most composites containing only 2 phr of graphite-based filler do not lead to a significant decrease in permeability. Anyhow, GO-ODA and GO-TESPT show a decrease by 10 % and 13 %, respectively, which is remarkable. Besides, GOX composites show the highest decrease in permeability of the composites with a reduction of 27 % at only 2 phr (0.6 vol%) loading. Kim et al [135] also reported enhanced barrier properties of thermally reduced graphite (TRG) dispersed at low loadings in TPU composites through melt mixing, as compared to pristine graphite composites. They achieved a 40 % decrease (with respect to the neat TPU matrix) in nitrogen permeability of TRG – TPU composites at 0.5 vol% while pristine graphite only reached a decrease of 5 % at the same loading. The authors attributed this effect to a better dispersion and exfoliation of the platelets in the TPU matrix.

At 15 phr loading, more significant decreases are observed. Strongest effects occur for GO-ODA (62 %), GOX (70 %) and commercial GE (72 %). These results may be explained by a better exfoliation and dispersion in the matrix than for the other composites, as observed in the morphological study (section

2.1). Scherillo et al [411] reported similar values with 50 % decrease in oxygen and nitrogen permeability of NR composites containing 5 vol% of chemically-reduced graphite oxide.

Herein, in comparison with the polyisoprene – carbon black reference sample (IR), pristine GO led to a 35 % decrease in air permeability at 15 phr, while GO-TESPT composites only showed a 22 % decrease in air permeability despite a better dispersion (observed by SEM). GO-allyl-IR composites also showed a moderate decrease of 28 % with respect to the permeability of the reference sample, and did not achieve the same permeability reduction as pristine GO composites (- 35 %). This may be due to the presence of polyisoprene chains on the surface of GO, shorter than those in the bulk, which increase the free volume around the filler and thus enable a faster diffusion of the permeant inside the composite.

Besides, a comparison of the crosslinking density of the composites could be of significant interest to be able to conclude whether the high performance of these composites is only related to the type of modification of graphite or is also affected by the crosslinking density. Hence, an increase in the crosslinking density of the polyisoprene composite may reduce more or less both chain mobility and free volume in the material, thus slowing down the permeant diffusion [412]. A change in the crosslinking density should then affect barrier properties of elastomer composites. For example, Barrer et al [413] reported a 10-fold decrease in the nitrogen permeability of neat NR upon increasing the sulfur concentration from 1.7 % to 11.3 %. However, such an increase in sulfur content is huge and the change of crosslinking density is much larger than what could possibly be expected between the samples of the present study (same sulfur content), where only the interaction between the modified filler and the curing system can influence the network density. Moreover, the presence of 50 phr of fillers in the polyisoprene composites of the present study may limit the impact of a small variation of the crosslinking density on the permeability of the composites. This parameter anyhow, has not been often studied in the literature.

To sum up, GOX and GO-ODA led to the most pronounced decreases in air permeability of polyisoprene composites when substituted to 15 phr of carbon black. The morphological study (section 2.1.) suggested a more homogeneous dispersion of these platelets, as compared to other graphite-based composites prepared in this study, however, no clear parameter affecting the barrier properties could be evidenced. The study of the mechanical properties of the composites could provide further information. Hence, tensile properties of graphite-based polyisoprene composites were investigated and are detailed in the following section.

2.4. Tensile properties of graphite-based polyisoprene composites

Graphite-based materials usually exhibit very high moduli compared to elastomers which are generally soft materials. Due to this important contrast, many studies have been performed on graphite incorporation into elastomers to improve their mechanical properties [237, 239, 255–259]. The influence of graphitic filler size, shape and surface functionalization has been discussed in Chapter 1. In the present study, the graphite modifications have been performed to evaluate the possibilities of achieving satisfactory dispersion of the filler in the matrix and possibly improved interfacial interactions, which are the key parameter for better mechanical properties. All composites have been prepared the same way as already mentioned (see Appendix 5.2).

This section compares the tensile properties of polyisoprene composites containing different graphite-based fillers.

2.4.1. Effect of graphite content

The tensile properties were measured for polyisoprene composites at 2 phr and 15 phr loadings of graphite-based fillers, in substitution for carbon black. The results are reported in Figure 102 and Figure 103.

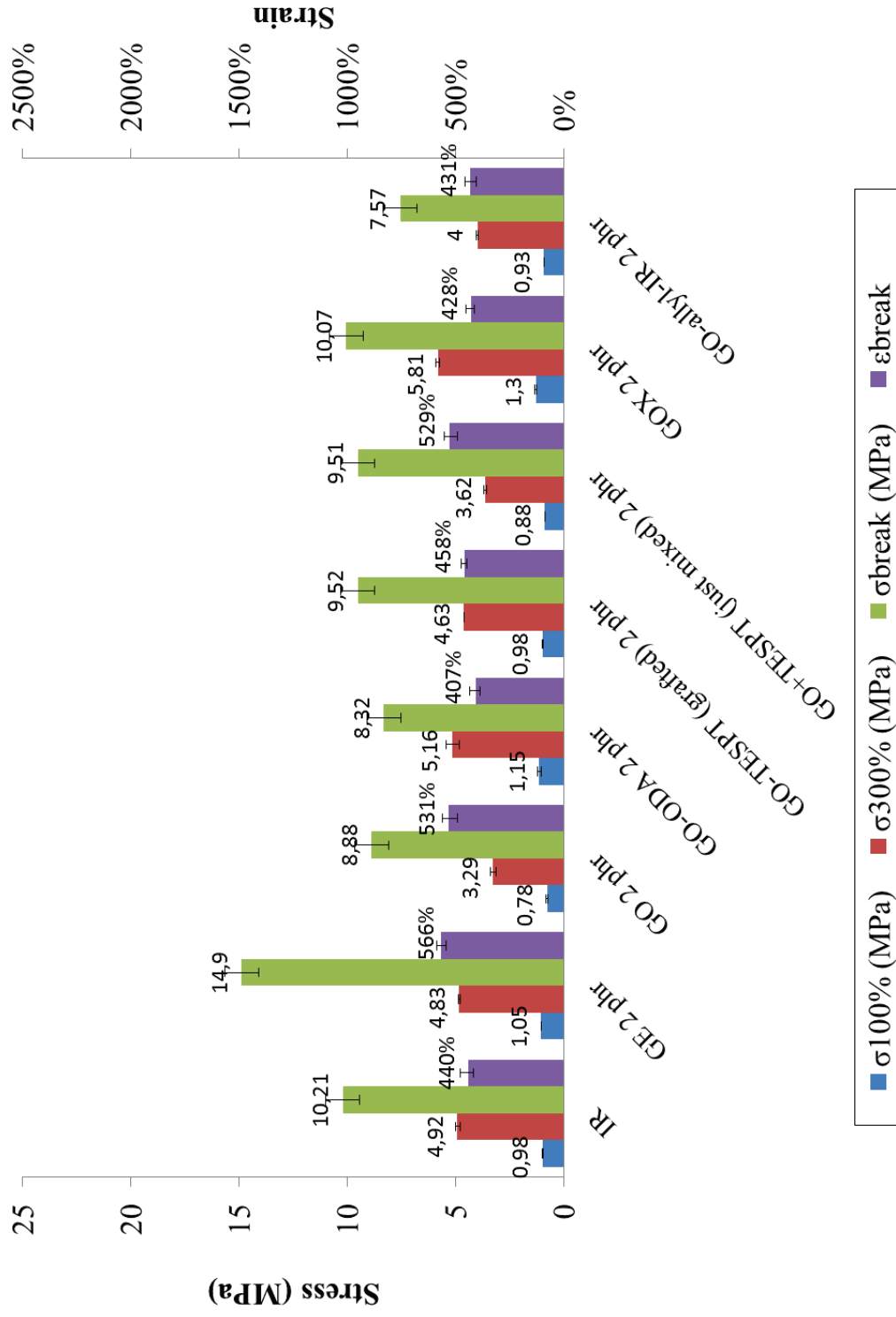


Figure 102: Tensile properties of graphite-based polyisoprene composites at 2 phr loading with 48 phr of carbon black (the IR reference sample contains 50 phr of carbon black).

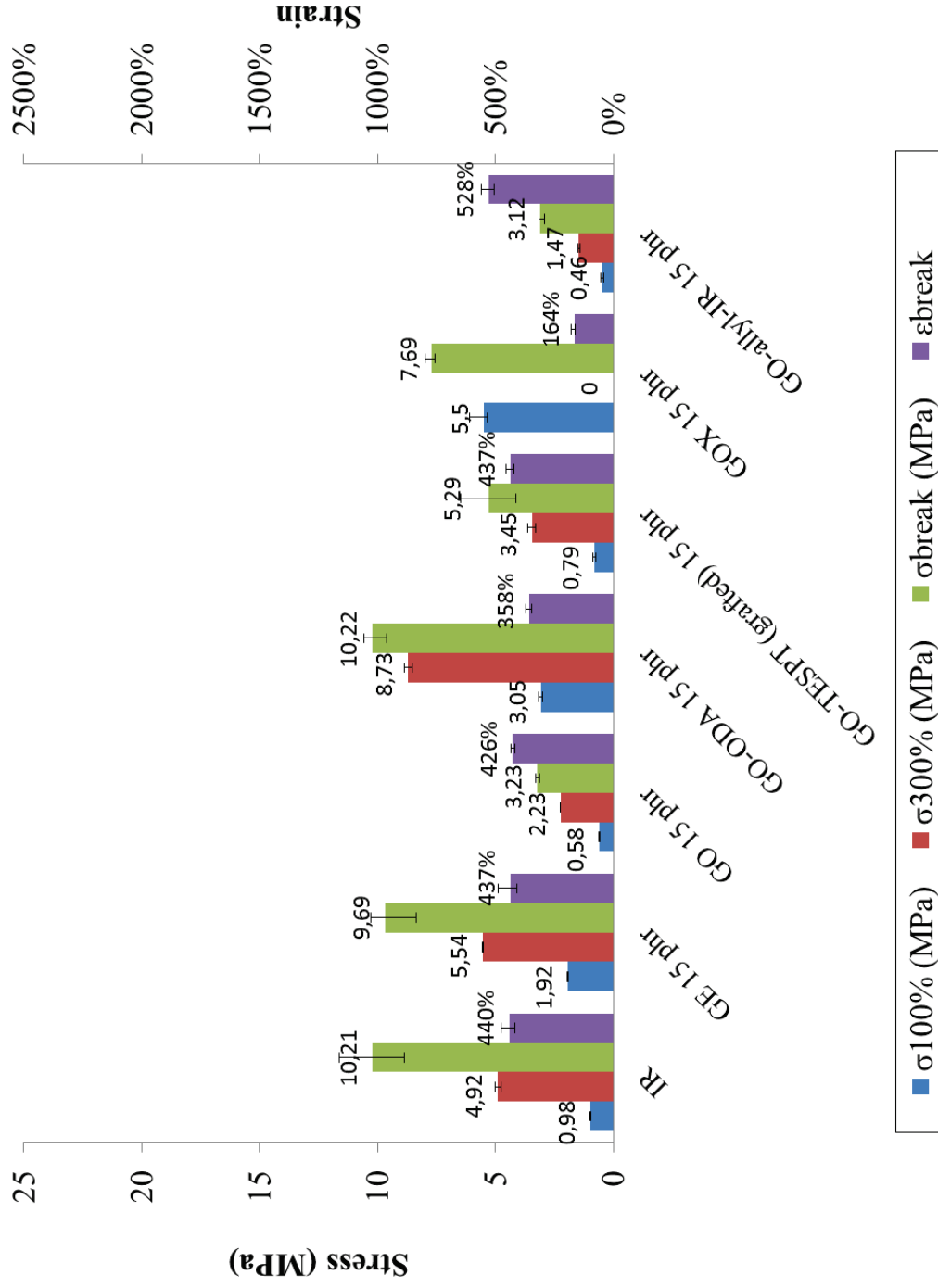


Figure 103: Tensile properties of graphite-based polyisoprene composites at 15 phr loading with 35 phr of carbon black (the IR reference sample contains 50 phr of carbon black).

From Figure 102, it is difficult to take any conclusion on the effect of 2 phr of graphite-based fillers on tensile properties, because little difference between the samples is visible at such a low loading. Anyhow, GE seems to induce a change in tensile strength for example, while most other fillers show similar values as the reference sample. No clear tendency could be evidenced from the results. The functionalization of the filler seems to induce small changes but they are not straightforward to predict.

At 15 phr loading (Figure 103), the modified-graphite fillers have stronger influence (either positive or negative) on the tensile properties of the polyisoprene composites, than at 2 phr loading. However no clear correlation with the results at 2 phr could be drawn: while some fillers tended to induce positive changes at 2 phr loading, most of them led to a decrease in tensile properties at 15 phr loading.

In the following section, the effect of the different fillers on the tensile properties of polyisoprene composites is discussed in more detail in order to analyze the effect of the chemical nature of the modification.

2.4.2. Effect of commercial GE (expanded graphite)

With a content of 2 phr of commercial graphite “GE”, and 48 phr of carbon black, the composite displays rather similar properties to the reference IR sample (containing 50 phr of carbon black). Only the stress at break increases from 10.2 MPa to 14.9 MPa due to the presence of graphite, which may provide stronger mechanical reinforcement than carbon black.

Besides, composites containing 15 phr of commercial GE tend to show improved stresses at 100 % and 300 % strain from 1 MPa to 1.9 MPa and from 4.9 MPa to 5.5 MPa, respectively, as compared to the reference sample. In addition, rupture properties are well preserved, with only a small decrease in tensile strength (from 10.2 MPa to 9.7 MPa). So, substitution of carbon black by graphite globally maintains the same tensile strength as samples filled with carbon black only, without impacting much strain at break of the composites. Beckert et al [414] also reported enhanced mechanical properties of SBR composites at 25 phr loading of graphite. They reported a 220 % increase in stress at 50 % strain with anyhow a 48 % increase in tensile strength and a 44 % decrease in strain at break, as compared to unfilled SBR matrix [414]. Although the composition and filler loading of these composites are quite different from those of the present study, the trend observed with graphitic fillers is similar.

2.4.3. Effect of GO (graphite oxide)

When 2 phr of carbon black are substituted by 2 phr of GO, tensile properties of polyisoprene composites tend to decrease. Stress at 300 % strain decreases from 4.9 MPa for the IR reference sample to 3.3 MPa for the GO-polyisoprene composite, and tensile strength decreases from 10.2 MPa to 8.9 MPa. This may be due to poor interfacial strength between GO and polyisoprene, which could be attributed to the polarity of GO and perhaps also to remaining physisorbed water on the surface, thus explaining the decrease in stresses as well as the increase in strain at break of GO composites as compared to the reference sample. Besides, the morphological study (section 2.1.) evidenced a heterogeneous dispersion with the presence of large platelets (> 100 μm), most likely to impact mechanical properties of the composites. A decrease in tensile strength was also reported by Bai et al [415] from 14.4 MPa to 10.3 MPa, upon addition of 1.3 vol% of GO in a XNBR matrix. However, other studies reported a reverse trend with enhanced mechanical properties upon addition of GO in SBR, NR and silicon matrices [238, 242, 256, 416].

At 15 phr loading, graphite oxide tends again to have a negative impact on tensile properties of polyisoprene composites, decreasing stresses at 100 % and 300 % strain, tensile strength and strain at break. With 15 phr loading of GO, composites display a tensile strength of 3.2 MPa while the reference sample reaches a value of 10.2 MPa. These low tensile properties may again be attributed to a poor compatibility between polar GO and non-polar polyisoprene. This filler could anyhow be of significant interest for a use in polar elastomers as well as in water-soluble polymers such as PVA [417].

2.4.4. Effect of modified GO on the tensile properties of polyisoprene composites

2.4.4.1. Effect of GO-ODA

Upon functionalization with ODA, stresses at 100 % and 300 % strain increase from 0.78 MPa to 1.15 MPa and from 3.29 MPa to 5.16 MPa for GO and GO-ODA composites, respectively. Liu et al [121] reported as well enhanced tensile properties for GO-ODA / SBR composites as compared to pristine GO / SBR composites, at 2 phr loading. They obtained increases in stresses at 100 % and 300 % strain from 1 MPa to 1.5 MPa and from 3 MPa to 4 MPa, respectively, upon functionalization of GO. The grafting of ODA seems able to decrease polarity of GO and to increase its affinity for non-polar organic media, thus creating a stronger interface between polyisoprene and the filler. The morphological study also evidenced improved dispersion and distribution of GO-ODA as compared to pristine GO polyisoprene composites. Besides, it can be noticed that GO-ODA filler provides slightly increased reinforcement at small strains, as compared to carbon black and to commercial graphite filler (GE). Indeed, a small increase (around 8 %) in stress at 300 % strain was observed (from 4.8 MPa for GE - polyisoprene composites to 5.2 MPa for GO-ODA composites), then suggesting stronger interactions of polyisoprene with GO-ODA than with GE.

At 15 phr loading, GO-ODA is able to increase tensile properties of the composites. A very high reinforcement is observed and a stress at 300 % strain as high as 8.73 MPa is achieved (compared to 5.5 MPa for commercial GE). ODA is believed to strengthen the interface between GO and polyisoprene. A high tensile strength (10.2 MPa) is also achieved, similar to the reference sample (containing 50 phr of carbon black). A small decrease in strain at break from 440 % for the reference sample to 358 % for GO-ODA composites, is observed. Such effect is often reported when fillers are incorporated into an elastomeric matrix for which elevated stresses at small strains and rupture properties often have to be balanced. As in most elastomeric materials, a compromise between reinforcement and large extension at break has to be achieved.

Besides, possible interaction of ODA with the curing system could be investigated. The crosslinking density of the composites should be compared in order to separate the effect of the surface modification and the effect of crosslinking density. Among additives used in the “curing system”, accelerators often contain amino groups that play a significant role in the vulcanization kinetics as well as on the nature of the final crosslinks. Lopez-Manchado et al [187] reported an increase in the curing rate of NR composites containing ODA-modified organoclays. They also reported synergistic effect of clays and ODA, leading to an increase in both the curing rate as well as the maximum torque. They explained that the amino groups of ODA could combine with benzothiazole accelerators to increase the reaction rate [187]. They also measured an increase in the crosslinking density of these composites as compared to neat NR [300]. In addition, Liu et al [121] observed an effect on crosslinking density of SBR composites measured through equilibrium swelling in toluene and using Flory-Rehner equation. At low loadings (1 phr of GO and GO-ODA) they observed a strong increase from 2.5×10^{-5} mol/cm³ to

7.5×10^{-5} mol/cm³ in the respective composites. On the contrary, at 7 phr, they observed a reversed effect with a strongly decreased crosslinking density from 8×10^{-5} mol/cm³ to 4.5×10^{-5} mol/cm³ for GO and GO-ODA composites respectively. Furthermore, they reported faster crosslinking kinetics for all GO-ODA composites with curing time differences ranging from 300 s at 1 phr to only 50 s at 5 phr. ODA has thus a complex effect on the crosslinking density of elastomer composites. The variations are not always straightforward to predict and monitor. Upon functionalization with ODA, it can thus be expected that a combination of better interfacial strength and increased crosslinking density, due to interaction with the curing system, may be responsible for the enhanced tensile properties of GO-ODA composites.

2.4.4.2. Effect of GO-TESPT

At 2 phr, GO-TESPT (grafted) composites exhibit slightly higher stresses as compared to pristine GO. Stress at 300 % strain is for example increased from 3.29 MPa to 4.63 MPa. Wu et al [127] also reported enhanced tensile properties of NR / GO-TESPT composites at 1 wt% loading. They observed enhanced tensile strength from 10 MPa to 14 MPa upon functionalization of GO with TESPT. The values obtained in the present study are very similar to commercial graphite composites, with anyhow a decreased strength at break for functionalized GO-TESPT composites. Besides, the effect of grafting can be evaluated from the comparison of GO-TESPT (grafted) and GO+TESPT (just mixed, not grafted) composites. While GO-TESPT composites contain grafted TESPT on the surface of GO, GO+TESPT composites are prepared by simple blending of GO and TESPT directly into the HAAKE mixing unit. The two samples exhibit similar properties at break but grafted TESPT-GO composite achieves higher stresses at 100 % and 300 % strain from 0.88 MPa to 0.98 MPa and from 3.62 MPa to 4.63 MPa, respectively. This effect may be attributed to better compatibility and interactions between the matrix and the filler when TESPT modifier is grafted on the surface.

Besides, TESPT may be able to react with rubber chains during vulcanization. Indeed, TESPT possesses S-S bonds that may break upon heating and then be involved in crosslinks between polyisoprene chains and GO-TESPT filler. Such covalent bonding of polyisoprene onto GO was described for example by Wu et al [127]. In addition, these authors reported a decrease in the swelling ratio from 4.4 to 4.1 at 2 phr loading of GO-TESPT in NR, thus suggesting an increase in the crosslinking density of the NR samples filled with GO-TESPT. This hypothesis is supported by the higher torque values reported for GO-TESPT composites. This increase in crosslinking density also affects the tensile properties of GO-TESPT composites [127]. In the present study, the crosslinking density of the composites should also be investigated to draw clear conclusions from the tensile testing results.

At 15 phr, GO-TESPT composites show higher stresses at 100 %, 300 % and at break, than pristine GO. However, these composites do not perform as well as commercial graphite (GE) composites. A stress at break of 5.29 MPa is achieved after functionalization while commercial graphite composites reach 9.69 MPa. Despite a more homogeneous dispersion (observed in section 2.1.), tensile properties of GO-TESPT composites are not as interesting as those of commercial graphite composites. This may be due to the possible interaction of TESPT with the curing system, as previously exposed. This reaction competes with the crosslinking reaction between polyisoprene chains and may thus affect mechanical properties of the composites. Thongsang et al [418] for example reported that TESPT was able to react either through creating filler-TESPT-rubber bondings or crosslinks between NR chains, but also could lead to the formation of polysiloxane layers by self-condensation. These reactions led mostly to

decreases in the crosslinking density of the composites, thus impairing the mechanical properties of the materials.

2.4.4.3. Effect of GOX (expanded GO)

Polyisoprene composites containing 2 phr of GOX filler exhibit increases in stresses at 100 % and 300 % strain of 35 % and 20 %, respectively, with respect to the reference sample containing 50 phr of carbon black. However, the composites break at lower strain (428 % vs 566 %) and exhibit a tensile strength reduced by around 30 %. It is anyhow of significant interest to reach a better level of reinforcement at low strains with a very low GOX loading (2 phr). Potts et al [257] also reported a 25 % increase in stress at 300 %, as compared to the neat NR matrix at 5 phr loading of thermally expanded graphite. They observed a decrease in strain at break from 900 % to 600 % but enhanced tensile strength (3-fold increase) compared to the unfilled matrix.

In addition, when a higher amount of carbon black (15 phr) was substituted by GOX, a very high increase in stress at small strain was observed for GOX composites. Hence, an increase in stress at 100 % strain from 1.9 MPa for GE composites to 5.5 MPa for GOX composites is observed. This very strong reinforcement may be induced by a better dispersion of the filler in the matrix due to the small size of the platelets (Figure 98). Nevertheless, it can be noticed that these composites break at very small strain (164 %) which is often not desirable for most applications where the ability to withstand large strains is often required. Schopp et al [255] reported similar enhancement in stresses at small strains upon addition of 25 phr of thermally-reduced graphite sheets into a SBR matrix. Their composites containing 25 phr of carbon black reached a strain at break of 350 % while composites containing thermally-expanded graphite at the same loading displayed less than 100 % strain at break. However, they reported a very strong increase in stress at 50 % strain from around 2 MPa for carbon black composites to 12 MPa for thermally-reduced graphite composites. Yang et al [16] observed a smaller increase in stress at 100 % strain from 1.0 MPa to 1.8 MPa at 20 phr loading of thermally-expanded graphite in NBR (as compared to pure NBR), with no significant decrease in tensile strength and strain at break, though.

As for previous modifications, it could be of significant interest to investigate the interaction of GOX filler with the curing additives. The better exfoliation of GOX (cf section 2.1.) as compared to commercial GE perhaps provides more available surfaces for curing additives to adsorb/react and so, could affect the crosslinking density of the final composites.

Such a high reinforcement using typical rubber processing techniques is seldom reported and could be valuable for applications that require withstanding elevated stresses [16, 255].

2.4.4.4. Effect of GO-allyl-IR

Substituting 2 phr of carbon black by polyisoprene-grafted-GO-allyl (GO-allyl-IR, see Chapter 2) induces a decrease in tensile strength from 10.2 MPa for the reference sample to 7.6 MPa for the composite containing the functionalized filler. A small decrease of the stress at 300 % strain from 4.9 MPa for the reference sample, to 4.0 MPa for the GO-allyl-IR composite is observed, which suggests a lower reinforcing effect for GO-allyl-IR filler than for carbon black. However, no significant changes in strain at break are observed.

Besides, similar tensile properties to pristine GO composites have been obtained at 15 phr loading. A 3-fold lower value than for the reference sample in tensile strength (3.1 MPa), comparable to pristine

GO composites, was obtained. Moreover, stresses at 100 % and 300 % strain were also decreased in comparison to the reference sample. Indeed, the stress at 300 % strain was reduced from 4.9 MPa to 1.5 MPa for GO-allyl-IR sample. These weak tensile properties may be attributed to weak interfacial strength between the GO-based filler and the polyisoprene matrix. However, a high strain at break (528 %) is achieved, as compared to 440 % for the reference sample containing only carbon black.

These behaviors are surprising since the presence of polyisoprene chains on the surface of GO was expected to improve compatibility and interfacial interactions between the filler and the matrix, and consequently to lead to more efficient load transfer. One explanation for these poor mechanical performances is that the polyisoprene chains polymerized on the surface of GO may be of very low molecular weight, then preventing entanglements with polyisoprene chains of the matrix. They could then fail at creating a strong interface between GO and the IR matrix in spite of supposedly better compatibility. The presence of many chain ends brings increased polymer mobility at the vicinity of the filler, which is detrimental to mechanical reinforcement and can be confronted to the results obtained for air permeability (see section 2.3.). However, no similar description could be found in the literature to support this hypothesis.

2.4.5. Comparison of the effect of different graphite-based fillers on the tensile properties

From the study of the tensile properties of graphite-based polyisoprene composites, it was shown that some modifications of the filler could lead to better properties of the polyisoprene composites.

With only 2 phr of carbon black (over 50 phr) being substituted by graphite-based filler, little effect was observed on the tensile properties of the composites. However, at 15 phr loading, GO appeared to have a strongly detrimental effect on the tensile properties of the composite, compared to the reference. Upon chemical functionalization of GO, tensile properties were improved as compared to GO-polyisoprene composites. The most pronounced effects were observed for GO-ODA and GOX composites. Indeed, GO-ODA composites exhibited increased stresses, for example stress at 300 % strain increased by almost 80 % and 50 % with respect to the reference sample and to the commercial GE composites, respectively. Besides, only a small decrease in strain at break was observed as compared these composites (around - 18 %).

In addition, GOX composites exhibited a 3-fold and almost 6-fold increase in stress at 100 % strain as compared to commercial GE composite and the reference sample, respectively. However, simultaneously the strain at break was observed to be divided by almost 3, thus limiting the potential applications of such a material. It is nevertheless interesting to be able to reinforce polyisoprene to such an extent.

From the tensile testing study, it was thus shown that GO-ODA and GOX led to the most significant improvement in tensile properties of IR composites. Most of these results are well supported by the literature, however most studies deal with the mere addition of graphite-based fillers in elastomeric matrices (which may or not contain any carbon black), but not as a partial substitution of carbon black by the same amount of graphite-based fillers.

From these results, it can also be concluded that the highest levels of reinforcement are obtained for modified-graphite polyisoprene composites at 15 phr loading. GOX filler provides the most effective

reinforcement at low strains while GO-ODA shows a significant increase in stresses at small strains with little impact on failure properties.

Conclusion

In this chapter, the influence of graphite modification on the thermal conductivity as well as barrier and mechanical properties of polyisoprene composites has been evaluated. The use of these modified fillers as partial substitution for the same amount of carbon black allows comparison of composites containing the same, relatively high, total filler loading (50 phr).

At 2 phr loading, most graphite-based fillers induced little difference in properties as compared to the reference sample, containing carbon black only. At 15 phr loading anyhow, the use of commercially-available expanded graphite (GE) led to a more than 3-fold increase in thermal conductivity, which is the highest value achieved in this study. Besides, this filler also led to the best performance in air permeability reduction (- 72 %) and to interesting mechanical properties. This behavior may be explained by a relatively uniform dispersion, as observed in the morphological study. The rather low cost of this product (~10 €/kg) suggests that an industrial use of this filler may be possible.

However, the interaction between graphite platelets and the elastomeric matrix are not well-known and the aim of the present study was to increase those interactions by the means of chemical modification. The use of modified graphite fillers led to complex effects on the polyisoprene composites properties. Hence, GO and GO-allyl-IR led to the poorest mechanical properties and did not perform as well as commercial GE in permeability reduction. These low properties could be related to a poor dispersion of these fillers inside the elastomer composite. However, some modifications of GO (GO-ODA and GOX mostly) enabled enhanced properties as compared to the reference sample. These fillers displayed more uniform dispersion and smaller aggregates in the composites than most other fillers. This confirms that dispersion is a key issue with graphite-based fillers.

Anyhow, these conclusions have to be balanced by the fact that ODA, and other modifiers such as TESPT, have been reported to interact with the sulfur curing system. This can influence the crosslinking density, and then affect both barrier and mechanical properties. This parameter should be taken into consideration in a further study, and measured by swelling measurements for example, to fully understand the effect of the functionalization on the properties of the composites.

In addition, materials without carbon black could also be studied to investigate the effect of graphite-based fillers on polyisoprene matrix. Indeed, interactions of carbon black with the elastomer, and perhaps also with the graphite-based filler, may influence the composite behavior. Besides, a lower total filler loading could enable an easier observation of the changes in properties, for example when only 2 phr of graphite-based filler are incorporated in the elastomeric matrix. This is anyhow less relevant industrially, as most elastomer products contain carbon black at a relatively high loading.

From a practical point of view, at 15 phr loading, GO-ODA and GOX fillers led to the most advantageous effect on polyisoprene composites properties. The choice of the appropriate filler should always be application-driven and while GOX showed the most enhanced reinforcement and the most pronounced air permeability decrease, GO-ODA composites exhibited better rupture properties and may thus be more suitable when the ability of the material to perform well at elevated strains is required.

It is essential to consider the compromise between the complexity of the filler treatment process and the benefit on the final properties of the composites. Therefore it is interesting to study and compare other routes of non-covalent functionalization of graphite by several modifiers such as surfactants or ionic liquids. The use of the latter will be described in the next chapter.

Chapter 5: Use of ionic liquids as dispersing agents in NR and NBR – graphite composites

Table of contents of Chapter 5

Introduction.....	194
1. Ionic liquids as dispersing agents	194
1.1. Ionic liquids in polymer materials: background	195
1.2. Scope of the study	196
2. NR composites.....	197
2.1. Influence of ILs on the vulcanization kinetics of NR – graphite composites.....	198
2.2. Thermal degradation of ILs and IL-based NR – graphite composites.....	201
2.3. Effect of ILs addition on the dispersion of graphite into NR	204
2.4. Effect of ILs addition on the tensile properties of NR – graphite composites	206
2.4.1. Effect of the addition of ILs in NR / carbon black composites	206
2.4.2. Effect of the addition of ILs in NR / graphite / carbon black composites	206
2.4.3. Conclusion on the influence of the addition of IL on tensile properties of NR – graphite composites	209
2.5. Influence of IL addition on the air permeability of NR – graphite composites.....	210
3. NBR composites.....	212
3.1. Influence of ILs on the vulcanization kinetics of NBR – graphite composites.....	212
3.2. Effect of ILs addition on the dispersion of graphite into NBR.....	212
3.3. Effect of ILs addition on tensile properties of NBR – graphite composites	214
3.3.1. Effect of the addition of ILs in NBR / carbon black composites	214
3.3.2. Effect of the addition of ILs in NBR / graphite / carbon black composites	214
4. Brief comparison of the changes in tensile properties of NR of NBR induced by the addition of graphite and ionic liquids	216
Conclusion	216

Introduction

In the previous chapters, chemical covalent functionalization of GO has been performed, involving several modification paths. Most of these modifications require to work in toxic organic solvents with many steps, sometimes long or critical. However, other graphite modification methods have been reported in the literature, involving simple strategies. Among these, non-covalent modification of graphite using surfactants has been widely performed. For example, Lomeda et al [419] adsorbed sodium dodecyl benzene sulfonate surfactant on reduced graphite oxide to enhance its dispersion in water and obtained stable suspensions at up to a concentration of 1 mg/mL.

In this section, a compatibilization strategy using several ionic liquids as dispersing agents is reported. The properties of NR and NBR composites containing graphite-based fillers and a compatibilizer have been investigated. The effect of the dispersing agent on the dispersion of the filler in the matrix has been observed through microscopy analysis. Besides, mechanical properties as well as air permeability measurements of the elastomer composites have been investigated. The influence of the ionic liquid addition on the performance of the materials has been evaluated.

1. Ionic liquids as dispersing agents

Elastomers and graphite-based nanofillers can interact in various ways such as non-covalent interactions through adsorption of elastomer chains onto the surface of graphite, ionic interactions through cation- π interactions and covalent bonding or mechanical entanglement of polymer chains in the case of fillers grafted with polymers. These interactions strongly affect the properties of the composites. Moreover, elastomers are highly viscous materials and thus, obtaining uniform dispersion and distribution of particles is challenging. Most elastomer nanocomposites exhibit poor properties when such features cannot be achieved. Besides, the absence of active sites on graphite-based materials is often responsible for low compatibility between these fillers and most elastomeric matrices. Some of the main challenges are therefore to be able to achieve a uniform distribution of well-dispersed nanofillers in the elastomeric matrix, to limit filler-filler aggregation as well as to increase filler-matrix interactions.

The chemical functionalization of graphite has been reported as a means to tune the hydrophilicity of this material and thus to improve its dispersion in various polymer matrices. Several modification paths have been studied in this work (Chapters 2 and 3) and one of the main limits to these methods is the difficulty to scale-up the modification process for industrial use.

Therefore, this section deals with another method commonly used to improve the dispersion of inorganic fillers in polymers: the use of dispersing agents. The use of surfactants has been widely reported in the literature [239, 265, 420, 421]. In this chapter, the focus will be put on an emerging class of dispersing agents: ionic liquids. These components are widely investigated nowadays because of their potential to bring new properties with possible industrial transpositions. Hence, Yang et al [239] prepared NBR – expanded graphite composites through latex blending, using sodium dodecyl sulfate (SDS) as a surfactant to enhance dispersion of expanded graphite platelets into the aqueous phase of the NBR latex. They observed that the surfactant prevented exfoliated expanded graphite from restacking [239].

1.1. Ionic liquids in polymer materials: background

A new class of dispersing agents has attracted much research interest over the last few years: ionic liquids (ILs). They are organic salts with a melting point below 100 °C. They exhibit low vapor pressure, they are non-flammable as well as thermally and chemically stable. Besides, due to their high ionic conductivities they may be used as electrolytes for lithium-ion batteries and actuators. The first generation of ILs showed air and moisture sensitivity. However, most recent generations of ILs such as imidazolium-based ILs are very stable chemically and thermally and have already shown promising results in the field of nanostructured materials, polymer blends, plasticized polymers and polymer nanocomposites [422]. The chemical structures of the cations of the main ILs families are displayed in Table 10.

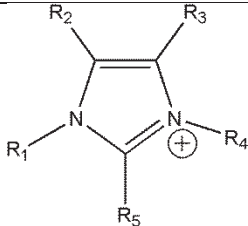
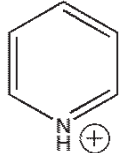
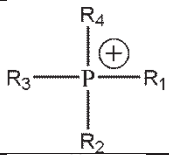
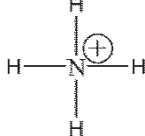
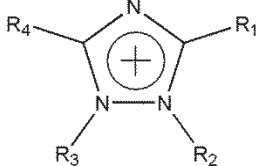
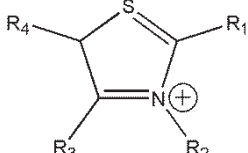
Cation name	Cation structure
Imidazolium	
Pyridinium	
Phosphonium	
Ammonium	
Triazolium	
Thiazolium	

Table 10: Chemical structures of the main ILs families.

From Table 10, it can be observed that several cation types are used in ionic liquids. They differ by their aromatic structure, the atom carrying the charge (nitrogen or phosphorous), the bulkiness etc. Besides, they may have various substituents such as short alkyl chains (ethyl for example), long alkyl chains (dodecyl for example) and may also include insaturations. They may then be associated with various organic or inorganic anions such as tetrafluoroborate, dicyanamide, chloride or bromide. It is thus possible to find a very wide variety of ionic liquids.

Many studies have dealt with the use of ILs as dispersing agents for MMT in polymers [422–425]. For example, Livi et al [425] reported a 50 % increase in the Young's modulus of a high density polyethylene matrix with 2 wt% of MMT - ILs. Recently, studies on CNT dispersion in elastomeric matrices through the use of ILs were reported by Heinrich et al [426–428]. They achieved the formation of a gel [429] with CNTs and several ILs and observed enhanced dispersion of the CNTs in presence of ILs in several elastomeric matrices such as styrene-butadiene copolymer (SBR) and polychloroprene (CR). Then, they investigated the effect of several ILs on the mechanical and electrical properties of CNT-SBR composites [428]. Upon addition of 1-allyl-3-methyl imidazolium chloride (AMIC) IL (1 mmol per g of CNTs), they reported an increase in tensile strength from 2.67 MPa to 4.12 MPa at 3 wt% CNTs content as well as an increase in the electrical conductivity from 4.5×10^{-6} S/cm to 7.7×10^{-4} S/cm [428]. Interactions between AMIC and SBR are reported to be cation- π interactions, as well as chemical covalent linkages through either an electrophilic addition of the imidazolium cation on SBR double bonds or via a sulfur crosslinking reaction of the double bond in the allylic group of AMIC and the double bonds on the SBR rubber matrix [430]. Similar positive effect of ILs on the mechanical properties of carbon black filled-elastomers have been reported [430].

Few studies have reported the use of ILs as dispersing agents to improve the dispersion of graphite-based fillers in elastomers. Xiong et al [431] prepared bromobutyl rubber (BIIR) composites with 1-butyl-3-methyl imidazolium hexafluorophosphate IL - modified GO. They reported an increased degree of exfoliation of GO (by XRD), and a slight increase (about 2 °C) in the glass transition temperature of the GO-IL composites at 4 wt% loading of GO and 0.2 phr of the IL (as compared to neat BIIR). They attributed this increase to enhanced interfacial adhesion between the filler and the matrix, but they did not characterize the nature of these interactions. They also observed a 3-fold increase in the thermal conductivity of BIIR composites containing 4 wt% of GO-IL, as compared to neat BIIR [431]. Besides, Yaragalla et al [432] prepared elastomer composites using ILs as dispersing agents. They reported that upon modification of CNT-graphene hybrid fillers with ILs, increased mechanical properties of NR composites were observed. Hence, stress at 300 % strain increased from 1.6 MPa to 2.8 MPa for IL-modified CNT-graphene hybrid fillers at 0.5 wt% loading [432].

ILs are believed to interact with graphene and CNT fillers through either interactions of the cations of the ILs with delocalized π -electrons from the fillers or, in the case of imidazolium-based ILs, through π - π interactions between imidazolium rings and graphene lattice. This results in increased distance between particles and thus in a better dispersion of the filler aggregates in the matrix [428].

1.2. Scope of the study

In this study, the influence of the addition of ionic liquids on the dispersion of commercially-available graphite in non-polar NR and polar NBR matrices has been investigated, as well as the mechanical and barrier properties of these composites. As in the previous chapters, graphite was incorporated in the elastomer as partial replacement of carbon black.

Two main IL types were used: imidazolium-based ILs and phosphonium-based ILs. The effect of these two cations on the dispersion of graphite and the properties of NR and NBR composites has been investigated. In addition, three different anions were used: bromide (Br), chloride (Cl) and bis(trifluoromethylsulfonyl)imide (TFSI). While Br and Cl anions are often reported to give a hydrophilic character to the IL, TFSI anion-based ILs exhibit increased hydrophobicity. Table 11 gathers the chemical structures of the seven ILs used in this study.

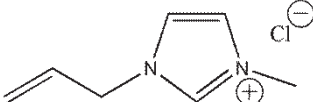
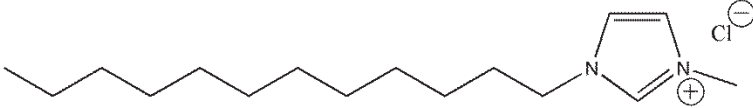
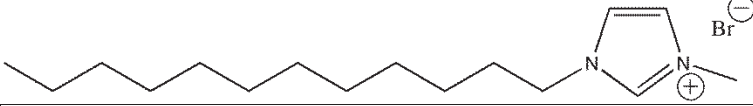
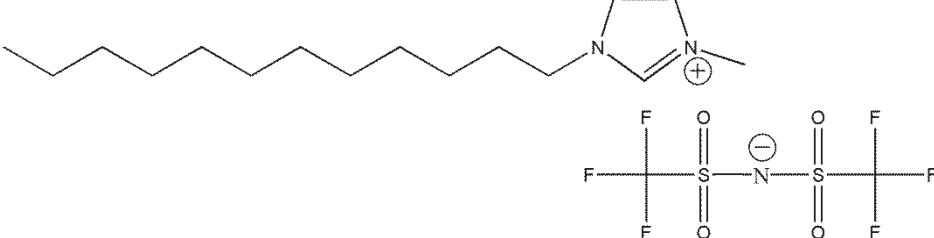
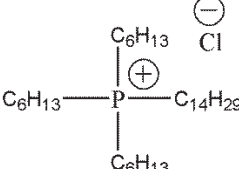
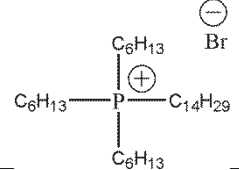
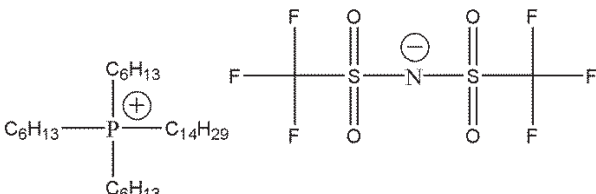
Name	Chemical structure
1-allyl-3-methylimidazolium chloride (AMIC)	
1-dodecyl-3-methylimidazolium chloride (DMIC)	
1-dodecyl-3-methylimidazolium bromide (DMIB)	
1-dodecyl-3-methylimidazolium bis(trifluoromethyl sulfonyl)imide (DMIT)	
Trihexyl(tetradecyl)phosphonium chloride (TTPC)	
Trihexyl(tetradecyl)phosphonium bromide (TTPB)	
Trihexyl(tetradecyl)phosphonium bis(trifluoromethyl sulfonyl)imide (TTPT)	

Table 11: Chemical structures of the 7 ionic liquids used in this study.

From Table 11, it can be noticed that two structures of imidazolium cations were used: one containing an allyl substituent (AMIC) and three other ones containing a C12 linear chain (DMIC, DMIB and DMIT). Phosphonium-based ILs all contain the same trihexyl(tetradecyl)phosphonium cation with the same counter-anions as imidazolium-based ILs (Cl, Br and TFSI).

NR and NBR composites were prepared with conventional rubber processing techniques ("bulk mixing") and the IL was added directly into the HAAKE mixer (see Appendix 6.1. and 6.2.). The effect of the IL structure on the properties of NR and NBR – graphite composites was investigated.

2. NR composites

Due to its exceptional properties, natural rubber is the elastomer most used worldwide. In the present chapter a more industrial approach has been developed compared to other chapters, since no modifications of the filler have been carried out prior to mixing. It was then chosen to use NR instead of IR, as it is more common in the industry and has a similar chemical structure to the polyisoprene.

In this section, the use of ILs as compatibilizing agents is investigated. Contrary to the previous approaches, no chemical bond is formed between the ILs and the filler and/or the elastomer. The IL is expected to adsorb on the surface of the filler, to decrease filler-filler interactions, and thus to promote its exfoliation within the matrix. In this study, the dispersing agents were added to the rubber mix directly during the bulk processing, no pre-modification was performed. This method was chosen to evaluate the ability of ILs to be used as efficient compatibilizing and dispersing agents for graphite, in an industrial process. Then the influence of the IL on several properties of the corresponding elastomer composites was evaluated.

2.1. Influence of ILs on the vulcanization kinetics of NR – graphite composites

Ionic liquids have been reported to affect processing of elastomer composites. Hence, Das et al [428] reported shorter curing times for CNT - SBR composites containing a few wt% of ILs. Besides, Przybyszewska et al [433] studied the effect of several imidazolium and ammonium-based ionic liquids on sulfur vulcanization of NBR. They observed that alkylammonium and alkylimidazolium salts were able to catalyze the crosslinking reactions, thus decreasing curing time. They also reported that ILs containing bromide and chloride anions led to a stronger decrease in the curing time than hexafluorophosphates. However, no mechanisms were put forward to explain this behavior [433]. Pernak et al [434] explained the increase in curing rate induced by ILs by a better dispersion of zinc oxide (ZnO), thus promoting a faster formation of accelerator-ZnO complexes and thus leading to an overall faster curing reaction. In the present study, the influence of the IL type on the curing times of NR – graphite composites was investigated.

NR composites containing variable loading of graphite ($x = 0, 2, 15$ phr) and carbon black ($50-x$ phr) were prepared through conventional rubber processing techniques (bulk mixing). The sample names are built with the following code: "Name of the rubber_amount of graphite in phr_amount of ionic liquid in wt%_name of the ionic liquid". For example, NR_0_1_TTPT is natural rubber filled with no graphite (and so, 50 phr of carbon black) and 1 wt% of TTPT ionic liquid.

Upon addition of 1 wt% of IL, curing times were found to decrease significantly for the reference NR compounds containing 50 phr of carbon black and no graphite (Figure 104).

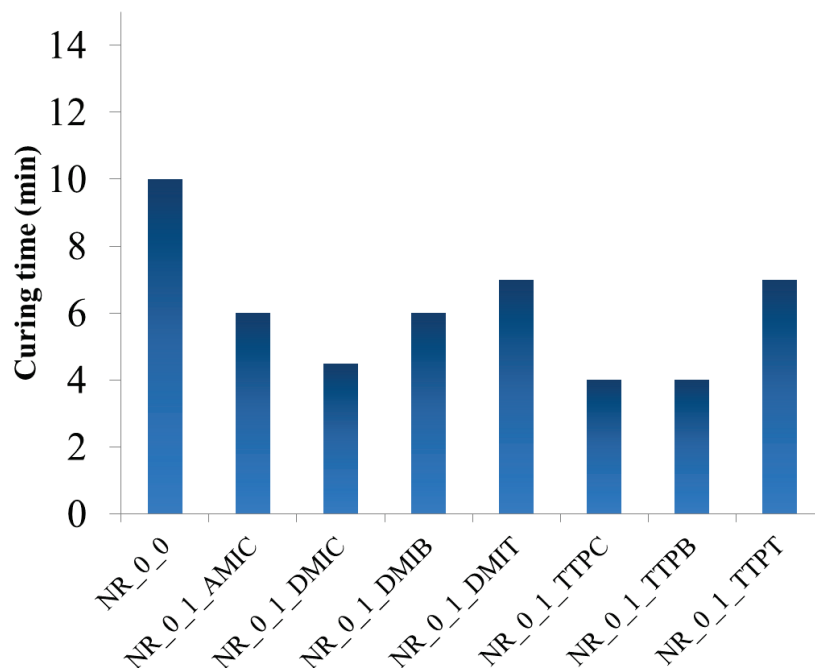


Figure 104: Curing time of NR samples filled with 50 phr of carbon black and 1 wt% of ionic liquids Curing times represents the optimum cure time (t₉₈) determined from rheological measurements as described in Appendix 1.14.2.1.

All ILs were found to effectively reduce curing times by at least 30 % and up to 60 % in the case of TTPC and TTPT. A greater effect was observed with ILs containing chloride and bromide anions (AMIC, DMIC, DMIB, TTPC, TTPB) than for ILs containing TFSI anion (DMIT and TTPT). Similar results were reported by Przybyszewska et al [433] who measured higher curing rates for rubber compounds containing alkylimidazolium chlorides and bromides than compounds containing alkylimidazolium hexafluorophosphates.

According to the results of the present study, upon addition of 1 wt% of AMIC, NR curing time decreases from 10 min to 6 min (and to as low as 4 min for TTPC and TTPB compounds). This is comparable to the results of Das et al [428] who reported a decrease of the curing time from 6.7 min to 3.2 min upon addition of AMIC in SBR/BR blends (without carbon black). The faster curing may be due to ionic interaction between the ionic liquid and the curing system, as suggested in 1.1., based on the work of Heinrich's group [428, 430, 435]. However, the exact mechanism is not known.

Next, the effect of ILs on the curing times of NR – graphite- carbon black composites was also addressed (Figure 105).

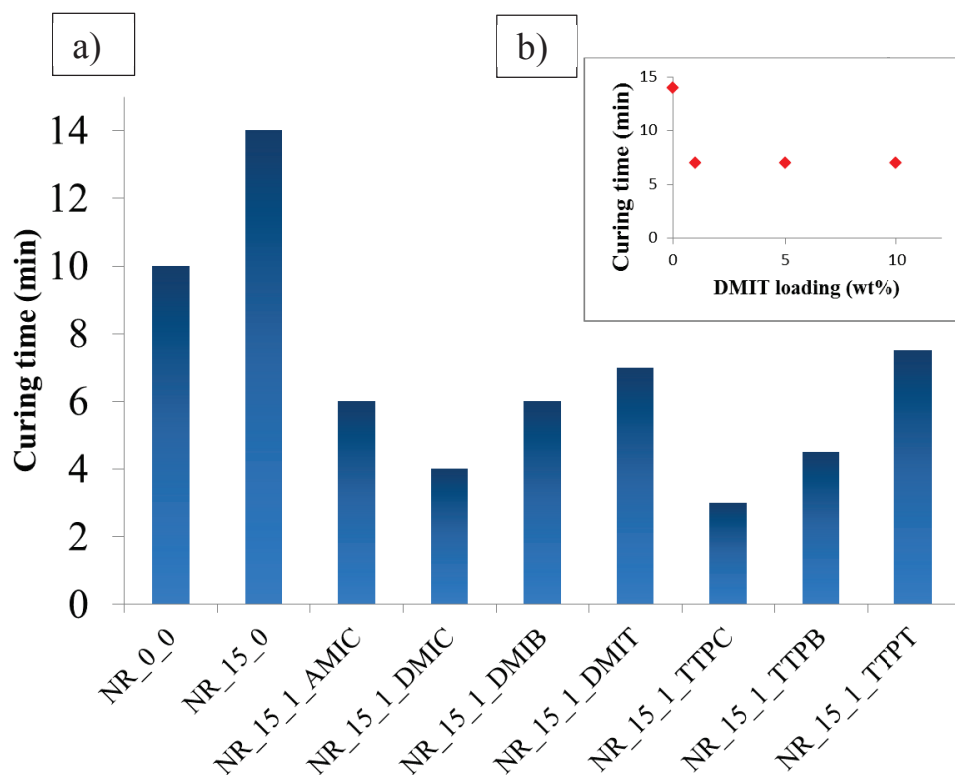


Figure 105: a) Curing time for NR and NR - graphite composites with 1 wt% ionic liquid and b) curing time of NR - graphite composites as a function of DMIT loading.

Upon addition of 15 phr of graphite in the reference NR-carbon black (50 phr) sample, curing time was found to increase from 10 min to 14 min, thus showing that inert graphite surface does not promote sulfur-curing activity, contrary to carbon black [436]. Upon addition of 1 wt% of ionic liquids, this curing time decreased significantly, down to 3 min for TTPC-containing NR composite. Das et al [428] reported similar results for SBR/BR blends filled with CNTs and ionic liquids. Upon addition of 5 phr of CNTs, curing time increased from 6.7 min to 10.2 min but was decreased to 3.7 min upon addition of 1 mmol of AMIC per gram of CNTs. However, no explanation was given by the authors. When comparing curing times of NR compounds containing 1 wt% ionic liquids, with or without graphite (Figure 104 and Figure 105), no significant difference was observed. The presence of graphite did not seem to affect the ionic liquid ability to increase reactions rates of CBS-accelerated sulfur vulcanization of NR.

However, at 10 wt% loading, most ILs prevented the vulcanization process to take place. For example, after 2 h at 160 °C, no increase in torque was observed for DMIB – NR – graphite composites (NR_15_10_DMIB) upon rheological testing. It may thus be expected that DMIB IL interacts with the curing system, thus inhibiting the reaction. DMIT was found to be the only imidazolium-based ionic liquid to be able to promote vulcanization at high loadings (10 wt%). The mechanism of IL interaction with the curing system is not known but the anion may be responsible for the inhibition since DMIC and DMIB prevented the NR composites to cure when loaded at 10 wt%, while DMIT did not seem to affect curing.

Besides, it should be taken into consideration (see section 1.), that AMIC IL may chemically react with the double bonds of the elastomeric matrix via an electrophilic addition of the imidazolium cation or

via sulfur crosslinking reaction of the double bond in the allylic group with the double bond of the rubber matrix [430]. Therefore, this reaction can compete favorably with the sulfur crosslinking reaction if the number of double bonds is limited. The effect is less prominent for elastomers such as NR that contain a large number of double bonds [430].

Another important feature when studying the vulcanization kinetics of elastomers, is the evolution of the maximum torque. In this work, the maximum torque was measured using a laboratory rheometer, which differs from common rubber rheometers using a closed oscillating cavity under controlled high pressure. The evolution of the reaction could thus be followed; however the maximum torque was not taken into account because the experimental setup did not allow the samples to cure under pressure. No conclusions on the crosslinking density were thus drawn from these measurements. Anyhow, to characterize the network density, three samples were additionally analyzed using a closed cavity rheometer: NR_0_0, NR_15_0 and NR_15_1_DMIT (see Appendix 1.14.2.2. and Appendix 6.4). No significant changes in the maximum torque were observed. The maximum torque of the reference sample reached a value of 11.1 dN.m while NR-graphite (with or without DMIT) reached a comparable value of 10.6 dN.m.

From rheological measurements, it has been evidenced that ILs interacted with the curing system. Shorter curing times were obtained when 1 wt% of the IL was added in the matrix, with TTPC having the strongest effect (3 min as compared to 10 min without IL). Besides, it was shown that the replacement of 15 phr of carbon black by 15 phr of graphite tended to increase curing times (14 min instead of 10 min), but did not modify the effect of the ILs. Indeed, similar curing times were obtained for NR composites containing ILs, whether graphite was present or not. In addition, it was shown that at higher loading (5 wt% to 10 wt%), some ILs inhibited the crosslinking reaction, due to interaction of the ILs with the curing system. However, as in most papers on this topic, no clear mechanism to explain this behavior could be found. Of course, it could be of significant interest to study the effect of the IL on the maximum torque, revealing the effect of the IL on the crosslinking density of the elastomer.

2.2. Thermal degradation of ILs and IL-based NR - graphite composites

Ionic liquids are known to exhibit a “high thermal stability” (> 400 °C) [422, 437]. For example, ethylmethylimidazolium bis(pentafluoroethylsulfonyl)imide IL was reported to have an onset degradation temperature of 462 °C, as determined by TGA under nitrogen at 10 °C/min [438].

Herein, the influence of the cation and the anion type on the thermal degradation of the ionic liquid was investigated using TGA (Figure 106). It must be noted that TGA measurements reveal the weight loss, which is associated with the degradation of the chemical component being studied. However, the absence of weight loss is not the guarantee that the material does not degrade in some way, via chemical modification. Therefore, the term “thermal degradation” will be used to refer to the occurrence of a weight loss in a sample, but no conclusion about the “thermal stability” (in the sense of no chemical modification occurring at lower temperature) will be possible.

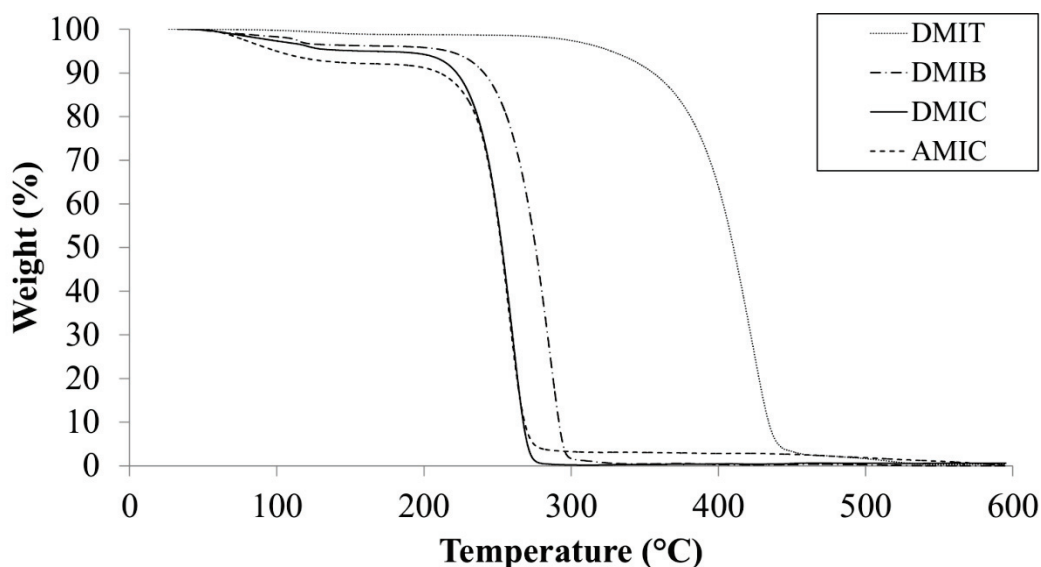


Figure 106: TGA thermograms of imidazolium ionic liquids DMIT, DMIB, DMIC and AMIC (weight loss recorded under helium with a heating rate of 10 °C/min).

First, the influence of the anion in the four imidazolium-based ILs of this study was examined. These imidazolium-based ILs show a main degradation stage at a temperature greater than 250 °C. A previous small mass loss (14 wt%, 12 wt% and 6 wt%, respectively) is observed for AMIC, DMIC and DMIB around 100 °C, showing their hydrophilic character, while hydrophobic DMIT does not exhibit any significant weight loss prior to 350 °C. The anion is thus responsible for the hydrophilicity of the ionic liquid. Besides, the cation chain length also affects significantly the hydrophilicity of the IL. Hence, while DMIC, containing a 12 carbon alkyl chain, and AMIC, containing an allylic group, undergo their main degradation at the same temperature (250 °C), AMIC shows a slightly greater weight loss (14 wt%) below 250 °C than DMIC (12 %). The imidazolium cation substituents thus affect the hydrophilicity of the IL but do not have any effect on the maximum degradation temperature of the IL. In addition, the anion seems to be of great influence on the thermal degradation of the ILs. While chloride-containing AMIC and DMIC degrade at 250 °C and bromide-containing DMIB degrades mainly at 270 °C, DMIT shows no weight loss up to 350-400 °C. It can thus be concluded that TFSI is the most stable anion and leads to a shifted temperature of degradation of the IL.

Then, the influence of the cation on the thermal degradation of the ionic liquid can be observed by comparing Figure 106 and Figure 107, where the thermograms of phosphonium-based ILs are shown.

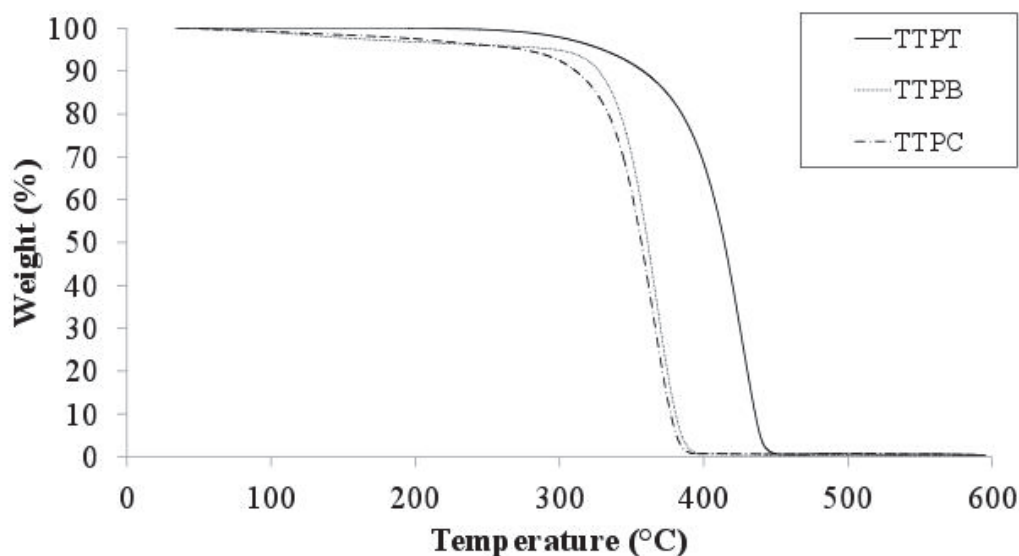


Figure 107: TGA thermograms of phosphonium ionic liquids TTPT, TTPB and TTPC.

As observed previously, chloride and bromide-containing ILs (TTPC and TTPB), show increased hydrophilicity as compared to TTPT. Besides, thermal stabilities of the ILs range in the same order as previously observed. Chloride-containing TTPC is the least stable with an onset degradation around 300 °C, bromide-containing TTPB shows slightly higher degradation temperature up to 325 °C and TFSI-containing TTPT shows delayed weight loss with a maximum degradation occurring at around 425 °C.

From the comparison of Figure 106 and Figure 107, the nature of the cation is shown to be of significant influence on the thermal degradation of the ILs. Hence, while imidazolium-based ILs degrade mainly between 250 °C and 300 °C, phosphonium-based ones show better stability with degradation temperature shifted upwards by up to 80 °C.

As a summary, the ranking of the degradation temperatures of the seven ILs of this study is the following: AMIC < DMIC < DMIB < TTPC < TTPB < DMIT < TTPT. In addition, the anion is responsible for the hydrophilic or hydrophobic character of the IL, with chloride and bromide anions having a hydrophilic character and TFSI hydrophobic. The hydrophilicity of the IL is of significant importance as it will drive the interactions between graphite and the elastomer. No study could be found on the hydrophilicity of the IL in elastomer composites with graphite filler. However, Laskowska et al [439] reported improved dispersion of silica and hydrotalcite in NBR and carboxylated NBR upon addition of 5 phr of hydrophobic 1-ethyl-3-methylimidazolium bis (trifluoromethylsulfonyl)imide IL (EMIM TFSI) whereas hydrophilic 1-ethyl-3-methylimidazolium thiocyanate IL (EMIM SCN) was not efficient in promoting dispersion of the particles. EMIM TFSI may adsorb onto filler particles and decrease the polarity of their surface, thus enhancing filler-elastomer compatibility [439].

It may thus be concluded from the results of the present study that the cation type, the anion type as well as the cation substituent chain length have an impact on the thermal stability of the IL. This is confirmed by the conclusions of Cao et al [440], who investigated the thermal degradation of sixty-six ionic liquids. Moreover, they observed that the anion type played a major role (with the main parameters being the anion coordination nature, its nucleophilicity and its hydrophilicity), while the cation type had a less significant effect on the thermal degradation of the IL. Besides, cation

modification (such as the substituent chain length) had less influence on the thermal degradation of ILs [440].

In addition, due to their high thermal stability, ILs have been reported in the literature to increase the temperature of thermal degradation of thermoplastic composites. However, in the present investigation no significant difference on the thermal degradation of NR composites could be observed upon addition of 1 wt% of an ionic liquid. All composites showed similar behavior. Likozar et al [441] also reported no significant changes in the thermal degradation of HNBR – CNTs (30 phr) composites upon addition of 3 wt% of 1-butyl-3-methylimidazolium tetrafluoroborate.

Besides, it is well-known that the glass transition temperature is related to the mobility of polymer chains. Upon addition of well-dispersed fillers showing strong interactions with the matrix, this mobility may decrease and the T_g may thus increase. The addition of an IL to improve the dispersion of a filler may lead to this effect. However, a neat T_g of – 61 °C was measured whatever the composite. No significant shift was observed upon addition of graphite and TTPT ionic liquid. Similar results were obtained with all ionic liquids tested in this study. Subramaniam et al [426] also reported no change in the glass transition temperature (- 39 °C) of polychloroprene elastomers filled with 3 phr of CNTs upon addition of 5 phr of 1-butyl 3-methyl imidazolium bis (trifluoromethylsulfonyl)imide. Therefore no detectable variation of chain mobility is observed but no conclusion can be drawn regarding filler-matrix interactions.

2.3. Effect of ILs addition on the dispersion of graphite into NR

The use of ILs as dispersing agents in elastomers has been reported to enhance dispersion of carbon-based fillers such as carbon black and CNTs [426, 428, 430, 435]. In this study, the effect of the ionic liquid on the dispersion of graphite in NR was investigated by SEM (Figure 108).

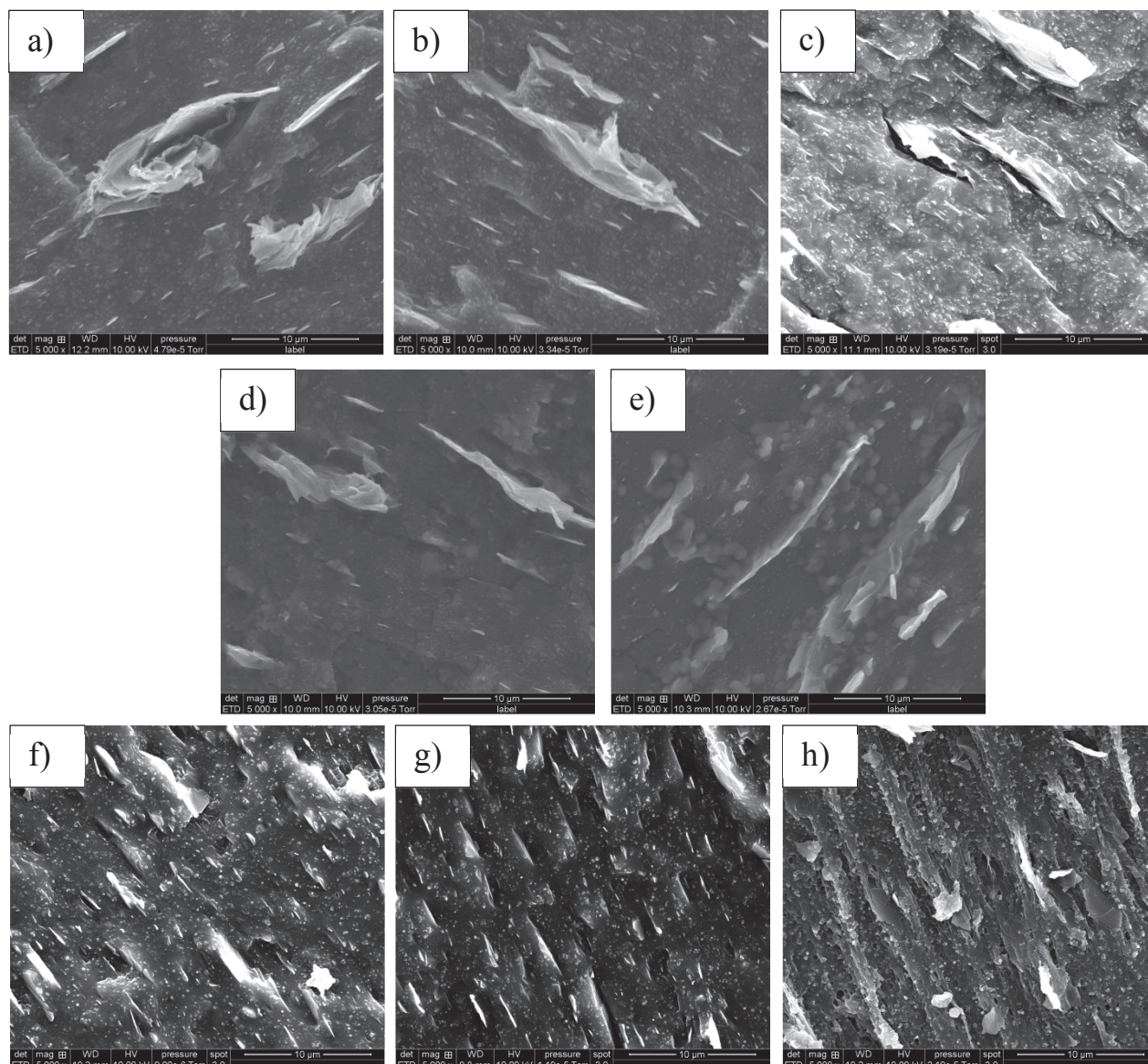


Figure 108: SEM images of NR composites with 35 phr of carbon black and 15 phr of graphite with a) no ionic liquid, 1 wt% of b) AMIC, c) DMIC, d) DMIB, e) DMIT, f) TTPC, g) TTPB and h) TTPT.

In Figure 108, SEM images of the morphologies of NR composites with 15 phr of graphite and the different ILs can be compared to the morphology of the neat composite which exhibits large aggregates up to 20 μm (Figure 108 a). Upon addition of 1 wt% of an ionic liquid, the size of the aggregates is either similar or reduced. The smallest aggregates are observed for the composite with TTPB, around 5 μm (Figure 108 g), suggesting that a more homogeneous dispersion is achieved. Phosphonium-based ILs seem to be more efficient in dispersing graphite than imidazolium-based ILs, since smaller aggregates are observed. Using TTPT ionic liquid, the morphology consists in graphite flakes of around 10 μm , coated with elastomer, thus suggesting a strong adhesion of the elastomer on the graphitic filler (Figure 108 h). Laskowska et al [439] reported similar results with enhanced dispersion of layered fillers in an elastomeric matrix (XNBR) upon addition of 5 phr of 1-ethyl-3-methylimidazolium bis(trifluoromethylsulfonyl)imide (comparable with TTPT).

The state of dispersion of fillers and the polymer-filler interactions are known to impact the mechanical properties. The composites were thus submitted to tensile testing.

2.4. Effect of ILs addition on the tensile properties of NR – graphite composites

Ionic liquids have been reported to have an influence on the mechanical properties of elastomer composites. According to several research papers, some ILs can induce enhancements in tensile properties of elastomer composites [422, 428]. For instance, Kreyenschulte et al [430] reported an increase in tensile strength (from 13 MPa to 15 MPa) and in strain at break (from 320 % to 400 %) by adding 0.8 phr of AMIC IL in carbon black – SBR/BR composites. In this study, tensile testing was used for mechanical characterization, but also as a means to reveal indirectly the state of dispersion of graphite in NR. As a consequence, only the first tensile solicitation was recorded. No cycle testing for Mullins effect was made.

2.4.1. Effect of the addition of ILs in NR / carbon black composites

The effect of some ionic liquids and on the tensile properties of NR (containing 50 phr of carbon black) has been investigated (see Appendix 6.7.1.).

Adding AMIC IL leads to very similar properties to the reference sample NR_0_0. However, DMIC and DMIT induce increased tensile strength (up to 21.9 MPa to be compared to 17 MPa for the reference material). The DMIC composite exhibits a slight increase in strain at break. Some authors attributed such an increase to a plasticizing effect of the IL on the NR matrix [435]. The term plasticization can be discussed since the other properties do not reveal the decrease of rigidity associated with the incorporation of a plasticizer and the glass transition is unchanged. More probably, the increase in stress at 100 % strain, stress at 300 % strain and strain at break may suggest a better dispersion of carbon black in the NR matrix, limiting the number of agglomerates in the composite, and thus leading to a better reinforcement and an increase in strain at break.

Furthermore, it appears that no significant effect can be noted on tensile properties with increasing ionic liquid content. This again questions some authors' conclusion about IL plasticization effect in the composites.

From this section, it was evidenced that ILs may have a dispersing effect on carbon black in elastomer composites. In the next section, the effect of ILs on composites containing graphite (in addition to carbon black) is investigated.

2.4.2. Effect of the addition of ILs in NR / graphite / carbon black composites

A similar study was performed in presence of graphite. The effect of the addition of IL in NR – graphite composites was then investigated.

First, the influence of the addition of IL and its loading in the composite were investigated. Hence, the effect of DMIT amount on the tensile properties of NR – graphite composites was investigated (Figure 109).

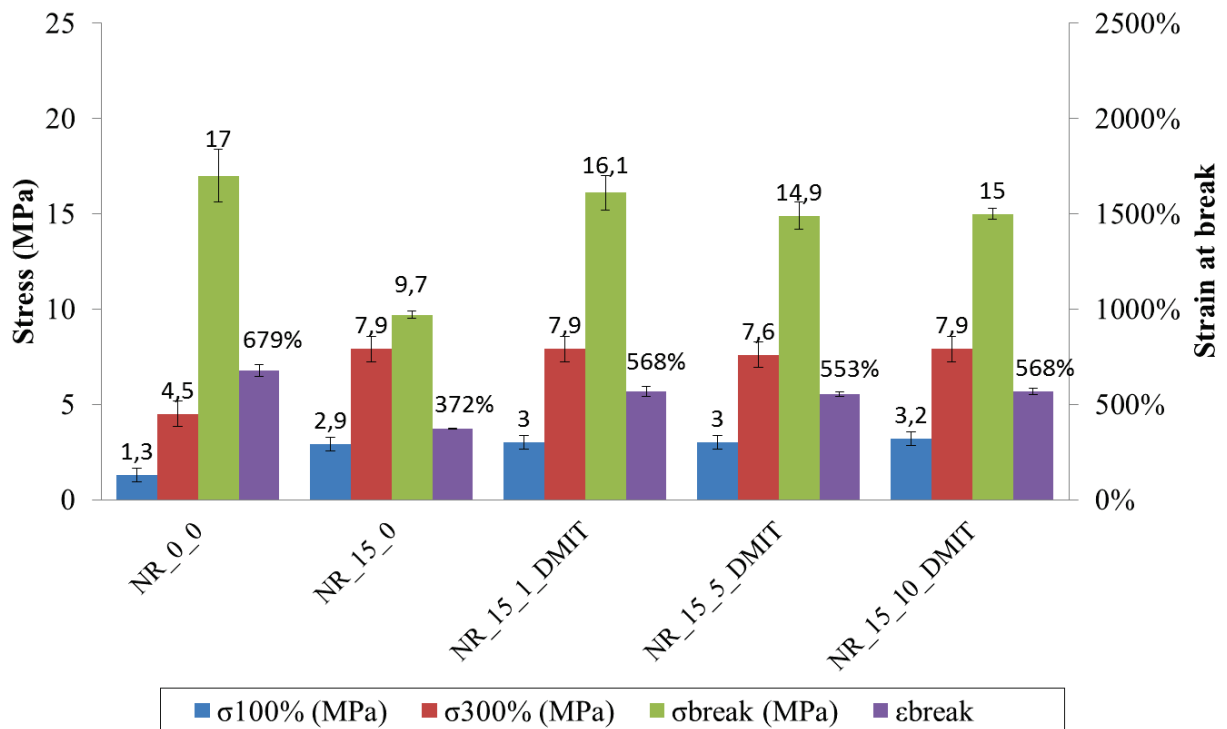


Figure 109: Effect of the amount of DMIT ionic liquid on the tensile properties of NR – graphite composites.

From Figure 109, it can be observed that NR composites containing 15 phr of graphite and 35 phr of carbon black (NR_15_0) exhibit increased stresses at 100 % and 300 % strain (from 1.3 MPa to 2.9 MPa and from 4.5 MPa to 7.9 MPa, respectively) and decreased stress and strain at break as compared to NR_0_0 containing carbon black only (50 phr). The increase in stresses at moderate strains indicates a greater reinforcing effect of graphite than carbon black. However, the noticeable decrease in tensile strength and strain at break may be attributed to a poor dispersion of graphite in the NR matrix.

Upon addition of 1 wt% of ionic liquid, no effect on stresses at small strains is observed as compared to NR_15_0 composite. However, the stress and strain at break are increased and reach similar values as NR_0_0. Besides, it is of significant interest that no decrease in stresses at moderate strains was observed with DMIT, which cannot be explained clearly on the basis of morphological observations.

Besides, it can be observed that the amount of IL does not seem to have any influence on the tensile properties of NR – graphite composites. Hence, when DMIT ionic liquid is incorporated in presence of 15 phr of graphite, similar values of stresses at small strains as well as tensile strength and strain at break are obtained, whatever the IL loading. Due to high costs of ILs (3.42 €/g for DMIT), it is thus of significant interest to limit to 1 wt% the IL loading into the NR composite.

In a second step, the influence of several ionic liquids, at 1 wt% loading, on the tensile properties of graphite-based polyisoprene composites was investigated (Figure 110).

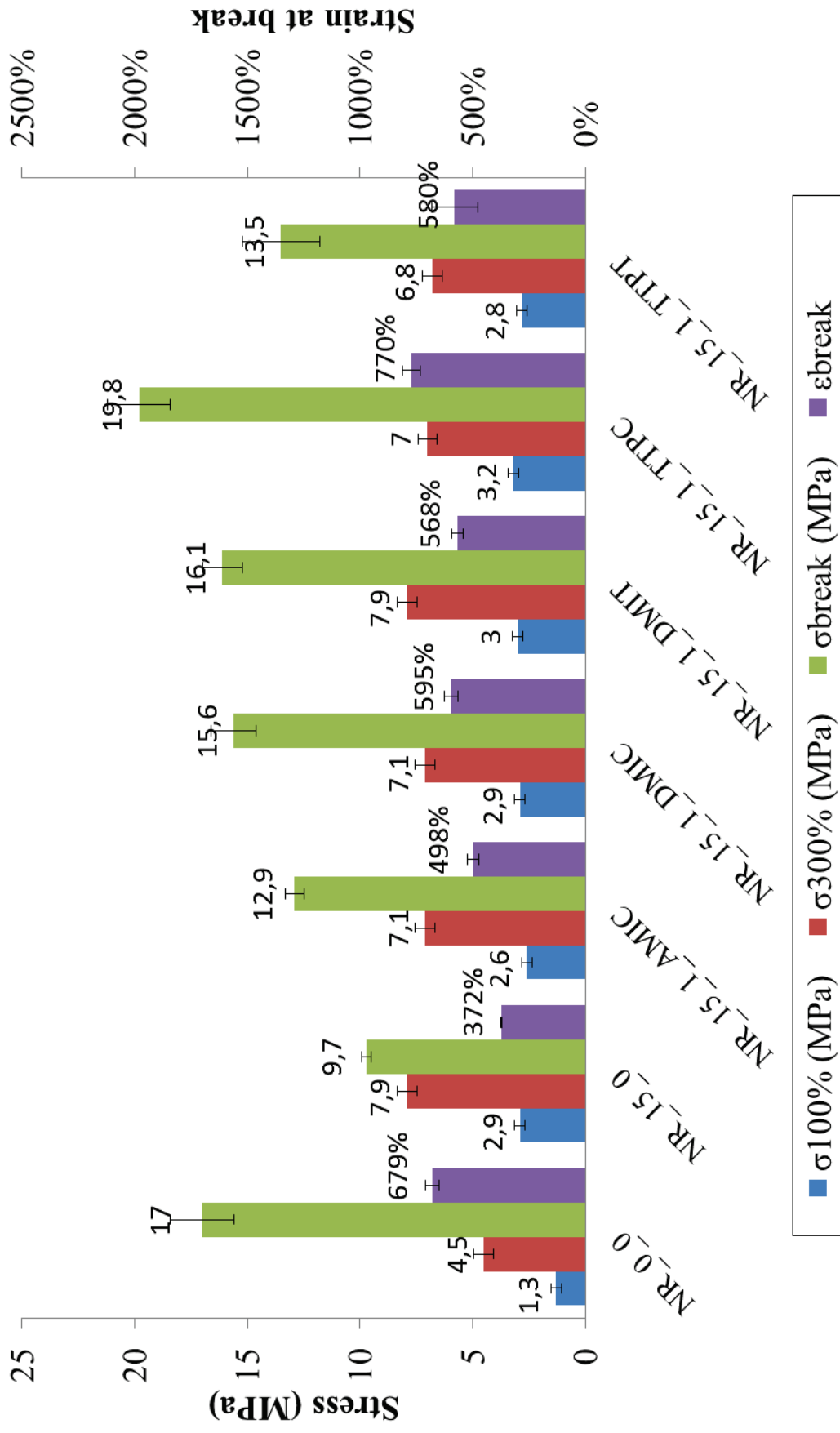


Figure 110: Effect of various ionic liquids on the tensile properties of NR – graphite composites.

For all composites containing 1 wt% of an IL, stresses at small strains are relatively well preserved while stress and strain at break increased in comparison to NR_15_0 sample. Compared to the composites containing DMIT, TTPT composites displays lower stress at 300 % (6.8 MPa as compared to 7.9 MPa for DMIT) but stress at break increased by 2.2 MPa and similar strain at break (568 % and 580 %, respectively). The TTPC composite exhibits the highest tensile strength and strain at break (superior to NR_0_0 sample). A value of 19.8 MPa is reached for tensile strength and a value of 770 % is obtained for strain at break. From morphological studies anyhow, TTPC did not appear as the best dispersing agent (Figure 108). Again, a complex influence of ILs is evidenced, with probably modifications of the dispersion and interactions.

Besides, a possible plasticizing effect was investigated through rheological measurements on uncured NR. However, the addition of 1 wt% of DMIT IL induced no significant change in the complex viscosity of NR – graphite composites, suggesting that the IL does not act as a plasticizer at 1 wt% loading in NR – graphite composites (Appendix 6.6).

In addition, the influence of the IL on the crosslinking density should be investigated. Hence, an increase in the crosslinking density of the composites would lead to an increase in stresses and would lower strain at break. Swelling experiments of NR composites, performed in cyclohexane, showed no significant change in the swelling ratio, thus suggesting no significant change in the crosslinking density of the composites (see Appendix 6.5.1).

A similar mechanical study was performed at 2 phr loading of graphite. However, no significant effect has been observed at such a low loading on tensile properties.

2.4.3. Conclusion on the influence of the addition of IL on tensile properties of NR – graphite composites

From the study of tensile properties of NR composites, it has been observed that ILs were efficient in increasing tensile strength and strain at break of NR composites containing 15 phr of graphite (and 35 phr of carbon black). These increases reached comparable values as NR vulcanizates with 50 phr loading of carbon black. Besides, no decrease in stresses at 100 % and 300 % strain were observed, as compared to pristine NR – graphite vulcanizates, thus preserving the reinforcement induced by graphite fillers. This result is of significant interest since reinforcement and rupture properties often have to be balanced.

Some selected results from the tensile testing study are gathered in Table 12.

	Stress at 100 % strain (MPa)	Stress at 300 % strain (MPa)	Tensile strength (MPa)	Strain at break (%)
NR_0_0	1.3	4.5	17.0	679
NR_0_1_DMIT	1.7	5.9	18.6	639
NR_15_0	2.9	7.9	9.7	372
NR_15_1_TTPC	3.2	7.0	19.8	770
NR_15_1_DMIT	3.0	7.9	16.1	568

Table 12: Selected results from the tensile properties of some NR composites.

From these data, a dispersing effect of the IL on the NR composites could be evidenced, leading to a reinforcement of the composite, and thus to an increase in stresses at moderate strains.

Upon addition of 1 wt% of an IL, such as DMIT, in a NR – carbon black composite (NR_0_0 and NR_0_1_DMIT), it can be noticed that stresses increase, thus suggesting a better dispersion or improved compatibility of carbon black within the NR matrix. The IL may be able to decrease the size of carbon black agglomerates, thus leading to a more efficient reinforcement of the matrix.

The substitution of 15 phr of carbon black by 15 phr of graphite (NR_15_0), leads to a noticeable increase in stresses at 100 % strain (from 1.3 MPa to 2.9 MPa) and at 300 % strain (from 4.5 MPa to 7.9 MPa), thus evidencing a greater reinforcing effect of graphite than carbon black. However, these composites break at lower strains (372 % instead of 679 %), which may be explained by the presence of large aggregates that create “defects” in the composites, initiating rupture.

The addition of 1 wt% on an IL in NR – graphite composites, enabled an increase in tensile strength and strain at break, while preserving the elevated stresses at moderate strains. This may be due to a dispersing effect of the IL in the composite. Hence, TTPC IL enables an increase in tensile strength from 9.7 MPa to 19.8 MPa and an increase in strain at break from 372 % to 770 %, due to a better dispersion of graphite in the elastomer matrix. Besides, it may be noticed that the nature of the IL influences the tensile properties of the NR composites. Hence, while DMIT well preserves the stress at 300 % strain (7.9 MPa), it induces a more moderate increase in strain at break than TTPC (568 % and 770 %, respectively). The nature of the interactions between the elastomer and the IL are not known but the polarity as well as the size of the cation and anions may be the main parameters.

In addition, it could be of significant interest to study Mullins effect in the NR composites. Hence, while the first tensile test gives an estimate of the state of dispersion, the study of Mullins effect would provide information on the stability of mechanical properties of the composites.

2.5. Influence of IL addition on the air permeability of NR – graphite composites

As mentioned in Chapter 1, good barrier properties can theoretically be expected for composites containing well-dispersed lamellar nanofillers. For instance, Das et al [435] reported a 64 % reduction in the oxygen permeability of bromobutyl rubber composites containing 5 phr of GNPs, as compared to the neat rubber matrix.

Herein, the dispersion in presence of ILs seemed improved with respect to the neat composite. Other results, such as changes in the tensile properties upon addition of ILs, tend to support the hypothesis of better dispersion. Therefore, a comparison of barrier properties with or without IL was undertaken.

The enhanced dispersion observed in SEM as well as elevated tensile properties may suggest that these composites could be efficient in gas barrier applications.

Air permeability of the NR – graphite composites in the present study, containing 15 phr of graphite and 35 phr of carbon black have thus been analyzed (Figure 111).

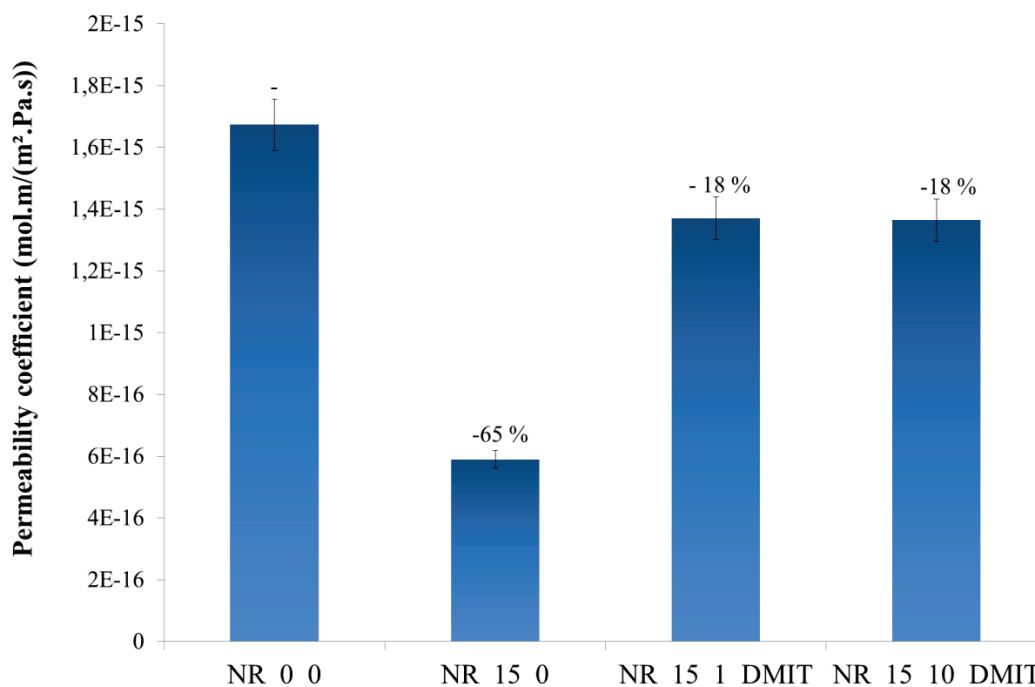


Figure 111: Air permeability coefficient of several NR composites.

From Figure 111, it can be observed that the substitution of 15 phr of carbon black by graphite enables a strong decrease in air permeability of NR composites (-65 %). This is supposedly due to the creation of a tortuous path, slowing down the permeant diffusion through the material. Upon addition of 1 wt% or 10 wt% of DMIT ionic liquid, no improvement of the barrier performance of the composite occurs. While SEM images (Figure 108) suggested a more homogeneous dispersion for NR_15_1_DMIT than NR_15_0 composite, the air permeability increases. It may be explained by an accumulation of the IL on the surface of the filler, leading to a faster diffusion of the permeant molecules at the interface [442]. Although with different filler and IL content, Das et al [435] reported similar behavior upon addition of 15 phr of IL into bromobutyl rubber filled with 5 phr of GNPs. Therefore, a possible hypothesis would be the creation of a diffusive interface, due to poor interactions of the elastomer with the filler and / or adsorption of IL on graphite, thus facilitating the diffusion of gas molecules at the vicinity of graphite platelets.

As already observed in Chapter 4, the addition of graphite-based impermeable filler into a rubber matrix is efficient in decreasing the air permeability of the composite. The addition of an IL has shown to improve the dispersion of graphite in NR but without decreasing permeability further. On the contrary, air permeability in presence of IL is larger than without IL and the amount of the IL in the composite has no influence on the air permeability of the material. An interaction of IL at the surface of the platelets can be suspected.

In the next section, the influence of several ILs on the properties on composites based on acrylonitrile-butadiene copolymer (NBR) is reported, in order to study the influence of the IL type on a polar elastomer matrix.

3. NBR composites

Acrylonitrile-butadiene copolymers (NBR) are polar elastomers that are commonly used in the automotive industry due to their good oil resistance. To study the effect of the polarity of the matrix on interactions between ILs and elastomer – graphite composites, it was chosen to work with the same ILs as described in the previous section.

Similarly to NR composites, NBR – carbon black and NBR – graphite – carbon black composites have been prepared and characterized. As for NR composites, some tests were carried out to assess the influence of ILs on the thermal stability and T_g of the NBR composites. No significant effect of the ionic liquid could be observed, either on the degradation temperature nor on the glass transition temperature of the NBR composites. Therefore, the following sections will focus on morphologies and mechanical properties.

3.1. Influence of ILs on the vulcanization kinetics of NBR – graphite composites

As for NR composites, the influence of the ILs in the vulcanization step of the composites was investigated. It was shown that partial substitution of carbon black by graphite increases curing time (from 6.5 min, for the carbon black reference, to 8.5 min) and the addition of an ionic liquid decreases this curing time. DMIC leads to the strongest reduction with 4 min curing time. However, DMIB IL has a reverse behavior and increases curing times (10 min). These observations are detailed in Appendix 6.3.

3.2. Effect of ILs addition on the dispersion of graphite into NBR

The influence of the addition of 1 wt% of an ionic liquid on the dispersion of the filler has been investigated through SEM (Figure 112).

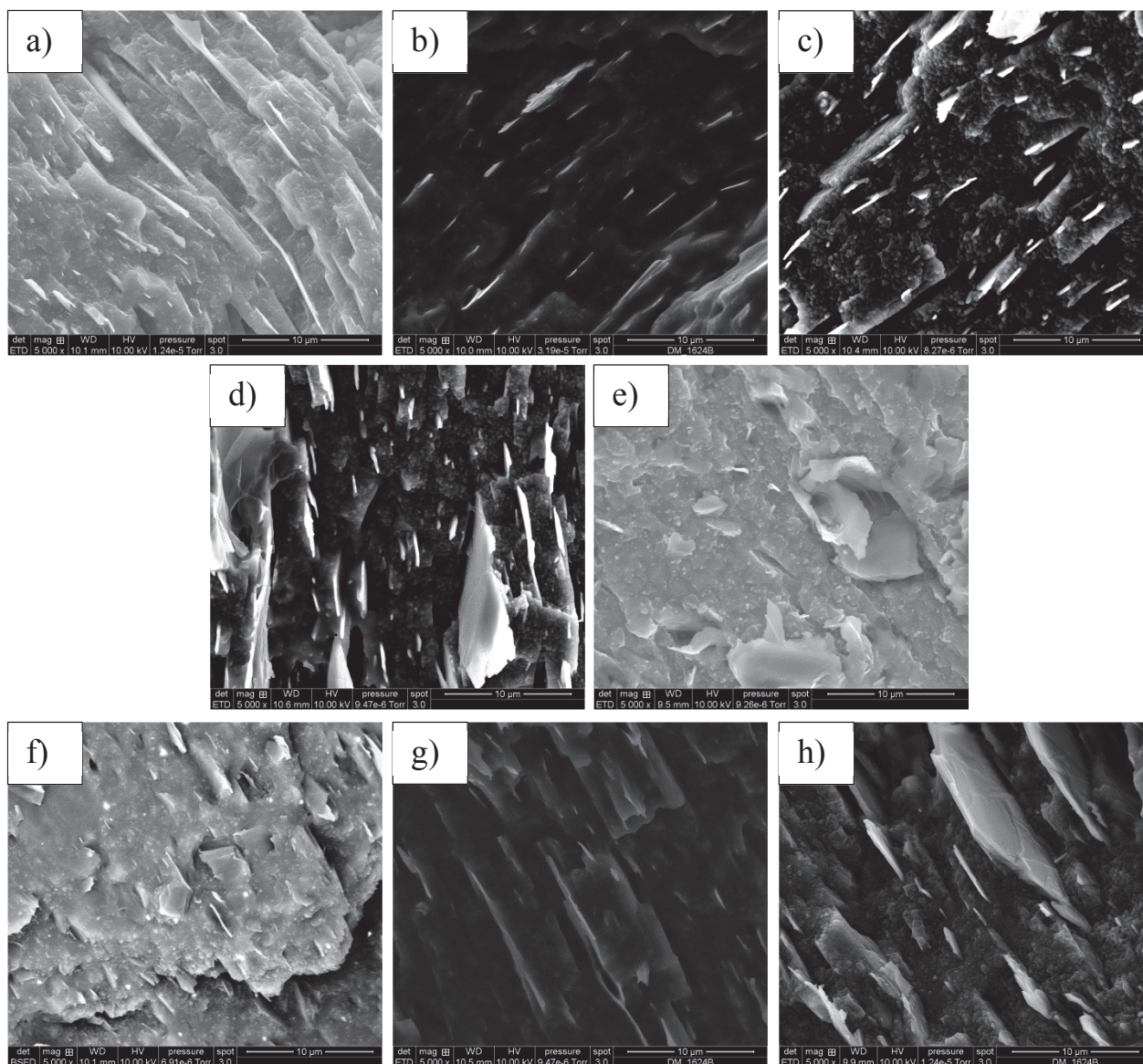


Figure 112: SEM images of NBR composites with 55 phr of carbon black and 15 phr of graphite with a) no ionic liquid, 1 wt% of b) AMIC, c) DMIC, d) DMIB, e) DMIT, f) TTPC, g) TTPB and h) TTPT.

From SEM images (Figure 112), the graphite sheet sizes seem to be reduced in composites containing AMIC, DMIC and TTPC (Figure 112 b, c and f, respectively) with the largest particles having a lateral dimension around 10 μm (as compared to 20 μm for graphite without IL in Figure 112 a). On Figure 112 e, small “filaments” are observed between graphite aggregates and the NBR matrix, thus suggesting that DMIT ionic liquid may provide good interfacial adhesion of the rubber onto the graphite platelets. However, the dispersion observed on Figure 112 h does not seem to be uniform. From these SEM images, a small improvement of the dispersion state seems to occur in chloride-based IL composites containing AMIC, DMIC and TTPC ionic liquids (Figure 112 b, c and f). It is however hard to precisely relate the nature of the anion and cation of the IL to the state of dispersion of graphite in NBR composites.

3.3. Effect of ILs addition on tensile properties of NBR – graphite composites

3.3.1. Effect of the addition of ILs in NBR / carbon black composites

The effect of ILs onto the tensile properties of NBR vulcanizates containing no graphite has been investigated (see Appendix 6.7.2).

An overall decrease in tensile strength and stresses at 100 % and 300 % strain is observed in comparison with the reference composite (NBR_0_0). AMIC induces high strains at break of 990 %. This effect may be explained by a decrease in the crosslinking density due to possible interactions of the IL with the curing additives. It might also be linked to a possible decrease of the aggregate sizes, due to the adsorption of the IL on the surface of the filler.

Besides, the effect of the amount of IL has been investigated and no significant difference between samples containing 1 wt%, 5 wt% and 10 wt% were observed.

3.3.2. Effect of the addition of ILs in NBR / graphite / carbon black composites

As for NR composites, tensile properties of NBR – graphite composites have been investigated (Figure 113).

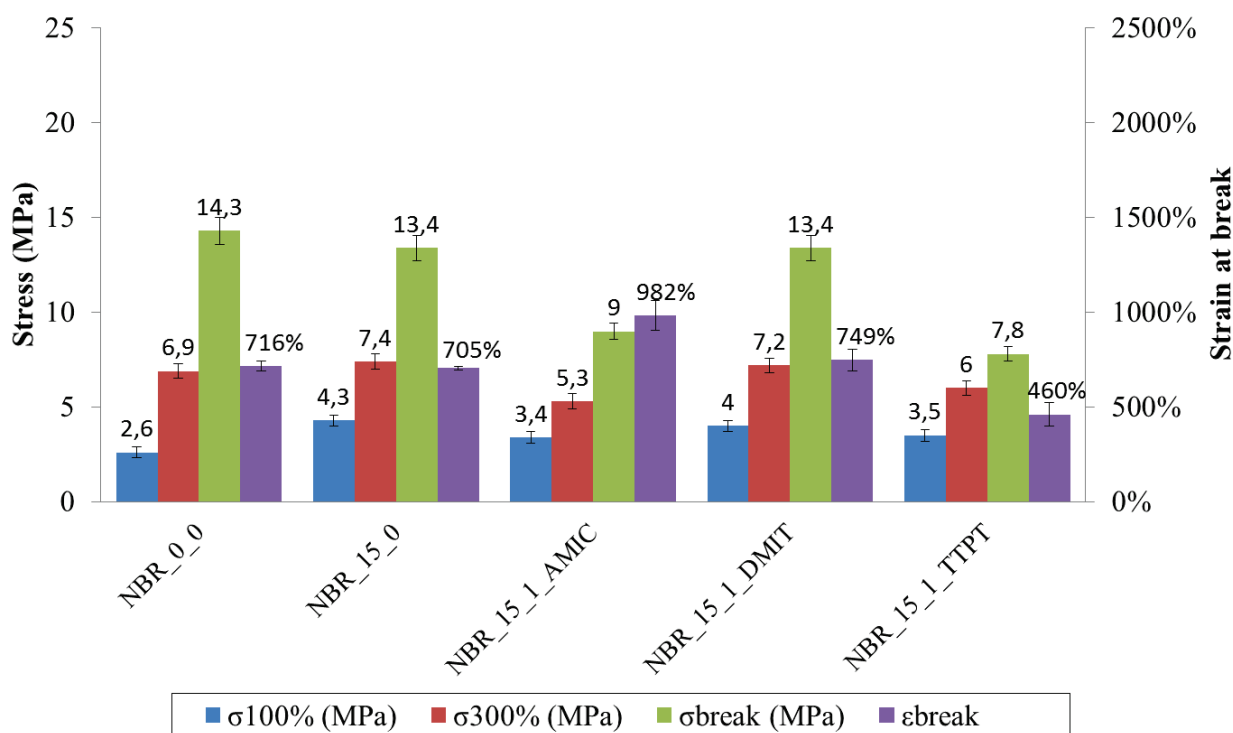


Figure 113: Effect of imidazolium ionic liquids on the tensile properties of NBR – graphite composites.

Contrary to NR-based similar composites, NBR-graphite composites do not exhibit a strong decrease in tensile strength and strain at break. A tensile strength of 13.4 MPa is reached at the maximum as compared to 14.3 MPa for NBR_0_0 vulcanizates. Upon addition of 1 wt% of ionic liquid, a decrease in stresses at small strains and at break is observed for AMIC - NBR samples. On the contrary, DMIT shows no effect on tensile properties of NBR – graphite composites at this loading. It may be noticed anyhow, that AMIC largely increases strain at break of the NBR – graphite composites (+ 40%). This increase

may be due to improvements of graphite dispersion and platelet size decrease but also to a decrease in crosslinking density. Hence, swelling experiments suggest that AMIC - NBR composites have a significantly lower crosslinking density than NBR_15_0 (see Appendix 6.5.2.). TTPT showed degraded tensile properties compared to NBR_15_0, since stresses at 100 % and 300 % strain were decreased, as well as tensile strength. Strain at break is also reduced to around 460 %.

Contrary to NR – graphite composites, the neat NBR – graphite composite (NBR_15_0) shows well-preserved rupture properties as well as an increase in stress at 100 % and 300 % strains compared to the reference sample NBR_0_0. The addition of an IL anyhow, mostly modified the tensile properties of NBR – graphite composites through a decrease in most stresses as compared to NBR_15_0.

The tensile testing study of NBR composites thus showed that ILs were not efficient in improving mechanical properties of NBR – graphite composites. Some selected results from the tensile testing study are gathered in Table 13.

	Stress at 100 % strain (MPa)	Stress at 300 % strain (MPa)	Tensile strength (MPa)	Strain at break (%)
NBR_0_0	2.6	6.9	14.3	716
NBR_0_1_DMIT	2.5	6.6	13.5	761
NBR_15_0	4.3	7.4	13.4	705
NBR_15_1_DMIT	4.0	7.2	13.4	749
NBR_15_1_AMIC	3.4	5.3	9.0	982

Table 13: Some selected tensile properties of NBR composites.

From Table 13, upon addition of 1 wt% of DMIT IL in NBR – carbon black composites, no significant changes could be observed. Similar trends were observed with other ILs. When 15 phr of carbon black are substituted by graphite, an increase in stress at 100 % strain from 2.6 MPa to 4.3 MPa and in stress at 300 % strain from 6.9 MPa to 7.4 MPa is observed, thus showing effective reinforcement of NBR by graphite. Besides, similar rupture properties to NBR_0_0 are reached.

It can also be noticed that AMIC leads to decreases in all stresses, thus suggesting that complex interactions occur between the IL and the composite components. The curing system used for NBR composites comprises different accelerators than NR composites. Hence, while CBS was used for NR, MBTS, TETD and TBzTD are used in NBR composites. These different components may thus have different interactions with the ILs. The choice of a different plasticizer (DOS instead of a paraffinic oil) as well as the addition of two antioxidants (6PPD and TMQ) may also have an influence on the interactions between the IL and the rubber.

From this study, it can be concluded that NBR – graphite composites show interesting tensile properties with increased stresses at small strains as compared to NBR_0_0 vulcanizates, without impacting much rupture properties of the material. The addition of ILs into NBR – graphite composite did not lead to better tensile properties. AMIC increased strain at break to a large extent, without preserving elevated stresses at small strain, due to a supposedly lower crosslinking density.

As for NR, it could thus be of significant interest to study the interaction of the IL with the curing system of NBR to fully attest the effect of the IL on the tensile properties of NBR – graphite composites.

4. Brief comparison of the changes in tensile properties of NR of NBR induced by the addition of graphite and ionic liquids

In this study, two matrices have been studied (NR and NBR) and the effect of the substitution of 15 phr of carbon black by 15 phr of graphite led to a different response depending on the matrix. The changes in tensile properties induced by the substitution of 15 phr of carbon black by 15 phr of graphite are gathered in Table 14.

	Stress at 100 % strain (MPa)	Stress at 300 % strain (MPa)	Tensile strength (MPa)	Strain at break (%)
NR_15_0	+ 123 %	+ 75 %	- 45 %	- 45 %
NBR_15_0	+ 65 %	+ 7 %	- 6 %	- 2 %

Table 14: Relative changes in tensile properties of NR and NBR composites upon substitution of 15 phr of carbon black by graphite. The results are given as comparison to NR_0_0 and NBR_0_0 reference samples, respectively.

From Table 14, it can be observed that the substitution of 15 phr of carbon black by 15 phr of graphite leads to a stronger impact on NR composites properties than on NBR composites. Indeed, NR – graphite composites display a strong increase in stresses at 100 % and 300 % strain (+ 123 % and + 75 %, respectively) while the stress at 300 % strain is hardly impacted by the substitution of 15 phr of carbon black by graphite in NBR. Besides, rupture properties are decreased by 45 % for NR composites while they remain identical for NBR composites.

Furthermore, the changes in tensile properties induced by the addition of 1 wt% of DMIT ionic liquid in NR and NBR – graphite composites (as compared to NR and NBR – graphite composites without IL) are gathered in Table 15.

	Stress at 100 % strain (MPa)	Stress at 300 % strain (MPa)	Tensile strength (MPa)	Strain at break (%)
NR_15_1_DMIT	+ 3 %	=	+ 66 %	+ 53 %
NBR_15_1_DMIT	- 7 %	- 3 %	=	+ 6 %

Table 15: Table 9: Relative changes in tensile properties of NR and NBR composites upon substitution of 15 phr of carbon black by graphite. The results are given as comparison to NR_0_0 and NBR_0_0 reference samples, respectively.

It can be observed that the addition of 1 wt% of DMIT ionic liquid has little impact on the tensile properties of NBR – graphite composites. However, the addition of 1 wt% of ionic liquid in NR – graphite composites leads to significant increases in stress and strain at break (+ 66 % and + 53 %, respectively).

It may thus be concluded that most significant effects on the tensile properties of NR and NBR were observed for NR composites. It is however unclear which mechanisms drive these changes. The polarity of the matrix may be one parameter but a more detailed study would be necessary to fully attest the effects of graphite and ionic liquids on NR and NBR composites.

Conclusion

In this study, the effect of addition of ionic liquids into NR and NBR – graphite composites has been investigated. Imidazolium and phosphonium-based ILs were used with chloride and bromide counterions, providing a hydrophilic character, as well as TFSI, more hydrophobic.

The main goal of this study was to investigate the use of ionic liquids as commercially-available compatibilizing agents between graphite and common elastomer matrices (NR and NBR). Similarly to

chapter 4, all composites contained carbon black, as in most industrial composites formulations. In the literature, several studies have reported contradictory results with anyhow the IL leading, in some cases, to enhanced mechanical properties of elastomer composites, by promoting a better dispersion of graphite-based fillers in the elastomer. In the present study anyhow, while some ILs led to apparently improved dispersion of graphite, no significant enhancements in mechanical properties were observed.

The ILs are believed to interact with both the filler and the matrix through physical interactions, which are dependent upon their hydrophilicity (anion type), the nature of the cation as well as the organic cation substituents (chain length and insaturations). However, no trends could be evidenced from this study. Hence, phosphonium-based TTPC led to the most prominent enhancement in mechanical properties of NR composites, while imidazolium-based DMIT was the best choice for NBR composites. Besides, only little differences between the ILs were observed and it is thus not possible to conclude on the effect of the nature of the IL on the dispersion of graphite in elastomer-based composites.

Another important parameter highlighted in this study, is the possible interaction of the IL with the curing systems of NR and NBR, which may also affect mechanical properties. Hence, a detailed study of the interactions (chemical and physical) between the IL and the vulcanization components could be interesting to perform.

From this study, it can thus be concluded that the IL did not bring the expected enhancements in mechanical and barrier properties of NR and NBR – graphite composites. Besides, due to the high cost of ILs, they may not be suitable for industrial use, as dispersing agents. In a further study, other compatibilizing agents could be investigated such as common surfactants (SDS etc).

Main conclusion

In this study, several modifications of graphite-based fillers have been investigated and their effects on the mechanical and barrier properties of polyisoprene-based composites have been characterized. The use of defect-free graphene as a filler in polymer matrices does not seem to be industrially possible yet. However, the use of graphite-based derivatives offers interesting opportunities. The literature review highlighted that graphite-based derivatives could lead to enhanced barrier and mechanical properties of elastomer composites. Besides, several studies evidenced the possibility to functionalize graphite derivatives to enhance filler-matrix interactions. This study thus focused on the enhancement of graphite – elastomer interactions through chemical modification.

In the next chapter, several functionalization strategies have been developed. While the grafting of compatibilizing molecules such as octadecylamine (ODA) has already been reported in the literature, the grafting of polymer chains was more challenging. Most research papers focused on the grafting of thermoplastic polymers chains onto the surface of graphite derivatives. However, anchoring elastomer chains had seldom been reported. In this work, an in situ polymerization technique has been developed, involving emulsion cationic polymerization of isoprene in the presence of graphite oxide (GO). Through this fast, one-pot technique, a high content of grafted polyisoprene, around 50 wt% could be achieved, which is not often reported in the literature.

In addition, new industrial materials with improved properties have been developed. The addition of the previously prepared graphite derivatives in elastomer composites has been performed and the properties of the corresponding composites have been investigated. While most studies reported the effect of the addition of graphite-based derivatives in a neat elastomer matrix, this work was carried out in a more industrially-relevant approach based on carbon black-filled elastomers. Then the modified fillers were added as partial substitution to carbon black. Complex effects on the barrier and mechanical properties were observed. Indeed, ODA-modified graphite oxide (GO-ODA) and thermally expanded graphite oxide (GOX) fillers, when loaded at 15 phr, led to prominent decreases in air permeability (~ 60-70 %) and to significant reinforcement of the polyisoprene composites.

Besides, while most studies focus on one modification path, several strategies have been investigated and compared in this work: (i) the grafting of short molecules on the surface of graphite oxide, (ii) the grafting of coupling agents between graphite oxide and the elastomer, (iii) the in situ polymerization of the monomer onto graphite oxide, (iv) the thermal treatment of graphite oxide and (v) the use of ionic liquids as dispersing agents. A wide variety of fillers has thus been prepared and in a second step, the properties of the corresponding composites have been investigated and compared. Such a global approach is seldom reported in the literature. Hence, most studies often describe one type of modification and, if a composite is prepared, its properties are usually not compared to other composites containing graphite derivatives. Besides, these materials are often compared to a reference matrix which does not contain any fillers. This is interesting to get a fundamental understanding of the effect of the modified filler on the neat elastomer matrix. In the present study, a direct comparison of the composites containing fillers with various modifications has enabled to separate the effect of the filler and the effect of the nature of the grafted molecule. Consequently, it was evidenced for example that the grafting of ODA on GO was more efficient than bis[3-

(triethoxysilyl)propyl]tetrasulfide (TESPT) in decreasing air permeability of polyisoprene-based composites.

Besides, in the present work, all the composites containing home-made modified fillers were compared to composites containing commercially-available graphite fillers, to evaluate the need for complex and time-consuming modification steps. For example, it was observed, that at 15 phr loading, commercially-available expanded graphite (GE) was as efficient as home-made GOX in reducing the air permeability of polyisoprene composites, thus suggesting that the commercial product could be used, to reduce costs. However, GOX composites displayed strongly enhanced reinforcement at small strains, compared to GE composites, which shows that for certain applications, the functionalization brings valuable changes. In addition, to further increase the barrier and mechanical properties of graphite-based elastomer composites, other modifications could be investigated in the future. For example, GO-ODA filler could be reduced, by a chemical or solvothermal process, to decrease its hydrophilicity while preserving the covalent grafting of ODA. This treatment would add an additional step to the preparation of the filler but should be valuable if it leads to a strong enhancement in barrier and mechanical properties of the polyisoprene composite. Besides, the reduction process would lead to partial recovery of the aromatic structure of the graphite-based filler and could thus induce an increase in the thermal conductivity of the composites.

This work highlighted the need for further research to fully understand and master the dispersion of platelet-like fillers in elastomer matrices. A greater understanding of exfoliation mechanisms for example could be valuable. Furthermore, another interesting feature in this study is that all composites were prepared using conventional rubber processing techniques, which are close to industrial processes. Anyhow, to attest whether these results may be industrially-relevant, a scale-up of the process should be performed as it would enable to evaluate whether the tendencies observed in this study at a laboratory scale, are confirmed.

In a further study, the dispersion of graphite-based derivatives could also be performed using a different industrial process, such as latex processing technique for example, to investigate the influence of the process on the dispersion and distribution of the filler in the elastomeric matrix. The latex processing could enable the addition of graphite derivatives as aqueous suspensions, which should limit their aggregation. Some preliminary research work on latex compounding method has already evidenced the formation of complex, segregated morphologies, which may lead to enhanced barrier properties of polymer composites. Since all the elastomers used in this study can be supplied in latex form, industrial applications of latex-compounded elastomers and graphite-based fillers can be considered.

Main conclusion

Main conclusion

References

1. Geim, A., Novoselov, K.S.: The Rise of Graphene.
2. Kim, H., Abdala, A.A., Macosko, C.W.: Graphene/polymer nanocomposites. *Macromolecules*. 43, 6515–6530 (2010).
3. Yoo, B.M., Shin, H.J., Yoon, H.W., Park, H.B.: Graphene and graphene oxide and their uses in barrier polymers: Review. *J. Appl. Polym. Sci.* 131, 39628 (2014).
4. Wan, X., Huang, Y., Chen, Y.: Focusing on Energy and Optoelectronic Applications: A Journey for Graphene and Graphene Oxide at Large Scale. *Acc. Chem. Res.* 45, 598–607 (2012).
5. Hagstrom, S., Lyon, H.B., Somorjai, G.A.: Surface Structures on the Clean Platinum (100) Surface. *Phys. Rev. Lett.* 15, 491–493 (1965).
6. Bepete, G., Anglaret, E., Ortolani, L., Morandi, V., Pénicaud, A., Drummond, C.: Surfactant-Free Single Layer Graphene in Water. *ArXiv Prepr. ArXiv160305421*. (2016).
7. Huang, K., Delport, G., Orcin-Chaix, L., Drummond, C., Lauret, J.-S., Penicaud, A.: Single layer nano graphene platelets derived from graphite nanofibres. *Nanoscale*. 8, 8810–8818 (2016).
8. Vallés, C., Drummond, C., Saadaoui, H., Furtado, C.A., He, M., Roubeau, O., Ortolani, L., Monthieux, M., Pénicaud, A.: Solutions of Negatively Charged Graphene Sheets and Ribbons. *J. Am. Chem. Soc.* 130, 15802–15804 (2008).
9. Catheline, A., Vallés, C., Drummond, C., Ortolani, L., Morandi, V., Marcaccio, M., Iurlo, M., Paolucci, F., Pénicaud, A.: Graphene solutions. *Chem. Commun.* 47, 5470 (2011).
10. Catheline, A., Ortolani, L., Morandi, V., Melle-Franco, M., Drummond, C., Zakri, C., Pénicaud, A.: Solutions of fully exfoliated individual graphene flakes in low boiling point solvents. *Soft Matter*. 8, 7882 (2012).
11. Pénicaud, A., Drummond, C.: Deconstructing Graphite: Graphenide Solutions. *Acc. Chem. Res.* 46, 129–137 (2013).
12. Varrla, E., Paton, K.R., Backes, C., Harvey, A., Smith, R.J., McCauley, J., Coleman, J.N.: Turbulence-assisted shear exfoliation of graphene using household detergent and a kitchen blender. *Nanoscale*. 6, 11810–11819 (2014).
13. Hof, F., Kampioti, K., Huang, K., Jaillet, C., Derré, A., Poulin, P., Yusof, H., White, T., Koziol, K., Paukner, C., Pénicaud, A.: Conductive inks of graphitic nanoparticles from a sustainable carbon feedstock. *Carbon*. 111, 142–149 (2017).
14. Sasikala, S.P., Henry, L., Yesilbag Tonga, G., Huang, K., Das, R., Giroire, B., Marre, S., Rotello, V.M., Penicaud, A., Poulin, P., Aymonier, C.: High Yield Synthesis of Aspect Ratio Controlled Graphenic Materials from Anthracite Coal in Supercritical Fluids. *ACS Nano*. 10, 5293–5303 (2016).
15. Gu, W., Zhang, W., Li, X., Zhu, H., Wei, J., Li, Z., Shu, Q., Wang, C., Wang, K., Shen, W., Kang, F., Wu, D.: Graphene sheets from worm-like exfoliated graphite. *J. Mater. Chem.* 19, 3367 (2009).
16. Yang, J., Tian, M., Jia, Q.-X., Zhang, L.-Q., Li, X.-L.: Influence of graphite particle size and shape on the properties of NBR. *J. Appl. Polym. Sci.* 102, 4007–4015 (2006).
17. Sadasivuni, K.K., Ponnamma, D., Thomas, S., Grohens, Y.: Evolution from graphite to graphene elastomer composites. *Prog. Polym. Sci.* 39, 749–780 (2014).
18. Xiu-Yun, C.: Graphene-like nanosheets synthesized by natural flaky graphite in Shandong, China. *Int. Nano Lett.* 3, 1–5 (2013).
19. Jacob George, J., Bandyopadhyay, A., Bhowmick, A.K.: New generation layered nanocomposites derived from ethylene-co-vinyl acetate and naturally occurring graphite. *J. Appl. Polym. Sci.* 108, 1603–1616 (2008).
20. Sun, Y., Yuan, L., Liang, G., Chang, J., Gu, A.: *In situ* vacuum exfoliation plus microwave curing: A facile and green technique for preparing polymeric composites with very good dispersion based on expanded graphite. *Polym. Compos.* 36, 385–388 (2015).

References

- Zheng, W., Wong, S.-C.: Electrical conductivity and dielectric properties of PMMA/expanded graphite composites. *Compos. Sci. Technol.* 63, 225–235 (2003).
- Ranjbar, B., Mirzazadeh, H., Katbab, A.A., Hrymak, A.N.: In situ dynamic vulcanization process in preparation of electrically conductive PP/EPDM thermoplastic vulcanizate/expanded graphite nanocomposites: Effects of state of cure. *J. Appl. Polym. Sci.* 123, 32–40 (2012).
- Bianco, A., Cheng, H.-M., Enoki, T., Gogotsi, Y., Hurt, R.H., Koratkar, N., Kyotani, T., Monthieux, M., Park, C.R., Tascon, J.M., others: All in the graphene family—a recommended nomenclature for two-dimensional carbon materials. *Carbon*. 65, 1–6 (2013).
- León, V., Quintana, M., Herrero, M.A., Fierro, J.L.G., Hoz, A. de la, Prato, M., Vázquez, E.: Few-layer graphenes from ball-milling of graphite with melamine. *Chem. Commun.* 47, 10936 (2011).
- León, V., Rodriguez, A.M., Prieto, P., Prato, M., Vázquez, E.: Exfoliation of Graphite with Triazine Derivatives under Ball-Milling Conditions: Preparation of Few-Layer Graphene *via* Selective Noncovalent Interactions. *ACS Nano*. 8, 563–571 (2014).
- Ji, X., Xu, Y., Zhang, W., Cui, L., Liu, J.: Review of functionalization, structure and properties of graphene/polymer composite fibers. *Compos. Part Appl. Sci. Manuf.* 87, 29–45 (2016).
- Georgakilas, V., Tiwari, J.N., Kemp, K.C., Perman, J.A., Bourlinos, A.B., Kim, K.S., Zboril, R.: Noncovalent Functionalization of Graphene and Graphene Oxide for Energy Materials, Biosensing, Catalytic, and Biomedical Applications. *Chem. Rev.* 116, 5464–5519 (2016).
- Georgakilas, V., Otyepka, M., Bourlinos, A.B., Chandra, V., Kim, N., Kemp, K.C., Hobza, P., Zboril, R., Kim, K.S.: Functionalization of graphene: Covalent and non-covalent approaches, derivatives and applications. *Chem. Rev.* 112, 6156–6214 (2012).
- Tasis, D., Tagmatarchis, N., Bianco, A., Prato, M.: Chemistry of Carbon Nanotubes. *Chem. Rev.* 106, 1105–1136 (2006).
- Karousis, N., Tagmatarchis, N., Tasis, D.: Current Progress on the Chemical Modification of Carbon Nanotubes. *Chem. Rev.* 110, 5366–5397 (2010).
- Liu, J., Tang, J., Gooding, J.J.: Strategies for chemical modification of graphene and applications of chemically modified graphene. *J. Mater. Chem.* 22, 12435 (2012).
- Voiry, D., Vallés, C., Roubeau, O., Pénicaud, A.: Dissolution and alkylation of industrially produced multi-walled carbon nanotubes. *Carbon*. 49, 170–175 (2011).
- Layek, R.K., Nandi, A.K.: A review on synthesis and properties of polymer functionalized graphene. *Polymer*. 54, 5087–5103 (2013).
- Maity, N., Mandal, A., Nandi, A.K.: Synergistic interfacial effect of polymer stabilized graphene *via* non-covalent functionalization in poly(vinylidene fluoride) matrix yielding superior mechanical and electronic properties. *Polymer*. 88, 79–93 (2016).
- Woszczyzna, M., Winter, A., Grothe, M., Willunat, A., Wundrack, S., Stosch, R., Weimann, T., Ahlers, F., Turchanin, A.: All-Carbon Vertical van der Waals Heterostructures: Non-destructive Functionalization of Graphene for Electronic Applications. *Adv. Mater.* 26, 4831–4837 (2014).
- Nottbohm, C.T., Turchanin, A., Beyer, A., Stosch, R., Götzhäuser, A.: Mechanically Stacked 1-nm-Thick Carbon Nanosheets: Ultrathin Layered Materials with Tunable Optical, Chemical, and Electrical Properties. *Small*. 7, 874–883 (2011).
- Luo, Z., Somers, L.A., Dan, Y., Ly, T., Kybert, N.J., Mele, E.J., Johnson, A.T.C.: Size-Selective Nanoparticle Growth on Few-Layer Graphene Films. *Nano Lett.* 10, 777–781 (2010).
- Zhong, X., Jin, J., Li, S., Niu, Z., Hu, W., Li, R., Ma, J.: Aryne cycloaddition: highly efficient chemical modification of graphene. *Chem. Commun.* 46, 7340 (2010).
- Sun, Z., Kohama, S., Zhang, Z., Lomeda, J.R., Tour, J.M.: Soluble graphene through edge-selective functionalization. *Nano Res.* 3, 117–125 (2010).
- Sainsbury, T., Passarelli, M., Naftaly, M., Gnaniyah, S., Spencer, S.J., Pollard, A.J.: Covalent Carbene Functionalization of Graphene: Toward Chemical Band-Gap Manipulation. *ACS Appl. Mater. Interfaces*. 8, 4870–4877 (2016).

References

41. Sicinski, M., Gozdek, T., Bielinski, D.M., Szymanowski, H., Kleczewska, J., Piatkowska, A.: Plasma-modified graphene nanoplatelets and multiwalled carbon nanotubes as fillers for advanced rubber composites. *IOP Conf. Ser. Mater. Sci. Eng.* 87, 12012 (2015).
42. Vadukumpully, S., Gupta, J., Zhang, Y., Xu, G.Q., Valiyaveetil, S.: Functionalization of surfactant wrapped graphenenanosheets with alkylazides for enhanced dispersibility. *Nanoscale*. 3, 303–308 (2011).
43. Park, J., Yan, M.: Covalent Functionalization of Graphene with Reactive Intermediates. *Acc. Chem. Res.* 46, 181–189 (2013).
44. Prato, M., Li, Q.C., Wudl, F., Lucchini, V.: Addition of azides to fullerene C₆₀: synthesis of azafulleroids. *J. Am. Chem. Soc.* 115, 1148–1150 (1993).
45. Cases, M., Duran, M., Mestres, J., Martín, N., Solà, M.: Mechanism of the Addition Reaction of Alkyl Azides to [60]Fullerene and the Subsequent N₂ Extrusion to Form Monoimino-[60]fullerenes. *J. Org. Chem.* 66, 433–442 (2001).
46. Han, J., Gao, C.: Functionalization of carbon nanotubes and other nanocarbons by azide chemistry. *Nano-Micro Lett.* 2, (2010).
47. Gao, C., He, H., Zhou, L., Zheng, X., Zhang, Y.: Scalable Functional Group Engineering of Carbon Nanotubes by Improved One-Step Nitrene Chemistry. *Chem. Mater.* 21, 360–370 (2009).
48. Tagmatarchis, N., Prato, M.: Functionalization of carbon nanotubes via 1,3-dipolar cycloadditions. *J. Mater. Chem.* 14, 437 (2004).
49. Choi, J., Kim, K., Kim, B., Lee, H., Kim, S.: Covalent Functionalization of Epitaxial Graphene by Azidotrimethylsilane. *J. Phys. Chem. C* 113, 9433–9435 (2009).
50. Strom, T.A., Dillon, E.P., Hamilton, C.E., Barron, A.R.: Nitrene addition to exfoliated graphene: a one-step route to highly functionalized graphene. *Chem. Commun.* 46, 4097 (2010).
51. Economopoulos, S.P., Tagmatarchis, N.: Chemical Functionalization of Exfoliated Graphene. *Chem. - Eur. J.* 19, 12930–12936 (2013).
52. Quintana, M., Spyrou, K., Grzelczak, M., Browne, W.R., Rudolf, P., Prato, M.: Functionalization of Graphene *via* 1,3-Dipolar Cycloaddition. *ACS Nano*. 4, 3527–3533 (2010).
53. Zhang, X., Hou, L., Cnossen, A., Coleman, A.C., Ivashenko, O., Rudolf, P., van Wees, B.J., Browne, W.R., Feringa, B.L.: One-Pot Functionalization of Graphene with Porphyrin through Cycloaddition Reactions. *Chem. - Eur. J.* 17, 8957–8964 (2011).
54. Liu, H., Ryu, S., Chen, Z., Steigerwald, M.L., Nuckolls, C., Brus, L.E.: Photochemical Reactivity of Graphene. *J. Am. Chem. Soc.* 131, 17099–17101 (2009).
55. Chua, C.K., Pumera, M.: Covalent chemistry on graphene. *Chem. Soc. Rev.* 42, 3222 (2013).
56. Voiry, D., Roubeau, O., Pénicaud, A.: Stoichiometric control of single walled carbon nanotubes functionalization. *J. Mater. Chem.* 20, 4385 (2010).
57. Kongsfelt, M.S., Cecato, M., Nilsson, L., Jørgensen, B., Hornekaer, L., Pedersen, S.U., Daasbjerg, K.: Chemical modifications of graphene using diazonium chemistry. In: *The Annual World Conference on Carbon 2010* (2010).
58. Dey, A., Chroneos, A., Braithwaite, N.S.J., Gandhiraman, R.P., Krishnamurthy, S.: Plasma engineering of graphene. *Appl. Phys. Rev.* 3, 21301 (2016).
59. Yang, Q., Pan, X., Clarke, K., Li, K.: Covalent Functionalization of Graphene with Polysaccharides. *Ind. Eng. Chem. Res.* 51, 310–317 (2012).
60. Cai, X., Lin, M., Tan, S., Mai, W., Zhang, Y., Liang, Z., Lin, Z., Zhang, X.: The use of polyethyleneimine-modified reduced graphene oxide as a substrate for silver nanoparticles to produce a material with lower cytotoxicity and long-term antibacterial activity. *Carbon*. 50, 3407–3415 (2012).
61. Xu, X., Luo, Q., Lv, W., Dong, Y., Lin, Y., Yang, Q., Shen, A., Pang, D., Hu, J., Qin, J., Li, Z.: Functionalization of Graphene Sheets by Polyacetylene: Convenient Synthesis and Enhanced Emission. *Macromol. Chem. Phys.* 212, 768–773 (2011).

References

62. Vuluga, D., Thomassin, J.-M., Molenberg, I., Huynen, I., Gilbert, B., Jérôme, C., Alexandre, M., Detrembleur, C.: Straightforward synthesis of conductive graphene/polymer nanocomposites from graphite oxide. *Chem. Commun.* 47, 2544 (2011).
63. Xu, L.Q., Yang, W.J., Neoh, K.-G., Kang, E.-T., Fu, G.D.: Dopamine-Induced Reduction and Functionalization of Graphene Oxide Nanosheets. *Macromolecules.* 43, 8336–8339 (2010).
64. Xu, Z., Gao, C.: *In situ* Polymerization Approach to Graphene-Reinforced Nylon-6 Composites. *Macromolecules.* 43, 6716–6723 (2010).
65. Sun, S., Wu, P.: A one-step strategy for thermal- and pH-responsive graphene oxide interpenetrating polymer hydrogel networks. *J. Mater. Chem.* 21, 4095 (2011).
66. Salavagione, H.J., Gómez, M.A., Martínez, G.: Polymeric Modification of Graphene through Esterification of Graphite Oxide and Poly(vinyl alcohol). *Macromolecules.* 42, 6331–6334 (2009).
67. Patten, T.E., Matyjaszewski, K.: Atom Transfer Radical Polymerization and the Synthesis of Polymeric Materials. *Adv. Mater.* 10, 901–915 (1998).
68. Wang, J.-S., Matyjaszewski, K.: Controlled/“living” radical polymerization. atom transfer radical polymerization in the presence of transition-metal complexes. *J. Am. Chem. Soc.* 117, 5614–5615 (1995).
69. Kato, M., Kamigaito, M., Sawamoto, M., Higashimura, T.: Polymerization of Methyl Methacrylate with the Carbon Tetrachloride/Dichlorotris-(triphenylphosphine)ruthenium(II)/Methylaluminum Bis(2,6-di-tert-butylphenoxide) Initiating System: Possibility of Living Radical Polymerization. *Macromolecules.* 28, 1721–1723 (1995).
70. Ren, P.-G., Yan, D.-X., Chen, T., Zeng, B.-Q., Li, Z.-M.: Improved properties of highly oriented graphene/polymer nanocomposites: Highly Oriented Graphene/Polymer Nanocomposites. *J. Appl. Polym. Sci.* 121, 3167–3174 (2011).
71. Fang, M., Wang, K., Lu, H., Yang, Y., Nutt, S.: Single-layer graphene nanosheets with controlled grafting of polymer chains. *J. Mater. Chem.* 20, 1982 (2010).
72. Ren, L., Wang, X., Guo, S., Liu, T.: Functionalization of thermally reduced graphene by in situ atom transfer radical polymerization. *J. Nanoparticle Res.* 13, 6389–6396 (2011).
73. Fang, M., Wang, K., Lu, H., Yang, Y., Nutt, S.: Covalent polymer functionalization of graphene nanosheets and mechanical properties of composites. *J. Mater. Chem.* 19, 7098 (2009).
74. Lee, S.H., Dreyer, D.R., An, J., Velamakanni, A., Piner, R.D., Park, S., Zhu, Y., Kim, S.O., Bielawski, C.W., Ruoff, R.S.: Polymer Brushes via Controlled, Surface-Initiated Atom Transfer Radical Polymerization (ATRP) from Graphene Oxide. *Macromol. Rapid Commun.* 31, 281–288 (2010).
75. Gonçalves, G., Marques, P.A.A.P., Barros-Timmons, A., Bdkin, I., Singh, M.K., Emami, N., Grácio, J.: Graphene oxide modified with PMMA via ATRP as a reinforcement filler. *J. Mater. Chem.* 20, 9927 (2010).
76. Yeole, N.: Thiocarbonylthio Compounds. *Synlett.* 2010, 1572–1573 (2010).
77. Ye, Y.-S., Chen, Y.-N., Wang, J.-S., Rick, J., Huang, Y.-J., Chang, F.-C., Hwang, B.-J.: Versatile Grafting Approaches to Functionalizing Individually Dispersed Graphene Nanosheets Using RAFT Polymerization and Click Chemistry. *Chem. Mater.* 24, 2987–2997 (2012).
78. Chen, G., Wu, C., Weng, W., Wu, D., Yan, W.: Preparation of polystyrene/graphite nanosheet composite. *Polymer.* 44, 1781–1784 (2003).
79. Kumar, M., Chung, J.S., Hur, S.H.: Controlled atom transfer radical polymerization of MMA onto the surface of high-density functionalized graphene oxide. *Nanoscale Res. Lett.* 9, 1–7 (2014).
80. Tripathi, S.N., Saini, P., Gupta, D., Choudhary, V.: Electrical and mechanical properties of PMMA/reduced graphene oxide nanocomposites prepared via in situ polymerization. *J. Mater. Sci.* 48, 6223–6232 (2013).
81. Liu, Y., Zhang, Y., Duan, L., Zhang, W., Su, M., Sun, Z., He, P.: Polystyrene/graphene oxide nanocomposites synthesized via Pickering polymerization. *Prog. Org. Coat.* 99, 23–31 (2016).

References

82. Beckert, F., Rostas, A.M., Thomann, R., Weber, S., Schleicher, E., Friedrich, C., Mülhaupt, R.: Self-Initiated Free Radical Grafting of Styrene Homo- and Copolymers onto Functionalized Graphene. *Macromolecules*. 46, 5488–5496 (2013).
83. Beckert, F., Friedrich, C., Thomann, R., Mülhaupt, R.: Sulfur-Functionalized Graphenes as Macro-Chain-Transfer and RAFT Agents for Producing Graphene Polymer Brushes and Polystyrene Nanocomposites. *Macromolecules*. 45, 7083–7090 (2012).
84. Patole, A.S., Patole, S.P., Kang, H., Yoo, J.-B., Kim, T.-H., Ahn, J.-H.: A facile approach to the fabrication of graphene/polystyrene nanocomposite by in situ microemulsion polymerization. *J. Colloid Interface Sci.* 350, 530–537 (2010).
85. Hu, H., Wang, X., Wang, J., Wan, L., Liu, F., Zheng, H., Chen, R., Xu, C.: Preparation and properties of graphene nanosheets–polystyrene nanocomposites via in situ emulsion polymerization. *Chem. Phys. Lett.* 484, 247–253 (2010).
86. Hummers Jr, W.S., Offeman, R.E.: Preparation of graphitic oxide. *J. Am. Chem. Soc.* 80, 1339–1339 (1958).
87. Dimiev, A.M., Tour, J.M.: Mechanism of Graphene Oxide Formation. *ACS Nano*. 8, 3060–3068 (2014).
88. Soldano, C., Mahmood, A., Dujardin, E.: Production, properties and potential of graphene. *Carbon*. 48, 2127–2150 (2010).
89. Lerf, A., He, H., Forster, M., Klinowski, J.: Structure of graphite oxide revisited. *J. Phys. Chem. B*. 102, 4477–4482 (1998).
90. He, H., Riedl, T., Lerf, A., Klinowski, J.: Solid-state NMR studies of the structure of graphite oxide. *J. Phys. Chem.* 100, 19954–19958 (1996).
91. Szabo T, Berkesi O, Forgo P, Josepovits K, Sanakis Y, Petridis D, Dekany I: Evolution of Surface Functional Groups in a Series of Progressively Oxidized Graphite Oxides. *Chem. Mater.* 18, 2740–2749 (2006).
92. Wang, G., Wang, B., Park, J., Yang, J., Shen, X., Yao, J.: Synthesis of enhanced hydrophilic and hydrophobic graphene oxide nanosheets by a solvothermal method. *Carbon*. 47, 68–72 (2009).
93. Gudarzi, M.M., Moghadam, M.H.M., Sharif, F.: Spontaneous exfoliation of graphite oxide in polar aprotic solvents as the route to produce graphene oxide – organic solvents liquid crystals. *Carbon*. 64, 403–415 (2013).
94. Guo, F., Kim, F., Han, T.H., Shenoy, V.B., Huang, J., Hurt, R.H.: Hydration-Responsive Folding and Unfolding in Graphene Oxide Liquid Crystal Phases. *ACS Nano*. 5, 8019–8025 (2011).
95. Aboutalebi, S.H., Jalili, R., Esrafilzadeh, D., Salari, M., Gholamvand, Z., Aminorroaya Yamini, S., Konstantinov, K., Shepherd, R.L., Chen, J., Moulton, S.E., Innis, P.C., Minett, A.I., Razal, J.M., Wallace, G.G.: High-Performance Multifunctional Graphene Yarns: Toward Wearable All-Carbon Energy Storage Textiles. *ACS Nano*. 8, 2456–2466 (2014).
96. Kim, J.E., Han, T.H., Lee, S.H., Kim, J.Y., Ahn, C.W., Yun, J.M., Kim, S.O.: Graphene Oxide Liquid Crystals. *Angew. Chem. Int. Ed.* 50, 3043–3047 (2011).
97. Dan, B., Behabtu, N., Martinez, A., Evans, J.S., Kosynkin, D.V., Tour, J.M., Pasquali, M., Smalyukh, I.I.: Liquid crystals of aqueous, giant graphene oxide flakes. *Soft Matter*. 7, 11154 (2011).
98. N, B., Lomeda, J.R., Green M J, Higginbotham A L, Sinitskii A, Kosynkin D, Tsentalovitch D, Parra-Vasquez G, Schmidt J, Kesselman E, Cohen Y, Talmon Y, Tour J M, Pasquali M: Spontaneous high-concentration dispersions and liquid crystals of graphene. *Nat. Nanotechnol.* 5, 406–411 (2010).
99. Paredes, J.I., Villar-Rodil, S., Martinez-Alonso, A., Tascon, J.M.D.: Graphene oxide dispersions in organic solvents. *Langmuir*. 24, 10560–10564 (2008).
100. Dreyer, D.R., Park, S., Bielawski, C.W., Ruoff, R.S.: The chemistry of graphene oxide. *Chem Soc Rev.* 39, 228–240 (2010).

References

101. Szabó, T., Tombácz, E., Illés, E., Dékány, I.: Enhanced acidity and pH-dependent surface charge characterization of successively oxidized graphite oxides. *Carbon*. 44, 537–545 (2006).
102. Li, D., Müller, M.B., Gilje, S., Kaner, R.B., Wallace, G.G.: Processable aqueous dispersions of graphene nanosheets. *Nat. Nanotechnol.* 3, 101–105 (2008).
103. Xu, Z., Gao, C.: Aqueous Liquid Crystals of Graphene Oxide. *ACS Nano*. 5, 2908–2915 (2011).
104. Ogino, I., Yokoyama, Y., Iwamura, S., Mukai, S.R.: Exfoliation of Graphite Oxide in Water without Sonication: Bridging Length Scales from Nanosheets to Macroscopic Materials. *Chem. Mater.* 26, 3334–3339 (2014).
105. Gómez-Navarro, C., Weitz, R.T., Bittner, A.M., Scolari, M., Mews, A., Burghard, M., Kern, K.: Electronic Transport Properties of Individual Chemically Reduced Graphene Oxide Sheets. *Nano Lett.* 7, 3499–3503 (2007).
106. Dikin, D.A., Stankovich, S., Zimney, E.J., Piner, R.D., Dommett, G.H.B., Evmenenko, G., Nguyen, S.T., Ruoff, R.S.: Preparation and characterization of graphene oxide paper. *Nature*. 448, 457–460 (2007).
107. Zhu, Y., Murali, S., Cai, W., Li, X., Suk, J.W., Potts, J.R., Ruoff, R.S.: Graphene and Graphene Oxide: Synthesis, Properties, and Applications. *Adv. Mater.* 22, 3906–3924 (2010).
108. Rourke, J.P., Pandey, P.A., Moore, J.J., Bates, M., Kinloch, I.A., Young, R.J., Wilson, N.R.: The Real Graphene Oxide Revealed: Stripping the Oxidative Debris from the Graphene-like Sheets. *Angew. Chem. Int. Ed.* 50, 3173–3177 (2011).
109. Chua, C.K., Pumera, M.: Chemical reduction of graphene oxide: a synthetic chemistry viewpoint. *Chem Soc Rev.* 43, 291–312 (2014).
110. Thomas, H.R., Day, S.P., Woodruff, W.E., Vallés, C., Young, R.J., Kinloch, I.A., Morley, G.W., Hanna, J.V., Wilson, N.R., Rourke, J.P.: Deoxygenation of Graphene Oxide: Reduction or Cleaning? *Chem. Mater.* 25, 3580–3588 (2013).
111. Kim, T., Lee, H., Kim, J., Suh, K.S.: Synthesis of Phase Transferable Graphene Sheets Using Ionic Liquid Polymers. *ACS Nano*. 4, 1612–1618 (2010).
112. Jurow, M., Manichev, V., Pabon, C., Hageman, B., Matolina, Y., Drain, C.M.: Self-Organization of Zr(IV) Porphyrinoids on Graphene Oxide Surfaces by Axial Metal Coordination. *Inorg. Chem.* 52, 10576–10582 (2013).
113. Liang, J., Huang, Y., Zhang, L., Wang, Y., Ma, Y., Guo, T., Chen, Y.: Molecular-Level Dispersion of Graphene into Poly(vinyl alcohol) and Effective Reinforcement of their Nanocomposites. *Adv. Funct. Mater.* 19, 2297–2302 (2009).
114. Xu, Y., Wang, Y., Liang, J., Huang, Y., Ma, Y., Wan, X., Chen, Y.: A hybrid material of graphene and poly(3, 4-ethyldioxythiophene) with high conductivity, flexibility, and transparency. *Nano Res.* 2, 343–348 (2009).
115. Yamada, Y., Suzuki, Y., Yasuda, H., Uchizawa, S., Hirose-Takai, K., Sato, Y., Suenaga, K., Sato, S.: Functionalized graphene sheets coordinating metal cations. *Carbon*. 75, 81–94 (2014).
116. Kuila, T., Bose, S., Mishra, A.K., Khanra, P., Kim, N.H., Lee, J.H.: Chemical functionalization of graphene and its applications. *Prog. Mater. Sci.* 57, 1061–1105 (2012).
117. Eigler, S., Hirsch, A.: Chemistry with Graphene and Graphene Oxide—Challenges for Synthetic Chemists. *Angew. Chem. Int. Ed.* 53, 7720–7738 (2014).
118. Lonkar, S.P., Deshmukh, Y.S., Abdala, A.A.: Recent advances in chemical modifications of graphene. *Nano Res.* 8, 1039–1074 (2015).
119. Park, S., Dikin, D.A., Nguyen, S.T., Ruoff, R.S.: Graphene Oxide Sheets Chemically Cross-Linked by Polyallylamine. *J. Phys. Chem. C*. 113, 15801–15804 (2009).
120. Bourlinos, A.B., Gournis, D., Petridis, D., Szabó, T., Szeri, A., Dékány, I.: Graphite Oxide: Chemical Reduction to Graphite and Surface Modification with Primary Aliphatic Amines and Amino Acids. *Langmuir*. 19, 6050–6055 (2003).
121. Liu, X., Kuang, W., Guo, B.: Preparation of rubber/graphene oxide composites with in-situ interfacial design. *Polymer*. 56, 553–562 (2015).

References

122. Li, W., Tang, X.-Z., Zhang, H.-B., Jiang, Z.-G., Yu, Z.-Z., Du, X.-S., Mai, Y.-W.: Simultaneous surface functionalization and reduction of graphene oxide with octadecylamine for electrically conductive polystyrene composites. *Carbon*. 49, 4724–4730 (2011).
123. Matsuo, Y., Fukunaga, T., Fukutsuka, T., Sugie, Y.: Silylation of graphite oxide. *Carbon*. 42, 2117–2119 (2004).
124. Matsuo, Y., Nishino, Y., Fukutsuka, T., Sugie, Y.: Introduction of amino groups into the interlayer space of graphite oxide using 3-aminopropylethoxysilanes. *Carbon*. 45, 1384–1390 (2007).
125. Matsuo, Y., Tabata, T., Fukunaga, T., Fukutsuka, T., Sugie, Y.: Preparation and characterization of silylated graphite oxide. *Carbon*. 43, 2875–2882 (2005).
126. Zhang, Y., Zhu, Y., Lin, G., Ruoff, R.S., Hu, N., Schaefer, D.W., Mark, J.E.: What factors control the mechanical properties of poly (dimethylsiloxane) reinforced with nanosheets of 3-aminopropyltriethoxysilane modified graphene oxide? *Polymer*. 54, 3605–3611 (2013).
127. Wu, J., Huang, G., Li, H., Wu, S., Liu, Y., Zheng, J.: Enhanced mechanical and gas barrier properties of rubber nanocomposites with surface functionalized graphene oxide at low content. *Polymer*. 54, 1930–1937 (2013).
128. Guimont, A., Beyou, E., Alcouffe, P., Martin, G., Sonntag, P., Cassagnau, P.: Synthesis and characterization of PDMS-grafted graphite oxide sheets. *Polymer*. 54, 4830–4837 (2013).
129. Jia, Z., Wang, Y.: Covalently crosslinked graphene oxide membranes by esterification reactions for ions separation. *J Mater Chem A*. 3, 4405–4412 (2015).
130. Niyogi, S., Bekyarova, E., Itkis, M.E., McWilliams, J.L., Hamon, M.A., Haddon, R.C.: Solution Properties of Graphite and Graphene. *J. Am. Chem. Soc.* 128, 7720–7721 (2006).
131. Stankovich, S., Piner, R.D., Nguyen, S.T., Ruoff, R.S.: Synthesis and exfoliation of isocyanate-treated graphene oxide nanoplatelets. *Carbon*. 44, 3342–3347 (2006).
132. Shen, J., Hu, Y., Li, C., Qin, C., Ye, M.: Synthesis of Amphiphilic Graphene Nanoplatelets. *Small*. 5, 82–85 (2009).
133. Bian, J., Wei, X.W., Gong, S.J., Zhang, H., Guan, Z.P.: Improving the thermal and mechanical properties of poly(propylene carbonate) by incorporating functionalized graphite oxide. *J. Appl. Polym. Sci.* 123, 2743–2752 (2012).
134. Malas, A., Pal, P., Das, C.K.: Effect of expanded graphite and modified graphite flakes on the physical and thermo-mechanical properties of styrene butadiene rubber/polybutadiene rubber (SBR/BR) blends. *Mater. Des.* 55, 664–673 (2014).
135. Kim, H., Miura, Y., Macosko, C.W.: Graphene/polyurethane nanocomposites for improved gas barrier and electrical conductivity. *Chem. Mater.* 22, 3441–3450 (2010).
136. Avinash, M.B., Subrahmanyam, K.S., Sundarayya, Y., Govindaraju, T.: Covalent modification and exfoliation of graphene oxide using ferrocene. *Nanoscale*. 2, 1762 (2010).
137. Guimont, A., Beyou, E., Cassagnau, P., Martin, G., Sonntag, P., D’Agosto, F., Boisson, C.: Grafting of polyethylene onto graphite oxide sheets: a comparison of two routes. *Polym. Chem.* 4, 2828 (2013).
138. Brauer, G.: *Handbook of Preparative Inorganic Chemistry*. Elsevier Science, Burlington (1965).
139. Park, S., An, J., Potts, J.R., Velamakanni, A., Murali, S., Ruoff, R.S.: Hydrazine-reduction of graphite- and graphene oxide. *Carbon*. 49, 3019–3023 (2011).
140. Dreyer, D.R., Murali, S., Zhu, Y., Ruoff, R.S., Bielawski, C.W.: Reduction of graphite oxide using alcohols. *J Mater Chem*. 21, 3443–3447 (2011).
141. Potts, J.R., Dreyer, D.R., Bielawski, C.W., Ruoff, R.S.: Graphene-based polymer nanocomposites. *Polymer*. 52, 5–25 (2011).
142. Park, S., Ruoff, R.S.: Chemical methods for the production of graphenes. *Nat. Nanotechnol.* 4, 217–224 (2009).
143. Thakur, S., Karak, N.: Alternative methods and nature-based reagents for the reduction of graphene oxide: A review. *Carbon*. 94, 224–242 (2015).

References

144. Gao, J., Liu, F., Liu, Y., Ma, N., Wang, Z., Zhang, X.: Environment-Friendly Method To Produce Graphene That Employs Vitamin C and Amino Acid. *Chem. Mater.* 22, 2213–2218 (2010).
145. Zhang, J., Yang, H., Shen, G., Cheng, P., Zhang, J., Guo, S.: Reduction of graphene oxide via L - ascorbic acid. *Chem Commun.* 46, 1112–1114 (2010).
146. Fernández-Merino, M.J., Guardia, L., Paredes, J.I., Villar-Rodil, S., Solís-Fernández, P., Martínez-Alonso, A., Tascón, J.M.D.: Vitamin C Is an Ideal Substitute for Hydrazine in the Reduction of Graphene Oxide Suspensions. *J. Phys. Chem. C.* 114, 6426–6432 (2010).
147. Bose, S., Kuila, T., Mishra, A.K., Kim, N.H., Lee, J.H.: Dual role of glycine as a chemical functionalizer and a reducing agent in the preparation of graphene: an environmentally friendly method. *J. Mater. Chem.* 22, 9696 (2012).
148. Tran, D.N.H., Kabiri, S., Losic, D.: A green approach for the reduction of graphene oxide nanosheets using non-aromatic amino acids. *Carbon.* 76, 193–202 (2014).
149. Stankovich, S., Dikin, D.A., Piner, R.D., Kohlhaas, K.A., Kleinhammes, A., Jia, Y., Wu, Y., Nguyen, S.T., Ruoff, R.S.: Synthesis of graphene-based nanosheets via chemical reduction of exfoliated graphite oxide. *Carbon.* 45, 1558–1565 (2007).
150. Stankovich, S., Piner, R.D., Chen, X., Wu, N., Nguyen, S.T., Ruoff, R.S.: Stable aqueous dispersions of graphitic nanoplatelets via the reduction of exfoliated graphite oxide in the presence of poly(sodium 4-styrenesulfonate). *J Mater Chem.* 16, 155–158 (2006).
151. Lotya, M., Hernandez, Y., King, P.J., Smith, R.J., Nicolosi, V., Karlsson, L.S., Blighe, F.M., De, S., Wang, Z., McGovern, I.T., Duesberg, G.S., Coleman, J.N.: Liquid Phase Production of Graphene by Exfoliation of Graphite in Surfactant/Water Solutions. *J. Am. Chem. Soc.* 131, 3611–3620 (2009).
152. Cao, N., Zhang, Y.: Study of Reduced Graphene Oxide Preparation by Hummers' Method and Related Characterization. *J. Nanomater.* 2015, 1–5 (2015).
153. Khan, M., Al-Marri, A.H., Khan, M., Mohri, N., Adil, S.F., Al-Warthan, A., Siddiqui, M.R.H., Alkhatlan, H.Z., Berger, R., Tremel, W., Tahir, M.N.: *Pulicaria glutinosa* plant extract: a green and eco-friendly reducing agent for the preparation of highly reduced graphene oxide. *RSC Adv.* 4, 24119 (2014).
154. Schniepp, H.C., Li, J.-L., McAllister, M.J., Sai, H., Herrera-Alonso, M., Adamson, D.H., Prud'homme, R.K., Car, R., Saville, D.A., Aksay, I.A.: Functionalized Single Graphene Sheets Derived from Splitting Graphite Oxide. *J. Phys. Chem. B.* 110, 8535–8539 (2006).
155. Bai, Y., Cai, H., Qiu, X., Fang, X., Zheng, J.: Effects of graphene reduction degree on thermal oxidative stability of reduced graphene oxide/silicone rubber nanocomposites. *High Perform. Polym.* 27, 997–1006 (2015).
156. Stankovich, S., Dikin, D.A., Dommett, G.H.B., Kohlhaas, K.M., Zimney, E.J., Stach, E.A., Piner, R.D., Nguyen, S.T., Ruoff, R.S.: Graphene-based composite materials. *Nature.* 442, 282–286 (2006).
157. Sharon, M., Sharon, M.: *Graphene: an introduction to the fundamentals and industrial applications.* Wiley, Hoboken, New Jersey (2015).
158. Wang, H., Robinson, J.T., Li, X., Dai, H.: Solvothermal Reduction of Chemically Exfoliated Graphene Sheets. *J. Am. Chem. Soc.* 131, 9910–9911 (2009).
159. Dubin, S., Gilje, S., Wang, K., Tung, V.C., Cha, K., Hall, A.S., Farrar, J., Varshneya, R., Yang, Y., Kaner, R.B.: A One-Step, Solvothermal Reduction Method for Producing Reduced Graphene Oxide Dispersions in Organic Solvents. *ACS Nano.* 4, 3845–3852 (2010).
160. Zhou, Y., Bao, Q., Tang, L.A.L., Zhong, Y., Loh, K.P.: Hydrothermal Dehydration for the “Green” Reduction of Exfoliated Graphene Oxide to Graphene and Demonstration of Tunable Optical Limiting Properties. *Chem. Mater.* 21, 2950–2956 (2009).
161. Lin, Z., Yao, Y., Li, Z., Liu, Y., Li, Z., Wong, C.-P.: Solvent-Assisted Thermal Reduction of Graphite Oxide. *J. Phys. Chem. C.* 114, 14819–14825 (2010).
162. Chen, W., Yan, L., Bangal, P.R.: Preparation of graphene by the rapid and mild thermal reduction of graphene oxide induced by microwaves. *Carbon.* 48, 1146–1152 (2010).

References

163. Zhu, Y., Murali, S., Stoller, M.D., Velamakanni, A., Piner, R.D., Ruoff, R.S.: Microwave assisted exfoliation and reduction of graphite oxide for ultracapacitors. *Carbon*. 48, 2118–2122 (2010).
164. De, S.K. ed: *Rubber technologist's handbook*. Rapra Technology Ltd, Shrewsbury, Shropshire (2001).
165. Ifoca: *Synthèse, Propriétés et Technologie des Elastomères*. Groupe français d'études et d'applications des polymères, Vitry-sur-Seine (1984).
166. Berthelot, K., Lecomte, S., Estevez, Y., Couлары-Salin, B., Bentaleb, A., Cullin, C., Deffieux, A., Peruch, F.: Rubber Elongation Factor (REF), a Major Allergen Component in *Hevea brasiliensis* Latex Has Amyloid Properties. *PLoS ONE*. 7, e48065 (2012).
167. Blackley, D.C.: Historical development of synthetic rubbers. In: *Synthetic rubbers: Their chemistry and technology*. pp. 17–31. Springer Netherlands, Dordrecht (1983).
168. Blow, C.M.: *Rubber technology and manufacture*. Butterworths for the Institution of the Rubber Industry, London (1971).
169. Blackley, D.C.: *Synthetic Rubbers: Their Chemistry and Technology*. Springer Netherlands, Dordrecht (1983).
170. Burfield, D.: Polymer glass transition temperatures. *J. Chem. Educ.* 64, 875 (1987).
171. Hsieh, H.L., Quirk, R.P.: *Anionic polymerization: principles and practical applications*. Marcel Dekker, New York (1996).
172. Odian, G.G.: *Principles of polymerization*. Wiley-Interscience, Hoboken, N.J (2004).
173. Ouardad, S., Bakleh, M.-E., Kostjuk, S.V., Ganachaud, F., Puskas, J.E., Deffieux, A., Peruch, F.: Bio-inspired cationic polymerization of isoprene and analogues: state-of-the-art. *Polym. Int.* 61, 149–156 (2012).
174. Rozentsvet, V.A., Kozlov, V.G., Ziganshina, E.F., Boreiko, N.P., Kostjuk, S.V.: Cationic polymerization of isoprene using zinc halides as co-initiators: towards well-defined oligo(isoprene)s under mild conditions: Cationic polymerization of isoprene with zinc halide co-initiators. *Polym. Int.* 62, 817–826 (2013).
175. Vasilenko, I.V., Yeong, H.Y., Delgado, M., Ouardad, S., Peruch, F., Voit, B., Ganachaud, F., Kostjuk, S.V.: A catalyst platform for unique cationic (co)polymerization in aqueous emulsion. *Angew. Chem.* 127, 12919–12923 (2015).
176. Du, G., Wei, Y., Ai, L., Chen, Y., Xu, Q., Liu, X., Zhang, S., Hou, Z., Li, X.: Living 3,4-polymerization of isoprene by cationic rare earth metal alkyl complexes bearing iminoamido ligands. *Organometallics*. 30, 160–170 (2011).
177. Germack, D.S., Wooley, K.L.: Isoprene polymerization via reversible addition fragmentation chain transfer polymerization. *J. Polym. Sci. Part Polym. Chem.* 45, 4100–4108 (2007).
178. Debuigne, A., Jérôme, C., Detrembleur, C.: Isoprene-Assisted Radical Coupling of (Co)polymers Prepared by Cobalt-Mediated Radical Polymerization. *Angew. Chem. Int. Ed.* 48, 1422–1424 (2009).
179. Jitchum, V., Perrier, S.: Living Radical Polymerization of Isoprene via the RAFT Process. *Macromolecules*. 40, 1408–1412 (2007).
180. Georges, M.K., Hamer, G.K., Listigovers, N.A.: Block copolymer synthesis by a nitroxide-mediated living free radical polymerization process. *Macromolecules*. 31, 9087–9089 (1998).
181. Cheong, I.W., Fellows, C.M., Gilbert, R.G.: Synthesis and cross-linking of polyisoprene latexes. *Polymer*. 45, 769–781 (2004).
182. Eirich Konrad, Eduard Tschunkur: *Verfahren zur Herstellung von Polymerisationsprodukten*, DE 658172 C, (1938).
183. Nagdi, K.: *Rubber as an engineering material: guideline for users*. Hanser Publishers, Munich ; New York (1993).
184. Bhowmick, A.K., Hall, M.M., Benarey, H.A. eds: *Rubber products manufacturing technology*. M. Dekker, New York (1994).

References

185. Ghosh, P., Katare, S., Patkar, P., Caruthers, J.M., Venkatasubramanian, V., Walker, K.A.: Sulfur vulcanization of natural rubber for benzothiazole accelerated formulations: from reaction mechanisms to a rational kinetic model. *Rubber Chem. Technol.* 76, 592–693 (2003).
186. Heideman, G., Datta, R.N., Noordermeer, J.W., van Baarle, B.: Activators in accelerated sulfur vulcanization. *Rubber Chem. Technol.* 77, 512–541 (2004).
187. López-Manchado, M.A., Arroyo, M., Herrero, B., Biagiotti, J.: Vulcanization kinetics of natural rubber–organoclay nanocomposites. *J. Appl. Polym. Sci.* 89, 1–15 (2003).
188. Wu, J., Xing, W., Huang, G., Li, H., Tang, M., Wu, S., Liu, Y.: Vulcanization kinetics of graphene/natural rubber nanocomposites. *Polymer.* 54, 3314–3323 (2013).
189. Trivette, C.D., Morita, E., Maender, O.W.: Pre-vulcanization Inhibitors. *Rubber Chem. Technol.* 50, 570–600 (1977).
190. Son, P.N., Andrews, K.E., Schooley, A.T.: Kinetics and Mechanism of the Reaction of 2-Mercaptobenzothiazole with N-(Cyclohexylthio)Phthalimide and Related Compounds. *Rubber Chem. Technol.* 45, 1513–1531 (1972).
191. Flory, P.J., Rehner, J.: Statistical Mechanics of Cross-Linked Polymer Networks I. Rubberlike Elasticity. *J. Chem. Phys.* 11, 512 (1943).
192. Mark, J.E., Erman, B. eds: Science and technology of rubber. Elsevier Academic Press, Amsterdam ; Boston (2005).
193. Plazek, D.J.: Effect of crosslink density on the creep behavior of natural rubber vulcanizates. *J. Polym. Sci. Part -2 Polym. Phys.* 4, 745–763 (1966).
194. Thirion, P., Chasset, R.: Proceedings International Conference on Physics of Non-Crystalline Solids. In: North Holland Publishing Co. p. 345. , Amsterdam (1965).
195. Cardarelli, F.: Materials handbook: a concise desktop reference. Springer, London (2008).
196. Brandrup, J., Immergut, E.H., Grulke, E.A. eds: Polymer handbook, 4th edition. Wiley, New York ; Chichester (2004).
197. R. T. Vanderbilt Company, George G Winspear: The Vanderbilt Rubber Handbook. R T Vanderbilt Co, Michigan University (1968).
198. Bussemaker, O.K.F.: Tack in Rubber. *Rubber Chem. Technol.* 37, 1178–1189 (1964).
199. Hamed, G.R.: Tack and Green Strength of Elastomeric Materials. *Rubber Chem. Technol.* 54, 576–595 (1981).
200. Barlow, F.W.: Rubber compounding: principles, materials, and techniques. M. Dekker, New York (1993).
201. Horn J B: In: Rubber technology and manufacture. pp. 202–218. C. M. Blow and C. Hepburn, London (1982).
202. Byers J T: Fillers, Part I, Carbon black. In: Rubber technology. pp. 59–85. M. Morton, New-York (1987).
203. Kraus G: Reinforcement of elastomers. Wiley & Sons, New-York (1965).
204. Leblanc, J.L.: Rubber–filler interactions and rheological properties in filled compounds. *Prog. Polym. Sci.* 27, 627–687 (2002).
205. Medalia, A.I.: Effect of Carbon Black on Dynamic Properties of Rubber Vulcanizates. *Rubber Chem. Technol.* 51, 437–523 (1978).
206. ASTM: ASTM D1765 - 14 Standard Classification System for Carbon Blacks Used in Rubber Products, (2014).
207. Meissner, B.: Theory of bound rubber. *J. Appl. Polym. Sci.* 18, 2483–2491 (1974).
208. Fielding, J.H.: Impact Resilience in Testing Channel Black. *Ind. Eng. Chem.* 29, 880–885 (1937).
209. Leblanc, J.L.: Rhéologie des caoutchoucs et de leurs mélanges. In: Rhéologie des élastomères et mise en oeuvre de polymères. pp. 253–294. Ed. Artel, Namur (1996).
210. Boehm, H P: Some aspects of the surface chemistry of carbon blacks and other carbons. *Carbon.* 32, 759–769 (1994).
211. Papirer, E., Dentzer, J., Li, S., Donnet, J.B.: Surface groups on nitric acid oxidized carbon black samples determined by chemical and thermodesorption analyses. *Carbon.* 29, 69–72 (1991).

References

212. Donnet, J.B.: Structure and reactivity of carbons: from carbon black to carbon composites. *Carbon*. 20, 267–282 (1982).
213. Leblanc, J.L.: Rhéologie des élastomères et mise en oeuvre des polymères. Ed. Artel, Namur (1996).
214. Stephen, R., Thomas, S.: Nanocomposites: State of the art, new challenges and opportunities. In: *Ruber nanocomposites*. pp. 1–19. Wiley & Sons (2010).
215. Thomas, S., Stephen, R. eds: *Rubber nanocomposites: preparation, properties, and applications*. John Wiley & Sons, Singapore ; Hoboken, NJ (2010).
216. Kuilla, T., Bhadra, S., Yao, D., Kim, N.H., Bose, S., Lee, J.H.: Recent advances in graphene based polymer composites. *Prog. Polym. Sci.* 35, 1350–1375 (2010).
217. Ma, J., Zhang, L.-Q., Geng, L.: Manufacturing techniques of rubber nanocomposites. In: *Rubber nanocomposites*. pp. 21–62. Wiley & Sons (2010).
218. Funt, J.F.: *Mixing of rubber*. Smithers Rapra Techn, Shawbury (2009).
219. Funt, J.M.: Rubber Mixing. *Rubber Chem. Technol.* 53, 772–779 (1980).
220. Collin, V., Boudimbu, I., Peuvrel-Disdier, E.: New insights in dispersion mechanisms of carbon black in a polymer matrix under shear by rheo-optics. *J. Appl. Polym. Sci.* 127, 2121–2131 (2013).
221. Collin, V., Peuvrel-Disdier, E.: Dispersion mechanisms of carbon black in an elastomer matrix. *Elastomery*. 9, 9 (2005).
222. Leblanc, J.L.: Aspects rhéologiques généraux des écoulements de mise en oeuvre. In: *Rhéologie des élastomères et mise en oeuvre des polymères*. pp. 107–136. Ed. Artel, Namur (1996).
223. Bolen, W., Colwell, R.: Intensive mixing. *Soc Plat Eng J.* 24 (1958).
224. Pavlidou, S., Papaspyrides, C.: A review on polymer-layered silicate nanocomposites. *Prog. Polym. Sci.* 33, 1119–1198 (2008).
225. Papageorgiou, D.G., Kinloch, I.A., Young, R.J.: Graphene/elastomer nanocomposites. *Carbon*. 95, 460–484 (2015).
226. Nawaz, K., Khan, U., Ul-Haq, N., May, P., O'Neill, A., Coleman, J.N.: Observation of mechanical percolation in functionalized graphene oxide/elastomer composites. *Carbon*. 50, 4489–4494 (2012).
227. Ozbas, B., O'Neill, C.D., Register, R.A., Aksay, I.A., Prud'homme, R.K., Adamson, D.H.: Multifunctional elastomer nanocomposites with functionalized graphene single sheets. *J. Polym. Sci. Part B Polym. Phys.* 50, 910–916 (2012).
228. Lape, N.K., Nuxoll, E.E., Cussler, E.L.: Polydisperse flakes in barrier films. *J. Membr. Sci.* 236, 29–37 (2004).
229. Mikell P. Groover: *Fundamentals of Modern Manufacturing. Materials, Processes, and Systems*. Michael McDonald, USA (2010).
230. Mabry, M., Rumpf, F., Podobnik, I., Westveer, S., Morgan, A., Chung, B., Andrews, M., Cabot corporation: *Methods for producing elastomeric compositions, US6040364A*, (2000).
231. Crank, J. ed: *Diffusion in polymers*. Academic Press, London (1977).
232. Klopffer, M.-H., Flaconneche, B.: Transport properties of gases in polymers: bibliographic review. *Oil Gas Sci. Technol.* 56, 223–244 (2001).
233. Charifou, R.: *Optimisation des propriétés barrière de matériaux polymères par association avec des composés inorganiques pour des applications biomédicales: influence des approches nanocomposites et dépôts de couches minces siliciées*, doctoral thesis, (2013).
234. Dhoot, S.N., Freeman, B.D., Stewart, M.E.: *Barrier polymers*. *Enycl. Polym. Sci. Technol.* (2002).
235. Fick, A.: Ueber Diffusion. *Ann. Phys. Chem.* 170, 59–86 (1855).
236. Song, S.H., Kim, J.M., Park, K.H., Lee, D.J., Kwon, O.-S., Kim, J., Yoon, H., Chen, X.: High performance graphene embedded rubber composites. *RSC Adv.* 5, 81707–81712 (2015).

References

237. Yan, N., Buonocore, G., Lavorgna, M., Kaciulis, S., Balijepalli, S.K., Zhan, Y., Xia, H., Ambrosio, L.: The role of reduced graphene oxide on chemical, mechanical and barrier properties of natural rubber composites. *Compos. Sci. Technol.* 102, 74–81 (2014).
238. Gan, L., Shang, S., Jiang, S.: Impact of vinyl concentration of a silicone rubber on the properties of the graphene oxide filled silicone rubber composites. *Compos. Part B Eng.* 84, 294–300 (2016).
239. Yang, J., Tian, M., Jia, Q.-X., Shi, J.-H., Zhang, L.-Q., Lim, S.-H., Yu, Z.-Z., Mai, Y.-W.: Improved mechanical and functional properties of elastomer/graphite nanocomposites prepared by latex compounding. *Acta Mater.* 55, 6372–6382 (2007).
240. Yang, X., Giese, U., Schuster, R.H.: Characterization of permeability of elastomers, Part I - HNBR. *Kautsch. Gummi Kunststoffe.* 61, 294 (2008).
241. Yang, X., Schneider, L.K.A., Giese, U., Schuster, R.H.: Characterization of permeability of elastomers, Part II. *Kautsch. Gummi Kunststoffe.* 63, 1 (2010).
242. Ha, H., Park, J., Ha, K., Freeman, B.D., Ellison, C.J.: Synthesis and gas permeability of highly elastic poly(dimethylsiloxane)/graphene oxide composite elastomers using telechelic polymers. *Polymer.* 93, 53–60 (2016).
243. Cui, Y., Kundalwal, S.I., Kumar, S.: Gas barrier performance of graphene/polymer nanocomposites. *Carbon.* 98, 313–333 (2016).
244. Nielsen, L.E.: Models for the Permeability of Filled Polymer Systems. *J. Macromol. Sci. Part - Chem.* 1, 929–942 (1967).
245. Bharadwaj, R.K.: Modeling the Barrier Properties of Polymer-Layered Silicate Nanocomposites. *Macromolecules.* 34, 9189–9192 (2001).
246. Gusev, A.A., Lusti, H.R.: Rational Design of Nanocomposites for Barrier Applications. *Adv. Mater.* 13, 1641–1643 (2001).
247. Fredrickson, G.H., Bicerano, J.: Barrier properties of oriented disk composites. *J. Chem. Phys.* 110, 2181 (1999).
248. Cussler, E.L., Hughes, S.E., Ward, W.J., Aris, R.: Barrier membranes. *J. Membr. Sci.* 38, 161–174 (1988).
249. Dunkerley, E., Schmidt, D.: Effects of Composition, Orientation and Temperature on the O₂ Permeability of Model Polymer/Clay Nanocomposites. *Macromolecules.* 43, 10536–10544 (2010).
250. Sadasivuni, K.K., Ponnamma, D., Kim, J., Thomas, S. eds: *Graphene-Based Polymer Nanocomposites in Electronics*. Springer International Publishing, Cham (2015).
251. Paul, D.R., Robeson, L.M.: Polymer nanotechnology: Nanocomposites. *Polymer.* 49, 3187–3204 (2008).
252. Kumar, V., Hanel, T., Galimberti, M., Giese, U.: Graphene / styrene butadiene rubber nanocomposite. *Kautsch. Gummi Kunststoffe.* 9, 29–36 (2014).
253. Kumar, V., Hanel, T., Giannini, L., Galimberti, M., Giese, U.: Graphene reinforced synthetic isoprene rubber nanocomposites. *KGK-Kautsch. GUMMI KUNSTSTOFFE.* 67, 38–46 (2014).
254. Giese, U., Fleck, F., Möwes, M.M., Dilman, T., Klüppel, M., Hanel, T.: Graphene filled nitrile butadiene rubber nanocomposites. *Kautsch. Gummi Kunststoffe.* 67, 69–79 (2015).
255. Schopp, S., Thomann, R., Ratzsch, K.-F., Kerling, S., Altstädt, V., Mülhaupt, R.: Functionalized Graphene and Carbon Materials as Components of Styrene-Butadiene Rubber Nanocomposites Prepared by Aqueous Dispersion Blending: Functionalized Graphene and Carbon Materials as Components *Macromol. Mater. Eng.* 299, 319–329 (2014).
256. Mao, Y., Wen, S., Chen, Y., Zhang, F., Panine, P., Chan, T.W., Zhang, L., Liang, Y., Liu, L.: High Performance Graphene Oxide Based Rubber Composites. *Sci. Rep.* 3, 2508 (2013).
257. Potts, J.R., Shankar, O., Murali, S., Du, L., Ruoff, R.S.: Latex and two-roll mill processing of thermally-exfoliated graphite oxide/natural rubber nanocomposites. *Compos. Sci. Technol.* 74, 166–172 (2013).

References

258. Zhao, X., Zang, C., Wen, Y., Jiao, Q.: Thermal and mechanical properties of liquid silicone rubber composites filled with functionalized graphene oxide. *J. Appl. Polym. Sci.* 132, 42582 (2015).
259. Wang, C., Liu, Z., Wang, S., Zhang, Y.: Preparation and properties of octadecylamine modified graphene oxide/styrene-butadiene rubber composites through an improved melt compounding method. *J. Appl. Polym. Sci.* 133, 42907 (2016).
260. Wang, L., Zhang, L., Tian, M.: Effect of expanded graphite (EG) dispersion on the mechanical and tribological properties of nitrile rubber/EG composites. *Wear.* 276–277, 85–93 (2012).
261. Potts, J.R., Shankar, O., Du, L., Ruoff, R.S.: Processing–Morphology–Property Relationships and Composite Theory Analysis of Reduced Graphene Oxide/Natural Rubber Nanocomposites. *Macromolecules.* 45, 6045–6055 (2012).
262. Cho, D., Lee, S., Yang, G., Fukushima, H., Drzal, L.T.: Dynamic Mechanical and Thermal Properties of Phenylethynyl-Terminated Polyimide Composites Reinforced With Expanded Graphite Nanoplatelets. *Macromol. Mater. Eng.* 290, 179–187 (2005).
263. Bokobza, L.: Elastomeric composites based on nanospherical particles and carbon nanotubes: a comparative study. *Rubber Chem. Technol.* 86, 423–448 (2013).
264. Payne, A R: Reinforcement of elastomers. Wiley & Sons, New-York (1965).
265. Kim, J.S., Yun, J.H., Kim, I., Shim, S.E.: Electrical properties of graphene/SBR nanocomposite prepared by latex heterocoagulation process at room temperature. *J. Ind. Eng. Chem.* 17, 325–330 (2011).
266. Araby, S., Meng, Q., Zhang, L., Kang, H., Majewski, P., Tang, Y., Ma, J.: Electrically and thermally conductive elastomer/graphene nanocomposites by solution mixing. *Polymer.* 55, 201–210 (2014).
267. Mu, Q., Feng, S.: Thermal conductivity of graphite/silicone rubber prepared by solution intercalation. *Thermochim. Acta.* 462, 70–75 (2007).
268. Heinrich, G., Basak, G.C. eds: Advanced rubber composites. Springer, Heidelberg ; New York (2011).
269. Dreyer, D.R., Bielawski, C.W.: Graphite oxide as an olefin polymerization carbocatalyst: Applications in electrochemical double layer capacitors. *Adv. Funct. Mater.* 22, 3247–3253 (2012).
270. Gangopadhyay, R., De, A.: Conducting Polymer Nanocomposites: A Brief Overview. *Chem. Mater.* 12, 608–622 (2000).
271. Bauhofer, W., Kovacs, J.Z.: A review and analysis of electrical percolation in carbon nanotube polymer composites. *Compos. Sci. Technol.* 69, 1486–1498 (2009).
272. Zhan, Y., Lavorgna, M., Buonocore, G., Xia, H.: Enhancing electrical conductivity of rubber composites by constructing interconnected network of self-assembled graphene with latex mixing. *J. Mater. Chem.* 22, 10464 (2012).
273. Munson-McGee, S.H.: Estimation of the critical concentration in an anisotropic percolation network. *Phys. Rev. B.* 43, 3331–3336 (1991).
274. Kim, H., Macosko, C.W.: Processing-property relationships of polycarbonate/graphene composites. *Polymer.* 50, 3797–3809 (2009).
275. Kim, H., Macosko, C.W.: Morphology and Properties of Polyester/Exfoliated Graphite Nanocomposites. *Macromolecules.* 41, 3317–3327 (2008).
276. Araby, S., Zhang, L., Kuan, H.-C., Dai, J.-B., Majewski, P., Ma, J.: A novel approach to electrically and thermally conductive elastomers using graphene. *Polymer.* 54, 3663–3670 (2013).
277. Guimont, A., Beyou, E., Alcouffe, P., Cassagnau, P., Serghei, A., Martin, G., Sonntag, P.: Pentadecane functionalized graphite oxide sheets as a tool for the preparation of electrical conductive polyethylene/graphite oxide composites. *Polymer.* 55, 22–28 (2014).
278. Wei, T., Song, L., Zheng, C., Wang, K., Yan, J., Shao, B., Fan, Z.-J.: The synergy of a three filler combination in the conductivity of epoxy composites. *Mater. Lett.* 64, 2376–2379 (2010).

References

279. Boland, C.S., Khan, U., Backes, C., O'Neill, A., McCauley, J., Duane, S., Shanker, R., Liu, Y., Jurewicz, I., Dalton, A.B., Coleman, J.N.: Sensitive, High-Strain, High-Rate Bodily Motion Sensors Based on Graphene–Rubber Composites. *ACS Nano*. 8, 8819–8830 (2014).
280. Romasanta, L.J., Hernández, M., López-Manchado, M.A., Verdejo, R.: Functionalised graphene sheets as effective high dielectric constant fillers. *Nanoscale Res. Lett.* 6, 508 (2011).
281. Kumar, S.K., Castro, M., Saiter, A., Delbreilh, L., Feller, J.F., Thomas, S., Grohens, Y.: Development of poly(isobutylene-co-isoprene)/reduced graphene oxide nanocomposites for barrier, dielectric and sensing applications. *Mater. Lett.* 96, 109–112 (2013).
282. Wu, S., Tang, Z., Guo, B., Zhang, L., Jia, D.: Effects of interfacial interaction on chain dynamics of rubber/graphene oxide hybrids: a dielectric relaxation spectroscopy study. *RSC Adv.* 3, 14549 (2013).
283. Hernández, M., Bernal, M. del M., Verdejo, R., Ezquerro, T.A., López-Manchado, M.A.: Overall performance of natural rubber/graphene nanocomposites. *Compos. Sci. Technol.* 73, 40–46 (2012).
284. Tian, M., Zhang, J., Zhang, L., Liu, S., Zan, X., Nishi, T., Ning, N.: Graphene encapsulated rubber latex composites with high dielectric constant, low dielectric loss and low percolation threshold. *J. Colloid Interface Sci.* 430, 249–256 (2014).
285. Singh, V.K., Shukla, A., Patra, M.K., Saini, L., Jani, R.K., Vadera, S.R., Kumar, N.: Microwave absorbing properties of a thermally reduced graphene oxide/nitrile butadiene rubber composite. *Carbon*. 50, 2202–2208 (2012).
286. Mensah, B., Kim, S., Arepalli, S., Nah, C.: A study of graphene oxide-reinforced rubber nanocomposite. *J. Appl. Polym. Sci.* 131, 40640 (2014).
287. Castelaín, M., Martínez, G., Marco, C., Ellis, G., Salavagione, H.J.: Effect of Click-Chemistry Approaches for Graphene Modification on the Electrical, Thermal, and Mechanical Properties of Polyethylene/Graphene Nanocomposites. *Macromolecules*. 46, 8980–8987 (2013).
288. Kuila, T., Bose, S., Hong, C.E., Uddin, M.E., Khanra, P., Kim, N.H., Lee, J.H.: Preparation of functionalized graphene/linear low density polyethylene composites by a solution mixing method. *Carbon*. 49, 1033–1037 (2011).
289. Liu, X., Kuang, W., Guo, B.: Preparation of rubber/graphene oxide composites with in-situ interfacial design. *Polymer*. 56, 553–562 (2015).
290. Brodie: Sur le poids atomique du graphite. *Ann. Chim. Phys.* (1860).
291. Kudin, K.N., Ozbas, B., Schniepp, H.C., Prud'homme, R.K., Aksay, I.A., Car, R.: Raman Spectra of Graphite Oxide and Functionalized Graphene Sheets. *Nano Lett.* 8, 36–41 (2008).
292. Jeong, H.-K., Noh, H.-J., Kim, J.-Y., Jin, M.H., Park, C.Y., Lee, Y.H.: X-ray absorption spectroscopy of graphite oxide. *EPL Europhys. Lett.* 82, 67004 (2008).
293. Zhang, Y., Ma, H.-L., Zhang, Q., Peng, J., Li, J., Zhai, M., Yu, Z.-Z.: Facile synthesis of well-dispersed graphene by γ -ray induced reduction of graphene oxide. *J. Mater. Chem.* 22, 13064 (2012).
294. Kim, W., Kang, B.-S., Cho, S.-G., Ha, C.-S., Bae, J.-W.: Styrene butadiene rubber-clay nanocomposites using a latex method: morphology and mechanical properties. *Compos. Interfaces*. 14, 409–425 (2007).
295. Gatos, K.G., Sawanis, N.S., Apostolov, A.A., Thomann, R., Karger-Kocsis, J.: Nanocomposite Formation in Hydrogenated Nitrile Rubber (HNBR)/Organo-Montmorillonite as a Function of the Intercalant Type. *Macromol. Mater. Eng.* 289, 1079–1086 (2004).
296. Gatos, K.G., Thomann, R., Karger-Kocsis, J.: Characteristics of ethylene propylene diene monomer rubber/organoclay nanocomposites resulting from different processing conditions and formulations. *Polym. Int.* 53, 1191–1197 (2004).
297. Gatos, K.G., Karger-Kocsis, J.: Effects of primary and quaternary amine intercalants on the organoclay dispersion in a sulfur-cured EPDM rubber. *Polymer*. 46, 3069–3076 (2005).

References

298. Gatos, K.G., Karger-Kocsis, J.: Effect of the aspect ratio of silicate platelets on the mechanical and barrier properties of hydrogenated acrylonitrile butadiene rubber (HNBR)/layered silicate nanocomposites. *Eur. Polym. J.* 43, 1097–1104 (2007).
299. Čapková, P., Pospíšil, M., Valášková, M., Měřínská, D., Trchová, M., Sedláková, Z., Weiss, Z., Šimoník, J.: Structure of montmorillonite cointercalated with stearic acid and octadecylamine: Modeling, diffraction, IR spectroscopy. *J. Colloid Interface Sci.* 300, 264–269 (2006).
300. López-Manchado, M., Herrero, B., Arroyo, M.: Preparation and characterization of organoclay nanocomposites based on natural rubber: Organoclay composites based on natural rubber. *Polym. Int.* 52, 1070–1077 (2003).
301. Zhang, Y., Mark, J.E., Zhu, Y., Ruoff, R.S., Schaefer, D.W.: Mechanical properties of polybutadiene reinforced with octadecylamine modified graphene oxide. *Polymer.* 55, 5389–5395 (2014).
302. Pramoda, K.P., Hussain, H., Koh, H.M., Tan, H.R., He, C.B.: Covalent bonded polymer-graphene nanocomposites. *J. Polym. Sci. Part Polym. Chem.* 48, 4262–4267 (2010).
303. Bandyopadhyay, P., Park, W.B., Layek, R.K., Uddin, M.E., Kim, N.H., Kim, H.-G., Lee, J.H.: Hexylamine functionalized reduced graphene oxide/polyurethane nanocomposite-coated nylon for enhanced hydrogen gas barrier film. *J. Membr. Sci.* 500, 106–114 (2016).
304. Kuila, T., Bose, S., Mishra, A.K., Khanra, P., Kim, N.H., Lee, J.H.: Chemical functionalization of graphene and its applications. *Prog. Mater. Sci.* 57, 1061–1105 (2012).
305. Saramolee, P., Sahakaro, K., Lopattananon, N., Dierkes, W.K., Noordermeer, J.W.M.: Comparative properties of silica-and carbon black-reinforced natural rubber in the presence of epoxidized low molecular weight polymer. *Rubber Chem. Technol.* 87, 320–339 (2014).
306. Sarkawi, S.S., Dierkes, W.K., Noordermeer, J.W.M.: Morphology of silica-reinforced natural rubber: The effect of silane coupling agent. *Rubber Chem. Technol.* 88, 359–372 (2015).
307. Yrieix, M., Da Cruz-Boisson, F., Majesté, J.-C.: Rubber/silane reactions and grafting rates investigated by liquid-state NMR spectroscopy. *Polymer.* 87, 90–97 (2016).
308. Rauline, R., Michelin: Rubber compound and tires based on such a compound, EP19920102313, (1992).
309. Nakaramontri, Y., Nakason, C., Kummerlöwe, C., Vennemann, N.: Enhancement of electrical conductivity and filler dispersion of carbon nanotube filled natural rubber composites by latex mixing and in situ silanization. *Rubber Chem. Technol.* 89, 272–291 (2016).
310. Nakaramontri, Y., Nakason, C., Kummerlöwe, C., Vennemann, N.: Effects of *in-situ* functionalization of carbon nanotubes with bis(triethoxysilylpropyl) tetrasulfide (TESPT) and 3-aminopropyltriethoxysilane (APTES) on properties of epoxidized natural rubber-carbon nanotube composites. *Polym. Eng. Sci.* 55, 2500–2510 (2015).
311. Nakaramontri, Y., Kummerlöwe, C., Nakason, C., Vennemann, N.: The effect of surface functionalization of carbon nanotubes on properties of natural rubber/carbon nanotube composites. *Polym. Compos.* 36, 2113–2122 (2015).
312. Jiang, H.-X., Ni, Q.-Q., Natsuki, T.: Design and evaluation of the interface between carbon nanotubes and natural rubber. *Polym. Compos.* 32, 236–242 (2011).
313. Mao, Y., Zhang, S., Zhang, D., Chan, T.W., Liu, L.: Enhancing graphene oxide reinforcing potential in composites by combined latex compounding and spray drying. *Mater. Res. Express.* 1, 25009 (2014).
314. Badri, A., Whittaker, M.R., Zetterlund, P.B.: Modification of graphene/graphene oxide with polymer brushes using controlled/living radical polymerization. *J. Polym. Sci. Part Polym. Chem.* 50, 2981–2992 (2012).
315. Deng, Y., Li, Y., Dai, J., Lang, M., Huang, X.: An efficient way to functionalize graphene sheets with presynthesized polymer via ATNRC chemistry. *J. Polym. Sci. Part Polym. Chem.* 49, 1582–1590 (2011).

References

316. He, H., Gao, C.: General approach to individually dispersed, highly soluble, and conductive graphene nanosheets functionalized by nitrene chemistry. *Chem. Mater.* **22**, 5054–5064 (2010).
317. Pan, Y., Bao, H., Sahoo, N.G., Wu, T., Li, L.: Water-Soluble Poly(*N*-isopropylacrylamide)-Graphene Sheets Synthesized via Click Chemistry for Drug Delivery. *Adv. Funct. Mater.* **21**, 2754–2763 (2011).
318. Sun, S., Cao, Y., Feng, J., Wu, P.: Click chemistry as a route for the immobilization of well-defined polystyrene onto graphene sheets. *J. Mater. Chem.* **20**, 5605 (2010).
319. Cano, M., Khan, U., Sainsbury, T., O'Neill, A., Wang, Z., McGovern, I.T., Maser, W.K., Benito, A.M., Coleman, J.N.: Improving the mechanical properties of graphene oxide based materials by covalent attachment of polymer chains. *Carbon.* **52**, 363–371 (2013).
320. Yu, D., Yang, Y., Durstock, M., Baek, J.-B., Dai, L.: Soluble P3HT-Grafted Graphene for Efficient Bilayer-Heterojunction Photovoltaic Devices. *ACS Nano.* **4**, 5633–5640 (2010).
321. Veca, L.M., Lu, F., Meziani, M.J., Cao, L., Zhang, P., Qi, G., Qu, L., Shrestha, M., Sun, Y.-P.: Polymer functionalization and solubilization of carbon nanosheets. *Chem. Commun.* 2565 (2009).
322. Eroğlu, M.S., Güven, O.: Thermal decomposition of poly(glycidyl azide) as studied by high-temperature FTIR and thermogravimetry. *J. Appl. Polym. Sci.* **61**, 201–206 (1996).
323. Gritsan, N., Platz, M.: Photochemistry of Azides: The Azide/Nitrene Interface. In: Brse, S. and Banert, K. (eds.) *Organic Azides*. pp. 311–372. John Wiley & Sons, Ltd, Chichester, UK (2009).
324. Oliveira, A.M., Barros, T., Martins, A., Cabral, M., Dias, A., Costa, L., Cabral, H., Moutinho, A., Jennings, K.R.: Mass spectrometry of aliphatic azides. *Rapid Commun. Mass Spectrom.* 559–561 (1999).
325. de Miguel, I., Velado, M., Herradón, B., Mann, E.: Synthesis of Functionalized Bicyclic Imines via Intramolecular Azide-Alkene 1,3-Dipolar Cycloaddition/Intramolecular Stork Alkylation Cascade Reaction. *Adv. Synth. Catal.* **355**, 1237–1242 (2013).
326. Janreddy, D., Kavala, V., Kuo, C.-W., Chen, W.-C., Ramesh, C., Kotipalli, T., Kuo, T.-S., Chen, M.-L., He, C.-H., Yao, C.-F.: Copper(I)-Catalyzed Aerobic Oxidative Azide-Alkene Cycloaddition: An Efficient Synthesis of Substituted 1,2,3-Triazoles. *Adv. Synth. Catal.* **355**, 2918–2927 (2013).
327. Zhou, Y., Murphy, P.V.: New Access to 1-Deoxyojirimycin Derivatives via Azide-Alkene Cycloaddition. *Org. Lett.* **10**, 3777–3780 (2008).
328. Damiron, D., Okhay, N., Akhrass, S.A., Cassagnau, P., Drockenmuller, E.: Crosslinked PDMS elastomers and coatings from the thermal curing of vinyl-functionalized PDMS and a diazide aliphatic crosslinker. *J. Polym. Sci. Part Polym. Chem.* **50**, 98–107 (2012).
329. González, L., Rodríguez, A., de Benito, J.L., Marcos-Fernandez, A.: Applications of an azide sulfonyl silane as elastomer crosslinking and coupling agent. *J. Appl. Polym. Sci.* **63**, 1353–1359 (1997).
330. López Manchado, M.A., Kenny†, J.M.: Use of Benzene-1,3-Bis(Sulfonyl)Azide as Crosslinking Agent of TPVs Based on EPDM Rubber—Polyolefin Blends. *Rubber Chem. Technol.* **74**, 198–210 (2001).
331. Zielinska, A.J., Noordermeer, J.W.M., Dierkes, W.K., Talma, A.G., Van Duin, M.: Azides as Effective Curing Agents for Saturated EPM-Rubber: Efficiency and Reactivity. *KGK Kautsch. Gummi Kunststoffe.* **63**, 308–315 (2010).
332. Park, S., An, J., Jung, I., Piner, R.D., An, S.J., Li, X., Velamakanni, A., Ruoff, R.S.: Colloidal Suspensions of Highly Reduced Graphene Oxide in a Wide Variety of Organic Solvents. *Nano Lett.* **9**, 1593–1597 (2009).
333. Roghani-Mamaqani, H.: Surface-initiated ATRP of styrene from epoxy groups of graphene nanolayers: twofold polystyrene chains and various graft densities. *RSC Adv.* **5**, 53357–53368 (2015).
334. Tan, Y., Fang, L., Xiao, J., Song, Y., Zheng, Q.: Grafting of copolymers onto graphene by miniemulsion polymerization for conductive polymer composites: improved electrical

References

- conductivity and compatibility induced by interfacial distribution of graphene. *Polym. Chem.* 4, 2939 (2013).
335. Kan, L., Xu, Z., Gao, C.: General Avenue to Individually Dispersed Graphene Oxide-Based Two-Dimensional Molecular Brushes by Free Radical Polymerization. *Macromolecules.* 44, 444–452 (2011).
 336. García-Valdez, O., Ledezma-Rodríguez, R., Saldívar-Guerra, E., Yate, L., Moya, S., Ziolo, R.F.: Graphene oxide modification with graft polymers via nitroxide mediated radical polymerization. *Polymer.* 55, 2347–2355 (2014).
 337. Wang, B., Wang, Z., Jiang, F., Fang, H., Wang, Z.: Synthesis and characterization of MWCNT-graft-polyisoprene via ARGET ATRP. *RSC Adv.* 4, 26468 (2014).
 338. Li, B., Hou, W., Sun, J., Jiang, S., Xu, L., Li, G., Memon, M.A., Cao, J., Huang, Y., Bielawski, C.W., Geng, J.: Tunable functionalization of graphene oxide sheets through surface-initiated cationic polymerization. *Macromolecules.* 48, 994–1001 (2015).
 339. Pazat, A., Beyou, E., Barrès, C., Bruno, F., Janin, C.: In situ emulsion cationic polymerization of isoprene onto the surface of graphite oxide sheets. *Appl. Surf. Sci.* 396, 902–911 (2017).
 340. Guimont, A., Beyou, E., Cassagnau, P., Martin, G., Sonntag, P., D'Agosto, F., Boisson, C.: Grafting of polyethylene onto graphite oxide sheets: a comparison of two routes. *Polym. Chem.* 4, 2828 (2013).
 341. Matsuo, Y., Nishino, Y., Fukutsuka, T., Sugie, Y.: Introduction of amino groups into the interlayer space of graphite oxide using 3-aminopropylethoxysilanes. *Carbon.* 45, 1384–1390 (2007).
 342. Guimont, A., Beyou, E., Martin, G., Sonntag, P., Cassagnau, P.: Viscoelasticity of Graphite Oxide-Based Suspensions in PDMS. *Macromolecules.* 44, 3893–3900 (2011).
 343. Hemraj-Benny, T., Wong, S.S.: Silylation of single-walled carbon nanotubes. *Chem. Mater.* 18, 4827–4839 (2006).
 344. Hou, S., Su, S., Kasner, M.L., Shah, P., Patel, K., Madarang, C.J.: Formation of highly stable dispersions of silane-functionalized reduced graphene oxide. *Chem. Phys. Lett.* 501, 68–74 (2010).
 345. Guimont, A., Beyou, E., Martin, G., Sonntag, P., Cassagnau, P.: Viscoelasticity of Graphite Oxide-Based Suspensions in PDMS. *Macromolecules.* 44, 3893–3900 (2011).
 346. Worsfold, D.J., Bywater, S.: Anionic polymerization of isoprene. *Can. J. Chem.* 42, 2884–2892 (1964).
 347. Fetters, L.J.: Anionic polymerization of isoprene at low concentrations of polyisoprenyllithium. *J. Res. Natl. Bur. Stand. Sect. Phys. Chem.* 69A, 159 (1965).
 348. Hou, S., Chan, W.K.: Preparation of functionalized polystyrene- *block* -polyisoprene copolymers and their luminescence properties. *Macromolecules.* 35, 850–856 (2002).
 349. Peng, Y., Wang, J., Liu, J., Dai, H., Cun, L.: Cationic copolymerization of 1,3-pentadiene with isoprene. *Polym. Int.* 39, 63–66 (1996).
 350. Kostjuk, S.V., Ouardad, S., Peruch, F., Deffieux, A., Absalon, C., Puskas, J.E., Ganachaud, F.: Carbocationic polymerization of isoprene co-initiated by $B(C_6F_5)_3$: An alternative route toward natural rubber polymer analogues? *Macromolecules.* 44, 1372–1384 (2011).
 351. Vasilenko, I.V., Yeong, H.Y., Delgado, M., Ouardad, S., Peruch, F., Voit, B., Ganachaud, F., Kostjuk, S.V.: A Catalyst Platform for Unique Cationic (Co)Polymerization in Aqueous Emulsion. *Angew. Chem.* 127, 12919–12923 (2015).
 352. Rozentsvet, V.A., Kozlov, V.G., Ziganshina, E.F., Boreiko, N.P., Khachaturov, A.S.: Cationic polyisoprene: Synthesis, structure, and some properties. *Russ. J. Appl. Chem.* 82, 148–152 (2009).
 353. Lasky, J.S., Garner, H.K., Ewart, R.H.: Catalysts for the Polymerization of Isoprene to trans-1,4-Polyisoprene (Synthetic Balata). *Ind. Eng. Chem. Prod. Res. Dev.* 1, 82–85 (1962).

References

354. Khachaturov, A.S., Ivanova, V.P., Estrin, A.S., Abramenko, Y.L., Valuev, V.I.: The initiation mechanism of isoprene polymerization on a heterogeneous ziegler system, as studied by a multiple pulse NMR method. *Polym. Sci. USSR.* 32, 581–587 (1990).
355. Liu, D., Cui, D., Gao, W.: Highly stereospecific polymerization of isoprene with homogeneous binary Ziegler-Natta catalysts based on NCN-pincer neodymium precursor. *Sci. China Chem.* 53, 1641–1645 (2010).
356. Phuphuak, Y., Bonnet, F., Vendier, L., Lorber, C., Zinck, P.: Isoprene polymerization mediated by vanadium-[ONNO] complexes. *Dalton Trans.* 45, 12069–12077 (2016).
357. Alnajrani, M.N., Mair, F.S.: The behaviour of β -triketimine cobalt complexes in the polymerization of isoprene. *RSC Adv.* 5, 46372–46385 (2015).
358. Annunziata, L., Duc, M., Carpentier, J.-F.: Chain Growth Polymerization of Isoprene and Stereoselective Isoprene–Styrene Copolymerization Promoted by an *ansa*-Bis(indenyl)allyl–Yttrium Complex. *Macromolecules.* 44, 7158–7166 (2011).
359. Bonnet, F., Visseaux, M., Pereira, A., Barbier-Baudry, D.: Highly *trans*-stereospecific isoprene polymerization by neodymium borohydrido catalysts. *Macromolecules.* 38, 3162–3169 (2005).
360. Gobran, R.H., Berenbaum, M.B., Tobolsky, A.V.: Bulk polymerization of isoprene: Kinetic constants from the dead-end theory. *J. Polym. Sci.* 46, 431–440 (1960).
361. Bar-Nes, G., Hall, R., Sharma, V., Gaborieau, M., Lucas, D., Castignolles, P., Gilbert, R.G.: Controlled/living radical polymerization of isoprene and butadiene in emulsion. *Eur. Polym. J.* 45, 3149–3163 (2009).
362. Orr, R.J., Williams, H.L.: The polymerization of isoprene and 2,3-dimethylbutadiene and copolymerization with styrene at -18 °C in emulsion. *Can. J. Chem.* 30, 108–123 (1952).
363. Cataldo, F., Ursini, O., Lilla, E.: Radiation induced polymerization of isoprene: A spectroscopic study. *J. Radioanal. Nucl. Chem.* 275, 9–16 (2008).
364. Maxwell, I.A., Morrison, B.R., Napper, D.H., Gilbert, R.G.: Entry of free radicals into latex particles in emulsion polymerization. *Macromolecules.* 24, 1629–1640 (1991).
365. Warson, H.: Emulsion polymerization, a mechanistic approach. R.G. Gilbert, London (1995).
366. Kongsinlark, A., Rempel, G.L., Prasassarakich, P.: Synthesis of monodispersed polyisoprene–silica nanoparticles via differential microemulsion polymerization and mechanical properties of polyisoprene nanocomposite. *Chem. Eng. J.* 193–194, 215–226 (2012).
367. Suppaibulsuk, B., Prasassarakich, P., Rempel, G.L.: Factorial design of nanosized polyisoprene synthesis via differential microemulsion polymerization. *Polym. Adv. Technol.* 467–475 (2010).
368. Chen, D., Shao, H., Yao, W., Huang, B.: Fourier Transform Infrared Spectral Analysis of Polyisoprene of a Different Microstructure. *Int. J. Polym. Sci.* 2013, 1–5 (2013).
369. Arjunan, V., Subramanian, S., Mohan, S.: Fourier transform infrared and Raman spectral analysis of *trans*-1,4-polyisoprene. *Spectrochim. Acta. A. Mol. Biomol. Spectrosc.* 57, 2547–2554 (2001).
370. Morton, M., Cala, J.A., Piirma, I.: Crosslinking in isoprene polymerization. *J. Polym. Sci.* 15, 167–182 (1955).
371. Baboo, M., Dixit, M., Sharma, K., Saxena, N.S.: Activation energy and thermo-mechanical properties of *trans*-polyisoprene and liquid *cis*-polyisoprene blends. *Thermochim. Acta.* 502, 47–50 (2010).
372. Brydson, J.A.: *Plastics materials.* Butterworth-Heinemann, Oxford ; Boston (1999).
373. Cui, L., Yu, J., Yu, X., Lv, Y., Li, G., Zhou, S.: In situ synthesis of polyisoprene/grafted single-walled carbon nanotube composites. *Polym. J.* 45, 834–838 (2013).
374. David, C., Geuskens, G., Rabek, J.F., Bamford, C.H., Tipper, C.F.H.: *Degradation of polymers.* Elsevier Scientific Pub. Co., Amsterdam; New York (1975).
375. Lu, H., Nutt, S.: Restricted relaxation in polymer nanocomposites near the glass transition. *Macromolecules.* 36, 4010–4016 (2003).
376. Lu, H., Nutt, S.: Enthalpy relaxation of layered silicate-epoxy nanocomposites. *Macromol. Chem. Phys.* 204, 1832–1841 (2003).

References

377. Tjong, S.C., Mai, Y.W.: Physical properties and applications of polymer nanocomposites. Woodhead Pub., Cambridge, U.K.; Philadelphia, Pa. (2010).
378. Zhan, Y., Wu, J., Xia, H., Yan, N., Fei, G., Yuan, G.: Dispersion and Exfoliation of Graphene in Rubber by an Ultrasonically-Assisted Latex Mixing and In situ Reduction Process. *Macromol. Mater. Eng.* 296, 590–602 (2011).
379. Tang, Y., Hu, X., Liu, C.: Perfect inhibition of CdS photocorrosion by graphene sheltering engineering on TiO₂ nanotube array for highly stable photocatalytic activity. *Phys Chem Chem Phys.* 16, 25321–25329 (2014).
380. Xia, W., Xue, H., Wang, J., Wang, T., Song, L., Guo, H., Fan, X., Gong, H., He, J.: Functionalized graphene serving as free radical scavenger and corrosion protection in gamma-irradiated epoxy composites. *Carbon.* 101, 315–323 (2016).
381. Qiu, Y., Wang, Z., Owens, A.C.E., Kulaots, I., Chen, Y., Kane, A.B., Hurt, R.H.: Antioxidant chemistry of graphene-based materials and its role in oxidation protection technology. *Nanoscale.* 6, 11744–11755 (2014).
382. Zhang, C., Chen, S., Alvarez, P.J.J., Chen, W.: Reduced graphene oxide enhances horseradish peroxidase stability by serving as radical scavenger and redox mediator. *Carbon.* 94, 531–538 (2015).
383. Cha, I., Yagi, Y., Kawahara, T., Hashimoto, K., Fujiki, K., Tamesue, S., Yamauchi, T., Tsubokawa, N.: Grafting of polymers onto graphene oxide by trapping of polymer radicals and ligand-exchange reaction of polymers bearing ferrocene moieties. *Colloids Surf. Physicochem. Eng. Asp.* 441, 474–480 (2014).
384. Zhang, L., Luo, Y., Hou, Z.: Unprecedented isospecific 3,4-polymerization of isoprene by cationic rare earth metal alkyl species resulting from a binuclear precursor. *J. Am. Chem. Soc.* 127, 14562–14563 (2005).
385. Ouardad, S., Lebarbé, T., Deffieux, A., Peruch, F.: Cationic polymerization of isoprene initiated by 2-cyclohexylidene ethanol-B(C₆F₅)₃: an insight into initiation and branching reactions. *Polym Chem.* 4, 407–413 (2013).
386. Du, W., Jiang, X., Zhu, L.: From graphite to graphene: direct liquid-phase exfoliation of graphite to produce single- and few-layered pristine graphene. *J. Mater. Chem. A.* 1, 10592 (2013).
387. Vogl, O.: Cationic polymerization of olefins: A critical inventory, J. P. Kennedy, Wiley-Interscience, New York, 1975, 337 pp. *J. Polym. Sci. Polym. Lett. Ed.* 13, 55–388 (1975).
388. Kim, I.-J., Faust, R.: Preparation of well-defined organic-inorganic hybrid nanostructures using living cationic surface-initiated polymerization from silica nanoparticles. In: *Polymer brushes.* pp. 119–128.
389. Pan, Y., Xu, Y., An, L., Lu, H., Yang, Y., Chen, W., Nutt, S.: Hybrid network structure and mechanical properties of rodlike silicate/cyanate ester nanocomposites. *Macromolecules.* 41, 9245–9258 (2008).
390. Zhu, L., Zhao, X., Li, Y., Yu, X., Li, C., Zhang, Q.: High-quality production of graphene by liquid-phase exfoliation of expanded graphite. *Mater. Chem. Phys.* 137, 984–990 (2013).
391. Wang, L., Zhang, L., Tian, M.: Effect of expanded graphite (EG) dispersion on the mechanical and tribological properties of nitrile rubber/EG composites. *Wear.* 276–277, 85–93 (2012).
392. Prud'Homme, R.K., Aksay, I.A., Adamson, D., Abdala, A.: Thermally exfoliated graphite oxide, US7,658,901B2, (2010).
393. Olsen, L., Scott, H.: Process for expanding pyrolytic graphite, US3885007A, (1975).
394. Drzal, L.T., Fukushima, H., Rook, B., Rich, M.: Continuous process for producing exfoliated nano-graphite platelets, US20060241237A1, (2006).
395. Kaschak, D., Reynolds, R., Krassowski, D., Ford, B.: Graphite intercalation and exfoliation process, US-7105108-B2, (2006).

References

396. Potts, J.R., Shankar, O., Du, L., Ruoff, R.S.: Processing–Morphology–Property Relationships and Composite Theory Analysis of Reduced Graphene Oxide/Natural Rubber Nanocomposites. *Macromolecules*. 45, 6045–6055 (2012).
397. Drzal, L.T., Fukushima, H.: Expanded graphite and products produced therefrom, US20040127621A1, (2004).
398. Zaleski, P.L., Derwin, D.J., Girkant, R.J.: Method for expanding lamellar forms of graphite and resultant product, US6287694B1, (2001).
399. Mamak, M., Stadler, U., Choi, S., Cordola, E.: Graphite nanoplatelets and compositions, US2010/0147188A1, (2009).
400. Franciszek, O.: Process for producing expanded graphite, US3323869A, (1967).
401. Hong, X., Chung, D.D.L.: Exfoliated graphite with relative dielectric constant reaching 360, obtained by exfoliation of acid-intercalated graphite flakes without subsequent removal of the residual acidity. *Carbon*. 91, 1–10 (2015).
402. Inagaki, M., Tashiro, R., Washino, Y., Toyoda, M.: Exfoliation process of graphite via intercalation compounds with sulfuric acid. *J. Phys. Chem. Solids*. 65, 133–137 (2004).
403. Hong, Y., Wang, Z., Jin, X.: Sulfuric Acid Intercalated Graphite Oxide for Graphene Preparation. *Sci. Rep.* 3, (2013).
404. Malas, A., Das, C.K.: Development of modified expanded graphite-filled solution polymerized styrene butadiene rubber vulcanizates in the presence and absence of carbon black. *Polym. Eng. Sci.* 54, 33–41 (2014).
405. Matsumoto, K., Minori, D., Takagi, K., Hagiwara, R.: Expansion of tetrachloroaluminate-graphite intercalation compound by reaction with anhydrous hydrogen fluoride. *Carbon*. 67, 434–439 (2014).
406. Jeongyun, K.I.M., Byounggon, K.I.M.: Chemical and low-expansion treatments for purifying natural graphite powder. *Physicochem. Probl. Miner. Process.* 41, 37–49 (2007).
407. Fukushima, K., Murariu, M., Camino, G., Dubois, P.: Effect of expanded graphite/layered-silicate clay on thermal, mechanical and fire retardant properties of poly(lactic acid). *Polym. Degrad. Stab.* 95, 1063–1076 (2010).
408. Hong, Y., Wang, Z., Jin, X.: Sulfuric Acid Intercalated Graphite Oxide for Graphene Preparation. *Sci. Rep.* 3, (2013).
409. Gao, Y., Müller-Plathe, F.: Increasing the Thermal Conductivity of Graphene-Polyamide-6,6 Nanocomposites by Surface-Grafted Polymer Chains: Calculation with Molecular Dynamics and Effective-Medium Approximation. *J. Phys. Chem. B*. 120, 1336–1346 (2016).
410. Gulotty, R., Castellino, M., Jagdale, P., Tagliaferro, A., Balandin, A.A.: Effects of Functionalization on Thermal Properties of Single-Wall and Multi-Wall Carbon Nanotube–Polymer Nanocomposites. *ACS Nano*. 7, 5114–5121 (2013).
411. Scherillo, G., Lavorgna, M., Buonocore, G.G., Zhan, Y.H., Xia, H.S., Mensitieri, G., Ambrosio, L.: Tailoring assembly of reduced graphene oxide nanosheets to control gas barrier properties of natural rubber nanocomposites. *ACS Appl. Mater. Interfaces*. 6, 2230–2234 (2014).
412. Klopffer, M.-H., Flaconnèche, B.: Transport properties of gases in polymers: bibliographic review. *Oil Gas Sci. Technol.* 56, 223–244 (2001).
413. Barrer, R.M., Skirrow, G.: Transport and equilibrium phenomena in gas–elastomer systems. I. Kinetic phenomena. *J. Polym. Sci.* 3, 549–563 (1948).
414. Beckert, F., Trenkle, S., Thomann, R., Mülhaupt, R.: Mechanochemical Route to Functionalized Graphene and Carbon Nanofillers for Graphene/SBR Nanocomposites: Mechanochemical Route to Functionalized Graphene. *Macromol. Mater. Eng.* 299, 1513–1520 (2014).
415. Bai, X., Wan, C., Zhang, Y., Zhai, Y.: Reinforcement of hydrogenated carboxylated nitrile–butadiene rubber with exfoliated graphene oxide. *Carbon*. 49, 1608–1613 (2011).
416. Dong, B., Liu, C., Zhang, L., Wu, Y.: Preparation, fracture, and fatigue of exfoliated graphene oxide/natural rubber composites. *RSC Adv.* 5, 17140–17148 (2015).

References

417. Cano, M., Khan, U., Sainsbury, T., O'Neill, A., Wang, Z., McGovern, I.T., Maser, W.K., Benito, A.M., Coleman, J.N.: Improving the mechanical properties of graphene oxide based materials by covalent attachment of polymer chains. *Carbon*. 52, 363–371 (2013).
418. Thongsang, S., Sombatsompop, N.: Effect of NaOH and Si69 treatments on the properties of fly ash / NR composites. *Polym. Compos.* 27, 30–40 (2006).
419. Lomeda, J.R., Doyle, C.D., Kosynkin, D.V., Hwang, W.-F., Tour, J.M.: Diazonium Functionalization of Surfactant-Wrapped Chemically Converted Graphene Sheets. *J. Am. Chem. Soc.* 130, 16201–16206 (2008).
420. Lian, H., Li, S., Liu, K., Xu, L., Wang, K., Guo, W.: Study on modified graphene/butyl rubber nanocomposites. I. Preparation and characterization. *Polym. Eng. Sci.* 51, 2254–2260 (2011).
421. Soltani, R., Katbab, A.A.: The role of interfacial compatibilizer in controlling the electrical conductivity and piezoresistive behavior of the nanocomposites based on RTV silicone rubber/graphite nanosheets. *Sens. Actuators Phys.* 163, 213–219 (2010).
422. Livi, S., Duchet-Rumeau, J., Gérard, J.-F., Pham, T.N.: Polymers and Ionic Liquids: A Successful Wedding. *Macromol. Chem. Phys.* 216, 359–368 (2015).
423. Livi, S., Duchet-Rumeau, J., Gérard, J.-F.: Effect of Ionic Liquid Modified Synthetic Layered Silicates on Thermal and Mechanical Properties of High Density Polyethylene Nanocomposites. *Macromol. Symp.* 342, 46–55 (2014).
424. Livi, S., Duchet-Rumeau, J., Pham, T.-N., Gérard, J.-F.: A comparative study on different ionic liquids used as surfactants: Effect on thermal and mechanical properties of high-density polyethylene nanocomposites. *J. Colloid Interface Sci.* 349, 424–433 (2010).
425. Livi, S., Duchet-Rumeau, J., Pham, T.N., Gérard, J.-F.: Synthesis and physical properties of new surfactants based on ionic liquids: Improvement of thermal stability and mechanical behaviour of high density polyethylene nanocomposites. *J. Colloid Interface Sci.* 354, 555–562 (2011).
426. Subramaniam, K., Das, A., Steinhauser, D., Klüppel, M., Heinrich, G.: Effect of ionic liquid on dielectric, mechanical and dynamic mechanical properties of multi-walled carbon nanotubes/polychloroprene rubber composites. *Eur. Polym. J.* 47, 2234–2243 (2011).
427. Das, A., Stöckelhuber, K.W., Jurk, R., Saphiannikova, M., Fritzsche, J., Lorenz, H., Klüppel, M., Heinrich, G.: Modified and unmodified multiwalled carbon nanotubes in high performance solution-styrene–butadiene and butadiene rubber blends. *Polymer*. 49, 5276–5283 (2008).
428. Das, A., Stöckelhuber, K.W., Jurk, R., Fritzsche, J., Klüppel, M., Heinrich, G.: Coupling activity of ionic liquids between diene elastomers and multi-walled carbon nanotubes. *Carbon*. 47, 3313–3321 (2009).
429. Fukushima, T., Kosaka, A., Ishimura, Y., Yamamoto, T., Takigawa, T., Ishii, N., Aida, T.: Molecular ordering of organic molten salts triggered by single-walled carbon nanotubes. *Science*. 300, 2072–2074 (2003).
430. Kreyenschulte, H., Richter, S., Götze, T., Fischer, D., Steinhauser, D., Klüppel, M., Heinrich, G.: Interaction of 1-allyl-3-methyl-imidazolium chloride and carbon black and its influence on carbon black filled rubbers. *Carbon*. 50, 3649–3658 (2012).
431. Xiong, X., Wang, J., Jia, H., Fang, E., Ding, L.: Structure, thermal conductivity, and thermal stability of bromobutyl rubber nanocomposites with ionic liquid modified graphene oxide. *Polym. Degrad. Stab.* 98, 2208–2214 (2013).
432. Yaragalla, S., Sindam, B., Abraham, J., Raju, K.C.J., Kalarikkal, N., Thomas, S.: Fabrication of graphite-graphene-ionic liquid modified carbon nanotubes filled natural rubber thin films for microwave and energy storage applications. *J. Polym. Res.* 22, (2015).
433. Przybyszewska, M., Zaborski, M.: Effect of ionic liquids and surfactants on zinc oxide nanoparticle activity in crosslinking of acrylonitrile butadiene elastomer. *J. Appl. Polym. Sci.* 116, 155–164 (2010).
434. Pernak, J., Walkiewicz, F., Maciejewska, M., Zaborski, M.: Ionic Liquids as Vulcanization Accelerators. *Ind. Eng. Chem. Res.* 49, 5012–5017 (2010).

References

435. Das, A., Leuteritz, A., Kavimani Nagar, P., Adhikari, B., Stöckelhuber, K.W., Jurk, R., Heinrich, G.: Improved gas barrier properties of composites based on ionic liquid integrated graphene nanoplatelets and bromobutyl rubber. *Int. Polym. Sci. Technol.* 43, 170–176 (2016).
436. Das, A., Ghosh, A.K., Pal, S., Basu, D.K.: The role of thiophosphoryl disulfide on the co-cure of CR-EPDM blends. *Polym. Adv. Technol.* 15, 197–208 (2004).
437. Villanueva, M., Coronas, A., García, J., Salgado, J.: Thermal Stability of Ionic Liquids for Their Application as New Absorbents. *Ind. Eng. Chem. Res.* 52, 15718–15727 (2013).
438. Maton, C., De Vos, N., Stevens, C.V.: Ionic liquid thermal stabilities: decomposition mechanisms and analysis tools. *Chem. Soc. Rev.* 42, 5963 (2013).
439. Laskowska, A., Marzec, A., Boiteux, G., Zaborski, M., Gain, O., Serghei, A.: Effect of imidazolium ionic liquid type on the properties of nitrile rubber composites: Effect of imidazolium ionic liquid on nitrile rubber composites. *Polym. Int.* 62, 1575–1582 (2013).
440. Cao, Y., Mu, T.: Comprehensive Investigation on the Thermal Stability of 66 Ionic Liquids by Thermogravimetric Analysis. *Ind. Eng. Chem. Res.* 53, 8651–8664 (2014).
441. Likozar, B.: The effect of ionic liquid type on the properties of hydrogenated nitrile elastomer/hydroxy-functionalized multi-walled carbon nanotube/ionic liquid composites. *Soft Matter.* 7, 970–977 (2011).
442. Labouffie, F., Hémati, M., Lamure, A., Diguët, S.: Effect of the plasticizer on permeability, mechanical resistance and thermal behaviour of composite coating films. *Powder Technol.* 238, 14–19 (2013).
443. Coleman, M.M., Shelton, J.R., Koenig, J.L.: Raman and ESR Spectroscopic Studies of Accelerator Systems. II. Thermal Degradation Vulcanizing Systems and Its Significance to Vulcanization Mechanisms. *Rubber Chem. Technol.* 46, 957–980 (1973).
444. Gradwell, M.H.S., Hendrikse, K.G., McGill, W.J.: The reactions of 2-(4-morpholiniothio)- and 2-(4-morpholinodithio) benzothiazole in the absence of polyisoprene. *J. Appl. Polym. Sci.* 72, 1235–1240 (1999).
445. Bateman, L., Moore, C.G., Porter, M., Saville, B.: The chemistry and physics of rubber-like substances. Maclaren & Sons Ltd., London (1963).
446. Krebs, H.: The Mechanism of Accelerator Action. *Rubber Chem. Technol.* 30, 962–971 (1957).
447. Scheele, W., Franck, A.: The Vulcanization of Elastomers. 20. Sulfur Vulcanization Accelerated with Thiuram Compounds. I. *Rubber Chem. Technol.* 32, 139–149 (1959).
448. Beckert, F., Trenkle, S., Thomann, R., Mülhaupt, R.: Mechanochemical Route to Functionalized Graphene and Carbon Nanofillers for Graphene/SBR Nanocomposites: Mechanochemical Route to Functionalized Graphene. *Macromol. Mater. Eng.* 299, 1513–1520 (2014).

Appendices

Table of appendices

1.	Characterization methods	252
1.1.	Sonication	252
1.2.	Fourier-Transform Infra-Red Spectroscopy (FTIR)	252
1.3.	Raman Spectroscopy	252
1.4.	X-Ray Photoelectron Spectroscopy (XPS).....	252
1.5.	X-Ray Diffraction (XRD).....	252
1.6.	Nuclear Magnetic Resonance (NMR)	252
1.7.	Gel Permeation Chromatography (GPC)	252
1.8.	Gas Chromatography in line with Mass Spectrometry (GC-MS)	252
1.9.	UV-vis spectroscopy	253
1.10.	Thermogravimetric Analysis (TGA).....	253
1.11.	Differential Scanning Calorimetry (DSC).....	253
1.12.	Scanning Electron Microscopy (SEM)	253
1.13.	Transmission Electron Microscopy (TEM)	253
1.14.	Rheology analysis	253
1.14.1.	Evolution of the complex viscosity and the shear moduli of uncured elastomer composites	253
1.14.2.	Vulcanization kinetics	253
1.15.	Equilibrium swelling	254
1.16.	Tensile testing.....	254
1.17.	Permeability measurements	254
1.18.	Thermal conductivity measurements.....	255
2.	Appendix to Chapter 1.....	256
2.1.	A possible mechanism of CBS-accelerated sulfur vulcanization	256
	Accelerator chemistry	256
	Crosslinking chemistry.....	257
	Post-cure chemistry.....	258
2.2.	Short literature review of barrier properties of graphitic fillers – elastomers composites	259
2.3.	Short literature review of tensile properties of graphitic fillers – elastomers composites	260
2.4.	Short literature review of electrical properties of graphitic fillers – elastomers composites	264

3.	Appendix to Chapter 2.....	265
3.1.	Preparation of graphite oxide (GO) through Hummers' method	265
3.2.	Preparation of GO-ODA.....	265
3.3.	Preparation of GO-TESPT.....	265
3.4.	Preparation of GO-azide-IR	266
3.4.1.	Esterification of GO with 1-azido-undecanol	266
3.4.2.	Cycloaddition of GO-azide onto polyisoprene	266
3.4.3.	Blank experiment	266
4.	Appendix to Chapter 3.....	267
4.1.	Experimental procedures	267
4.1.1.	APTMS grafting onto GO	267
4.1.2.	Isoprene emulsion free radical polymerization.....	267
4.1.3.	In situ emulsion free radical polymerization of isoprene in presence of GO-APTMS .	267
4.1.4.	Allyltrimethoxysilane grafting onto GO.....	267
4.1.5.	Isoprene cationic polymerization.....	268
4.1.6.	In situ emulsion cationic polymerization of isoprene onto GO-allyl.....	268
4.2.	Characterization of allyltrimethoxysilane grafting onto GO	268
4.3.	Characterization of APTMS grafting onto GO	269
4.3.1.	FTIR spectra of GO and GO-APTMS	269
4.3.2.	Raman spectra of GO and GO-APTMS.....	270
4.3.3.	XRD analysis of GO and GO-APTMS.....	271
4.3.4.	TGA thermogram of GO and GO-APTMS.....	271
4.3.5.	Stability of suspensions of GO-APTMS	272
4.3.6.	Morphology of GO-APTMS.....	272
5.	Appendix to Chapter 4.....	273
5.1.	Thermal expansion of graphite oxide.....	273
5.2.	Preparation of graphite-based polyisoprene composites.....	273
5.3.	Morphologies of graphite-based polyisoprene composites	274

6.	Appendix to Chapter 5.....	275
6.1.	Experimental procedure for the preparation of NR composites	275
6.2.	Experimental procedure for the preparation of NBR composites	276
6.3.	Effect of the ILs on the curing times of NBR composites	277
6.3.1.	Effect of the ILs on the curing times of NBR – carbon black composites.....	277
6.3.2.	Effect of the ILs on the curing times of NBR – graphite composites.....	278
6.4.	Evolution of torque during vulcanization of NR composites.....	278
6.5.	Swelling ratio of NR and NBR composites.....	279
6.5.1.	Swelling ratio of NR composites.....	279
6.5.2.	Swelling ratio of NBR composites.....	279
6.6.	Rheometric curves of uncured NR composites	280
6.7.	Tensile testing results for NR and NBR – carbon black composites	281
6.7.1.	Effect of the addition of ILs in NR carbon black composites.....	281
6.7.2.	Effect of the addition of ILs in NBR carbon black composites.....	282

1. Characterization methods

1.1. Sonication

Sonication was accomplished using an Elma S40 Ultrasonic apparatus (Sheller, 37 kHz, 140 W).

1.2. Fourier-Transform Infra-Red Spectroscopy (FTIR)

FTIR spectra were recorded on a Nicolet FTIR 460 spectrometer using powder-pressed KBr pellets. Specimens for the measurements were prepared by mixing 1 mg of the sample powder with 150 mg of KBr and by pressing the mixture into pellets. FTIR spectra were obtained at a resolution of 6.0 cm^{-1} at room temperature in a wavenumber range between 4000 and 400 cm^{-1} and averaged over 70 scans. Some samples were also analyzed using attenuated total reflectance (ATR) diamond apparatus.

1.3. Raman Spectroscopy

Raman spectroscopy was performed on a ThermoFisher Scientific DXR Smart Raman spectrometer using a green laser with a wavelength of 532 nm, at a power of 7 mW, in the 500 - 3500 cm^{-1} range and with a resolution of 4 cm^{-1} . The measure was performed at room temperature on powders.

1.4. X-Ray Photoelectron Spectroscopy (XPS)

The X-ray photoelectron spectroscopy (XPS) analyses were performed with a PHI Quantera SXM instrument equipped with a 180° hemispherical electron energy analyzer and a monochromatized Al $K\alpha$ (1486.6 eV) source operated at 15 eV and 4 mA. The analysis spot had a diameter of $200\text{ }\mu\text{m}$ and the detection angle relative to the substrate surface was 45° .

1.5. X-Ray Diffraction (XRD)

X-ray diffraction was performed on a Bragg-Brentano Bruker D8 Advance diffractometer (Ni-filtered Cu $K\alpha$ radiation, 1.5405 \AA) at a voltage of 40 kV with an intensity of 40 mA using a Bruker LynxeyeXE detector. $d(002)$ basal spacings were calculated from 2θ values using Bragg's law.

1.6. Nuclear Magnetic Resonance (NMR)

^1H Liquid Nuclear Magnetic Resonance (NMR) spectra were recorded using a 5 mm BBFO + probe on a Bruker AVANCE II spectrometer at 400MHz. Deuterated toluene was used as a solvent.

1.7. Gel Permeation Chromatography (GPC)

Molar mass of polyisoprene samples was determined using a Viscotek 270 max Size Exclusion Chromatography (SEC) apparatus from Malvern. A high-mass column maintained at $35\text{ }^\circ\text{C}$ was used with a volume flow rate of $1\text{ mL}\cdot\text{min}^{-1}$ and a resulting pressure of 2.8 MPa. Pure toluene purchased from Carlo Erba was used as the eluent with diethyl ether as the flow marker. A differential refractometer (RI VE3580 with a tungsten lamp) and a viscosimeter (4 capillaries in Wheatstone bridge configuration) were used for detection. 5 mg/mL solutions of the samples were prepared in toluene with a drop of the flow marker, then filtered on $0.20\text{ }\mu\text{m}$ filter. An injection volume of $100\text{ }\mu\text{L}$ was used. Calibration was done with standard polystyrene. Molar mass data given in this study are calculated with a universal calibration method.

1.8. Gas Chromatography in line with Mass Spectrometry (GC-MS)

Gas chromatography in line with mass spectrometry was performed on a 6890N-GC with a MS Agilent Instruments 5973N mass detector. Gas chromatography with HP-5MS column ($20\text{ m} \times 0.18\text{ mm} \times 0.18$

μm), was performed using helium as a vector gas. Mass spectra were obtained as a function of elution time with a mass range of 10 to 700 u.

1.9. UV-vis spectroscopy

UV-vis experiments were recorded on a Perkin Elmer UV/VIS Spectrometer Lambda 35 with a slit width of 2 nm. The samples were put in a 0.2 mL cuvette with 1 cm path length and the spectrum was recorded in the 200-900 nm range with a scan speed of 240 nm/min.

1.10. Thermogravimetric Analysis (TGA)

Thermogravimetric analysis (TGA) was carried out with a TA SDT Q600 (TA Instruments). Samples were heated at $5\text{ }^\circ\text{C}\cdot\text{min}^{-1}$ under helium flow ($25\text{ mL}\cdot\text{min}^{-1}$).

1.11. Differential Scanning Calorimetry (DSC)

Differential Scanning Calorimetry analysis was performed with a DSC 2920 apparatus (TA Instruments). The initial temperature was set at $-100\text{ }^\circ\text{C}$, the sample was then heated at $10\text{ }^\circ\text{C}\cdot\text{min}^{-1}$ up to $100\text{ }^\circ\text{C}$, cooled down to $-100\text{ }^\circ\text{C}$ at the same rate and finally heated to $100\text{ }^\circ\text{C}$ at $10\text{ }^\circ\text{C}\cdot\text{min}^{-1}$. The last heating stage was used to determine the glass transition temperature of the product.

1.12. Scanning Electron Microscopy (SEM)

Scanning electron microscopy (SEM) images were taken by a commercial FEI Quanta 250 FEG. The powder was deposited onto carbon tape and observed with an accelerating voltage of 15 kV. Composites were fractured in liquid nitrogen and deposited on carbon tape. The observation was made at 15 kV. GO-allyl-IR sample was cut in 1 mm thick band, cooled in liquid nitrogen and fractured inside a cryotransfer GATAN Alto 2500 at $-150\text{ }^\circ\text{C}$ using a scalpel. The observation was done in cryo mode at $-150\text{ }^\circ\text{C}$ with an accelerating voltage of 2 kV.

1.13. Transmission Electron Microscopy (TEM)

Transmission electronic microscopy (TEM) analysis was performed on a Philips CM120 electron microscope operating at 80 kV. In a typical experiment, one drop of the colloidal dispersion was deposited on a carbon film supported by a copper grid and allowed to air-dry before observation.

1.14. Rheology analysis

1.14.1. Evolution of the complex viscosity and the shear moduli of uncured elastomer composites

Evolution of the complex viscosity, storage modulus and loss modulus of uncured elastomer composites were recorded on a TA ARES 4800 rheometer with parallel plates geometry, at a temperature of $100\text{ }^\circ\text{C}$, and at 1 % strain over a frequency range of 0.01 rad/s to 100 rad/s. The measurements were performed with a fixed gap, under a nitrogen flow and the samples were allowed to relax during 5 minutes before starting the measurement. The samples were 3 mm thick disks with a diameter of 25 mm.

1.14.2. Vulcanization kinetics

1.14.2.1. Using an ARES rheometer

Cure times were measured on a TA ARES 4800 rheometer with parallel plates geometry, at a temperature of $160\text{ }^\circ\text{C}$, at a frequency of 10 rad/s and at 7 % strain. The measurements were

performed with a fixed gap, under a nitrogen flow and the increase in torque was recorded as a function of time. The samples were 3 mm thick disks with a diameter of 25 mm.

1.14.2.2. Using a closed cavity rheometer

Curing data of NR_0_0, NR_15_0 and NR_15_1_DMIT were additionally recorded using a Moving Die Rheometer (MDR) MDR2000 according to ISO 6502 standard. The chamber temperature was set at 160 °C and the oscillation was performed at a frequency of 1.66 Hz with an amplitude of $\pm 0.5^\circ$. Each sample was a cut as a disk of 5 g.

1.15. Equilibrium swelling

Equilibrium swelling measurements were performed on crosslinked elastomer composites. Each sample was cut in three pieces and they were soaked in cyclohexane for NR composites and butanone for NBR composites at room temperature, until a constant weight was reached. They were then dried in a vacuum oven at 80 °C until a constant weight was reached. The swelling ratio (S_r) was then calculated according to the following equation.

$$S_r = \frac{m_{swollen} - m_{dry}}{m_{dry}}$$

Where $m_{swollen}$ is the mass of the swollen sample and m_{dry} is the mass after drying.

1.16. Tensile testing

Tensile testing was performed according to ISO standard 37:2011 on an Alpha T2000 on type 2 dumbbells (2 mm thick). A pre-load of 1 MPa was applied prior to the measurement. The analysis was then performed at 500 mm/min speed and the strain was recorded using an extensometer.

1.17. Permeability measurements

Permeability measurements were performed on a home-made equipment. The sample was attached between two chambers against a microporous steel plate. The upper cell (volume $> 25 \text{ cm}^3$) was maintained at 5 bars and the lower cell pressure was set at 1 bar at the beginning of the experiment. The volume of the measuring cell was 3.3 cm^3 and the surface of the sample in contact with the permeant was 15.2 cm^2 . The samples were cut in circular shape with a diameter of 700 mm and a thickness of 1 mm. Air was used as the permeant and the experimental device was maintained at 23 °C during the measurement. Permeability coefficients were calculated according to ISO 2782: 2007 standard in $\text{mol.m.m}^{-2}.\text{s}^{-1}.\text{Pa}^{-1}$ using equation (1).

$$Q = \frac{V_0 \times e}{A \times P_u \times T \times R} \times \frac{dP}{dt} \times 10^2 \quad (1)$$

Where:

- V_0 is the volume of the measurement chamber (m^3)
- e is the thickness of the membrane (m)
- A is the diffusion surface (m^2)
- P_u is the relative pressure in the upper chamber (Pa)
- T is the temperature (K)

- R is the gas constant ($8.31 \text{ Pa}\cdot\text{m}^3\cdot\text{K}^{-1}\cdot\text{mol}^{-1}$)
- dP is the increase in pressure during a certain time dt ($\text{Pa}\cdot\text{s}^{-1}$)

1.18. Thermal conductivity measurements

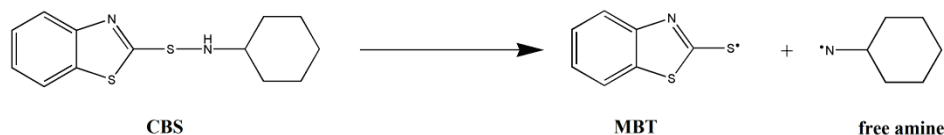
Thermal conductivity was measured using a Hot Disk TPS 500S with a diameter 3.189 mm probe. Each sample was cut in 2 pieces of 125 mm × 125 mm × 6 mm. The measure was performed at room temperature, with a power of 60 mW and during a time of 10 s to 40 s, in accordance with ISO 2207-2 standard. A minimum time of 2 minutes was left between two measures and for each sample, the measure was repeated three times.

2. Appendix to Chapter 1

2.1. A possible mechanism of CBS-accelerated sulfur vulcanization

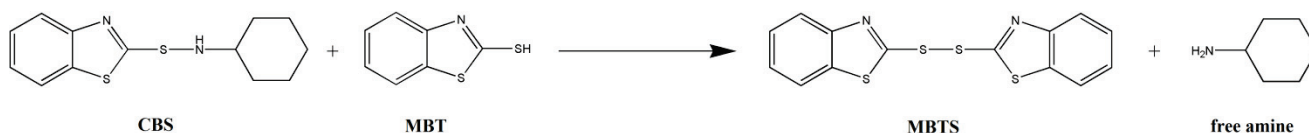
Accelerator chemistry

In a first step, upon heating, CBS is reported to homolytically cleave to form 2-mercaptobenzothiazole (MBT) and a free amine as shown on Scheme 24.



Scheme 24: CBS homolytic dissociation.

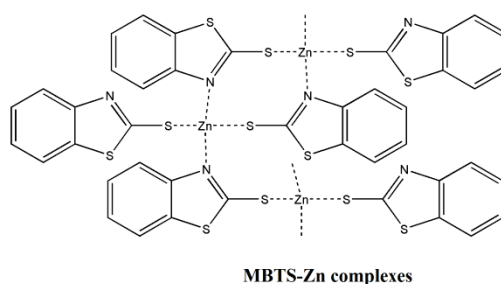
CBS dissociates into MBT molecule and a free amine is formed (supplementary hydrogen atoms are believed to come from surrounding molecules such as stearic acid). The resulting MBT can then react with CBS, to form MBTS (Scheme 25) [443].



Scheme 25: Formation of MBTS from CBS and MBT.

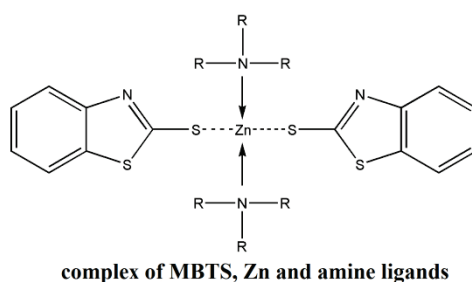
The nature of the reaction is postulated to be either ionic or radical [190, 444]. It can be noted that MBT and MBTS are activators that are commercially available and that could be used directly, instead of CBS. However, the use of CBS induces a delay in the onset of the vulcanization reaction (scorch time) that is often desirable in the industry.

In a next step, an activator such as ZnO may catalyze the formation of macromolecular complexes with MBTS (Scheme 26).



Scheme 26: MBTS-zinc complexes.

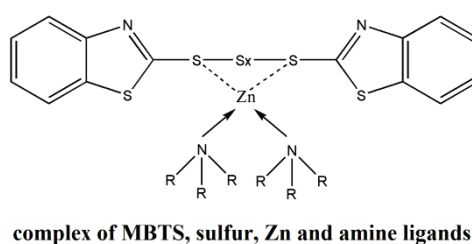
These complexes have low solubility in most elastomeric matrices and low reactivity towards sulfur. However, they may coordinate with amines and carboxylate ligands to increase solubility and reactivity (Scheme 27).



Scheme 27: MBTS-zinc complexes with amine ligands.

Amines can be released from the CBS cleavage and carboxylic ligands can be provided by stearic co-agent incorporation [185].

In a following step, elemental sulfur is added in the MBTS complex as shown in Scheme 28.

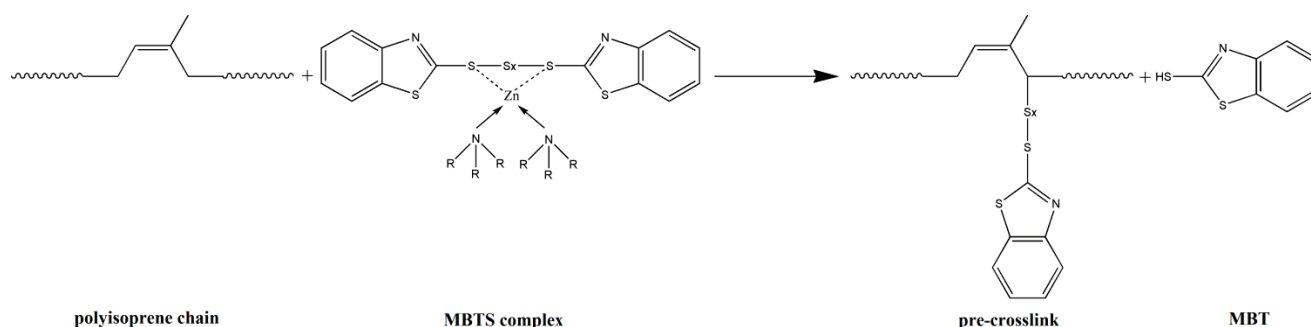


Scheme 28: Sulfur insertion into MBTS-zinc complexes with amine ligands.

Several studies have shown that sulfur addition in MBTS structures is sequential however the exact mechanism of this reaction is not fully understood yet [445, 446].

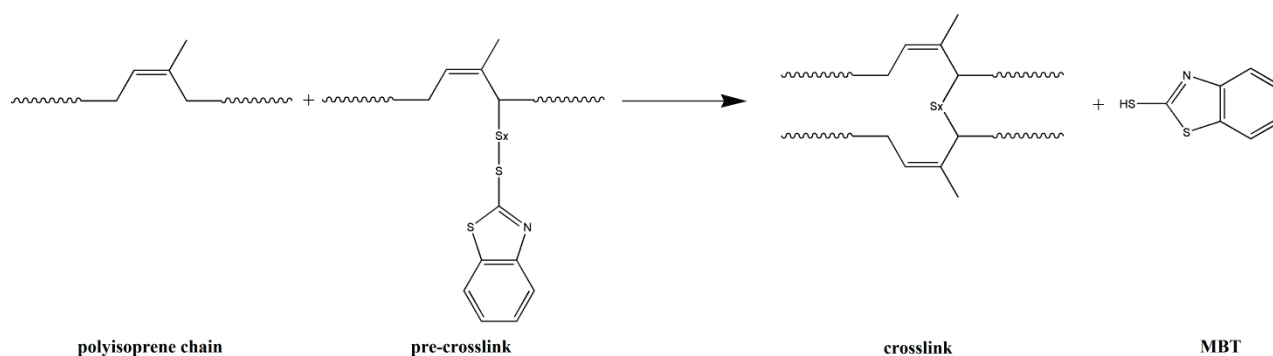
Crosslinking chemistry

Crosslinking reactions occur in two main steps: first precursors are formed, then crosslinks between elastomer chains are formed [447]. In the first step, polysulfide complexes react with elastomer chains through abstraction of an allylic hydrogen, to form crosslink precursors or “pre-crosslinks” [185]. Scheme 29 shows the reaction paths.



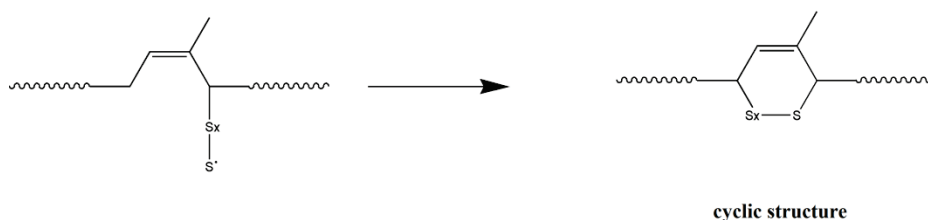
Scheme 29: Pre-crosslinks formation.

Crosslinking precursors are formed when the polysulfidic bonds of the accelerator complex react with rubber chains. Accelerator-terminated polysulfidic pendant group are attached to a rubber molecule, forming reactive “pre-crosslinks”. In a second step, these highly reactive species can react with elastomer chains again (through abstraction of an allylic hydrogen) to create crosslinks (Scheme 30).



Scheme 30: Formation of crosslinks from pre-crosslinks.

Polysulfide crosslinks between rubber chains are thus formed. From Scheme 30, it seems that MBT is regenerated after the crosslink is formed and may react again to form new crosslinking precursors. Besides, crosslinking precursors may also rearrange to form polysulfide cyclic structures on elastomer chains (Scheme 31) [185].



Scheme 31: Formation of a polysulfide cyclic structure onto an elastomer chain.

These cyclic structures are « elastically ineffective » as they do not enable covalent bonding of two elastomer chains together, and thus do not participate in the creation of a three-dimensional network.

Post-cure chemistry

As detailed above, crosslinks that are formed are mainly polysulfidic. They can then undergo modification through two main mechanisms: desulfuration and decomposition. In the former, polysulfidic crosslinks rearrange into more stable mono and disulfide crosslinks. In the latter, polysulfidic crosslinks degrade to elastically ineffective cyclic sulfides, inactive pendant groups and other main chain modifications (Figure 18 c and d). Besides, the sulfur released during those rearrangements may react to form new crosslinks [185].

2.2. Short literature review of barrier properties of graphitic fillers – elastomers composites

Many studies investigated graphitic fillers-elastomer barrier properties [135, 227, 236–239]. Table 14 provides a short review of the literature regarding barrier properties of elastomers filled with graphitic fillers.

Filler	Loading	Matrix	Processing	Permeant	Relative reduction (/ pristine polymer)	Reference
GO	1 wt% (=0.43 vol%)	PDMS	Solution (THF)	N ₂	-45 %	[238]
				O ₂	-45 %	
				H ₂	-45 %	
				CH ₄	-45 %	
				CO ₂	-45 %	
Low defect graphene flakes	5 phr	SBR	Latex	O ₂	-35 %	[236]
rGO	4 phr	NR	Latex	O ₂	-70 %	[237]
rGO	4 phr	NR	Latex + two-roll mill	O ₂	-30 %	[237]
TRG (aspect ratio L/W= 1000)	5 wt%	PDMS	Solution	Air	-80 %	[227]
TRG (aspect ratio L/W= 400)	5 wt%	PDMS	Solution	Air	-60 %	[227]
Graphite	1.6 vol%	TPU	Solution Melt in situ polymerization	N ₂	-5 %	[135]
TRG	1.6 vol%	TPU	Melt mixing	N ₂	-50 %	[135]
TRG	1.6 vol%	TPU	In situ polymerization	N ₂	-70 %	[135]
TRG	1.6 vol%	TPU	Solution	N ₂	-80 %	[135]
GO	1.6 vol%	TPU	In situ polymerization	N ₂	-60 %	[135]
Phenyl isocyanate - GO	1.6 vol%	TPU	Solution	N ₂	-98 %	[135]
Acetyl phenyl isocyanate - GO	1.6 vol%	TPU	Solution	N ₂	-94 %	[135]
Exfoliated graphite (using microwaves)	10 phr		Latex + HAAKE + two-roll-mill	N ₂	-38 %	[239]

Table 16: Gas permeability of graphene/graphite - elastomer composites.

2.3. Short literature review of tensile properties of graphitic fillers – elastomers composites

Some tensile properties of graphene-rubber composites found in the literature are reported in Table 15. The values in parenthesis refer to the increase / decrease in properties as compared to the neat matrix.

Filler	Loadi ng	Mat rix	Processing	Strain at break	Tensile strengt h	50% modu lus	100% modul us	300% modul us	Refere nce
Thermally reduced GO	5 phr	NR latex	Pre-mixing in latex phase followed by two-roll mill	950 % (× 1.1 as compared to neat NR)	6 MPa (× 1.5 as compared to neat NR)		1 MPa (× 2 as compared to neat NR)	5 MPa (× 6 as compared to neat NR)	[257]
Thermally reduced GO	5 phr	NR latex	two-roll mill	600 % (/ 1.5)	11 MPa (× 2.8)		0.5 MPa (× 1)	1 MPa (× 1.25)	[257]
Chemically reduced GO	5 phr	NR latex	Pre-mixing in latex phase followed by two-roll mill	500 % (/ 2)	9 MPa (× 2)		1 MPa (× 2)	4 MPa (× 4)	[261]
Chemically reduced GO	5 phr	NR latex	Pre-mixing in latex phase followed by solution mixing	< 100 % (/ 8)	10 MPa (× 5)		-	-	[261]
Graphite	25 phr	SBR	Solution (THF), HAAKE and two-roll mill	66 % (of the value obtained for the neat matrix)	148%	320 %			[448]
Graphite milled with THF	25 phr	SBR	Solution (THF), HAAKE and two-roll mill	118 %	561 %	680 %			[448]
Graphite milled under argon	25 phr	SBR	Solution (THF), HAAKE and two-roll mill	123 %	550 %	260 %			[448]

Graphite milled under CO₂ pressure	25 phr	SBR	Solution (THF), HAAKE and two-roll mill	240 %	380 %	180 %				[448]
TRG	25 phr	SBR	Solution (THF), HAAKE and two-roll mill	37 %	991 %	1520 %				[448]
TRG	25 phr	SBR	Latex mixing, internal mixer and two-roll mill	88 % (/ 3.7)			17.5 MPa (× 3)	10.9 MPa (× 14)		[255]
Chemically reduced graphite (using vitamin C)	25 phr	SBR	Latex mixing, internal mixer and two-roll mill	295 % (/ 1.1)			12.6 MPa (× 2.5)	2.8 MPa (× 3.5)	12.4 MPa (× 2.6)	[255]
Multilayer graphene (<10 layers)	25 phr	SBR	Latex mixing, internal mixer and two-roll mill	91 % (/ 3.6)			9.9 MPa (× 2)	6.5 MPa (× 8)		[255]
Expanded graphite	25 phr	SBR	Latex mixing, internal mixer and two-roll mill	334 % (× 1)			4.6 MPa (× 1)	1.1 MPa (× 1.4)	4.2 MPa (/ 1.1)	[255]
CNT	25 phr	SBR	Latex mixing, internal mixer and two-roll mill	260 % (/ 1.2)			9.2 MPa (× 2)	2.1 MPa (× 2.6)		[255]
CB	25 phr	SBR	Latex mixing, internal mixer and two-roll mill	365 % (× 1.1)			8.2 MPa (× 1.6)	1.2 MPa (× 1.5)	6.7 MPa (× 1.4)	[255]
GO-octadecylamine	4 wt%	TPU	Solution (THF)	850 % (/ 1.1)	35 MPa (× 1.3)		4 MPa (× 1.6)	10 MPa (× 1.4)		[226]

Appendices

GO-octadecylamine	10 wt%	TPU	Solution (THF)	600 % (/ 1.6)	17 MPa (/ 1.6)	4 MPa (× 1.6)	7 MPa (× 2)	[226]
GO-octadecylamine	50 wt%	TPU	Solution (THF)	10 % (/ 9.5)	9 MPa (/3)			[226]
subMicro graphite	10 phr	NBR	Two-roll mill	511 % (× 1.1)	3.9 MPa (× 1.3)	1.2 MPa (× 1.2)	2.1 MPa (× 1.3)	[16]
Micro graphite	10 phr	NBR	Two-roll mill	539 % (× 1.1)	3.8 MPa (× 1.3)	1.2 MPa (× 1.2)	1.9 MPa (× 1.2)	[16]
Expanded graphite	10 phr	NBR	Two-roll mill	488 % (× 1)	3.3 MPa (× 1.1)	1.5 MPa (× 1.5)	2.0 MPa (× 1.2)	[16]
Spherical graphite	10 phr	NBR	Two-roll mill	512 % (× 1.1)	2.8 MPa (/ 1.1)	1.1 MPa (× 1.1)	1.7 MPa (× 1.1)	[16]
subMicro graphite	60 phr	NBR	Two-roll mill	563 % (× 1.2)	10.2 MPa (× 3.4)	4.3 MPa (× 4.3)	7.1 MPa (× 4.4)	[16]
Micro graphite	60 phr	NBR	Two-roll mill	647 % (× 1.3)	9.8 MPa (× 3.3)	4.6 MPa (× 4.6)	5.4 MPa (× 3.4)	[16]
Expanded graphite	60 phr	NBR	Two-roll mill	529 % (× 1.1)	3.6 MPa (× 1.2)	2.7 MPa (× 2.7)	2.8 MPa (× 1.7)	[16]
Spherical graphite	60 phr	NBR	Two-roll mill	610 % (× 1.3)	5.1 MPa (× 1.7)	2.8 MPa (× 2.8)	3.5 MPa (× 2.2)	[16]
Reduced graphite oxide	2 phr	NR latex	Latex coagulation followed by twin-roll mill	550 % (/ 1.6)	27 MPa (× 2.7)			[237]
Reduced graphite oxide	2 phr	NR latex	Latex coagulation (segregated morphology of the composites)	600 % (/ 1.5)	18 MPa (× 1.8)			[237]
GO	0.3 wt%	LSR	In situ polymerization	40 % (/ 1.3)	1.5 MPa (× 1.8)			[258]
GO-TEVS	0.3 wt%	LSR	In situ polymerization	46 % (/ 1.5)	2 MPa (× 2.3)			[258]

Appendices

Expanded graphite	10 phr	NBR latex	Latex compound ing method followed by internal mixer	110 % (/ 3.7)	11.8 MPa (× 3)	11.5 MPa (× 10.5)	[239]
Expanded graphite	10 phr	NBR latex	Internal mixer	610 % (× 1.5)	5.8 MPa (× 1.5)	1.8 MPa (× 1.6)	[239]
Carbon black	2 wt%	NR latex	Ultrasonic ally-assisted latex mixing and two-roll mill	586 % (× 1)	18.2 MPa (× 1.1)	0.96 MPa (× 1)	2.6 MPa (× 1.1) [378]
CNT	2 wt%	NR latex	Ultrasonic ally-assisted latex mixing and two-roll mill	534 % (/ 1.1)	18.6 MPa (× 1.1)	1.13 MPa (× 1.1)	3.3 MPa (× 1.4) [378]
rGO	2 wt%	NR latex	Ultrasonic ally-assisted latex mixing and two-roll mill	564 % (/ 1.1)	25.2 MPa (× 1.5)	1.7 MPa (× 1.7)	6.6 MPa (× 2.8) [378]
rGO	2 wt%	NR latex	Two-roll mill	600 % (× 1)	18.8 MPa (× 1.1)	0.99 MPa (× 1)	2.47 MPa (× 1) [378]
Expanded graphite	10 phr	NBR latex	Latex compound ing + two-roll mill	225 % (/ 1.3)	9.5 MPa (× 1.7)	6 MPa (× 4)	[260]
Expanded graphite	10 phr	NBR latex	two-roll mill	260 % (/ 1.2)	6.5 MPa (× 1.2)	2.5 MPa (× 1.7)	[260]
GO	1.3 vol%	XNBR	Solution (THF) and two-roll mill	248 % (/ 2.2)	10.3 MPa (/ 1.4)	M200 6.5 MPa (× 3.8)	

Table 17: Literature review of tensile properties of some elastomer-graphene composites.

2.4. Short literature review of electrical properties of graphitic fillers – elastomers composites

Table 16 gives an insight of the performance of graphene-rubber composites on electrical properties.

Filler	Loading	Matrix	Process	Percolation threshold	Electrical resistivity	Electrical conductivity	Reference
GNPs	17 vol%	SBR	Solution and twin-roll mill	5 vol%	$5 \cdot 10^6 \Omega / \text{cm}$		[266]
GNPs	25 vol%	SBR	Twin-roll mill	16.5 vol%	$10^{17} \Omega / \text{cm}$		[276]
Graphite	13 vol%	TPU	melt	3 vol%	$10^6 \Omega / \text{cm}$		[135]
TRG	2.2 vol%	TPU	melt	0.25 vol%	$10^3 \Omega / \text{cm}$		[135]
TRG	1.5 vol%	TPU	In situ polymerization	0.25 vol%	$10^3 \Omega / \text{cm}$		[135]
TRG	1.7 vol%	TPU	solution	< 0.1 vol%	$10^2 \Omega / \text{cm}$		[135]
rGO	1.78 vol%	NR	Latex mixing	0.62 vol%		$0.03 \Omega / \text{cm}$	[272]
rGO	5 vol%	NR	Latex mixing and twin-roll milling	4.62 vol%		$0.04 \Omega / \text{cm}$	[272]

Table 18: Short literature review of graphene-rubber electrical properties.

3. Appendix to Chapter 2

3.1. Preparation of graphite oxide (GO) through Hummers' method

7.51 g of expanded graphite were introduced into an Optimax glass reactor with 177 mL of sulfuric acid and 3.77 g (0.044 mol) of sodium nitrate. The mixture was maintained at 0 °C for 1 h under mechanical stirring (with a glass stirrer). Then, 22.53 g (0.143 mol) of potassium permanganate were added slowly. The solution was then heated to 35 °C for 30 min and 188 mL of distilled water were added dropwise. After heating at 90 °C for 15 min the reaction was quenched by a quick addition of 750 mL of distilled water and 66.23 mL of hydrogen peroxide. The brown suspension was then repeatedly washed with 5 % hydrochloric acid solution and distilled water until a neutral pH was reached. The dark brown product was then dried under vacuum at 80 °C for 16 h. Figure 114 shows the product obtained before and after drying.

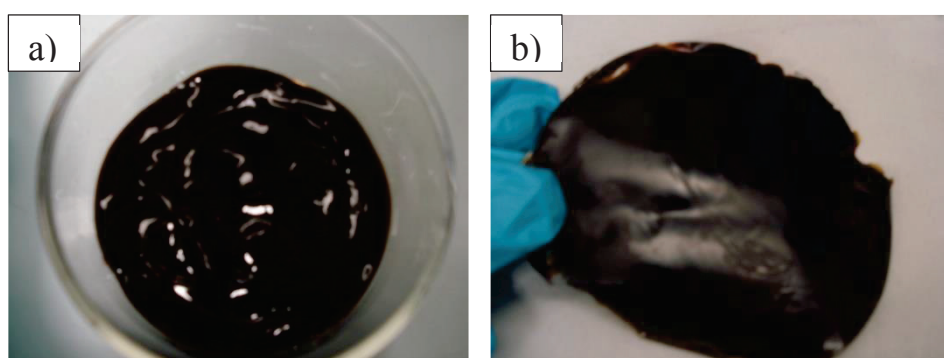


Figure 114: Digital images of graphite oxide a) before drying, b) after drying under vacuum. Product b) is sometimes reported as “GO paper” in the literature [106, 107].

The dried product was subsequently grinded using a cryo-grinder.

3.2. Preparation of GO-ODA

100 mg of graphite oxide prepared according to Hummers' method were added in a 250 mL round-bottom flask with 100 mL ethanol. 1 g of ODA (3.71 mmol) was added and the mixture was stirred for 5 min with a magnetic stirrer. The black suspension was then sonicated for 5 h at room temperature.

The product was then collected by centrifugation and washed 6 times with ethanol. It was then dried under vacuum at 60 °C for 16 h.

3.3. Preparation of GO-TESPT

0.5 g of GO introduced in a Schlenk flask and were sonicated in NMP for 30 min. 5.5 g (0.34 mmol) of TESPT were then added. Three freeze-pump-thaw cycles were then performed to remove oxygen from the Schlenk that was then filled with argon. The reaction was allowed to perform at 70 °C for 24 h. The resultant product was then washed several times with methanol, distilled water and acetone to remove ungrafted TESPT. Finally, the product was dried under vacuum at 60 °C during 16 h.

3.4. Preparation of GO-azide-IR

3.4.1. Esterification of GO with 1-azido-undecanol

200 mg of GO were dispersed in 40 mL of dimethylformamide (DMF) during 7 h in a sonication bath. 400 mg (1.94 mmol) of N-N'-dicyclohexylcarbodiimide (DCC) and 20 mg (0.164 mmol) of 4-dimethylaminopyridine (DMAP) were added and the mixture was sonicated during 4 h. 200 mg (0.938 mmol) of 1-azido-undecanol were then added with 40 mL DMF and the flask was protected from light and sonicated for 24 h followed by 24 h magnetic stirring at room temperature.

The product was subsequently isolated with centrifugation and washed several times (12) with tetrahydrofuran (THF). The black powder was then dried under vacuum at 60 °C during 16 h.

3.4.2. Cycloaddition of GO-azide onto polyisoprene

100 mg of polyisoprene were solubilized in 4.3 mL of 1,2,4-trichlorobenzene at 70 °C during 2.5 h in a Schlenk flask. 100 mg of GO-azide powder were added and dispersed in the solution under sonication for 2 h. Four freeze-pump-thaw cycles were then performed to remove oxygen from the flask. Then the Schlenk flask was backfilled with argon and heated at 190 °C during 64 h.

The product was then filtered on 0.45 µm Millipore Teflon filter and washed with 100 mL of boiling toluene. The powder was finally dried in vacuum oven at 80 °C during 16 h.

3.4.3. Blank experiment

A blank experiment was carried out with pristine GO to investigate the effect of the heating process on GO structure.

100 mg of GO powder were added and dispersed in 4.3 mL of 1,2,4-trichlorobenzene under sonication for 2 h. Four freeze-pump-thaw cycles were then performed and the Schlenk was filled with argon. The suspension was allowed to heat at 190 °C during 64 h. It was then filtered on 0.45 µm Millipore Teflon filter and washed with 100 mL of boiling toluene. The powder was finally dried in vacuum oven at 80 °C during 16 h.

4. Appendix to Chapter 3

4.1. Experimental procedures

4.1.1. APTMS grafting onto GO

1.0 g of graphite oxide was dispersed in 20 mL of N-methylpyrrolidone (NMP) using an ultrasonication bath for 30 min. 6.9 g (0.029 mol) of 3-acryloxypropyltrimethoxysilane (APTMS) were then added to the Schlenk flask. Four freeze-pump-thaw cycles were performed and the Schlenk was then filled with argon and heated at 110 °C for 24 h. The black suspension was then centrifuged nine times with methanol, distilled water and acetone to remove ungrafted APTMS and dried under vacuum at 80 °C for 10 h.

4.1.2. Isoprene emulsion free radical polymerization

In a typical experiment, 40 mg (0.15 mmol) of potassium peroxydisulfate (KPS, initiator, > 99.9 %) were added in a 50 mL glass Schott reagent bottle with 140 mg (1.67 mmol) of sodium hydrogenocarbonate and 14 mL of distilled water. Argon inert gas was bubbled into the mixture for 20 min. Then, sodium dodecyl sulfonate (120 mg, 0.42 mmol) was added under argon flow in the flask. Isoprene monomer (5.9 mL, 58.94 mmol) was first slowly distilled over argon and immediately collected with a syringe under argon. It was then quickly added in the Schott reagent flask under a light argon flow. The bottle was well sealed and heated at 75 °C in an oil bath, during 16 h under vigorous magnetic stirring.

The vessel was then removed from the oil bath and cooled in an ice bath. 20 mL of butanone were added for isoprene coagulation, forming a white elastic product. The mixture was then centrifuged several times with butanone, methanol and distilled water to fully precipitate the polymer and remove the remaining surfactant. Eventually, the product was dried in a vacuum oven at 50 °C during 16 h.

4.1.3. In situ emulsion free radical polymerization of isoprene in presence of GO-APTMS

Similarly to the procedure previously described, NaHCO₃ (140 mg, 1.67 mmol), KPS (40 mg, 0.15 mmol) and water (14 mL) were introduced in a Schlenk flask. 32 mg (GO-APTMS-p1) or 322 mg (GO-APTMS-p10) of GO-APTMS were added and the flask was sonicated for 20 min to disperse GO-APTMS in water. Then, argon was bubbled for 20 min. SDS (120 mg, 0.42 mmol) was added under argon flow and finally freshly distilled isoprene (5.9 mL, 58.94 mmol) was introduced in the flask under a light argon flow. The mixture was heated at 75 °C for 16 h under vigorous magnetic stirring.

After completion of the reaction, the flask was cooled in an ice bath and 20 mL of butanone were added. The product was then centrifuged with butanone, methanol and distilled water. It was finally dried at 50 °C under vacuum for 16 h.

4.1.4. Allyltrimethoxysilane grafting onto GO

1.0 g of graphite oxide was dispersed in 20 mL of N-methylpyrrolidone (NMP) using an ultrasonication bath for 30 min. 6.9 g (0.043 mol) of allyltrimethoxysilane (allyl) were then added to the Schlenk flask. Four freeze-pump-thaw cycles were performed and the Schlenk was then filled with argon and heated at 110 °C for 24 h. The black suspension was then centrifuged several times with methanol, distilled water and acetone to remove ungrafted allyltrimethoxysilane and dried under vacuum at 80 °C for 10 h.

4.1.5. Isoprene cationic polymerization

Cationic polymerization of isoprene was performed using a Lewis acid surfactant-combined catalyst (LASC). The LASC was prepared by stirring 0.21 g of ytterbium chloride hexahydrate ($\text{YbCl}_3 \cdot 6\text{H}_2\text{O}$) and 0.78 g of highly-branched sodium dodecyl benzenesulfonate (hbDBSNa) in purified water (3.5 g). After a few minutes the solution aspect turned from milky-white to a translucent orange coloration. Finally, 1.5 mL of distilled isoprene was added and the Schlenk reactor was heated at 50 °C for 16 h. The polymer was collected by coagulation with cold methanol and centrifugation. It was dried at 50 °C for 16 h under vacuum.

4.1.6. In situ emulsion cationic polymerization of isoprene onto GO-allyl

In situ polymerization of isoprene onto GO-allyl was performed following the same procedure as previously described. The LASC was prepared by stirring 0.21 g of ytterbium chloride hexahydrate ($\text{YbCl}_3 \cdot 6\text{H}_2\text{O}$) and 0.78 g of highly-branched sodium dodecyl benzenesulfonate (hbDBSNa) in purified water (3.5 g). After a few minutes the solution aspect turned from milky-white to a translucent orange coloration. 80 mg of graphite oxide were then added in the mixture and sonicated 1 h. Finally, 1.5 mL of distilled isoprene were added and the Schlenk reactor was heated at 50 °C for 16 h. The polymer was collected by coagulation with cold methanol and centrifugation. It was dried at 50 °C for 16 h under vacuum. To remove ungrafted polymer, washing with hot toluene was performed and the obtained product was subsequently dried under vacuum at 50 °C for 16 h.

4.2. Characterization of allyltrimethoxysilane grafting onto GO

High resolution XPS spectra of GO and GO-allyl are displayed in Figure 115.

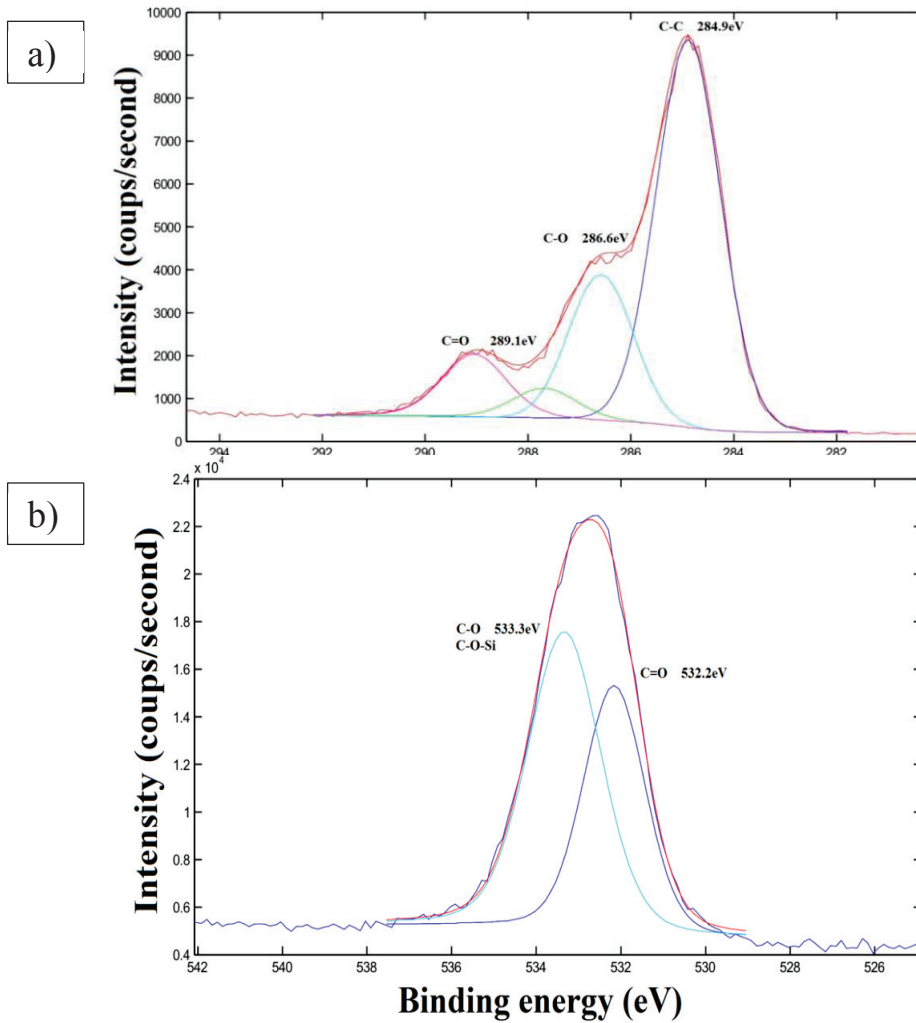


Figure 115: XPS spectra of GO-allyl. a) C 1s spectrum and b) O 1s spectrum.

From Figure 87, no clear evidence of allyltrimethoxysilane onto GO could be observed.

4.3. Characterization of APTMS grafting onto GO

4.3.1. FTIR spectra of GO and GO-APTMS

The FTIR spectra of GO and GO-APTMS are displayed in Figure 116.

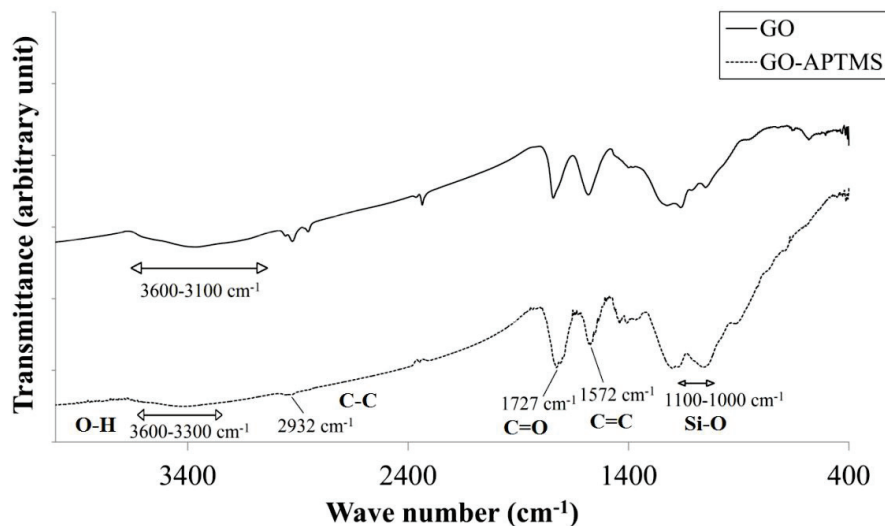


Figure 116: FTIR spectra of GO and GO-APTMS.

Similar observations as for GO-allyl could be made, the main difference between the two spectra being the reduction of the intensity and width of the O-H vibration band around 3400 cm^{-1} .

4.3.2. Raman spectra of GO and GO-APTMS

The Raman spectra of GO and GO-APTMS are displayed in Figure 117.

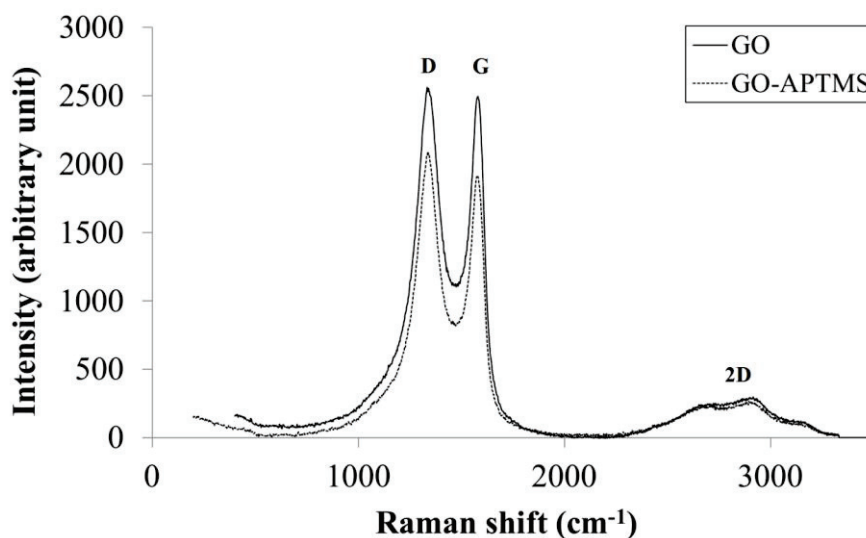


Figure 117: Raman spectra of GO and GO-APTMS.

No significant differences could be observed between the two Raman spectra. The structure of GO is well preserved after grafting of APTMS.

4.3.3. XRD analysis of GO and GO-APTMS

XRD spectra of GO and GO-APTMS are displayed in Figure 118.

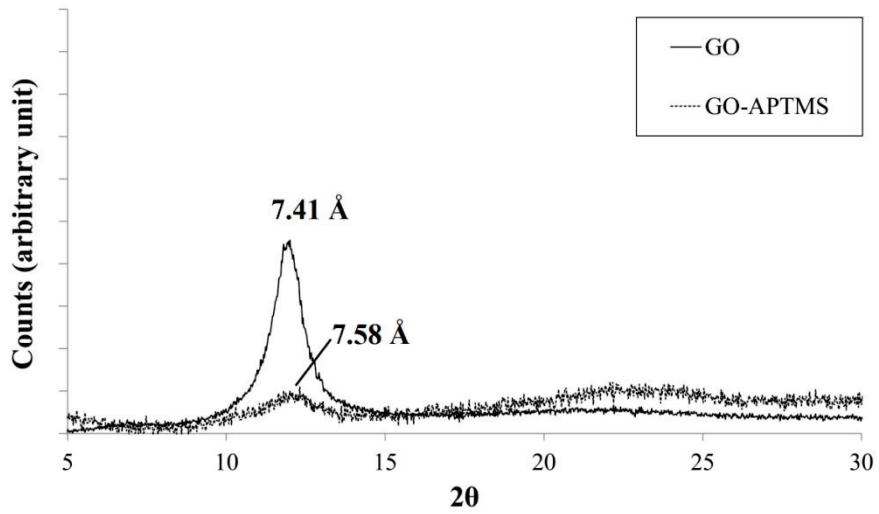


Figure 118: XRD spectra of GO and GO-APTMS.

A small increase from 7.41 Å to 7.58 Å could be observed upon grafting of APTMS onto GO.

4.3.4. TGA thermogram of GO and GO-APTMS

TGA analysis was performed to quantify the amount of APTMS on GO (Figure 119).

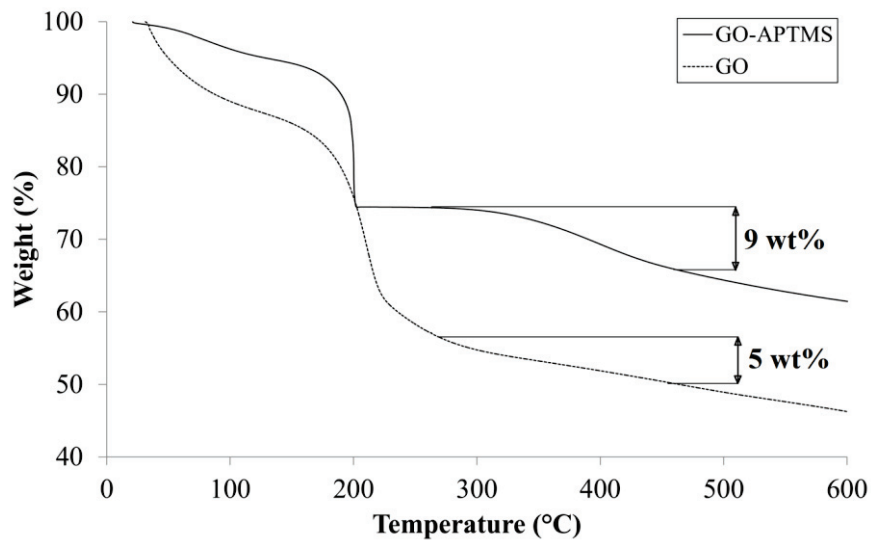


Figure 119: TGA thermogram of GO-APTMS and GO.

A 4 wt% grafting content was calculated from the thermogram, which is similar to the value obtained for GO-allyl.

4.3.5. Stability of suspensions of GO-APTMS

The stability of suspensions of GO-APTMS in an organic solvent has been evaluated (Figure 120).



Figure 120: Suspensions of GO (left) and GO-APTMS (right) in toluene at a concentration of 0.1 mg/mL.

As for GO-allyl, when placed in toluene, GO-APTMS sheets, at a concentration of 0.1 mg.mL⁻¹, disperse well and yield a homogeneous black suspension for at least 24 h, while GO sheets sediment almost immediately.

4.3.6. Morphology of GO-APTMS

The morphology of APTMS-modified GO was investigated by SEM (Figure 121).

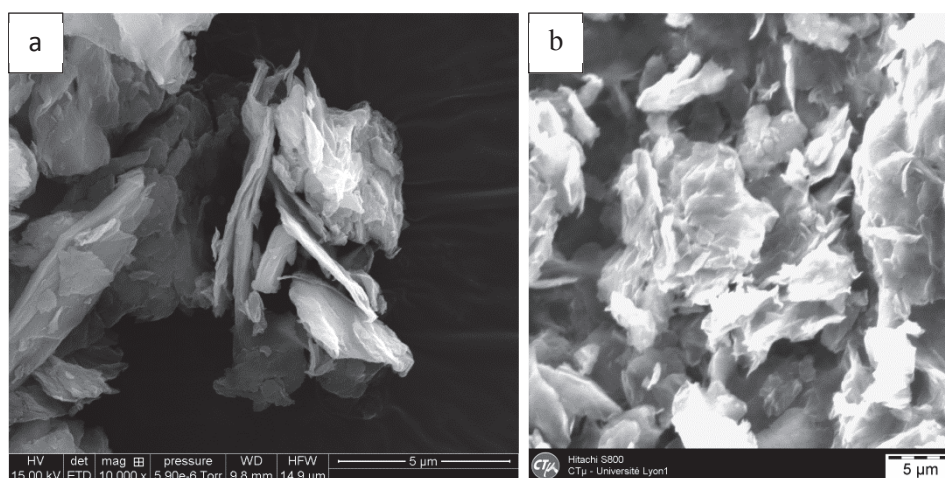


Figure 121: SEM image of a) GO and b) GO-APTMS.

No significant changes were observed in the morphology of the GO-APTMS sample, indicating that the structure of GO is preserved. Wrinkled sheets of various sizes with small “oxidized patches” on the surface of the platelets are seen. Sheet sizes in GO and GO-allyl are similar (from 5 to 10 μm).

5. Appendix to Chapter 4

5.1. Thermal expansion of graphite oxide

200 mg of GO were introduced in a nickel crucible and then placed into a muffle furnace and heated at the desired temperature (200 °C, 300 °C, 400 °C, 500 °C, 700 °C or 900 °C) during the desired time (30 s, 1 min, 5 min). The optimal parameters were 700 °C and 30 s. When removed from the furnace, the crucible was allowed to cool down for 1 min and then the fluffy powder was collected.

5.2. Preparation of graphite-based polyisoprene composites

Nanocomposites were prepared through conventional rubber processing. The formulations are given in Table 19.

Constituent	Loading (phr = parts per hundred rubber)
Polyisoprene (Nipol, ZEON)	100
Carbon black N550	50-x
Graphite-based filler	x = 0 ; 2 ; 15
SUNPAR paraffinic oil	5
Zinc oxide	3
Stearic acid	1
N-Cyclohexylbenzothiazole-2-sulphenamide 80 % (CBS)	0.75
Sulfur	1

Table 19: Formulation of the nanocomposites. Graphite-based fillers were incorporated in the composites as a replacement for the same amount of carbon black.

In a first step, polyisoprene was introduced into an internal mixer (Thermo Scientific, HAAKE rheomix) equipped with Banbury rotors. The capacity of the mixer is 50 cm³, temperature was set at 80 °C and a 40 rpm rotor speed was chosen. After 2 minutes, zinc oxide, stearic acid, oil, carbon black, and the graphite-based filler were added and mixed for 3 more minutes. The blend was then discharged and sheared on a twin-roll mill regulated at 40 °C for 8 min to incorporate CBS and sulfur. It was then taken out of the cylinder in the form of a 3 mm-thick sheet. The optimum curing time was measured on an ARES (TA) rheometer at 160 °C with a frequency of 1 Hz and at 7 % strain. Finally the compounds were compression molded into 2 mm-thick sheets, in a press at 160 °C, under 150 bars, during the optimum curing time.

5.3. Morphologies of graphite-based polyisoprene composites

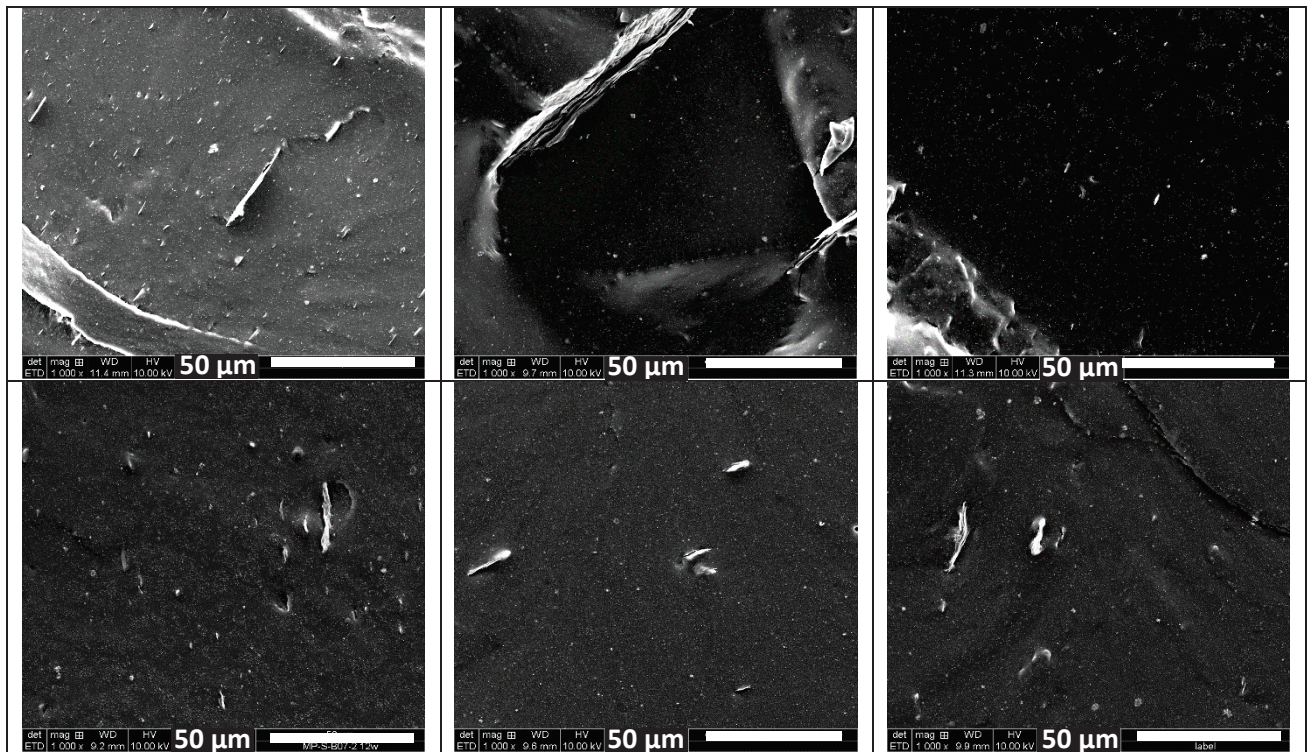


Figure 122: SEM images of graphite-based polyisoprene composites at 2 phr loading (and 48 phr of carbon black).

The same tendencies as composites at 15 phr loading can be observed. While GO leads to less uniform dispersions in polyisoprene composites, its functionalization seems to improve the dispersion and distribution of the platelets.

6. Appendix to Chapter 5

6.1. Experimental procedure for the preparation of NR composites

Nanocomposites were prepared through conventional rubber processing. The formulations are given in Table 20.

Constituent	Loading (phr = parts per hundred rubber)
Natural rubber (SMR 10CV60)	100
Carbon black N550	50-x
Graphite (TIMCAL, C-THERM 002)	x = 0 ; 2 ; 15
SUNPAR paraffinic oil 2280	5
Ionic liquid	1.95 (1 wt%) ; 10 (5 wt%) ; 19.5 (10 wt%)
Zinc oxide	3
Stearic acid	1
N-Cyclohexylbenzothiazole-2-sulphenamide (CBS)	0.75
Sulfur	1

Table 20: Formulation of the nanocomposites. Graphite was added in substitution for the same amount of carbon black.

In a first step, NR was introduced into an internal mixer (Thermo Scientific, HAAKE rheomix) equipped with Banbury rotors. The capacity of the mixer is 50 cm³, temperature was set at 80 °C and a 40 rpm rotor speed was chosen. After 2 minutes, zinc oxide, stearic acid, oil, carbon black, graphite and the ionic liquid were added and mixed for 3 more minutes. The blend was then discharged and sheared on a twin-roll mill regulated at 40 °C for 8 min to incorporate CBS and sulfur. It was finally put into a 3 mm-thick sheet when taken from the cylinders. The optimum curing time was measured on an ARES (TA) rheometer at 160 °C with a frequency of 1 Hz and at 7 % strain. Finally the compounds were compression molded in a press at 160 °C under 150 bars during the optimum curing time into 1 mm and 2 mm sheets.

6.2. Experimental procedure for the preparation of NBR composites

Nanocomposites were prepared through conventional rubber processing. The formulations are given in Table 21.

Constituent	Loading (phr = parts per hundred rubber)
NBR (Krynac 4450F, 43.5 % ACN)	100
Carbon black N550	70-x
Graphite (TIMCAL, C-THERM 002)	x = 0 ; 2 ; 15
DOS	10
Ionic liquid	1.95 (1 wt%) ; 10 (5 wt%) ; 19.5 (10 wt%)
Zinc oxide	3
Stearic acid	1
Antioxidant (N-1,3-Dimethylbutyl-N'-phenyl-p-phenyldiamine, 6PPD)	2
Antioxidant (2,2,4-trimethyl-1,2-dihydroquinoline)	1
Tetrabenzylthiuram disulfide (TBzTD, 70 %)	4.3
Tetraethylthiuram disulfide (TETD)	2.5
Dibenzothiazyl disulfide (MBTS)	2
Sulfur	0.2

Table 21: Formulation of the nanocomposites. Graphite was added in substitution for the same amount of carbon black.

In a first step, NBR was introduced into an internal mixer (Thermo Scientific, HAAKE rheomix) equipped with Banbury rotors. The capacity of the mixer is 50 cm³, temperature was set at 25 °C and a 40 rpm rotor speed was chosen. After 1 minute, zinc oxide, stearic acid, DOS, 6PPD, TMQ, carbon black, graphite and the ionic liquid were added and mixed for 3 more minutes. The blend was then discharged and sheared on a twin-roll mill regulated at 40 °C for 8 min to incorporate CBS and sulfur. It was finally put into a 3 mm-thick sheet when taken from the cylinders. The optimum curing time was measured on an ARES (TA) rheometer at 170 °C with a frequency of 1 Hz and at 7 % strain. Finally the compounds were compression molded in a press at 170 °C under 150 bars during the optimum curing time into 2 mm sheets.

6.3. Effect of the ILs on the curing times of NBR composites

The influence of the ILs on the curing time of NBR composites is displayed in Figure 123 and Figure 124.

6.3.1. Effect of the ILs on the curing times of NBR – carbon black composites

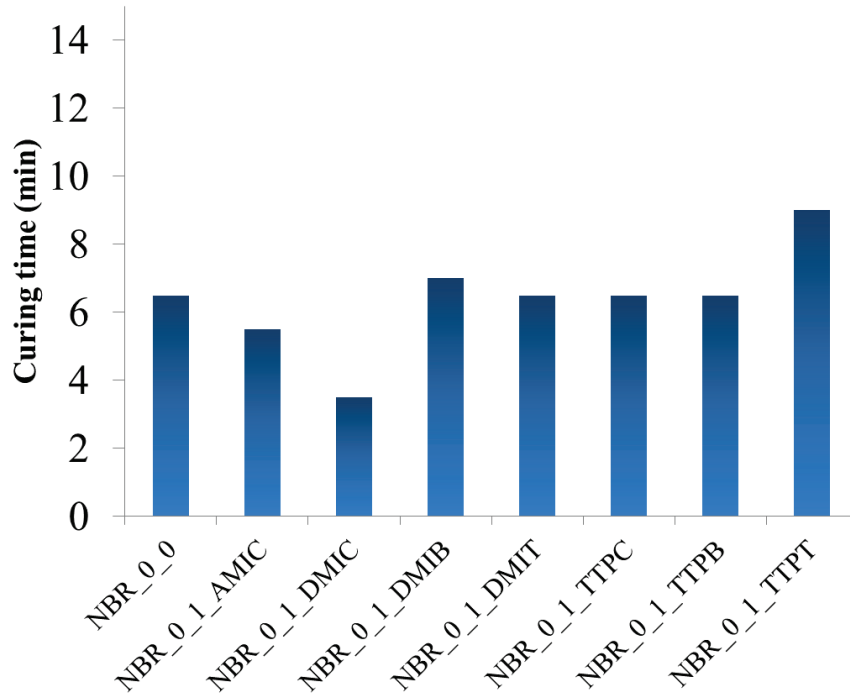


Figure 123: Curing time of NBR samples filled with 50 phr of carbon black and 1 wt% of ionic liquids.

For NBR composites containing only carbon black, DMIT, TTPC and TTPB induce no change in the curing times (6.5 min), while DMIB and TTPT increase the curing time (7 min and 9 min, respectively) and AMIC and DMIC decrease curing times (5.5 min and 3.5 min). It may thus be suggested that both the anion and the cation play a complex role on the vulcanization kinetics of NBR – carbon black composites.

6.3.2. Effect of the ILs on the curing times of NBR – graphite composites

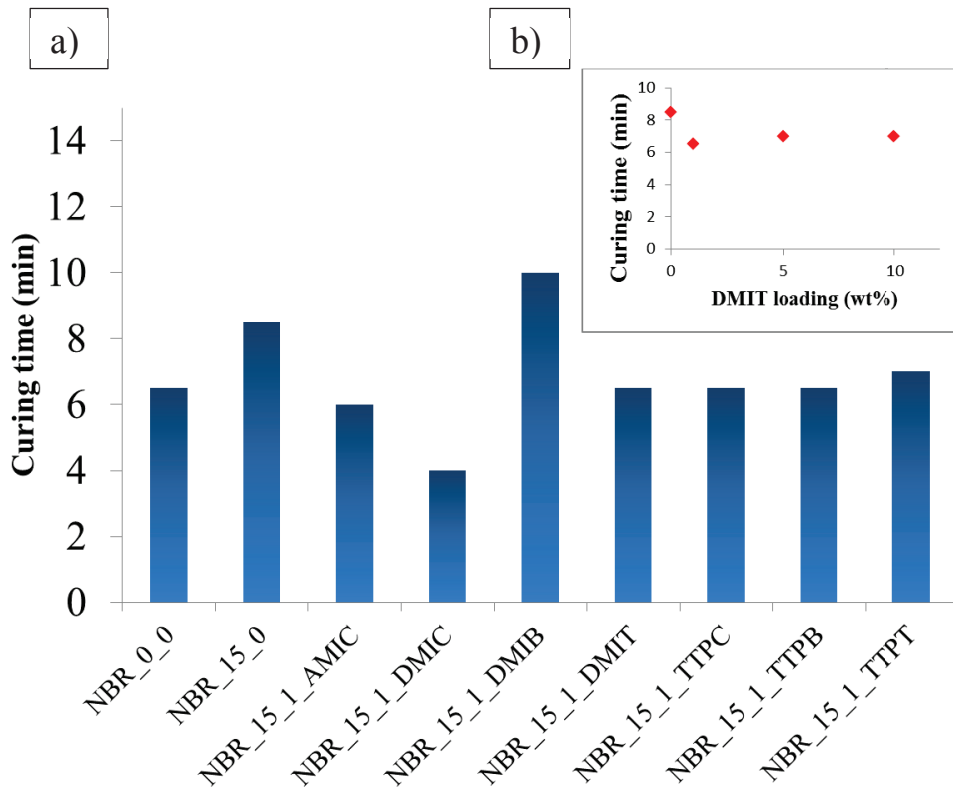


Figure 124: a) Curing time for NBR and NBR - graphite composites with 1 wt% ionic liquid and b) curing time of NBR - graphite composites as a function of DMIT loading.

As for NR composites, the substitution of 15 phr of carbon black by graphite leads to an increase in the curing time (from 6.5 min to 8.5 min). Upon addition of 1 wt% of IL, the same trend as for NBR – carbon black composites is observed. AMIC and DMIC decrease curing times, while DMIB and TTPT increase the curing times. The amount of IL in the composite does not seem to have an influence on the curing time, with no significant change observed for DMIT composites between 1 wt% and 10 wt% loading in NBR – graphite composites.

6.4. Evolution of torque during vulcanization of NR composites

NR composites were prepared and investigated with a closed cavity rheometer (Moving Die Rheometer, MDR).

	M_L	M_{HR}	$M_{HR}-M_L$
NR_0_0	1.5 dN.m	11.1 dN.m	9.6 dN.m
NR_15_0	1.4 dN.m	10.6 dN.m	9.3 dN.m
NR_15_1_DMIT	1.3 dN.m	10.6 dN.m	9.3 dN.m

Table 22: Minimum and maximum torque of NR composites.

No significant changes in the minimum and maximum torque were observed upon addition of 15 phr of graphite and 1 wt% of DMIT IL in NR composites.

6.5. Swelling ratio of NR and NBR composites

6.5.1. Swelling ratio of NR composites

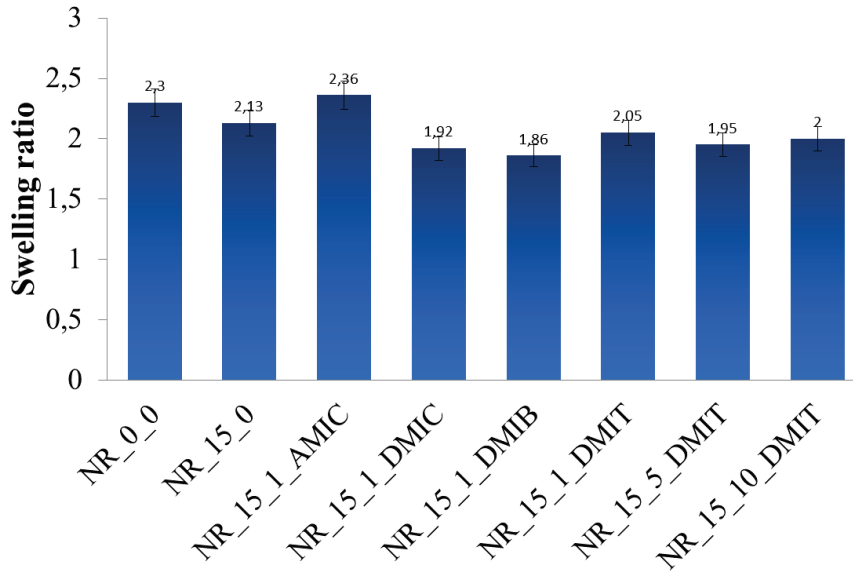


Figure 125: Swelling ratio of NR composites in cyclohexane.

Figure 125 displays the swelling ratio of NR composites in cyclohexane. All composites show a swelling ratio around 2, thus suggesting no significant differences between the crosslinking densities.

6.5.2. Swelling ratio of NBR composites

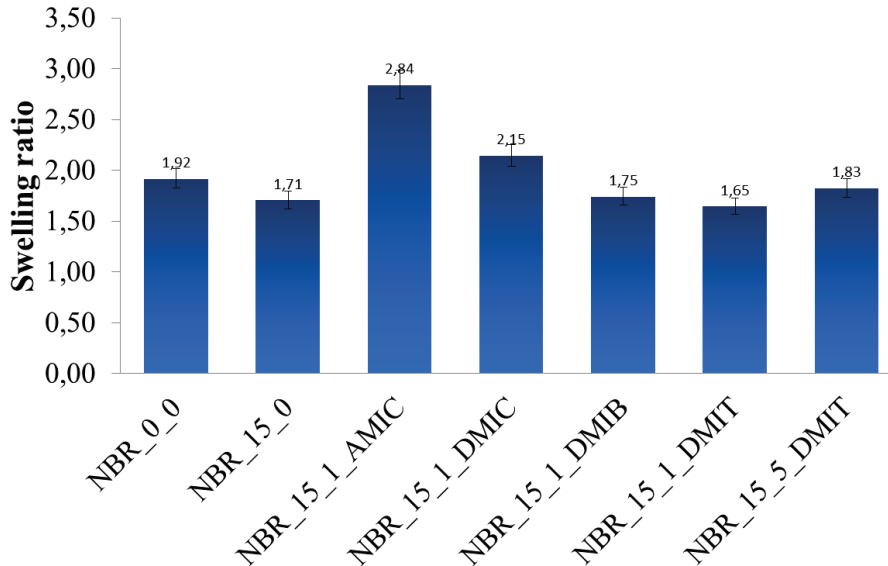


Figure 126: Swelling ratio of NBR composites in MEK.

Figure 126 displays the swelling ratio of NR composites in cyclohexane. Most composites show a swelling ratio around 1.7-1.8. The addition of 1 wt% of AMIC IL induces anyhow an increase in the swelling ratio up to 2.8, thus suggesting a decrease in the crosslinking density of the composite. DMIC IL also displays a small increase in the swelling ratio up to 2.1.

6.6. Rheometric curves of uncured NR composites

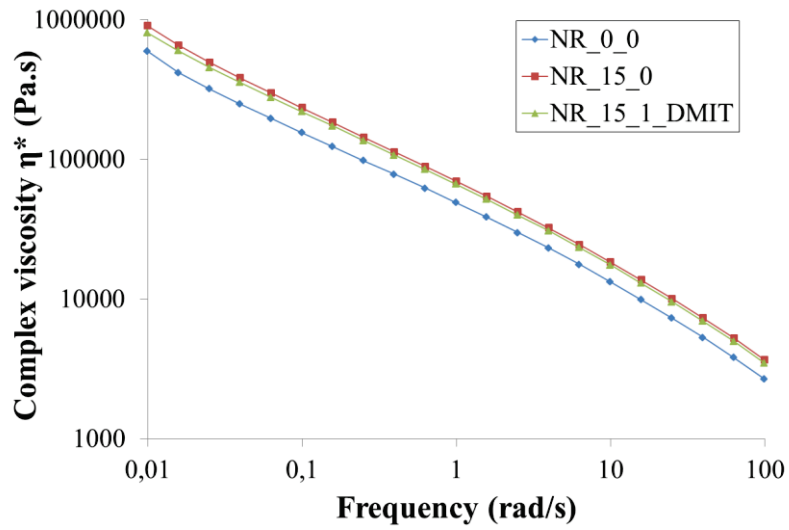


Figure 127: Evolution of the complex viscosity as a function of frequency for uncured NR composites.

Figure 127 displays the evolution of the complex viscosity as a function of the frequency. Upon substitution of 15 phr of carbon black by graphite, the complex viscosity increases from 5.9×10^5 Pa.s to 9.0×10^5 Pa.s at 0.01 rad/s (+ 52 %). The addition of 1 wt% of DMIT IL only leads to a small decrease of 1×10^5 Pa.s at 0.01 rad/s (- 10 %).

6.7. Tensile testing results for NR and NBR – carbon black composites

6.7.1. Effect of the addition of ILs in NR carbon black composites

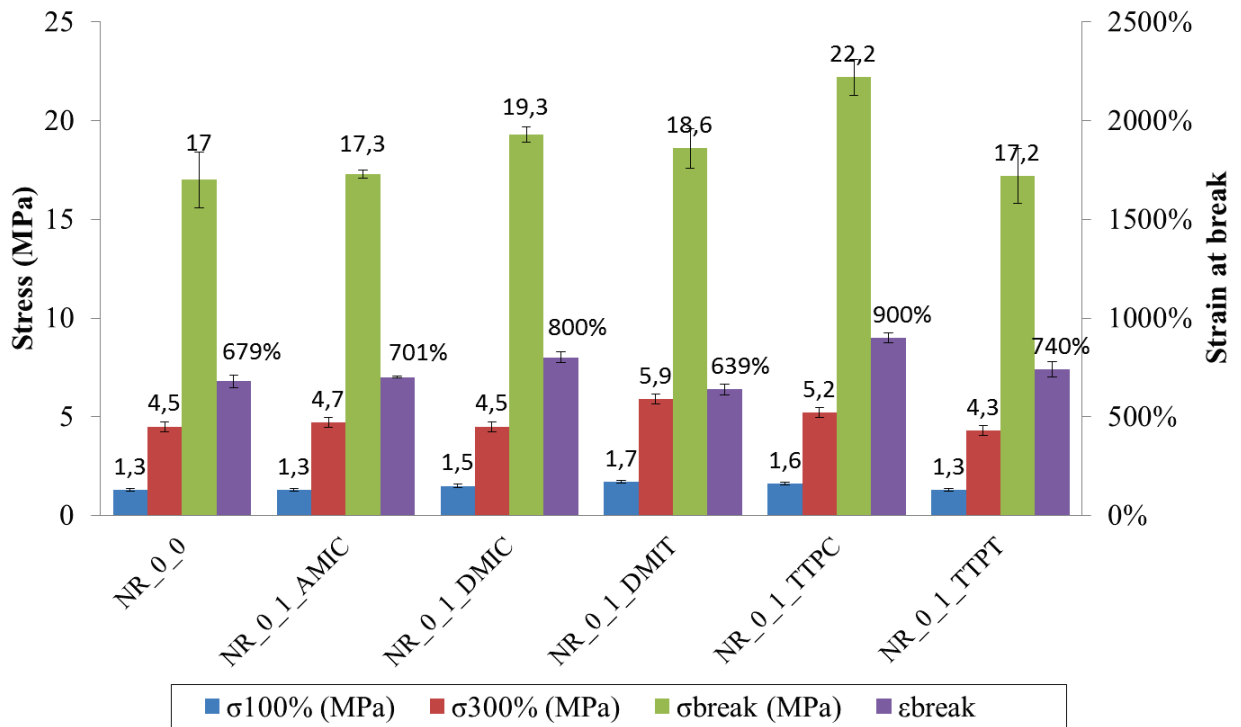


Figure 128: Effect of ionic liquids on the tensile properties of NR – carbon black composites.

From Figure 128, it may be observed that the addition of 1 wt% of IL on the tensile properties of NR – carbon black composites has little effect. DMIC and TTTC anyhow tend to increase strain at break (up to 900 % or TTTC - based composites). Besides, DMIT and TTTC display a small increase in stress at 300 % strain, thus suggesting a dispersing effect on carbon black, which may lead to enhanced reinforcement of the NR composite.

6.7.2. Effect of the addition of ILs in NBR carbon black composites

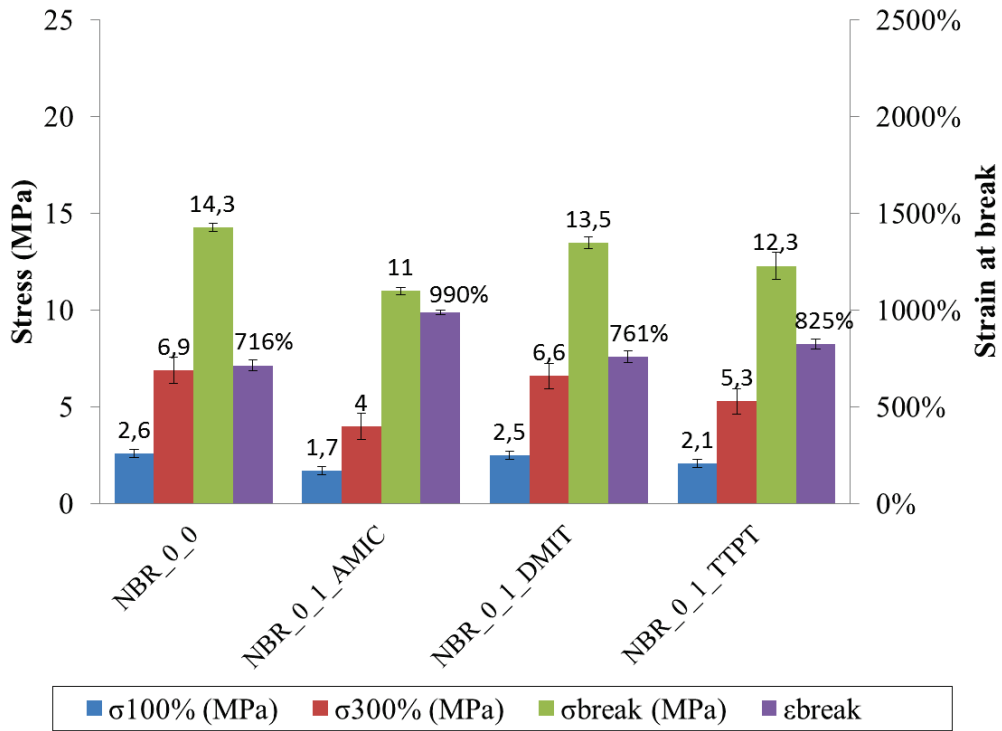


Figure 129: Effect of ionic liquids on the tensile properties of NBR – carbon black composites.

AMIC ionic liquid leads an increase in strain at break from 716 % to 990 % with reduced stresses at 100 % and 300 %. TTPT has a comparable effect, less pronounced anyhow. However, DMIT ionic liquid does not seem to induce any significant changes in tensile properties of carbon black – NBR composites.